Summer 8-15-2018

Functional and Skeletal Muscle Impairments In Progressive Diabetic CKD

Daniel Bittel
Washington University in St. Louis

WASHINGTON UNIVERSITY IN ST. LOUIS

Department of Physical Therapy
Movement Science

Dissertation Examination Committee:

David R. Sinacore

Todd Cade

Gretchen Meyer

Brent Miller

Michael Mueller

Arun Varadhachary

Functional and Skeletal Muscle Impairments In Progressive Diabetic CKD

by
Daniel C. Bittel, PT, DPT

A dissertation presented to
The Graduate School
of Washington University in
partial fulfillment of the
requirements for the degree
of Doctor of Philosophy

August 2018
St. Louis, Missouri

Table of Contents

List of Figures

List of Tables

Acknowledgments

An especially deserved acknowledgement is due to my primary mentor, Dr. David Sinacore. Dr. Sinacore has been an ideal mentor to me over the past 5 years – I will forever be grateful for his enthusiasm, passion, excitement, and most of all, his willingness to allow me to pursue my interests and curiosity, while always encouraging me to see them through. I couldn't imagine completing this PhD with anyone else's mentorship. I will always remember the efforts you've put in to my own professional development, and will be forever grateful.

I would also like to thank members of my dissertation committee, especially Drs. Varadhachary and Meyer. Dr. Varadhachary's ready willingness to help an unknown PhD student from another department, and become an integral source of knowledge, technical expertise, and feedback for this work has truly made this dissertation something much more than it would have been otherwise. I will always be indebted to Dr. Varadhachary for his critical role in not only this dissertation, but my research training as well. I would like to especially thank Dr. Gretchen Meyer, who I have always viewed as a second mentor in my research training. She has always been more than willing to answer all inquiries, teach me any technique, provide invaluable insights and feedback, and expand my interests, not to mention the countless pipette tips of hers I have used. My career trajectory has completely changed for the better, largely because of Dr. Meyer, and I cannot express my gratitude enough for all she has done for me. I would also like to thank Dr. Todd Cade for his efforts in expanding my knowledge of basic science and physiology early in my training, and for his constructive feedback and willingness to help with any aspect of my training or research. Additionally, Dr. Michael Mueller has been a tremendous source of encouragement and expertise in my training from the first semester of my time here, and his constant willingness to help in any way he can, is immensely appreciated. Kay Bohnert also deserves specific acknowledgement for her

upbeat attitude and positivity, and showing me, from my first day in the lab, how to conduct research and get a project off the ground. These skills are crucial for any trainee, and Kay was a tremendous source of knowledge and insight whenever I needed. Thank you.

I would also like to thank members of the nutrition-obesity-research-center, specifically Terri Pietka. Terri has been instrumental in making this work possible, and her patience, guidance, and enthusiasm in teaching me numerous methods has made this process immeasurably more enjoybale. Terri served as a bridge between impossible and easy for this research, and I will be forever in her debt. Thank you also to Dr. Gammon Earhart, Dr. Catherine Lang, and Dr. Marcie Harris-Hayes for your professional guidance and feedback throughout my training – from keeping me on track, to helping me grow as an educator, I am extremely grateful. Laslty, I would like to thank the APTA Foundation for Physical Therapy – their graciousness in awarding me promotion of doctoral studies (PODSI, PODS2) scholarships made all the difference in my training, dissertation efforts, and my career path. Their generosity has given me a tremendous foothold and a clear career path moving forward. I would also like to acknowledge the NIDDK of the NIH for their training support (F31 training grant), and the ICTS of WASHU for providing critical funds for key aspects of this work.

Daniel Bittel

Washington University in St. Louis

August 2018

ABSTRACT OF THE DISSERTATION

Functional and Skeletal Muscle Impairments In Progressive Diabetic CKD

by

Daniel Christopher Bittel

Doctor of Philosophy in Movement Science

Program in Physical Therapy

Washington University in St. Louis, 2018

Professor David R. Sinacore, PT, PhD, FAPTA, Chair

1-in-3 persons with type 2 diabetes (T2DM) develop chronic kidney disease (CKD), which is characterized by progressive renal dysfunction leading to end-stage renal disease. In response to elevated blood glucose and systemic inflammation of diabetes, a process of active thickening of the renal glomerular basement membrane ensues with concomitant damage to the structural supports (podocytes) of the kidney's filtration barrier. This results in impaired renal filtration. The metabolic sequelea of T2DM and CKD also, synergistically, alter skeletal muscle's degradative pathways, satellite cell function (muscle reparative cells), and mitochondrial health (muscle energetic machinery) -- resulting in muscle breakdown, poor muscle quality, and exercise intolerance, and immobility that exacerbates CKD. *The temporal nature and extent of these changes in CKD, however, remains unknown*. With mandates from the Center for Disease Control (CDC) urging avenues of treatment that impede the progression of CKD, it is critical now, more than ever, to gain a better understanding of the factors that contribute to disease progression. This will inform more effective targeted interventions. We therefore aim to determine how renal dysfunction dictates the activity of muscle degredative pathways, the status of muscle reparative cells, and the energetic production of muscle, to ultimately influence muscle quality, performance and physical mobility. This will be determined across stages of CKD.

In chapter 1, we examine how CKD progression in T2DM, impacts muscle performance and physical function. Our results suggest that muscle performance of the lower extremity, particularly the quadriceps, and physical function decline in-parallel with progression of CKD in T2DM, with these declines becoming clinically evident in stage 3. Moreover, we find that CKD-stage, and renal filtration/function (eGFR) are both significant predictors of overall physical function, with increasing CKD stage/worsening kidney filtration predicting worse functional mobility. In chapter 2, we examine the CKD-stage specific functional status of skeletal muscle mitochondrial ATP production, and electron transport chain kinetics, as these are critical cellular processes to fuel muscle cross-bridge cycling, contraction and movement. We find that intrinsic skeletal muscle mitochondrial electron transport chain function is reduced with progression of CKD, with significant reductions in ATP-production capacity emerging as early as stage 3 CKD. Moreover, these changes may derive from transcriptome-level alterations in gene networks governing muscle mitochondrial health and function. In Chapter 3, we examine muscle regenerative and maintenance capacity in relationship to CKD progression. We find the muscle-resident satellite cell pool to decline significantly with CKD progression, and exhibit impaired myogenic capacity with altered gene activation patterns, that relate strongly to findings of poor muscle quality with progressive CKD stage. Using transcriptomics, we report signi ficant dowregulation in gene networks that influence muscle SC behavior and myogenesis.

Overall, our data suggests that the progression of diabetes-induced chronic kidney disease, is paralleled by impairments in skeletal muscle ATP-producing capacity, and these energetic deficits are accompanied by CKD-associated reductions in muscle SC abundance, and reparative function. Both changes perhaps stem from alterations in gene pathway expression that is imparted by the

altered uremic environment. These impairments may promote the development of poor muscle quality and performance that ultimately impairs functional capacity, even in middle-stage CKD.

Background and Significance:

Over 30 million persons in the United States (~10%) have diabetes, with type 2 diabetes (T2DM) constituting 95% of all cases (**1**). T2DM is increasingly prevalent health condition, with 1.5 million new diagnosed cases each year (**1**). Diabetes is a syndrome characterized primarily by dysfunction in glucose regulation leading to hyperglycemia (**2**). The two principles of blood glucose regulation are insulin secretion by the pancreatic B-cell, and insulin sensitivity by peripheral tissues. Glucose absorbed from the meal is sensed, stimulating pancreatic insulin production and secretion (ie. by GLP1 and GLP2 peptides) (**3**). Insulin stimulates the uptake of glucose by peripheral insulin-sensitive tissues like skeletal muscle and adipose tissue by binding to, and activating the insulin receptor, which leads to phosphorylation of several different substrates, namely the insulin-receptor substrates (IRSs) (**4**). This phospho-activation leads to subsequent pathway signaling cascades resulting in glucose, fatty acid and amino acid uptake by both skeletal muscle and adipose tissue. Insulin resistance is defined by a failure of insulin, at even normal concentrations, to exert its effects, predictably leading to elevated blood glucose concentrations (**4**). A common index of glycemic control is the hemoglobin A1C test (HbA1c). HbA1c provides an indication of chronic hyperglycemia over a 120 day period, as it fundamentally asesses glycation of hemoglobin (red-blood cells) that provides evidence of an individuals average blood glucose levels during the previous ~3 months (**5**). Thus, diabetes results from impairment at either end of the insulin sensitivity/insulin secretion axis.

The more prevalent phenotype of diabetes (T2DM), results from an interaction between genetic predisposition and behavioral (excess nutrient intake, obesity, sedentary behavior, obesity) and environmental risk factors (**3**). T2DM often demonstrates as impaired glucose tolerance, reflected by a decrease in glucose-responsive insulin secretion resulting in postprandial hyperglycemia (excess blood glucose after a meal). This is generally understood to stem from insulin

resistance of peripheral tissues like skeletal muscle, as impaired insulin action at these tissues results in inadequate glucose uptake, thus prompting the pancreas to produce and secrete more insulin, and tissues like skeletal muscle to instead rely upon fats and protein for oxidation and energy production (**6, 7, 8**). With this postprandial deficit in mind, peripheral insulin sensitivity and insulin secretion assessment with glucose ingestion is the hallmark of T2DM diagnosis (**8**). While numerous clinical tests are utilized, among the most common are the oral glucose tolerance test (OGTT) and homeostatic model assessment (HOMA). The OGTT is administered as a single glucose bolus ingestion following an overnight fast and subsequent tracking of blood glucose and insulin concentrations over a 2-hour "post-prandial" period. Higher glucose excursions despite elevated insulin secretion provides a reasonable index of insulin resistance, and/or impaired insulin secretion. Conversely, the HOMA relies on the product of fasting plasma glucose and fasting plasma insulin concentrations, which shows a reasonable estimate of tissue sensitivity to insulin (**8**).

While the root cause of T2DM from a pathophysiological perspective remains debated, it is hypothesized that caloric excess and adiposity contributes largely to peripheral insulin resistance and ultimately pancreatic B-cell exhaustion (**9**). Adipose tissue accrual, a hallmark of obesity and development of T2DM, is linked with a litany of hormonal systemic effects. Of chief importance is the inflammatory response (**10**). With diabetes and obesity, hypertrophic adipocytes become hypoperfused, leading to local upregulation of hypoxia-inducible factor-1, along with activation of signaling cascades, mainly JNK1 and NFkB pathways, and genes involved in inflammation and endoplasmic reticulum stress. This leads to chemokine release from adipose tissue, and generalized low-grade systemic inflammation in T2DM (**11**). This adipose-tissue-mediated inflammation contributes to peripheral insulin resistance. Due to the insensitivity of skeletal muscle to insulin, and subsequent reduction in glucose uptake, utilization, and storage, skeletal muscle instead relies upon

other metabolic substrates, namely fatty acids. Not surprisingly, obese individuals express a higher rate of fatty acid breakdown, uptake and fatty acid flux (**9**). The increased fatty acid flux of T2DM results in elevated circulating free-fatty acids (FFA) and increased FFA uptake into muscle. Within skeletal muscle, FFA are converted to fatty acyl CoAs and transported into the energetic powerhouse of skeletal muscle – mitochondria, via carnitine palmitoyl transferase (CPT), for beta oxidation and energy production. In the event of mitochondrial inadequacy (due to oversupply of FFA, or reduction in oxidation capacity, or mitochondrial abundance, or all 3), fatty acyl CoAs are instead converted to diacylglycerol (DAG) and used to re-synthesize triglyceride. This leads to 1. ectopic lipid accumulation known as intermuscular adipose tissue (IMAT) beneath fascia and between muscle fascicles, and 2. intramuscular adipose tissue accumulation within muscle cells themselves (**9,12,13**).

In support of this theory, it has been shown that in T2DM, the oversupply of fatty acids exhausts skeletal muscle mitochondria, leading to accrual of fatty acid intermediates (DAG, ceramide, fatty acyl-CoA, etc.) in muscle that impairs insulin receptor signaling and contributes to insulin resistance (**11, 14, 15, 16**). More specifically, lipid intermediates have been shown to activate protein kinase C – a potent inhibitor of tyrosine phosphorylation of the insulin receptor and its substrates, while other intermediates (ie. ceramide) dephosphorylate Akt/protein kinase B, resulting in inhibition of GLUT4 translocation and subsequent glucose uptake (**17,11**). As skeletal muscle is responsible for 90% of peripheral glucose uptake, disruption in its ability to take up glucose and oxidize it (via glucose-fatty acid cycle or randle cycle competition) is a well-established key pathophysiological feature of T2DM and its progression (**18**). However, while T2DM is characterized by impairments in insulin signaling, sensitivity, and secretion, the potential causative metabolic deficits in skeletal muscle also serve to hinder overall muscle health and function.

Accrual of the aforementioned IMAT depot may impair extrinsic muscle contractile performance by interfering with muscle fascicle arrangement, pennation angle, excursion during contraction and perimysial function (**19, 20, 21**). Indeed, numerous studies have demonstrated reduced muscle strength, power, and twitch speed with increased IMAT deposition (**19,22**). Moreover, intermuscular fat storage is associated with enhanced lipid peroxidation, which, along with accumulation of fatty acid metabolic intermediates like DAG and ceramides, not only impair contractile mechanics, but act through inflammatory cytokines (TNF-alpha, IL-6) and signaling pathways (NF-KB, JNK) to upregulate protein-degrading machinery – ubiquitin proteasome system, and E3 ubiquitin-ligase MuRF1 (**23**,**11**,**24**). This upregulation promotes muscle atrophy – a negative balance between muscle protein synthesis and breakdown rates. In support of the presence of this signaling cascade, those with T2DM indeed exhibit muscle atrophy that is initially mild, and becomes more substantial with older age and severity of disease. In addition to systemic inflammation and lipid intermediates promoting muscle atrophy in T2DM, the reduced insulin sensitivity and signaling in T2DM skeletal muscle results in muscle atrophy as well (**21**).

Under normal conditions, insulin and insulin-like growth factor 1 (IGF-1) interact with their cell membrane receptors, which in-turn phosphorylate insulin receptor substrate 1 (IRS-1) (**26**). Phosphorylated IRS-1 then acts as a docking site to recruit and activate phosphatidylinositol-3-kinase (PI3K), which subsequently phosphorylates muscle inner membrane phospholipids, and generates phosphoinositide-3,4,5-triphosphate (PIP3). PIP3 acts as a docking site for the kinase Akt, which, upon binding, is phosphorylated and activated. This activated Akt inhibits protein degredation by phosphorylating and thus repressing the FoxO family – which transcriptionally upregulate production and activity of the E3 ubiquitin ligases of the ubiquitin proteasome, Atrogin-1/MAFbx, and MuRF-1 (**26**). Thus, deficient insulin and IGF-1 signaling in T2DM leads to

dephosphorylated IRS-1, dephosphorylated (inactive) Akt, in-turn upregulating FoxO transcription factors, leading to a more active ubiquitin proteasome pathway while simultaneously inhibiting mTOR pathway signaling, the primary protein synthesis pathway (**19**). Thus, muscle contractile function may be hampered in T2DM due to mechanical disruption secondary to IMAT accrual, and loss of muscle mass through overactive protein degradation. However, it is theorized that these interconnected impairments of T2DM skeletal muscle may stem from upstream mitochondrial dysfunction.

As mentioned previously, mitochondrial inadequacy may be a prime causative factor in skeletal muscle metabolic derangments and insulin resistance in T2DM. Mitochondria have 4 functions in their host cell – 1. provision of ATP for cell function, 2. mediation of cell death via apoptosis, 3. heat production, and 4. calcium homeostasis. Abundant in skeletal muscle, mitochondria are suspended in cytoplasm at locations where energy is needed -- between myofibrils to fuel muscle contraction, under the sarcolemma to assist in ion exchange and substrate transport and cell signaling, and near the nucleus (**27**). Mitochondria couple substrate oxidation (ie. glucose, fatty acids, and amino acids) with phosphorylation of ADP to ATP through generation and utilization of a proton gradient over the inner mitochondrial membrane - termed oxidative phosphorylation (**28**). Impaired functional capacity of mitochondria is a factor that may contribute to perturbations in glucose and fatty acid substrates in T2DM. Indeed, a reduction in the activity of enzymes of oxidative pathways observed in T2DM skeletal muscle correlates with severity of insulin resistance (**29**,**13**). This suggests impairment in mitochondrial function as a key aspect of the pathogenesis of insulin resistance, presumably due to decreased lipid oxidation and production of lipid intermediates (**13,14**). Moreover, studies have found smaller and damaged mitochondria in T2DM (~30% smaller), reduced activity of mitochondrial TCA cycle enzymes, downregulation of

genes involved in mitochondrial oxidative phosphorylation and those encoding proteins of respiratory chain complexes, specifically the B-subunit of ATP synthase (**30**). T2DM also seems to negatively impact skeletal muscle mitochondrial function, namely through inhibition of a coactivator of nuclear gene transcription factors, PGC-1a. PGC-1a, which is reduced in T2DM, regulates the expression of key genes governing mitochondrial replication, oxidative phosphorylation, and energy homeostasis (**31**). Thus, impaired mitochondrial function may serve as a key initial factor in the pathogenesis of skeletal muscle metabolic derangements in T2DM. However, while skeletal muscle metabolic deficiencies may serve as a linchpin of T2DM and development of hyperglycemia, poor glycemic control also contributes to a host of sequelae in other tissues of the body.

T2DM, and its associated hyperglycemia, can lead to macrovascular disease involving large vessels, and microvascular complications involving capillaries and arterioles. Specific macrovascular complications include atherosclerosis affecting arteries in the limbs, those supplying the brain, and coronary arteries (**7**). This can cause reduced blood supply to the limbs, promoting reduced wound healing, and can also impair bloodflow in the cerebro-vascular network resulting in stroke, dementia and other neurological deficits. Coronary artery alterations, both in structure and function with T2DM promotes cardiovascular disease, a common comorbidity of diabetes (**7**). Microvascular complication are thought to mostly stem from glycation-induced thickening of the capillary basement membrane rendering it impermeable, stiffer, and less compliant (**7**,**33**). As capillary permeability and compliance is critical for nutrient and oxygen delivery to target tissues, these microvascular complications predictably lead to elevated blood pressure (HTN), eye problems (retinopathy), nerve impairments (neuropathy), and kidney issues (nephropathy) (**7**,**33**). Proper glycemic control and oxygenation is important for the maintenance of neuronal structural integrity and function. Chronic hyperglycemia is implicated in peripheral nerve demyelination, excess

thickening of endoneurial microvessels, decline in nerve conduction velocity, axonal atrophy and degeneration and loss, glial insult and lipid peroxidation (**33**,**34**). Diabetes-induced neuropathic changes can affect large-fiber sensory, small fiber sensory, autonomic, and motor nerves. These metabolic, structural and functional alterations synthesize to produce classic neuropathic symptoms most commonly in sensorimotor nerves and termed diabetic sensorimotor polyneuropathy (**33,34**). This peripheral neuropathy is characterized first by a painful "pins and needles" sensation, and followed by a lack of cutaneous sensation in a stocking and glove distribution, that when paired with macrovascular-induced deficits in bloodflow, lead to impaired circulation, wound healing, and sensation, resulting in things like cutaneous ulceration (**35**). Such occurrences are usually found primarily in distal regions like the foot, that may lead, in some cases, to amputation. However, motor nerve involvement is not atypical, and can affect large and small fibers resulting neuromuscular deficits. While T2DM and hyperglycemia clearly result in a wide array of whole-body alterations in metabolism, sensation, and endocrine and cardiovascular function, of growing epidemiological significance is the pervasiveness of T2DM-induced kidney problems, or diabetic nephropathy.

One out of every 3 individuals with diabetes, have what is known as chronic kidney disease (CKD) (**36**). Diabetes, and in particular, T2DM, is the most common cause of CKD, and constitutes 70% of all cases of end-stage renal disease, the end-point of CKD (**36**). CKD and its progression, is characterized by declining renal function and can be classified into 5 different stages according to the presence of albuminuria (protein in the urine) and degree of renal impairment (renal filtration rate decrements) (**37**,**38, 39**) (see below charts). The genesis of CKD development and progression is thought to stem from the metabolic and hemodynamic abnormalities of T2DM. Blood travels via the renal artery to afferent arterioles and subsequently into capillaries of the glomerulus (the basic filtration unit of the kidney). As blood travels through these glomerular capillaries, plasma filters out

into the glomerular capsule through several layers – 1. Slats and fenestrated holes of capillary endothelium, 2. Slits in the squamous endothelium (basement membrane), and 3. Slits between interdigitating feet of podocytes (glomerular capillary structural support proteins), to filter unnecessary toxins and metabolic bi-products in circulation (**40**). However, the microvascular alterations induced by T2DM mentioned previously, result in glomerular hyperfiltration, hypertrophy and hyperperfusion within the kidney. A "silent phase" follows this hyperfiltration and is associated with morphological changes of the glomerulus and its capillaries that include glomerular basement membrane thickening, glomerular hypertrophy, and mesangial cell expansion that leads to protein leaking in the filtrate and overt proteinuria with declining renal filtration capacity and function (**41**).

While there are numerous interactive factors that predispose individuals with T2DM to developing CKD, a primary causative factor is accumulation of the extracellular matrix of the renal glomerulus. The chronic hyperglycemia, glycated albumin (AGEs), low-grade systemic inflammation, and excess glomerular capillary pressure and hypertrophy of T2DM, stimulate production of the pro-fibrotic protein TGF-B in the glomerulus, where it localizes to glomerular podocytes (**42**). Once localized, TGFB induces connective tissue growth factor (CTGF) and vascular endothelial growth factor (VEGF), and type 4 collagen production, the main component

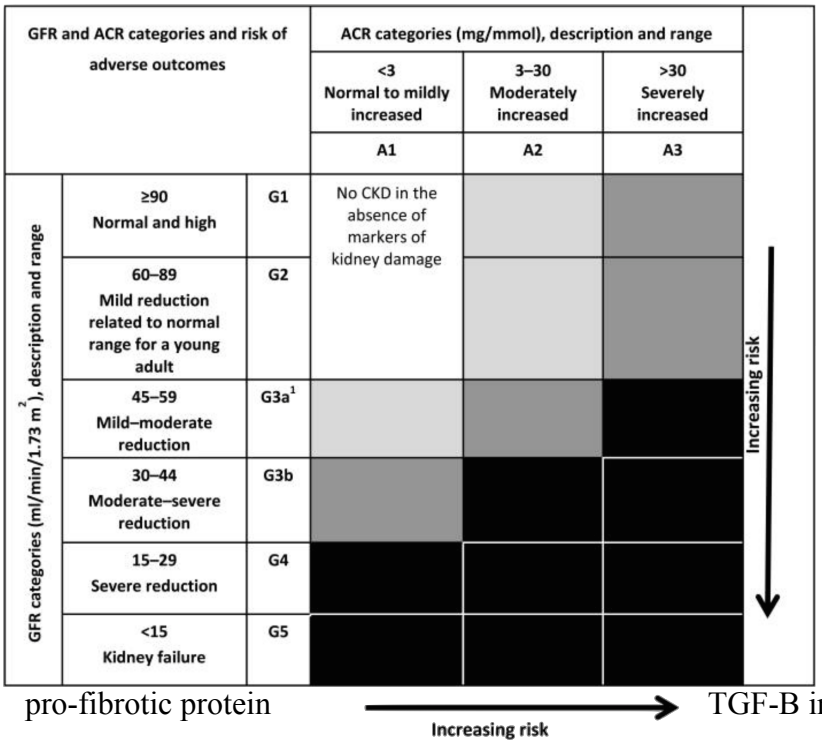

of the glomerular basement membrane to promote renal fibrosis (**42, 43**). This process becomes routine in nature in T2DM, leading to a progressive cycle of basement membrane thickening, glomerular hypertrophy and declining renal filtration (**42**). Accordingly, CKD is divided into 5 stages, the defining criteria of which are degree of proteinuria and renal filtration rate. Staging is shown above, and below (NICE Clinical Guidelines, No.182, National Clinical Guideline Centre (UK), 2014.)

Spot Urinary Albumin:Creatinine Ratio (index of renal filtration barrier integrity)

Microalbuminuria	>30 mg albumin/g creatinine
Macroalbuminuria	>300 mg albumin/g creatinine

Physical mobility is independently associated with renal functional decline in T2DM-CKD. However, CKD-associated muscle wasting and metabolic impairments complicate the clinical pathways and progression of CKD (**44**). The collective term for the state of muscle wasting and multifactorial metabolic impairment in CKD, is uremic myopathy. This uremic myopathy is superimposed on the T2DM-induced skeletal muscle metabolic derangements to exacerbate skeletal muscle decline in this population. Uremic myopathy was first described by Serratric et al. (1967), in a group of patients with chronic renal failure (ESRD) and progressive proximal muscle weakness caused by an intrinsic disorder of muscle function (**45**). Presently, though often debated, uremic myopathy – a collection of functional and structural muscle abnormalities in patients with CKD – is considered to be a consequence of the uremic state itself (**46**, **47**). The uremic state is a term used to describe the excess metabolic bi-products (ie. urea, creatinine, etc.) in the blood that, due to the declining filtration capacity of CKD, are no longer filtered by the kidneys and excreted in the urine,

most often associated with ESRD (stage 5 CKD) (**48**). Indeed, subsequent studies have shown that the progression of uremic myopathy runs parallel to the decline in renal function, with clinical signs becoming obvious upon ESRD (**47**). Muscle morphological features of uremic myopathy include – 1. **fiber atrophy and loss of myofilaments,** 2. **reduced mitochondrial content, with mitochondrial damage and increased lipid droplet content,** and 3. **internalized nuclei (indicative of attempted regeneration of muscle fibers) with z-band damage and cellular degeneration** (**47**). This constellation of muscle cellular alterations implicates dysfunction of systems governing muscle protein degradation, mitochondrial dysfunction, and systems governing new muscle fiber formation and injury repair in uremic myopathy. These dysfunctional systems are best examined in the context of the structural effects they produce in uremic muscle.

1. <u>Fiber atrophy and loss of myofilaments in CKD</u>: The decrease in muscle fiber size and number observed in CKD is due, in part, to protein degradation (**49**). As mentioned previously, protein degradation indicates an outpacing of protein synthesis, by protein breakdown, with small persistent imbalances causing substantial protein loss (**44**)**.** The loss of these cellular proteins increases the risk of morbidity and mortality in CKD and hampers muscle performance and mobility. The main cause of this loss of contractile protein in uremic myopathy is the upregulation of the ubiquitin proteasome pathway.

The ATP-dependent ubiquitin proteasome pathway (UBP) confers a specificity to muscle breakdown through its unique ubiquitin tagging process in which the muscle protein to be degraded is marked with a heat-shock family protein (ubiquitin). Ubiquitin is equipped with lysine residues (adherence ions that allow it to tag proteins) by an E1 ubiquitin-activating enzyme (**50**). Ubiquitin is subsequently transferred to an E2 carrier protein, which shuttles it to the muscle protein to be degraded. Once at the protein site, a highly specific E3 enzyme joins ubiquitin to the selected

protein. Specificity is realized through the 20 different E2 carrier proteins, and >500 forms of E3 enzyme, with each specific E2 carrier and E3 enzyme recognizing a specific set of muscle proteins (**44**). This process is repeated, ultimately producing a 5-ubiquitin "tag" attached to the protein, allowing its recognition by the degradative complex – the 26S proteasome. The proteasome contains 19S complexes at each of its ends, which serve to cleave the protein of its ubiquitin tag, unfold it, and feed the protein into an assembly line of proteases and peptides within the proteasome (**51,50).** In the uremic myopathy of CKD, there is drastic (4-15 fold) upregulation of the genes encoding components of the UBP – FOXO32 and FOXO1 (encoding Atrogin-1/MAFbx, and MuRF-1, both E3 ubiquitin ligases specific for contractile proteins of muscle), proteasome 19S subunit non-ATPase 11 (PSMD11, a "gatekeeper" 19S complex that recognizes, and unfolds muscle proteins before entry into the proteasome), and ubiquitin B and C (UBB and UBC, ubiquitin tags) (**51,52,53**). The physiological impetus for this upregulation of the UBP is multifaceted. One primary cause is a state of insulin resistance of T2DM, A second causative factor in ubiquitin proteasome upregulation in uremic myopathy is systemic inflammation that is characteristic of CKD (**44**).

Inflammatory cytokines, such as IL-6, TNF-alpha, and C-reactive protein are increasingly generated in CKD in response to uremic toxins (methylguanidine, ouabain, creatinine, urea) and reduced renal clearance (**54).** These inflammatory cytokines phosphorylate signal transducer and activator of transcription 3 (Stat3), which in-turn increases expression of suppressor of cytokine signaling 3 (SOCS-3). SOCS-3 dephosphorylates and inhibits IRS-1 production, thereby further interfering with the insulin/PI3K/Akt signaling pathway, and allowing FoXO transcription of the E3 ligases to go unchecked (**44,54**). However, the inflammatory cytokines also activate a TGF-beta family protein – myostatin. Stat3 independently increases the expression of CCAAT/enhancer binding protein-δ (C/EBPδ), which subsequently activates myostatin, resulting in dephosphorylation

of Akt via the Smad2/3 pathway, leading to activation of the ubiquitin proteasome pathway (**44).** Additionally, in rodent models of CKD, the uremic toxins that accumulate with impaired renal filtration/function contribute to metabolic acidosis – a condition that increases expression of ubiquitin mRNA and key 19S subunits of the proteasome (**44,47**)**.** Yet, other metabolic contributors to the activation of the degredative ubiquitin proteasome system are present in uremic myopathy, a primary protein being angiotensin 2.

Angiotensin 2 is the main effector of the renin-angiotensin-aldosterone system that controls fluid and electrolyte balance through coordinated effects on the heart, vasculature, and kidneys. Renin is secreted from the glomeruli of the kidney, and through a conversion cascade, generates angiotensin 2 (**55**). Angiotensin 2 acts on the kidney by binding to specific g-protein-coupled receptors, causing subsequent vasoconstriction and hypertrophy of afferent glomerular arterioles, leading to excess intraglomerular pressure and progressive damage and death of renal nephrons that is characteristic of CKD progression (**55**). Angiotensin 2 is upregulated in T2DM and even early CKD (**56**). However, angiotensin 2 also promotes endogenous production of various inflammatory cytokines (TNF-apha, IL-6, monocyte chemotactic protein-1, and nuclear factor-KB), which interfere with insulin signaling and thus promote E3 ligase production of the UBP as mentioned above (**57,55,44**).

Beyond these multifactorial contributions to UBP-mediated muscle breakdown in uremic myopathy, there is a primary muscle protein-cleaving enzyme that actively feeds the UBP in CKD – caspase 3. Caspases are a family of proteases that cleave proteins. In the uremic state, caspase-3 is activated, and subsequently cleaves actomyosin to be tagged for degredation in the UBP, allowing for more rapid protein degradation (**58**). Indeed, studies have shown that in those with ESRD of CKD, the enzyme-specific activity of caspase-3 is drastically increased, along with the transcription

of the FoxO-generated Atrogin-1/MAFbx and MuRF-1 E3 ubiquitin ligases, and *in-vitro* studies have even shown a direct stimulation of the proteasome by caspase-3 (**58**). Given the numerous contributing metabolic pathways of CKD that stimulate it, the UBP is responsible for the bulk of muscle breakdown observed in uremic myopathy. However, the second major route of muscle proteolysis – the autophagy lysosome system – may also play a role in the muscle atrophy of uremic myopathy.

The autophagy pathway is a homeostatic mechanism that degrades cytoplasmic constituents – organelles (mitochondria), protein aggregates (including protein toxins), and intracellular metabolites and pathogens (**59**). Autophagy is initiated by the formation of a semicircular double-membrane phagaphore that expands and engulfs selected intracellular components (including muscle proteins), and fuses to create a closed vesicle – the autophagasome (**59**). This autophagasome subsequently fuses with lysosomes which degrade the contained proteins and organelles, and expels the vacuolar debris via exocytosis (**60**). A crucial step in this degredative process is the conjugation of cytosolic microtubule-associated protein light chain 3 version 1 (LC3-1) to LC3-2. This protein must be conjugated to LC3-2 during the growth of the autophagasome, to act as both a structural support of the membrane, and as a sequesterer/docking site with proteins and organelles to be degraded (**59**,**61**). The overall formation of the autophagasome, however, is instigated by the Bnip3 gene. The Bnip3-produced protein localizes to the outer mitochondrial membrane and endoplasmic reticulum, and may induce cell death by perturbing mitochondrial function and calcium handling of the ER. Moreover, Bnip3 protein serves as the interactive docking site with LC3-2 of the autophagasome, resulting in autophagic degradation of mitochondria and cristae of the endoplasmic reticulum (**62,59)**. Predictably, an overactive autophagic system would remove excess proteins, organelles, and cytoplasm, resulting in atrophy and muscle cell death (**63**). Conversely, with

deficient autophagy, toxic protein aggregates and defective organelles (ie damaged mitochondria) may accumulate, promoting muscle degredation and atrophy as well (**59,63**). However, autophagy is inhibited by phosphorylated Akt, as pAkt stops the conjugation of LC3-1 to LC3-2, prevents the transcription of LC3 proteins, and inhibits the transcription of the Bnip3 gene (**64**). Yet, in uremic myopathy of CKD, Akt is dephosphorylated, leading to an upregulation of the FoxO family transcription factors that interact with key autophagy genes. FoxO3 for instance, may access 3 binding sites in the promoter region of the LC3 and Bnip3 genes, thus upregulating autophagy (**61,64**). Indeed, in CKD, FoxO3 is upregulated, leading to enhanced transcription of LC3 protein and Bnip3, which synergistically activate autophagy, and provide enough requisite protein to keep it active, resulting in muscle breakdown (**44**). However, the contribution of autophagy to CKD and uremic myopathy has only recently garnered investigative attention. The findings of reduced mitochondrial number and damaged mitochondria in uremic myopathy, certainly lend theoretical support for involvement of the aforementioned autophagic genes and protein (ie Bnip3). However, such findings also strongly implicate dysfunctional mitochondrial regulation.

***2. Reduced mitochondrial content/mitochondrial damage/ increased lipid droplet content in CKD*:** Mitochondrial production, or biogenesis, is critical in maintaining the functional and structural integrity of muscle, as it serves as muscle's main energy-generating system (**65).** Studies have shown low concentrations of aerobic enzymes, with impairment of ATP synthesis and increased rate of intracellular acidification in uremic myopathy. This indicates that uremic muscle depends more upon anaerobic metabolism (**47**). *However, this begs the question, is this due to deficient mitochondrial function, or deficient number of mitochondria*? While the answer remains unclear, evidence suggests both may be true. Several studies have demonstrated in the deltoid, gastrocnemius, rectus femoris, and vastus lateralis of hemodialysis patients (those in ESRD), there is

reduced oxidative enzyme activity, increased type 2 fiber percentage, low capillary density, mitochondrial inclusions (damaged mitochondria) and low myoglobin content (**66,67,68,69**). These are suggestive of an oxygen-independent energy metabolism preference in uremic myopathy (**66**). One study examined the *in-vitro* function of mitochondrial electron transport chain complex 2, SDH, in uremic muscle of an ESRD rodent-model, and found impaired ability of the complex to transfer electrons from administered succinate, down the transport chain (**70**). This predictably leads to impaired generation of ATP. Similar results are echoed in other works showing decreased activity/capacity of mitochondrial oxidative enzymes – cytochrome C (responsible for electron transport between ETC complexes), and citrate synthase (pace-maker for the 1st step of the citric acid cycle - catalyzes the reaction between acetyl CoA and oxaloacetate to form citrate and CoA-SH) (**71**). *In-vivo*, these results have been corroborated with 31P-MRS studies examining phosphocreatine depletion with contraction of uremic muscle. In these studies, with dynamic repetitive contraction, uremic muscle produces a greater and more rapid reduction in PCr concentration, suggesting reduced oxidative generation of ATP (**66**). A hypothesized reason for this deficient ATP production and storage, is an exhaustion of mitochondrial machinery due to 1. Reduced mitochondrial number, 2. Greater fractional energy expenditure for non-contractile ATP-dependent processes (ie ion pumping), and 3. Lower pH. This leads to increased demand for oxidative ATP production from the fewer remaining mitochondria, exhausting these energetic systems, and leading to mitochondrial morphological changes. Indeed, Tamaki et al (2014) showed in a CKD mouse model, that these mice exhibited classic morphological features of uremic myopathy, and had reduced levels of PGC-1-alpha and phosphorylated AMPK (indicative of reduced mitochondrial content) in all fiber types (**72**). These results are also confirmed through observations of reduced mitochondrial DNA copy number (a measure of mitochondrial content)

(**73**). Interestingly, however, other studies examining *in-vivo* mitochondrial function, have observed no difference in mitochondrial oxidative capacity between those receiving dialysis with diagnosed uremic myopathy and a control group (**67,47)**. After administration of glutamate, succinate, and ascorbate, ADP phosphorylation to ATP was not deficient in uremic myopathy, and function of all 5 complexes of the ETC had similar specific activity. However, these studies did not account for the well-established acidic cellular environment of uremic myopathy which could interfere with ATP production, and were limited to those undergoing maintenance hemodialysis for ESRD (**47**). These studies suggest that deficient ATP production *in-vivo* likely stems from reduced mitochondrial number, and lower intracellular pH, that together may place undue burden on remaining mitochondria, leading to mitochondrial DNA mutations, structural damage observed in histological studies, and respiration deficits. Indeed, Lim et al. (2002) has shown that in those with uremic myopathy, there are large-scale deletions (mtDNA4977, 8,041-bp deletion), and higher content of lipid peroxides and protein carbonyls in mitochondrial membranes (**74**). The 70-fold increase in mtDNA-4977 deletion in uremic myopathy, causes removal of major structural genes of cytochrome c oxidase, and ATPases that are crucial to proper mitochondrial function, structure, and integrity (**75**). With the increased burden on existing mitochondria, and large-scale mtDNA deletions that exacerbate deficient mitochondrial energy production and structure, it is not surprising that oxidation of metabolites such as fatty acids, may be impaired, leading to lipid droplet accumulation observed in histological samples of uremic muscle. In support of this theory, numerous studies have shown carnitine deficiency in uremic myopathy, which would predictably lead to deficient fatty acid transport within the intermembranous space of the mitochondria, and ultimately lead to impaired beta-oxidation, and lipid accumulation above that experienced in T2DM alone (**74,75,47**). Moreover, AMP-activated protein kinase (AMPK), a key regulator that inactivates acetyl CoA carboxylase

(thereby promoting FA oxidation), is downregulated in uremic myopathy (**71**). The status of mitochondria in uremic muscle remains understudied, and may be a large contributor to muscle dysfunction in this disease. However, known histological and morphological changes in skeletal muscle also raise other questions regarding muscle health in this population.

3. <u>Internalized nuclei with z-band damage and cellular degeneration</u>: These findings in uremic muscle of CKD implicate muscle-repair mechanisms may be deficient, resulting in structurally weak and perpetually remodeling muscle fibers. Skeletal muscle is a highly plastic tissue that responds to a variety of physiological and pathological stimuli due, in part, to constant turnover or remodeling of muscle proteins, organelles and cell populations. Muscle repair is the duty of satellite cells, a normally quiescent cell population located beneath the basal lamina of myofibers (**76**). Muscle homeostasis requires that these cells proliferate, differentiate and fuse to repair injured muscle fibers, form new muscle fibers, or return to a quiescent state to re-populate the cell pool (**76**). With muscle injury, among other signaling mechanisms, Notch ligand-delta is upregulated, and binds to notch-1 receptors on satellite cells, and activates the myogenic transcription of satellite cell functional genes Myf5, MyoD, and myogenin leading to satellite cell proliferation, and differentiation to repair damaged or necrosed fibers (**76,77**). However, obligatory to this repair process, is the simultaneous mobilization of fibroblasts, a cell population charged with producing temporary extracellular matrix components (collagen type 1 and 3, fibronectin, elastin, laminin, etc.) to stabilize the tissue and act as scaffolds for generation of new fibers (**78**). In rodent models of CKD with signs of uremic myopathy however, transcription of satellite cell function genes (MyoD, Myf5 – proliferation, Myogenin – differentiation) and contractile proteins (eMyHC) are decreased (**79**). Additionally, these satellite cells, when grown *in*-vitro and *in*-vivo to examine their proliferative and differentiation capacity, display slower rates of myotube formation, with significantly reduced

myosin content in resultant muscle fibers (**79**). This is paired with persistently elevated low-grade systemic inflammation observed in CKD – a state that provides positive feedback to muscle-resident fibroblasts in ECM deposition. Thus, with deficient satellite cell function, daily weight-bearing and activity induces muscle damage that is poorly rectified. Muscle repair becomes slowed, with deficient synthesis of key structural and functional proteins in new muscle cells, with simultaneous replacement with non-contractile fibrotic or adipose tissue (**78**). This may explain the appearance of centrally located nuclei in uremic myopathy, as this is indicative of newly formed muscle fibers in a perpetually damaged environment, though the degree of non-contractile tissue accrual in uremic muscle remains unknown. In uremic myopathy, theoretically, newly formed muscle fibers are not strong enough to withstand the continual demands of daily activity, and incur damage. Satellite cell response to this continual damage is both inadequate and delayed, and muscle atrophy ensues with potential concomitant fibrous or fatty replacement. The underlying reason for the proposed deficient satellite cell repair mechanism in uremic myopathy is still largely unknown, and remains to be determined in human muscle. However, some evidence suggests that insulin and IGF-1 signaling deficits, inflammation, and angiotensin 2, synergistically inhibit satellite cell function (**79**).

Satellite cells possess an angiotensin type 1 receptor, which upon activation by angiotensin 2, suppresses notch signaling and subsequent satellite cell functional gene transcription (**80**). IGF-1 is necessary for activation of satellite cells, and is also deficient in a state of insulin resistance as in CKD and T2DM (**79**). Additionally, IGF-1 binds to its receptor IGF-1BP-5, which in-turn modulates the extracellular matrix surrounding satellite cells and facilitating their proliferation (**52**).

The z-disc streaming seen in uremic muscle is theorized to stem from 2 causes in uremic myopathy – altered extracellular matrix protein production, and immature muscle fiber generation. As described theoretically above, the immature myofibers produced by deficient satellite cells, are

incapable of withstanding the high strain rates placed upon them, resulting in z-disc rupture and damage (**66**). Concurrently, evidence shows reduced mRNA levels for extracellular matrix proteins (filamin C, vinculin, talin) linking costameres (a tether linking and reinforcing the z-disc to the extracellular matrix lattice) to z-discs in skeletal muscle in uremic myopathy (**81,66**). Lacking these proteins, uremic muscle may possesses a less-stable z-disc that is predictably prone to damage during contraction. Moreover, muscle satellite cells and their purported dysfunction in uremic myopathy may also impact inherent metabolic health of mature skeletal muscle fibers through improper maintenance of myonuclear domain sizes of the muscle fibers.

Each myonucleus of a mature, elongated, multinucleated muscle cell, governs an area of surrounding cytoplasm, and produces enough protein and regulates signaling to support the limited area of cytoplasmic and structural components and organelles within it. This is called the nuclei's domain (**82**). With changes in the metabolic health of skeletal muscle, and in conditions of muscle wasting or atrophy (ie. uremic myopathy), myonuclear domain sizes continually shift, and the required incorporation (via satellite cell fusion) or removal (via autophagy or apoptosis) of nuclei becomes critical to the maintained functional and metabolic viability of the muscle cell (**82**). For instance, protein synthesis requires steady supply of nuclear derived genetic information to code the building of new proteins. Accumulation of DNA damage and deregulation of gene expression results in decreased tissue remodeling, and required nuclear removal and replacement through satellite cell mobilization (**83**). Thus, it is not unreasonable to suggest that satellite cell dysfunction or loss, may also contribute to conditions of muscle wasting and metabolic impairment through inadequate myonuclear contribution or regulation (**84**), though this remains to be investigated.

In community-dwelling elderly, research has examined the connection between anemia, electrolyte, and acid-base disturbances, and cardiovascular complications in CKD with functional

mobility deficits. Indeed, functional mobility/physical activity decrements in advanced stage CKD, is strongly associated with mortality and poor clinical outcomes (**86**). However, while mobility and physical activity are independently associated with renal function and overall health in this population, the aforementioned uremic myopathy (CKD-induced loss of muscle proteins, organelles, energetic deficiencies, and regenerative deficits) presumably imparts a state of muscle dysfunction that hinders continued mobility (**44**,**85**). Indeed, those with T2DM and late CKD exhibit fast-onset muscle fatigue and reduced exercise capacity and physical performance, stemming from dysfunction of muscle regulatory mechanisms and impaired muscle mitochondrial energy production (**37**). Together, muscle breakdown and impaired energy production may produce poor muscle quality that exacerbates mobility deficits and renal decline. These underlying factors that drive uremic myopathy in CKD has largely been examined in the context of advanced CKD, and ESRD in particular. When in the progression of CKD in T2DM, the effects of this process become apparent, and to what extent, is unknown. Determining when along the progression of CKD, these muscle regulatory pathways implicated in uremic myopathy become dysfunctional, may reveal key windows of opportunity to prescribe conservative exercise intervention to preserve muscle performance, mobility, and quality of life in T2DM-induced CKD.

Primary Purpose: To determine the unique contributions and temporal nature of CKD progression on skeletal muscle health, regulation, performance, and overall physical mobility in those with T2DM. In determining when along the progression of T2DM-induced CKD, skeletal muscle regulatory pathways become dysfunctional, and how this dysfunction manifests poor muscle health and performance, clinicians may then better understand the specific muscular sub-systems to target with conservative management approaches (ie. exercise), and when intervention is best.

Specific Aims and Hypotheses:

Specific Aim 1 (Chapter 1)- Determine how renal function (filtration capacity) and associated systemic factors (hyperglycemia, uremic status) relate to physical function and skeletal muscle performance across stages of T2DM-CKD.

Approach – Renal filtration capacity and stage of CKD determined via serum creatinine and CKD-EPI equation, and denoted as estimated glomerular filtration rate (eGFR). Glycemic control/insulin sensitivity using HbA1c. Uremic status determined via blood-urea-nitrogen concentration (BUN). Physical function is to be determined using the 9-item physical performance test (PPT) score, while muscle performance of major lower extremity muscle groups is determined via isokinetic dynamometry (to measure knee extensor peak torque at different contraction velocities and at optimal sarcomere length).

Aim 1 – Hypotheses: *Elevated BUN (uremia), and poor glycemic control (HbA1c) will both positively correlate with renal filtration rate (eGFR). Physical mobility (PPT score) will directly correlated with eGFR, even when controlling for comorbidities. Declining eGFR will correlate with declines in proximal muscle strength of the lower extremities (knee extensor torque production).*

Specific Aim 2 (Chapter 2) - Determine the functional status of muscle mitochondria, and activity of gene pathways governing muscle health, protein and organelle turnover and regulation, across stages of CKD. These measures will be additionally assessed for their relationships to muscle performance and physical function.

Approach – 1. Stage of CKD and filtration rate determined as in aim 1, with additional assessment of renal filtration barrier stability determined via proteinuria quantification (urinary spot albumin:creatinine ratio – ACR) 2. Skeletal muscle mitochondrial function/energy production

(oxidative phosphorylation capacity, electron transport system capacity, ETC-complex 1 function, ROS production) assessed via high-resolution respirometry of permeabilized muscle fibers, 3. Mitochondrial enzyme activity determined by enzymatic spectrophotometric assay, 4. Mitochondrial abundance determined via mitochondrial DNA copy number and qPCR, and citrate synthase enzyme activity. 5. RNA-sequencing to analyze the transcriptome of gene pathways governing mitochondrial oxidative phosphorylation, turnover, and protein import 6. Muscle performance and physical function will be determined for major lower extremity muscle groups via isokinetic dynamometry (to measure hip and knee extensor peak torque, work, average power -watts, and fatigue resistance).

Aim 2 – Hypotheses: *Reductions in renal filtration rate in CKD will positively correlate with:1. Lower extremity muscle performance, 2. Physical function (PPT score, gait speed, chair rise capacity), 3 mitochondrial function. With CKD progression, there will be stage-wise reductions in mitochondrial abundance, and enzyme activity. Mitochondrial function will significantly positively correlate with muscle performance and physical function. The skeletal muscle transcriptome will reveal altered gene expression in pathways governing mitochondrial regulation and function in later stages of CKD compared to early-stage.*

Specific Aim 3 (Chapter 3) - Determine the status of muscle quality and regenerative capacity, and explore the abundance and myogenic function of skeletal muscle satellite cells and muscle-resident inflammatory cells with CKD progression. Secondarily, explore how these measures relate to muscle quality and performance, and determine the relationship to relevant myogenic gene networks. These measures will also be assessed for their relationships to systemic inflammatory indices and uremic status across stages of CKD.

Approach – 1. Genome-wide expression analysis of protein-coding gene families governing satellite cell function, extracellular matrix deposition and collagen synthesis, inflammation via RNA-

sequencing. 2. Stage of CKD and filtration rate determined as in aims one and two. 3. Skeletal muscle satellite cell abundance determined via fluorescence-activated cell sorting (FACS) of muscle biopsies, and functional status (proliferative capacity, myogenic function and gene expression) determined via cell culture and qPCR. 4. Muscle quality determined via histology and image quantification of non-contractile- tissue accumulation. 5. Muscle performance determined as described in aim two. 6. Systemic inflammatory indices determined via plasma cytokine concentrations (IL-6, TNF-a), and uremic status via serum BUN levels as in aim one.

Aim 3 – Hypotheses: *Reductions in renal filtration rate in CKD will correlate with: 1. Reduced satellite cell abundance, 2. Impaired satellite cell myogenic capacity, and 3. Increased non-contractile tissue accumulation in skeletal muscle. Muscle-resident inflammatory cell population will increase with progression of CKD. Poor muscle quality will correlate with poor muscle performance and increased systemic inflammation and uremia in CKD. 4. The skeletal muscle transcriptome will reveal altered gene expression in gene networks that influence SC regenerative function (cell morphology pathways, growth factor signaling, extracellular matrix regulation, and inflammatory signaling).*

References

1. CDC National Center for Chronic Disease Prevention and Health Promotion – Division of Diabetes Translation. (2017) *National Diabetes Statistics Report*. Atlanta, GA, 2017.

2. Tuomilehto, J., & Wolf, E. (1987) Primary prevention of diabetes mellitus. *Diabetes Care*. 10(2); 238-248.

3. Scheen, A.J. (2014) Pathophysiology of type 2 diabetes. *Acta Clinica Belgica*. 335-341

4. Kahn, S.E., Cooper, M.E., & Del Prato, S. (2014) Pathophysiology and treatment of type 2 diabetes: perspectives on the past, present and future. *Lancet*, 383(9922); 1068-1083.

5. Sherwani, S., Kahn, H.A., Ekhzaimy, A., Masood, A., & Sakharkar, M.K. (2016) Significance of HbA1c test in diagnosis and prognosis of diabetic patients. *Biomark Insights*, 11; 95-104.

6. Nathan, D.M., Davidson, M.B., DeFronzo, R.A., Heine, R.J., Henry, R.R., Pratley, R., & Zinman, B. (2007) Impaired fasting glucose and impaired glucose tolerance. *Diabetes Care*, 30(3); 753-759

7. Frayn, K.N., Metabolic Regulation – A human perspective, 3rd Ed. Wiley-Blackwell, Oxford, UK.

8. Matsuda, M., & DeFronzo, R.A. (1999) Insulin sensitivity indices obtained from oral glucose tolerance testing: comparison with the euglycemic insulin clamp. *Diabetes Care*, 22(9); 1462-1470.

9. Capurso, C., & Capurso, A. (2012) From excess adiposity to insulin resistance: the role of free fatty acids, *Vasc Pharmacol*, 57(2-4); 91-7

10. Hardy, O.T., Czech, M.P., & Corvera, S. (2012) What causes the insulin resistance underlying obesity? *Curr Opin Endocrinol Diabetes Obes*, 19(2); 81-87.

11. Cefalu, W.T. (2009) Inflammation, insulin resistance, and type 2 diabetes: back to the future? *Diabetes*, 58(2); 307-308.

12. Mittendorfer, B. (2011) Origins of metabolic complications in obesity: adipose tissue and free fatty acid trafficking, *Curr Opin Clin Nutr Metab Care*, 14(6); 535-541.

13. Koves TR, et al. (2008) Mitochondrial overload and incomplete fatty acid oxidation contribute to skeletal muscle insulin resistance. *Cell Metab*. 7(1):45–56

14. Chavez JA, et al. (2003) A role for ceramide, but not diacylglycerol, in the antagonism of insulin signal transduction by saturated fatty acids. *J Biol Chem*. 278(12):10297–10303.

15. Holland WL, et al. (2007) Inhibition of ceramide synthesis ameliorates glucocorticoid-, saturated-fat-, and obesity-induced insulin resistance. *Cell Metab*. 5(3):167–179.

16. Long SD, Pekala PH. (1996) Lipid mediators of insulin resistance: Ceramide signalling down-regulates GLUT4 gene transcription in 3T3-L1 adipocytes. *Biochem J*. 319(Pt 1):179–184

17. De Fea K, Roth RA. (1997) Protein kinase C modulation of insulin receptor substrate-1 tyrosine phosphorylation requires serine 612. *Biochemistry*. 36(42):12939–12947.

18. Randle PJ, Garland P, Hales C, Newsholme E. (1963) The glucose-fatty acid cycle: its role in insulin sensitivity and the metabolic disturbances of diabetes mellitus. *Lancet*. 13:786–789.

19. Bittel, D.C., Bittel, A.J., Tuttle, L.J., Hastings, M.K., et al. (2015) Adipose tissue content, muscle performance and physical function in obese adults with type 2 diabetes mellitus and peripheral neuropathy. *J Diabetes Complications*, 29(2); 250-257.

20. Gillies AR, Lieber RL. (2011) Structure and function of the skeletal muscle extracellular matrix. *Muscle & Nerve*. 44(3):318–331

21. Wakeling JM, Blake OM, Wong I, Rana M, Lee SS. (2011) Movement mechanics as a determinate of muscle structure, recruitment and coordination. *Philos Trans R Soc Lond B Biol Sci.* 366(1570):1554–1564.

22. Casas-Herrero, A., Cadore, E.L., Zambom-Ferraresi, F., Idoate, F., et al. (2013) Functional capacity, muscle fat infiltration, power output, and cognitive impairment in institutionalized frail oldest old. *Rejuvenation Res*, 16(5); 396-403.

23. Addison, O., Marcus, R.L., LaStayo, P.C., & Ryan, A.S. (2014) Intermuscular fat: a review of the consequences and causes. *International Journal of Endocrinology*, 2014(2014); 1-11.

24. Hamrick, M.W., McGee-Lawrence, M.E., & Frechetter, D.M. (2016) Fatty infiltration of skeletal muscle: mechanisms and comparisons with bone marrow adiposity. *Front Endocrinol*.

25. Wang, X., Hu, Z., Hu, J., Du, J., & Mitch, W.E. (2006) Insulin resistance accelerates muscle protein degradation: activation of the ubiquitin-proteasome pathway by defects in muscle cell signaling. *Endocrinology*, 147(9); 4160-8

26. Schiaffino, S. & Mammucari, C. (2011) Regulation of skeletal muscle growth by the IGF1-Akt/PKB pathway: insights from genetic models. *Skeletal Muscle*, 1:4

27. Gouspillou, G., Hepple, R. T., eds. (2017). Mitochondria in Skeletal Muscle Health, Aging and Diseases. Lausanne: Frontiers Media. doi: 10.3389/978-2-88945-073-2

28. Conley, K.E. (2016) Mitochondria to motion: optimizing oxidative phosphorylation to improve exercise performance. *Journal of Experimental Biology*, 2019(2016); 243-249.

29. Rabol, R., Boushel, R., & Dela, F. (2006) Mitochondrial oxidative function and type 2 diabetes. *Appl Physiol Nutr Metab*, 31(6); 675-83.

30. Mogensen, M., Sahlin, K., Fernstrom, M., Glintborg, D., Vind, B.F., Beck-Nielsen, H., & Hojlund, K. (2007) Mitochondrial respiration is decreased in skeletal muscle of patients with type 2 diabetes. *Diabetes*, 56(6); 1592-9

31. Zorzano, A., Hernandez-Alvarez, M., Palacin, M., & Mingrone, G. (2010) Alterations in the mitochondrial regulatory pathways constituted by the nuclear co-factors PGC-1a or PGC-1B and mitofusin 2 in skeletal muscle in type 2 diabetes. *Biochimica et Biophysica Acta – Bioenergetics*, 1797(6); 1028-1033

32. Fowler, M.J. (2008) Microvascular and macrovascular complications of diabetes. *Clinical Diabetes*, 26(2); 77-82

33. Yagihashi, S., Mizukami, H., & Sugimoto, K. (2011) Mechanism of diabetic neuropathy: where are we now and where to go? *J Diabetes Investig.*, 2(1); 18-32

34. Dobretsov, M., Romanovsky, D., & Stimers, J.R. (2007) Early diabetic neuropathy: triggers and mechanisms. *World J Gastroenterol*, 13(2); 175-191

35. Tesfaye, S., & Selvarajah, D. (2012) Advances in the epidemiology, pathogenesis and management of diabetic peripheral neuropathy. *Diabetes Metab Res Rev*, 28(S1); 8-14

36. Center for Disease Control and Prevention (CDC). National Chronic Kidney Disease Fact Sheet: General Information and National Estimates on Chronic Kidney Disease in the United States, 2014. Atlanta, GA: US Dept. of Health and Human Services, CDC; 2014.

37. Taal, M.W., and Brenner, B.M.(2006) Kidney International - Predicting initiation and progression of chronic kidney disease: Developing renal risk scores. *Kidney International* (70), 1694-1705

38. Cao, Z., Cooper, M.E. (2011) Pathogenesis of diabetic nephropathy. *J Diabetes Investig.* 2(4); 243-247.

39. National Clinical Guideline Center (2014) NICE Clinical Guidelines, No.182, UK.

40. Holechek, M.J. (2003) Glomerular filtration: an overview. *Nephrol Nurs J*, 30(3); 285-90

41. Cooper, M.E. (1998) Pathogenesis, prevention, and treatment of diabetic nephropathy. *Lancet*, 352(9123); 213-9.

42. Pantsulaia,T.(2006)Role of TGF-β in pathogenesis of diabetic nephropathy. *Georgian Med News*, 131:13-18.

43. Gomes, K.B., Rodrigues, K.F., & Fernandes, A.P. (2014) The role of transforming growth factor-beta diabetic nephropathy. *International Journal of Medical Genetics*, 2014; 1-6.

44. Wang, X.H., & Mitch, W.E. (2014) Mechanisms of muscle wasting in chronic kidney disease. *Nat Rev Nephrol*, 10(9): 504-16

45. Serratric, G., Toga, M., Roux, H. et al. (1967) Neuropathies, myopathies and neuromyopathies in chronic uremic patients. *Presse Med*, 75; 1835-1838

46. Kaltsatou, A., Sakkas, G.K., Poulianiti, K.P., Koutedakis, Y., et al. (2015) Uremic myopathy: is oxidative stress implicated in muscle dysfunction in uremia. *Front Physiol*, 2015(6); 102.

47. Campistol, J.M. (2002) Uremic myopathy. *Kidney International*, 62(5); 1901-1913.

48. Chikotas, N., Gunderman, A., & Oman, T. (2006) Uremic syndrome and end-stage renal disease: physical manifestations and beyond. *J Am Acad Nurse Pract.*, 18(5); 195-202.

49. Fahal, I.H. (2014) Uraemic sacropenia: aetiology and implications. *Nephrol Dial Transplant*, 29(2): 1655-65. doi: 10.1093/ndt/gft070

50. Attaix, D., Combaret, L., Bechet, D., & Taillandier, D. (2008) Role of the ubiquitin-proteasome pathway in muscle atrophy in cachexia. *Curr Opin Support Palliat Care*, 2(4); 262-6.

51. Workeneh, B.T., & Mitch, W.E. (2010) Review of muscle wasting associated with chronic kidney disease. *Am J Clin Nutr*, 91(4): 1128S-1132S

52. Lecker, S.H., Jagoe, R.T., Gilbert, A., et al. (2004) Multiple types of skeletal muscle atrophy involve a common program of changes in gene expression. *FASEB*, 18(1): 39-51

53. Yokoi, H. & Yanagita, M. (2014) Decrease of muscle volume in chronic kidney disease: the role of mitochondria in skeletal muscle. *Kidney International*, 85: 1258-1260

54. Neirynck, N. Glorieux, G., Schepers, E., Dhondt, A., Verbeke, F., & Vanholder, R. (2015) Pro-inflammatory cytokines and leukocyte oxidative burst in chronic kidney disease: culprits or innocent bystanders. *Nephrol Dial Transplant*, 30(6); 943-51.

55. Remuzzi, G., Perico, N., Macia, M., & Ruggenenti, P. (2005) The role of renin-angiotensin-aldosterone system in the progression of chronic kidney disease. *Kidney Int Suppl*, 99: S57-65

56. Fogo, A.B. (2007) Mechanisms of progression of chronic kidney disease. *Pediatr Nephrol*, 22(12): 2011-2022

57. Rajan, V.R., & Mitch, W.E. (2008) Muscle wasting in chronic kidney disease: the role of the ubiquitin proteasome system and its clinical impact. *Pediatr Nephrol*, 23(4); 527-535.

58. Boivin, M.A., Battah, S.I., Dominic, E.A. et al. (201) Activation of caspase-3 in the skeletal muscle during haemodialysis. *Eur J Clin Invest*, 40(10): 903-10

59. Masiero, E. Agatea, L., Mammucari, C. et al. (2009) Autophagy is required to maintain muscle mass. *Cell Metab*, 10(6): 507-15

60. Johansen, T. & Lamark, T. (2011) Selective autophagy mediated by autophagic adapter proteins. *Autophagy*, 7(3): 279-96

61. Mammucari, C. Milan, G., & Romanello, V. et al. (2007) FoxO3 controls autophagy in skeletal muscle in vivo. *Cell Metab*, 6(6): 458-71

62. Hanna, R.A. Quinsay, M.N., Orogo, A.M. et al. (2012) Microtubule-associated protein 1 light chain 3 (LC3) interacts with Bnip3 protein to selectively remove endoplasmic reticulum and mitochondria via autophagy. *J Biol Chem*, 287(23): 19094-104

63. Sandri, M. (2013) Protein breakdown in muscle wasting: role of autophagy-lysosome and ubiquitin-proteasome. *Int J Biochem Cell Biol*, 45(10); 2121-2129.

64. Sridharan, S., Jain, K., & Basu, A. (2011) Regulation of autophagy by Kinases. *Cancers*, 3: 2630-2654

65. Balakrishnan, V.S., Rao, M., Menon, V. et al. (2010) Resistance training increases muscle mitochondrial biogenesis in patients with chronic kidney disease. *Clin J Am Soc Nephrol*, 5(6): 996-1002.

66. Bautista, J.E., Gil-Necija, J., Castill, I. et al. (1983) Dialysis myopathy: report of 13 cases. *Acta Neuropathol*, 61: 71-75

67. Gamboa, J.L., Billings, F.T., Bojanowski, M.T., Gilliam, L.A., et al. (2016) Mitochondrial dysfunction and oxidative stress in patients with chronic kidney disease. *Physiological Reports*, 4(9); e12780

68. Stenvinkel, P., Carrero, J.J., von Walden, F., Ikizler, T.A., & Nader, G.A. (2015) Muscle wasting in end-stage renal disease promulgates premature death: established, emerging and potential novel treatment strategies. *Nephrology Dialysis Transplantation*, 31(7); 1070-1077.

69. Lewis, M.I., Fournier, M. Wang, H. et al. (1985) Metabolic and morphometric profile of muscle fibers in chronic hemodialysis patients. *J Appl Physiol*, 112(1): 72-8

70. Yazdi, P.G., Moradi, H., Yang, J.Y., Wang, P.H., & Vaziri, N.D. (2013) Skeletal muscle mitochondrial depletion and dysfunction in chronic kidney disease, *Int J Clin Exp Med*, 6(7); 532-539

71. Yokoi, H., & Yanagita, M. (2014) Decrease of muscle volume in chronic kidney disease: the role of mitochondria in skeletal muscle, *Kidney International*, 86(6); 1258-1260.

72. Tamaki, M., Miyashita, K., Wakino, S. et al. (2014) Chronic kidney disease reduces muscle mitochondria and exercise endurance and its exacerbation by dietary protein through inactivation of pyruvate dehydrogenase. *Kidney Int*, 85: 1330-1339

73. Madhumathi, R., Bertrand, L., & Vaidyanathapuram, S. (2018) Chronic kidney disease and acquired mitochondrial myopathy. *Current Opinion in Nephrology and Hypertension*, 27(2); 113-120.

74. Lim, P.S., Ma, Y.S., Cheng, Y.M., et al. (2002) Mitochondrial DNA mutations and oxidative damage in skeletal muscle of patients with chronic uremia. *J Biomed Sci*, 9(6 Pt1): 549-60

75. Lim, P.S., Cheng, Y.M., & Wei, Y.H. (2000) Large-scale mitochondrial DNA deletions in skeletal muscle of patients with end-stage renal disease. *Free Radical Biology and Medicine*, 29(5): 454-463

76. Dayanidhi, S., & Lieber, R.L. (2014) Skeletal muscle satellite cells: mediators of muscle growth during development and implications for developmental disorders. *Muscle Nerve*, 50(5); 723-732.

77. Conboy, I.M., & Rando, T.A. (2002) The regulation of notch signaling controls satellite cell activation and cell fate determination in postnatal myogenesis. *Developmental Cell*, 3(2); 397-409

78. Mann, C.J., Perdiguero, E., Kharraz, Y., Aguilar, S., et al. (2011) Aberrant repair and fibrosis development in skeletal muscle. *Skeletal Muscle*, 2011; 1-21.

79. Zhang, L., Wang, X.H., Wang, H., Du, J., & Mitch, W.E. (2010) Satellite cell dysfunction and impaired IGF-1 signaling cause CKD-induced muscle atrophy. *J Am Soc Nephrol*, 21(3): 419-27.

80. Yoshida, T., Galvez, S., Tiwari, S., Rezk, B.M. et al. (2013) Angiotensin II inhibits satellite cell proliferation and prevents skeletal muscle regeneration. *The Journal of Biological Chemistry*, 288; 23823-23832.

81. Peter, A.K., Cheng, H., Ross, R.S., Knowlton, K.U., & Chen, J. (2011) The costamere bridges sarcomeres to the sarcolemma in striated muscle. *Prog Pediatr Cardiol*, 31(2): 83-88

82. Brooks, N.E., & Myburgh, K.H. (2014) Skeletal muscle wasting with disuse atrophy is multi-dimensional: the response and interaction of myonuclei, satellite cells and signaling pathways. *Front Physiol*, 2014, doi: https://doi.org/10.3389/fphys.2014.00099

83. Burd, N.A., & De Lisio, M. (2017) Skeletal muscle remodeling: interconnections between stem cells and protein turnover. *Exerc Sport Sci Rev*, 45(3); 187-191.

84. Brooks, N.E., & Myburgh, K.H. (2014) Skeletal muscle wasting with disuse atrophy is multi-dimensional: the response and interaction of myonuclei, satellite cells and signaling pathways. *Front Physiol*, 5;99.

85. Oberg, B.P, et al. (2004). Increased prevalence of oxidant stress and inflammation in patients

with moderate to severe chronic kidney disease. *Kidney Int* (65)3;1009-1016

86. Ikizler TA, et al. (2002) Hemodialysis stimulates muscle and whole body protein loss and alters substrate oxidation. *Am J Physiol Endocrinol Metab*. 282:E107–E116

Chapter 1

Progressive CKD in Type 2 Diabetes Impairs Skeletal Muscle Performance and Physical Function

Background

Over 29 million persons in the United States (~9%) have diabetes mellitus, with 90% exhibiting the obese type 2 phenotype (T2DM). Nearly two thirds of those with diabetes have or will develop chronic kidney disease (CKD) – an early complication of T2DM (**1**). CKD, or diabetic nephropathy, is characterized by a progressive and persistent decline in kidney function classified into 5 categorical stages according to the degree of renal filtration impairment, or renal filtration rate (**2**). Renal filtration rate, or glomerular filtration rate (GFR), is the volume of fluid filtered from the glomerular capillaries in the bowmans capsule of the kidney per unit time (minute) (**3).** The genesis of CKD and its progression in T2DM is thought to stem from the metabolic and hemodynamic abnormalities of T2DM. Specifically, a key causative factor identified is the accumulation of extracellular matrix of the renal glomerulus. Chronic hyperglycemia, among other factors including glycated albumin -AGEs, low-grade systemic inflammation, and excess glomerular capillary pressure and hypertrophy observed in T2DM, stimulates production of pro-fibrotic protein TGF-B in the glomerulus, where it localizes to podocytes – a key filtration-barrier support protein (**4**). Once localized, TGFB induces connective tissue growth factor (CTGF) and vascular endothelial growth factor (VEGF), and type 4 collagen production- the main components of the glomerular basement membrane, to ultimately result in renal fibrosis (**4,5**). This process promotes progressive basement membrane thickening, glomerular hypertrophy and ultimately declining renal filtration and degradation of the filtration barrier leading to proteinuria (**4**). Accordingly, CKD is divided into 5 stages characterized by decline in the rate of glomerular filtration, estimated from serum creatinine concentrations, as creatinine derives from creatine degradation, and is freely filtered by the kidney and not reabsorbed or metabolized there (**3).**

Given the pathophysiology of CKD in T2DM, its not surprising that those with T2DM exhibit a more rapid decline in kidney function above their age-matched counterparts. Indeed, in a 10-year prospective longitudinal study of 1682 participants with T2DM, and baseline eGFR >60 mL/min, the authors found between a 1 ("non-decliner") and 6 ("rapid decliner") mL/min annual decline in kidney function in those with T2DM (**2**). The authors also found that HbA1c (glycemic control), and diabetes duration and severity (ie. presence of peripheral neuropathy), were significant modifiers of the annual rate of decline (**2**). Other studies have supported a faster rate of renal decline in those with T2DM, ranging from 1 mL/min per year for those without proteinuria, to nearly 3 mL/min per year decline when proteinuria is present (**6**,**2**). These data all support the observations of a faster rate of kidney decline in those with T2DM, as non-diabetic individuals of similar age experience <1 mL/min annual decline (**7,8,9**). However, a key modifiable factor in the rate of renal decline in progressive CKD is physical activity and function. Evidence shows that among those in stage 4 CKD (eGFR 15-29 mL/min), those who reported no leisure time physical activity over a typical 4-week period, had an annual decline in kidney function of ~10%. This was contrasted by an annual decline in renal filtration of only 6% in those who reported meeting consensus guidelines for physical activity in the general population (150 minutes/wk) (**10**). However, despite the seeming renal-protective effect of physical activity, it is well established that in those in ESRD (stage 5 CKD – eGFR <15 mL/min), there is marked impairment in aerobic capacity and physical performance, and subsequent lower activity compared to healthy populations (**11**). Thus, the disease state may hinder physical mobility. This hindrance may stem from secondary impairments in muscle function, something often observed in advanced CKD.

CKD configures well to a geriatric syndrome model, specifically in its propensity to promote a frailty state. Frailty is commonly thought of as a complex phenotype of aging characterized by a

combination of objective and subjective findings such as slowed gait, physical inactivity, exhaustion or fatigue, muscle weakness and loss of muscle mass (**12**). Bao et al. found that 74% of those undergoing maintenance hemodialysis (end-stage renal disease - ESRD) were frail, and at 57% increased risk of death (**13**). Similarly, in the Canadian Frailty Observation and Interventions Trial (CanFIT), examining 600 advanced stage CKD participants (stage 4-5, pre-dialysis) over a 2 year period, 56% of individuals exhibited reduced physical function (assessed with short physical performance battery), and 8-times higher risk of physical frailty (**14**). This frailty state and impaired physical function may stem from uremia-induced muscle dysfunctions, collectively referred to as uremic myopathy.

Uremic myopathy was first described by Serratric et al. (1967), in a group of patients with chronic renal failure (ESRD) and progressive proximal muscle weakness caused by an intrinsic disorder of muscle function (**15**). Presently, though often debated, uremic myopathy – a collection of functional and structural muscle abnormalities in patients with CKD – is considered to be a consequence of the uremic state itself (**16,17**). The uremic state is a term used to describe the excess metabolic bi-products (ie. urea, creatinine, etc.) in the blood that, due to the declining filtration capacity of CKD, are no longer filtered by the kidneys and excreted in the urine, most often associated with ESRD (stage 5 CKD) (**18**). Urea, a nitrogenous end-product of protein and amino acid catabolism, is produced by the liver and distributed throughout intra- and extracellular fluid, and filtered out of circulation by glomeruli. This rise in blood urea concentration in CKD is due to a disequilibrium between the rate of amino acid incorporation into skeletal muscle, rate of amino acid release from tissue and muscle breakdown, and the capacity of the liver to form urea from these amino acids (**19**). Urea is of critical importance in the implicated pathophysiology of uremic myopathy, as elevated urea concentrations are known to disrupt proteins, and are frequently used in

biochemical preparations to denature them (**20**). In fact, increasing urea concentrations have been shown to alter tertiary structure of skeletal muscle myosin by selectively targeting its globular catalytic domain, specifically interfering with protein structure to alter ATP-binding and cross-bridge cycling that drives muscle contraction (**20**). However, this has been demonstrated in a laboratory setting in-vitro, and the precise mechanisms that drive uremic myopathy and muscle impairment in CKD remain unknown.

While the physiological basis for uremic myopathy remains poorly understood, the clinical manifestation has been readily documented. Liu et al. (**21**) examined lower extremity function in community-dwelling elderly, with eGFR <60 mL/min with or without CKD, and found that those with CKD-induced kidney deficits had greater decline in walking speed over a 6.5 year observation period compared to non-CKD. Similarly, those with CKD were 55% more likely to have self-reported dependence in walking or climbing stairs compared to their non-CKD counterparts (**21**). Additionally, Roshanravan et al. studied 385 participants with mean eGFR of 41 mL/min (stage 3 CKD) with or without CKD, and assessed lower extremity physical performance via timed-up-and-go (TUG), 4-minute walk distance, 6-min walk distance, and grip strength (**22**). While upper extremity function was preserved, performance on lower extremity functional tasks – such as gait speed, TUG, and 6-minute walk distance, were at least 30% impaired in those with CKD compared to non-CKD (**22**). To compound the findings of impaired functional mobility in CKD, this functional deficit translates into a significantly elevated risk of death in those with CKD. Indeed, lower extremity performance measures have been shown to be stronger predictors of mortality than kidney function in those with CKD (both those in ESRD and those pre-dialysis) (**22**). A small, .1 m/second drop in gait speed increases the risk of death by 26%, while a 1-second increase in timed-up-and-go time is associated with 8% greater risk of death (**22**). Thus, CKD, even prior to ESRD, negatively

affect functional performance, that subsequently increases risk for mortality and disease progression, and this may be due to the CKD-related metabolic and systems affects on skeletal muscle health and function, though this remains unknown. Similarly, while the vast majority of research has been devoted to advanced or progressed CKD on physical function and mortality risk, some studies, as mentioned previously, have demonstrated impairments in function in earlier CKD. However, these findings are largely in respect to matched controls without CKD. Given that progression of uremic myopathy runs parallel to the decline in renal function (**17**), and other studies reporting a mere 14% prevalence of frailty in those with earlier stages of CKD (contrasted with reports of 74% of frailty in those undergoing hemodialysis in ESRD)(**12**), there is a need to investigate the relationship between CKD progression and muscle performance decrements and physical mobility impairments across stages of CKD in those with T2DM. Thus, the purpose of this study is to determine the relationship between CKD progression (ie. stage of CKD, and eGFR decline) and muscle performance and physical function, and to investigate the contribution and predictive value of uremia, and CKD-predisposing factors (glycemic control, severity and duration of diabetes) to these measures in those with T2DM.

Methods and Procedures

Participants

Ninety five subjects participated in this study – 80 with diagnosed T2DM and peripheral neuropathy (PN), and 15 without evidence of PN. Participants of each categorical stage of CKD progression were – n = 21 in stage 1 CKD (16 male, 5 female), n=25 in stage 2 CKD (16 male, 9 female), n=24 in stage 3 CKD (15 male, 9 female), and n=20 in pre-dialysis stages 4&5 combined (15 male, 5 female). The groups were matched for diabetes severity (based on the presence of PN), BMI, and

duration of T2DM (TABLE 1). Participants were recruited from the Washington University School of Medicine Diabetes Clinic, Washington University's Volunteers for Health, the Center for Community Based Research, the Washington University Medical School Renal Clinic, and from the surrounding St. Louis community. Study inclusion criteria included individuals with BMI >27 kg/m^2, with diagnosis of diabetes mellitus and diabetes-induced CKD (diabetic nephropathy), with or without evidence of peripheral neuropathy. DM status was based on clinical report of a diagnosis of DM from a physician, confirmation of medication usage for DM (insulin, oral hypoglycemic agents or both) and verification of HbA1c levels either currently or at the time of diagnosis >6.5%. Participants were excluded from the study if they weighed more than 300 pounds (equipment weight limit), presented with any illness or hospitalization within the last 6 months, had any infection or ulceration of either foot, had prior botulinum toxin injections, severe foot deformity or amputation, or any co-morbidity (ie. rheumatic disease, peripheral arterial disease, dialysis, current cancer treatment, acute coronary syndrome, heart failure requiring medication, anemia, uncontrolled proliferative retinopathy) or medication that would limit participant on physical activity testing. Each participant read and signed an IRB-approved protocol and informed consent that was approved by the Human Research Protection Office at Washington University in St. Louis, MO.

CKD Staging (eGFR)

CKD staging was performed using serum creatinine concentrations. Serum creatinine was measured with a standardized assay, and used to estimate glomerular filtration rate (eGFR) - computed based on the Chronic Kidney Disease Epidemiology Collaboration equation and was classified into 5 categories: eGFR $\geq$ 90 mL/min per 1.73 m^2 (stage 1 CKD), 60-90 mL/min (stage 2 CKD), 30-60 mL/min (stage 3 CKD), 15-30 mL/min (stage 4 CKD), <15 mL/min (stage 5 CKD) with no kidney transplant or dialysis.

Laboratory Measures

Laboratory measures including serum creatinine (mg/dl) as above, blood-urea nitrogen - BUN (mg/dl), HbA1c (%)

Participant Demographics-

Participants age, duration of T2DM, weight, height, and BMI (calculated as weight in kg divided by the square of height in meteres, used to define obesity) were collected through participant interview, weight balance, and stadiometer, respectively at the initial visit, prior to any dynamometry or physical performance testing.

Neuropathy Assessment-

Determined by the presence of either diminished or absent plantar sensation to light touch or pressure or vibration perception threshold. Lower extremity sensation was assessed via biothesiometry and semmes Weinstein monofilament testing. Neuropathy was defined clinically as the inability to feel the 5.07 (10 gram) monofilament on at least one non-callused site on the plantar aspect of either foot or the inability to perceive vibration <25 volts on the biothesiometer (Biomedical Instrument, Newbury, OH, USA) applied to the hallux (**23**).

Physical Function –

Functional physical performance was assessed using the 9-item modified physical performance test (PPT). The PPT is a timed observational assessment of performance on nine daily physical activities including: 5 consecutive sit-to-stand transfers without arm assistance, climbing a flight of stairs with 10 steps, a 50-ft. walk test, turning 360 degrees, picking up a coin from the floor, donning/doffing a jacket, lifting a 7-lb book onto an overhead shelf, a Romberg standing balance assessment with eyes

open, and ability to ascend 4 flights of stairs (**23**). Each item is scored from 0-4 based on the time taken to complete each task, with a maximum score of 36 (higher scores indicate better physical function/performance). Each task is performed twice with the average time used to score the task. Interrater reliability, validity with other functional assessments, and predictive validity of lack of independence and mortality have all been well established for the mPPT (**24,25,26,27**). The mPPT possesses a test-retest reliability of .964, while individual sub-items have reliability ranging from .51-.99, and Cronbach alpha of .785 (**25,26**).

Stair Vertical Power-

Stair vertical power was calculated from the stair-climbing component of the PPT, using the equation as previously described (**23**)

Stair Power = [(weight in Kg)(9.8)(1.95)] / (avg. stair climb time in seconds)

1.95 → cumulative height of the 10 steps (each step is 19.5 cm)

Muscle Performance Assessment-

Maximal isokinetic torque was measured at 60 deg/sec and 180 deg/sec for knee extension, using a Biodex System 3 Isokinetic Dynamometer (Shirley, NY, USA). Each isokinetic movement was repeated three times, with the average of the three trials used in the final analysis. Additionally, isometric peak knee extensor torque was measured at optimal quadriceps sarcomere length (knee flexion angle of 60^0) and averaged from 3 repetitions, each held maximally for 5 seconds.

Physical Frailty Classification –

Physical frailty was classified as described previously (**26**). Briefly, from the PPT scoring, a score <29 point indicates moderate physical frailty, as scores less than 30 are functionally below the 75^{th}

percentile of community dwelling older adults, and scores less than or equal to 21 indicates function below the 25th percentile (**25**). Thus, frailty was subsequently classified based on PPT score as – mild/no frailty (PPT=30-36), moderate frailty (PPT=22-29), and severe frailty (PPT=21 or less).

Statistical Analysis -

Pearson Chi-square test for equality of proportions was used to determine the homogeneity of sex distribution, and neuropathy status between CKD-staged groups (stage 1, stage 2, stage 3, and stage4&5). CKD-group differences in PPT score, PPT sub-item measures, muscle performance measures, and stair power, were analyzed using 1-way ANOVAs and analysis of covariance (ANCOVA) to control for potential covariate confounders. Post-hoc testing for CKD-staged group differences was determined using Tukey's HSD or Games-Howell in the event of a violation of homogeneity of variance. Bivariate pearson correlation coefficients were used to assess relationships between eGFR and the aforementioned measures, including lab measures. All analyses were evaluated at an alpha level set at .05.

Forced entry multiple regressions were used to predict **1**. 9-item PPT score using predictors – group status (using stage 1 CKD as reference), HbA1c, age, BMI, and duration of diabetes (years). **2**. 9-item PPT score using eGFR and the same predictors as model 1. **3**. 9-item PPT score using predictors – BUN, HbA1c, age, duration of diabetes, and BMI. **4**. Stair power using predictors – group status (using stage 1 CKD as reference), eGFR, BUN, HbA1c, age, duration of diabetes, BMI. Overall model fit was assessed using the Hosmer-Lemeshow goodness of fit test, and the potency of the model was determined using Nagelkerke's Pseudo R^2. All statistical analyses were performed in IBM SPSS Version 21 (Armonk, NY: IBM Corp).

Results

Group Demographics-

As shown in Table 1, there were no group differences in gender composition, PN status, BMI, or duration of diabetes. Groups did differ with respect to HbA1c, and age. For this reason, subsequent analyses for CKD-stage-based differences were performed with ANCOVA, adjusting for the covariates of age and HbA1c. Additionally, these variable were included in multiple regression analyses to ensure statistical control when analyzing for CKD progression contributions to functional declines.

Muscle Performance-

eGFR was significantly positively correlated with knee extensor torque production (60^0/sec – r=.523, p<.001/ and 180^0/sec – r=.5, p<.001), and knee extensor isometric strength (r=.49, p<.001) (Table 2). As shown in Figure 1, there was a significant step-wise decline in muscle performance of the lower extremity with progression of CKD. Specifically, those in stage 3 exhibit a 33% decline in knee extensor torque at 60^0/sec, and 40% decline at 180^0/sec (p=.001), while those in stages 4/5 exhibit a 43% and 50% decline respectively (p<.001). Similar relationships were demonstrated in isometric force production of the knee extensors (23% decline from stage 1 to 3, p=.05, 41% decline in stage 4/5, p<.001) (Figure 1). These declines in muscle performance across CKD stages persist, even after controlling for age, and HbA1c (knee extensor isometric torque – p=.004, knee extensor torque 180^0/sec – p=.003, knee extensor torque 60^0/sec – p=.006). There was no significant different in muscle performance between stages 1 and 2 CKD. Interestingly, muscle performance was negatively correlated with serum BUN concentration (Table 2).

Physical Function-

As shown in Table 2, eGFR was significantly negatively correlated with 50-ft walk time (lower time = faster gait speed) (r=-.434, p<.001), and time to climb 1 flight of stairs (r=-.3, p=.005). eGFR was, however, positively correlated with stair power (r=.482, p<.001), and PPT score (r=.43, p<.001). As shown in Figure 2, there is a significant decline in PPT score across stages of CKD, however, this is not significant until reaching stage 3 CKD, even after adjusting for age, and HbA1c (p=.05). Similarly, there is significant reduction in gait speed from stage 1 to stages 3 and 4 and 5, even after controlling for age and HbA1c (Figure 2**)**. However, there is significant step-wise decline in functional stair power (watts), from stage 1 to stage 2 (p=.03), stage 1 to stage 3 (p=.009), and from stage 1 to stages 4 and 5 (p<.001) (Figure 2). Additionally, similar to its relationship to muscle performance, serum BUN concentrations were significantly positively correlated to 50-ft walk time (r=.471, p<.001), time to climb 1 flight of stairs (r=.39, p<.001). However, BUN was negatively correlated with stair power (r=-.342, p=.001), PPT score (r=-.48, p<.001). Additionally, those in stages 3 and 4 exhibited significantly higher frequency (Fishers exact, p=.018) of frailty (both moderate frailty and severe frailty) than those in stages 1 and 2, and those in stage 4 exhibited significantly fewer than expected individuals without frailty.

However, the predictive value of kidney decline in muscle performance and functional impairment requires predictive regression modeling.

Multiple Linear Regression-

Model 1 (predicting PPT score from CKD stage, HbA1c, age, BMI, and duration of diabetes). Using these predictors, the model accounted for nearly 50% of the variance in PPT score in this population (p<.001). Even after accounting for age, BMI, HbA1c (glycemic control), and

duration of T2DM, CKD stage was a significant negative predictor of PPT score, with those in later stages (4 or 5) exhibiting a striking ~6 point decline in physical function scores ($p<.001$). (Table 3)

Model 2 (9-item PPT score from eGFR, HbA1c, age, BMI, and duration of diabetes). Using these predictors, the resultant model accounts for 43% of the variance in physical function score ($p<.001$). eGFR, even after controlling for HbA1c, age, duration of diabetes, and BMI, is a significant positive predictor of PPT score ($p=.005$). (Table 3)

Model 3 (9-item PPT score from BUN, HbA1c, age, duration of diabetes, and BMI). Using this combination of predictors, which accounted for 48% of the variance in PPT score, BUN is a significant negative predictor of physical function, even after controlling for potential confounding factors ($p<.001$). Specifically, for every 10 mg/dL increase in BUN, PPT score declines nearly 2 points (Table 3).

Model 4 (Stair power from CKD stage - using stage 1 CKD as reference, eGFR, BUN, HbA1c, age, duration of diabetes, BMI). This model accounted for 33% of the variance in stair power ($p<.001$), and when accounting for glycemic control, age, duration of diabetes, and BMI, CKD stage was a significant negative predictor of stair power, where stage 3 and stages 4 and 5, significantly negatively predict functional stair performance ($p=.04$, and $p=.001$ respectively). (Table 3)

Discussion

Lower extremity muscle performance plays an essential role in mobility, as sufficient strength of the knee extensors is a requisite for optimal performance of weight-bearing tasks (**27).** Indeed, in other chronic conditions, progressive weakness of the quadriceps muscles constitute an early clinical finding, subsequently followed by decline in functional abilities, and loss of ambulation (**27)**.

Moreover, disability in CKD may be associated more with muscle strength than muscle mass, as recent studies in patients undergoing hemodialysis report poorer muscle function than matched controls for a given muscle mass (**28).** While we did not assess muscle mass, our findings support this notion, and demonstrate across the spectrum of CKD severity. Specifically, eGFR was significantly positively correlated with muscle performance of the quadriceps (r=.49 knee extensor isometric torque, r=.52 knee extensor torque 60 deg/sec, r=.5 knee extensor torque 180 deg/sec), a key mobility-dictating lower extremity muscle group. Predictably, muscle performance of the knee extensors exhibits moderate to strong correlations with functional performance, from gait speed, to stair climbing, and functional battery test scores (PPT). Moreover, when analyzed by CKD stage, muscle performance decrements become significant when considering differences between early CKD (stages 1 and 2), middle (stage 3), and late (stages 4 and 5) stages. Specifically, stage 3 CKD marks the earliest stage where muscle performance declines to a significant extent compared to early CKD (30-40% decline in torque production, p=.001). This is exacerbated by CKD progression to later stages. These findings are supported by other studies demonstrating performance deficits at stage 3 CKD and beyond (**21, 22**). Although conducted in a different population, the Heart and Soul Study (average age 67, n=1,024) found that those with eGFR <60 mL/min (stage 3+) had 6x higher odds of possessing exercise capacity below 5 metabolic equivalents (METS), a level constituting only moderate-level daily activity similar to, for instance, raking leaves or easy swimming (**29**). Moreover, exercise capacity was graded - with lower eGFR associated with worsening activity capacity. The investigators theorized this was secondary to poor muscle performance and strength that increased the physiological and metabolic cost of such activity (**29,30).** Similarly, the Health Aging and Body Composition study observed significant reductions in grip strength in those with eGFR <60 mL/min (**31**). Thus, it becomes apparent that CKD progression upon reaching stage 3

seems to surpass a threshold whereby muscle performance decrements become significantly negatively impacted. This is of critical importance, as it is well established that declining physical performance may signal a high-risk state, even before overt disease-specific thresholds have been crossed (**32).** Much work has been conducted to dissect the mechanisms that drive these muscle performance decrements in CKD, mostly in the ESRD and late-stage CKD population. A large portion of this work has been dedicated to the network of atrophy signals that lead to protein-energy wasting in skeletal muscle (**33,34,35**).

Loss of lean mass secondary to CKD is termed CKD-cachexia and appears clinically as an accelerated form of sarcopenia (**36)**. It has been theorized, among other potential causes, that uremic toxins, like urea, creatinine, etc. that accumulate in the circulation with impaired renal filtration, contributes to metabolic acidosis – a condition that increases expression of ubiquitin mRNA and key 19S subunits of the proteasome that degrade contractile muscle proteins (**34**,**17**). This may predictably lead to loss of muscle mass, quality, and performance. This is supported, in part, by our findings that BUN is not only significantly negatively correlated with muscle performance (r=-.32-(-.37)), but also with physical function (gait speed, stair climbing capacity, whole-body functional battery scores). BUN was a significant negative predictor of PPT scores (B=-.169, p<.001) and accounts for 24% of its variance (when controlling for potential confounding factors, model 3). However, despite the potentially harmful signaling cascades exerted upon skeletal muscle in CKD, the Singapore Longitudinal Aging Study of 1,315 community-dwelling older adults, found that eGFR was not predictive of muscle or functional performance limitations (**37)**. Given that muscle homeostasis is complex and depends on hormonal, immunologic factors, and muscle stem cell function, this balance may be adversely or differentially affected by different pathomechanisms driving kidney decline. Diabetic nephropathy (diabetes-induced CKD) is accompanied by a litany of

metabolic complications such as insulin-like growth factor 1 resistance, not observed to the same extent with aging-induced CKD, excess inflammation, dietary and nutrient metabolism deficits, and excess angiotensin 2 production above that observed in aging-induced CKD. Angiotensin 2, though not measured in this study, also promotes inflammation (upregulating TNF-a, IL-6, NFK-B) and interferes with insulin signaling that promotes muscle degradation (**38,39,34**,**36)**. Hence, diabetic nephropathy progression, as shown in this study, significantly predicts muscle performance where other aging-induced models may not. This may, perhaps, be due to the metabolic environment and unique factors that challenge muscle homeostasis differently than simple aging-induced kidney changes. However, aside from significant impairments in muscle performance, perhaps of greater clinical significance, are the apparent deficits in functional mobility with CKD progression.

Those in stage 3 CKD exhibit, on average, a 4.5 point deficit in PPT functional scores, while those in later stages of disease experience a ~10 point drop, and these are both significant (p=.05, p=.001 respectively). However, while there appears to be a trend, there are not significant differences between stage 3 and stages 4 and 5 CKD with respect to any functional or muscle performance measures. This may indicate that underlying skeletal muscle pathology is present as early as stage 3 and already significantly affects muscle performance and subsequent function, and further progression of CKD beyond this point imparts more subtle progressive deficits. Additionally, even when accounting for glycemic control (HbA1c), age, duration of diabetes, and BMI, eGFR is a significant predictor of PPT score (B=.062, p=.005), and accounts for 10% of its variance. Given previous research that establishes the clinically significant decline threshold for PPT score at 2.4, this indicates that a ~39 mL/min drop in eGFR results in clinically meaningful declines in functional capacity (**27**). Given our results, when applied to the standard delineations for CKD stage, theoretically if an individual in stage 1 CKD (90 mL/min) were considered with our model, and

experiences a 39 point decline in eGFR, this would put them in stage 3 CKD (eGFR=52 mL/min) and would be predicted to exhibit a significant decline in functional capacity (PPT score). Such functional performance decrements may result in profound impairments in exercise capacity, engagement in physical activity, and ability to complete key activities of daily living (ADL). Indeed, in agreement with our results, in a study of aging-associated CKD in the United Kingdom (13,179 participants), the authors report a parallel in functional impairment deficits with CKD progression, as those with eGFR <30 mL/min had a 2.2x higher odds of impairment in ADLs, while those with eGFR 30-44 mL/min exhibit a 1.6x higher odds of impairment, compared to those with eGFR >60 mL/min (**40)**. However, aside from decrements in a battery of functional measures, specific sub-items of the PPT also emerged with significant differences between CKD stages.

Slow gait is a robust biomarker of health, and a predictor of functional decline and death in older adults. In this study, there were step-wise significant increases in 50-ft walk time (slower gait speeds) across all stages of CKD, when compared to stage 1 (stage 2-p=.04, stage 3-p=.004, stages 4&5-p=.001). This is also in agreement with the findings of the Health Aging and Body Composition study that measured 400 meter walk times, and lower extremity performance in a large cohort of 3,075 people, and found that those with eGFR <60 mL/min, took 20 seconds longer to complete the 400 meter walk (**31)**. While the mechanistic underpinnings of slowed gait in CKD progression may stem from aforementioned muscle impairments, the Baltimore Longitudinal Study of Aging assessed energetic cost of walking over a 7-year period with portable indirect calorimetry and tracked its longitudinal association with 6-meter gait speed (**41)**. Not surprisingly, increased energetic cost of walking significantly predicted rate of gait speed decline, as increased energetic cost of walking had an associated 57% greater risk of developing slowed gait (**41)**. While not conducted in a CKD population, the focus of the Baltimore Study investigation carries implications

for CKD progression and skeletal muscle energetics. Mitochondria serve as the muscle's main energy-generating system (**42**), and studies have shown low concentrations of aerobic enzymes, mitochondrial inclusions (damaged mitochondria), and impaired electron transport in muscle mitochondria of an ESRD rodent model (**42,43,17,44**). However, in light of our results, the implications that mitochondrial dysfunction may increase the metabolic cost of simple activities such as walking, and may even present earlier than ESRD to reduce gait speeds and impair skeletal muscle, are intriguing and warrant further study.

The ability to climb stairs strongly correlates with other measures of functional disability and decline in medical status (**45**). Our previous work has demonstrated that along the continuum of metabolic and morphological impairments in those with type 2 diabetes alone, individuals who produce less than 441 watts of power while ascending stairs are very likely to be in a sarcopenic state (**46**). In this study, while those in stage 1 CKD exhibit only slight reduction in stair power from this cutoff (~411 watts), those in stages 3, 4 and 5, exhibit drastic deficits in stair power capacity (278 and 193 watts respectively). Although not conducted in a CKD population, Shimada and colleagues (**47**) found that among older community dwelling adults (avg. age of 80), leg extensor power of 484 watts differentiated those who reported difficulty with ascending stairs from those who did not (<484 watts equated with self-reported difficulty). In this respect, our results lend support to the notion that CKD represents an accelerated geriatric syndrome model, and may promote a sarcopenic process. Interestingly, our results also suggest that this geriatric, and potentially sarcopenic, state is imparted as early as stage 3 CKD. This is further supported by the BUN results from model 3. BUN, as mentioned prior, may serve as a potent atrophy-inducing agent (**48,49**). Given the results of model 3, possessing an elevated BUN ($\geq$20 mg/dL) translates into a significant (3+ point) decline in PPT score (**27**). This once again, coincides with our findings that functional and

muscle-specific performance is impaired upon reaching stage 3 CKD. This may be due, in part, to BUN elevations exceeding a threshold at stage 3, that negatively affects function and skeletal muscle. For instance, the average BUN in stage 2 CKD was within normal limits (~19 mg/dL), however, BUN was substantially elevated in stage 3 CKD (32 mg/dL). However, the specific underlying mechanisms behind this relationship require further study.

Conclusion

The findings of this study demonstrate that muscle performance of the lower extremity and physical function decline in-parallel with progression of CKD in T2DM, with these declines becoming clinically evident in stage 3. CKD-associated metabolic bi-products, like BUN was a significant negative predictor of functional mobility, and those in stage 3+ CKD demonstrate functional deficits that reflect a pre-mature geriatric state. The mechanistic causes that drive skeletal muscle impairments in CKD progression remains to be determined, but given the functional deficits observed relatively early in disease progression, such mechanistic studies should be devoted to exploring stage-related changes in muscle health across the full spectrum of CKD in T2DM.

Tables for Chapter 1:

Table 1 (Demographics)

	Stage 1 CKD (n=21)	Stage 2 CKD (n=25)	Stage 3 CKD (n=24)	Stage 4&5 CKD (n=20)	p
Age	48 (10)	59 (9)	60 (9)	59 (10)	*p<.001 ^(p=.001) +(p<.001) #(p=.001)
Gender					
Male	16	16	15	15	p=.7
Female	5	9	9	5	
BMI	33 (5.6)	32 (5.3)	33 (5)	33 (7)	p=.85
Duration of Diabetes (years)	15 (13)	13 (11)	15 (7)	21 (11)	p=.07
Glycemic Control (HbA1c %)	9.3 (2)	7.9 (1.6)	7.8 (1.4)	7.6 (1.8)	*p=.011 ^(p=.022) +(p=.026) #(p=.047)
Peripheral Neuropathy (Yes, No)	20,1	19,6	20,4	16,4	p=.35

Table 1: Demographics. * denotes significant F-test indicating difference between groups. The following symbols represent post-hoc pairwise comparisons: ^ (between CKD stage 1 and 4&5), $^{+}$ (between CKD stage 1 and 3), #(between stage 1 and 2), ɜ (between CKD stage 3 and 4&5), δ (between CKD stage 2 and 3)

Table 2 (correlations)

	eGFR	Knee Extensor Isometric Torque (ft-lbs)	Knee Extensor Torque (60^0/sec)	Knee Extensor Torque (180^0/sec)	BUN	50-ft walk time	Time to climb 1 flight of stairs	Stair Power (watts)	PPT Score
eGFR	r=1 p=----	r=.49 p<.001	r=.52 p<.001	r=.504 p<.001	r=-.77 p<.001	r=-.43 p<.001	r=-.3 p=.005	r=.48 p<.001	r=.43 p<.001
Knee Extensor Isometric Torque (ft-lbs)	r=.49 p<.001	r=1 p=----	r=.88 p<.001	r=.78 p<.001	r=-.32 p=.003	r=-.53 p<.001	r=-.40 p<.001	r=.60 p<.001	r=.54 p<.001
Knee Extensor Torque (60^0/sec)	r=.52 p<.001	r=.88 p<.001	r=1 p=----	r=.91 p<.001	r=-.34 p=.002	r=-.67 p<.001	r=-.50 p<.001	r=.68 p<.001	r=.61 p<.001
Knee Extensor Torque (180^0/sec)	r=.50 p<.001	r=.78 p<.001	r=.91 p<.001	r=1 p=----	r=-.37 p=.001	r=-.65 p<.001	r=-.5 p<.001	r=.69 p<.001	r=.60 p<.001
BUN	r=-.77 p<.001	r=-.32 p=.003	r=-.34 p=.002	r=-.37 p=.001	r=1 p=----	r=.47 p<.001	r=.39 p<.001	r=-.34 p=.001	r=-.50 p<.001
50-ft walk time	r=-.43 p<.001	r=-.53 p<.001	r=-.67 p<.001	r=-.65 p<.001	r=.47 p<.001	r=1 p=----	r=.84 p<.001	r=-.69 p<.001	r=-.85 p<.001
Time to climb 1 flight of stairs	r=-.30 p=.005	r=-.40 p<.001	r=-.50 p<.001	r=-.50 p<.001	r=.39 p<.001	r=.84 p<.001	r=1 p=----	r=-.71 p<.001	r=-.75 p<.001
Stair Power (watts)	r=.48 p<.001	r=.60 p<.001	r=.68 p<.001	r=.69 p<.001	r=-.34 p=.001	r=-.69 p<.001	r=-.71 p<.001	r=1 p=----	r=.66 p<.001
PPT Score	r=.43 p<.001	r=.54 p<.001	r=.61 p<.001	r=.60 p<.001	r=-.50 p<.001	r=-.85 p<.001	r=-.75 p<.001	r=.66 p<.001	r=1 p=----

TABLE 2- Bivariate pearson correlation coefficients were calculated between measures of physical function (PPT score, Stair power, stair climb time, 50-ft walk time), muscle performance (Knee extensor torque – 180^0/sec, 120^0/sec, isometric), and serum chemistries (eGFR, BUN). Inset within each block is the r-value correlation coefficient between the two correlated variables (row vs. column), with the corresponding p-value. Color coding is as follows

r= (-.25)-(-.5), r=(-.5)-(-.75), r=(-.75)-(-1) , r=.25-.5, r=.5-.75, r=.75-1

Table 3 (models)

Model 1 predicting PPT score

Model	Unstandardized Coefficients		Standardized Coefficients		
	B	Std. Error	Beta	t	Sig.
Constant	61.9	6.9		8.98	.000
HbA1c	-.56	.38	-.14	-1.5	.144
BMI	-.33	.11	-.26	-2.97	.004
Duration of Diabetes (yrs)	-.046	.06	-.07	-.74	.46
Age	-.330	.071	-.485	-4.644	.000
CKD stage 2	-.020	1.940	-.001	-.010	.992
CKD stage 3	-1.259	1.990	-.077	-.633	.529
CKD stage 4&5	-5.599	2.126	-.317	-2.633	.010

Model Significance → F=8.8, p<.001
Nagelkerke R^2 = .45

Model 2 predicting PPT score

Model	Unstandardized Coefficients		Standardized Coefficients		
	B	Std. Error	Beta	t	Sig.
Constant	56.516	7.278		7.765	.000
HbA1c	-.647	.379	-.162	-1.708	.092
Age	-.296	.068	-.434	-4.335	.000
eGFR	.062	.022	.286	2.889	.005
Duration of Diabetes (yrs)	-.072	.060	-.108	-1.196	.235
BMI	-.355	.111	-.283	-3.203	.002

Model Significance → F=11.8, p<.001
Nagelkerke R^2 = .43
eGFR accounts for 10% of the variance in PPT in this model (get this by squaring the partial correlations)

Model 3 predicting PPT from BUN

Model	Unstandardized Coefficients		Standardized Coefficients		
	B	Std. Error	Beta	t	Sig.
(Constant)	64.305	6.712		9.581	.000
HbA1c	-.743	.373	-.181	-1.991	.050
Age	-.331	.063	-.469	-5.252	.000
Duration of Diabetes (yrs)	.008	.060	.012	.132	.895
BMI	-.277	.108	-.215	-2.572	.012
BUN	-.169	.034	-.444	-4.940	.000

Model Significance → F=14.8, p<.001
Nagelkerke R^2 = .48
BUN accounts for 24% of the variance in PPT score in this model

Model 4 predicting stair power from CKD stage

Model	Unstandardized Coefficients		Standardized Coefficients		
	B	Std. Error	Beta	t	Sig.
(Constant)	616.301	162.615		3.790	.000
HbA1c	-9.064	8.894	-.110	-1.019	.311
Age	-4.582	1.654	-.323	-2.769	.007
Years of diabetes	.573	1.433	.042	.400	.690
BMI	2.934	2.588	.112	1.134	.261
CKD stage 2	-78.438	44.753	-.233	-1.753	.084
CKD stage 3	-96.414	46.242	-.282	-2.085	.041
CKD stage 4&5	-178.958	49.605	-.479	-3.608	.001

Model Significance → F=5.2, p<.001
Nagelkerke R^2 = .33
Total of 25% of variance in stair power is accounted for by CKD stage

TABLE 3
Linear regression model to determine 9-item PPT score (models 1-3) from various combinations of predictor variables, and a linear regression model to predict stair power from different predictors. Beta coefficients for each predictor represent change in PPT score or stair power, due to disease status or 1 unit change in the respective predictor. Model significance, amount of variance in 9-item PPT score or stair power, explained by the model (R^2), and amount of variance in PPT or stair power, explained by each predictor are shown in the bottom panel. *UPPER LEFT* – **Model 1**. Predicting PPT score from HbA1c (glycemic control), BMI, duration of diabetes, age, and CKD stage (stage 1 is reference). 45% of the variance in PPT is explained by this model, with age, BMI, and CKD stage being significant negative predictors of PPT score (all $p<.05$). *UPPER RIGHT* – **Model 2.** Predicting PPT score from HbA1c (glycemic control), age, renal filtration rate (eGFR), duration of diabetes, and BMI. 43% of the variance in PPT is explained by this model, with age and BMI being significant negative predictors and eGFR being a significant positive predictor of PPT score (all $p<.05$). Note- shown below, eGFR accounts for 10% of the variance in PPT score. *LOWER LEFT* – **Model 3.** Predicting PPT score from HbA1c (glycemic control), age, duration of diabetes, BMI, and serum BUN. 48% of the variance in PPT is explained by this model, with age, BMI, and BUN being significant negative predictors of PPT

score (all $p<.05$). Note- shown below, BUN accounts for a surprising 24% of the variance in PPT score. *LOWER RIGHT* – **Model 4.** Predicting stair power (watts), from HbA1c, age, duration of diabetes, BMI, and CKD-stage (CKD stage 1 is reference). This model accounts for 33% of the variance in stair power, with CKD-stage and age being significant negative predictors of stair power.

Figures for Chapter 1:

Figure 1 (muscle performance)

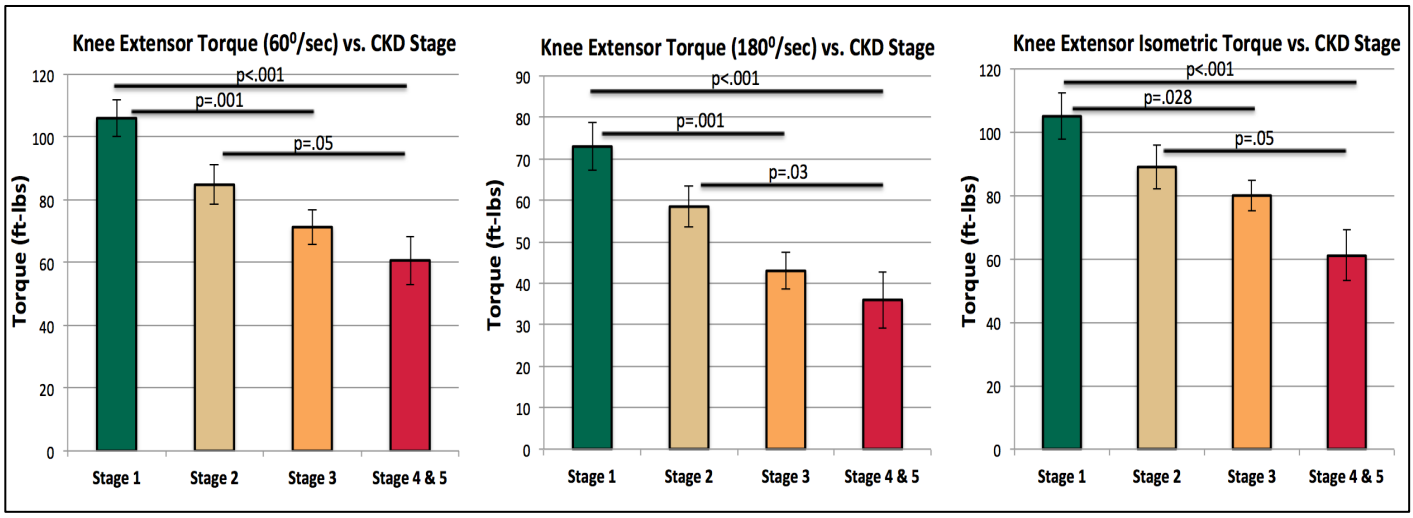

Figure 1. Lower extremity muscle strength (knee extensor peak torque, and isometric torque) was assessed across CKD-stage groups with 1-way ANOVAs. Bar heights indicate group means, with error bars indicating ± SD. The black lines connect two groups for post-hoc comparisons, with the corresponding p-value noted above it. *LEFT*- Group differences in knee extensor torque (assessed at isokinetic speed of 60^0/sec, knee extensor torque measured in ft-lbs) ($p<.05$). Significant differences were found between stage 1 and 3 ($p=.001$), stage 1 and 4&5 ($p<.001$), and stage 2 and 4&5 ($p=.05$). *MIDDLE* - Knee extensor torque (180^0/sec, ft-lbs) ($p<.05$). Significant differences were found between stage 1 and 3 ($p=.001$), stage 1 and 4&5 ($p<.001$), and stage 2 and 4&5 ($p=.03$). *RIGHT* - Knee extensor isometric peak torque (measured in ft-lbs) ($p<.05$). Significant differences were found between stage 1 and 3 ($p=.05$), stage 1 and 4&5 ($p<.001$), and stage 2 and 4&5 ($p=.028$).

Figure 2 (physical function)

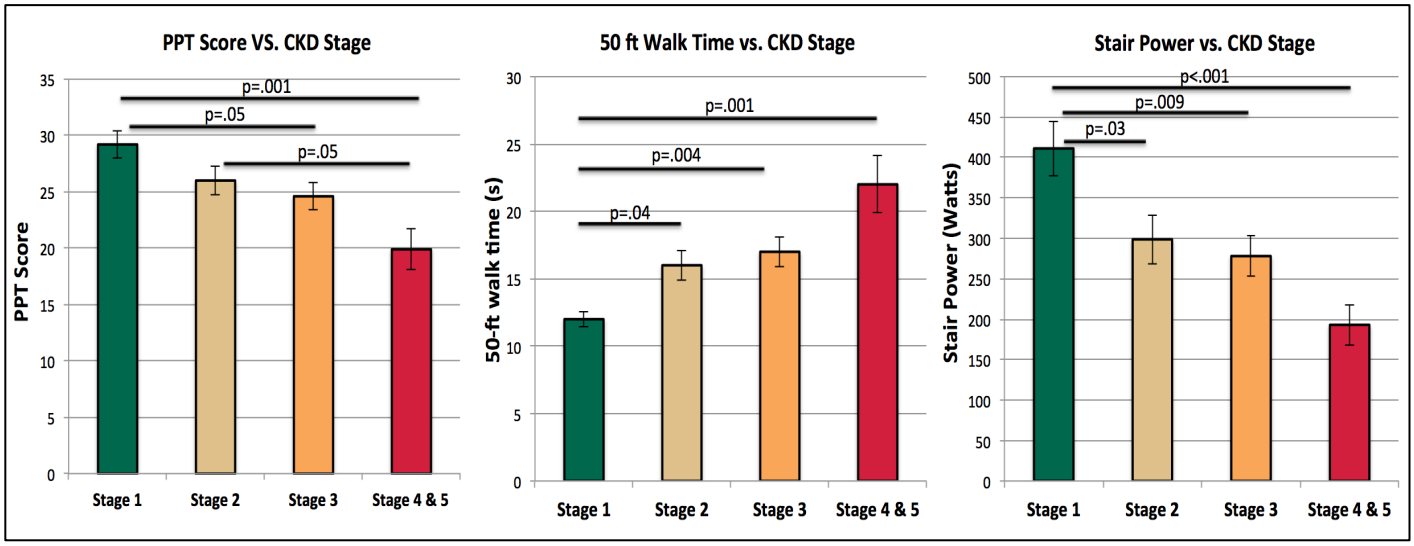

Figure 2. Physical function capacity (PPT score, stair power, 50-ft walk time) was assessed across CKD-stage groups with 1-way ANOVAs. Bar heights indicate group means, with error bars indicating ± SD. The black lines connect two groups for post-hoc comparisons, with the corresponding p-value noted above it. *LEFT*- Group differences in PPT score (scored 0-36, higher scores = better performance) ($p<.05$). Significant differences were found between stage 1 and 3 ($p=.05$), stage 1 and 4&5 ($p=.001$), and stage 2 and 4&5 ($p=.05$). *MIDDLE* -50-ft walk time (seconds) ($p<.05$). Significant differences were found between stage 1 and 3 ($p=.004$), stage 1 and 4&5 ($p=.001$), and stage 1 and 2 ($p=.04$). *RIGHT* – Stair power (watts) ($p<.05$). Significant differences were found between stage 1 and 3 ($p=.009$), stage 1 and 4&5 ($p<.001$), and stage 1 and 2 ($p=.03$).

References

1. Center for Disease Control and Prevention (CDC). National Chronic Kidney Disease Fact Sheet: General Information and National Estimates on Chronic Kidney Disease in the United States, 2014. Atlanta, GA: US Dept. of Health and Human Services, CDC; 2014.

2. Zapponi, G., Targher, G., Chonchol, M., Ortalda, V., et al. (2012) Predictors of estimated GFR decline in patients with type 2 diabetes and preserved kidney function. *Clin J Am Soc Nephrol*, 7(3); 401-8.

3. Lopez-Giacoman, S., & Madero, M. (2015) Biomarkers in chronic kidney disease, from kidney function to kidney damage. *World J Nephrol*, 4(1); 57-73.

4. Pantsulaia,T.(2006)Role of TGF-β in pathogenesis of diabetic nephropathy. *Georgian Med News*, 131:13-18.

5. Gomes, K.B., Rodrigues, K.F., & Fernandes, A.P. (2014) The role of transforming growth factor-beta diabetic nephropathy. *International Journal of Medical Genetics*, 2014; 1-6.

6. Hemmelgarn, B.R., Zhang, J., Manns, B.J., Tonelli, M., et al. (2006) Progression of kidney dysfunction in the community-dwelling elderly. *Kidney Int*, 69(12); 2155-61.

7. Lindeman RD, Tobin J, Shock NW. Longitudinal studies on the rate of decline in renal function with age. J Am Geriatr Soc. 1985 Apr;33(4):278–285

8. Rule AD, Amer H, Cornell LD, et al. The association between age and nephrosclerosis on renal biopsy among healthy adults. Ann Intern Med. 2010 May 4;152(9):561–567

9. Denic, A., Glassock, R.J., & Rule, A.D. (2016) Structural and functional changes with the aging kidney. *Adv Chronic Kidney Dis*, 23(1); 19-28.

10. Robinson-Cohen C, Littman AJ, Duncan GE, et al. Physical activity and change in estimated GFR among persons with CKD. J Am Soc Nephrol 2014; 25(2):399–406.

11. Weiner, D.E., & Seliger, S.L. (2014) Cognitive and physical function in chronic kidney disease. *Curr Opin Nephrol Hypertens*, 23(3); 291-7.

12. Roshanravan B, Khatri M, Robinson-Cohen C, et al. A prospective study of frailty in nephrology-referred patients with CKD. Am J Kidney Dis 2012; 60:912–921

13. Bao Y, Dalrymple L, Chertow GM, et al. Frailty, dialysis initiation, and mortality in end-stage renal disease. Arch Intern Med 2012; 172:1071–1077

14. Walker, S.R., Brar, R., Eng, F., Komenda, P. et al. (2015) Frailty and physical function in chronic kidney disease: the CanFIT study. *Can J Kidney Health Dis*, 2:32.

15. Serratric, G., Toga, M., Roux, H. et al. (1967) Neuropathies, myopathies and neuromyopathies in chronic uremic patients. *Presse Med*, 75; 1835-1838

16. Kaltsatou, A., Sakkas, G.K., Poulianiti, K.P., Koutedakis, Y., et al. (2015) Uremic myopathy: is oxidative stress implicated in muscle dysfunction in uremia. *Front Physiol*, 2015(6); 102.

17. Campistol, J.M. (2002) Uremic myopathy. *Kidney International*, 62(5); 1901-1913.

18. Chikotas, N., Gunderman, A., & Oman, T. (2006) Uremic syndrome and end-stage renal disease: physical manifestations and beyond. *J Am Acad Nurse Pract.*, 18(5); 195-202.

19. Dossetor, J.B. (1996) Creatininemia versus uremia: the relative significance of blood urea nitrogen and serum creatinine concentrations in azotemia. *Ann Intern Med*, 65(6); 1287-1299.

20. Ortiz-Costa, S., Sorenson, M.M., & Sola-Penna, M. (2002) Counteracting effects of urea and methylamines in function and structure of skeletal muscle myosin. *Archives of Biochemistry and Biophysics*, 408(2); 272-78.

21. Liu CK, Lyass A, Massaro JM, D'Agostino RB, Sr., Fox CS, Murabito JM. (2013) Chronic Kidney Disease Defined by Cystatin C Predicts Mobility Disability and Changes in Gait Speed: The Framingham Offspring Study. *J Gerontol A Biol Sci Med Sci*. 69(3); 301-307.

22. Roshanravan, B., Robinson-Cohen, C., Patel, K.V., Ayers, E., et al. (2013) Association between physical performance and all-cause mortality in CKD. *J Am Soc Nephrol*, 24(5); 822-30.

23. Bittel D.C., Bittel A.J., Tuttle, L.J., Hastings, M.K. et al. (2015) Adipose tissue content, muscle performance and physical function in obese adults with type 2 diabetes mellitus and peripheral neuropathy. *J Diabetes Complications*, 29(2); 250-7.

24. Brown M, Sinacore DR, Binder EF, Kohrt WM. Physical and performance measures for the identification of mild to moderate frailty. *J Gerontol A Biol Sci Med Sci* 2000; 55:M350–M355

25. Reuben DB, Siu AL. An objective measure of physical function of elderly outpatients: the Physical Performance Test. *J Am Geriatr Soc*.1990;38:1105–12.

26. Reuben DB, Siu AL, Kimpau S. (1992) The predictive validity of self-report and performance-based measures of function and health. *J Gerontol*. 47:M106–10.

27. King MB, judge JO, Whipple R, Wolfson L (2000). Reliability and responsiveness of two physical performance mesures examined in the context of a functional training intervention. *Phys Ther* 80(1):8-16.

25. Host HH, Sinacore DR, Brown M, Holloszy JO (1996) Reliability of the modified Physical Performance Test in older adults. *Phys Ther*. 76:S23–S24.

26. Tuttle, L.J. Bittel, D.C., Bittel, A.J., & Sinacore, D.R. (2017) Early-onset physical frailty in adults with diabesity and peripheral neuropathy. *Canadian Journal of Diabetes*, (17); 30118-1.

27. Lowes, L.P., Alfano, L., Viollet, L., Rosales, X.Q. et al. (2012) Knee extensor strength exhibits potential to predict function in sporadic inclusion-body myositis. *Muscle Nerve*, 45(2);163-8

28. Marcus, R.L., LaStayo, P.C., Ikizler, T.A., Wei, G. et al. (2015) Low physical function in maintenance hemodialysis patients is independent of muscle mass and comorbidity. *Journal of Renal Nutrition*, 25(4); 371-375.

29. McManus, D., Slipak, M., Ix, J.H., Ali, S. et al. (2007) Association of cystatin c with poor exercise capacity and heart rate recovery: data from the heart and soul study. *Am J Kidney Dis*, 49(3); 365-72.

30. Anand, S., Johansen, K.L., & Tamura, M.K. (2014) Aging and chronic kidney disease: the impact on physical function and cognition. *J Gerontol A Biol Sci Med Sci*, 69A(3); 315-322.

31. Odden, M.C., Chertow, G.M., Fried, L.F., Newman A.B. et al. (2006) Cystatin C and measures of physical function in elderly adults: the health, aging, and body composition (HBAC) study. *American Journal of Epidemiology*, 164(12); 1180-1189

32. Carrero, J.J., Johansen, K.L., Lindholm, B., Stenvinkel, P., et al. (2016) Screening for muscle wasting and dysfunction in patients with chronic kidney disease. *Kidney Int*, 90(1); 53-66

33. Wang, X., Hu, Z., Hu, J., Du, J., & Mitch, W.E. (2006) Insulin resistance accelerates muscle protein degradation: activation of the ubiquitin-proteasome pathway by defects in muscle cell signaling. *Endocrinology*, 147(9); 4160-8

34. Wang, X.H., & Mitch, W.E. (2014) Mechanisms of muscle wasting in chronic kidney disease. *Nat Rev Nephrol*, 10(9): 504-16

35. Workeneh, B.T., & Mitch, W.E. (2010) Review of muscle wasting associated with chronic kidney disease. *Am J Clin Nutr*, 91(4): 1128S-1132S

36. Hernandez, H.J., Obamwonyi, G., & Harris-Love, M.O. (2018) Physical therapy considerations for chronic kidney disease and secondary sarcopenia. *J Funct Morphol Kinesiol*, 3(1); 5.

37. Feng L, Yap KB, Yeoh LY, Ng TP. Kidney function and cognitive and functional decline in elderly adults: findings from the Singapore longitudinal aging study. *J Am Geriatr Soc*. 2012;60(7):1208–1214

38. Remuzzi, G., Perico, N., Macia, M., & Ruggenenti, P. (2005) The role of renin-angiotensin-aldosterone system in the progression of chronic kidney disease. *Kidney Int Suppl*, 99: S57-65

39. Rajan, V.R., & Mitch, W.E. (2008) Muscle wasting in chronic kidney disease: the role of the ubiquitin proteasome system and its clinical impact. *Pediatr Nephrol*, 23(4); 527-535.

40. Roderick PJ, Atkins RJ, Smeeth L, et al. Detecting chronic kidney disease in older people; what are the implications? Age Ageing. 2008;37(2):179–186

41. Schrack, J.A., Zipunnikov, V., Simonsick, E.M., Studenski, S., & Ferrucci, L. (2016) Rising energetic cost of walking predicts gait speed decline with aging. *J Gerontol A Biol Sci Med Sci*, 71(7); 947-53.

42. Balakrishnan, V.S., Rao, M., Menon, V. et al. (2010) Resistance training increases muscle mitochondrial biogenesis in patients with chronic kidney disease. *Clin J Am Soc Nephrol*, 5(6): 996-1002.

43. Bautista, J.E., Gil-Necija, J., Castill, I. et al. (1983) Dialysis myopathy: report of 13 cases. *Acta Neuropathol*, 61: 71-75

44. Yazdi, P.G., Moradi, H., Yang, J.Y., Wang, P.H., & Vaziri, N.D. (2013) Skeletal muscle mitochondrial depletion and dysfunction in chronic kidney disease, *Int J Clin Exp Med*, 6(7); 532-539

45. Riener R, Rabuffetti M, Frigo C. Stair ascent and descent from different inclinations. Gait Posture. 2001;15(1):32–44.

46. Bittel, A.J., Bittel, D.C., Tuttle, L.J., Strube, M.J., et al. (2017) Explanators of sarcopenia in individuals with diabesity: a cross-sectional analysis. *Journal of Geriatric Physical Therapy*, 40(2); 86-94.

47. Shimada M, Nomura Y, Kimura Y, et al Functional performance levels of strength and power needed for independence in 80-year-old individuals. Open J Epidemiol. 2012;2(3):61–69

48. Sun, D.F., Chen, Y., Rabkin R. (2006) Work-induced changes in skeletal muscle IGF-1 and myostatin gene expression in uremia. *Kidney Int*, 70; 377-9.

49. Ortiz-Costa, S., Sorenson, M.M., & Sola-Penna, M. (2002) Counteracting effects of urea and methylamines in function and structure of skeletal muscle myosin. *Archives of Biochemistry and Biophysics*, 408(2); 272-78.

Chapter 2

Skeletal muscle energetic impairments in progressive CKD: from the transcriptome to whole-body functional deficits

Background

Type 2 diabetes mellitus (T2DM) is the leading cause of chronic kidney disease (CKD) in the United States, as nearly two thirds of those with diabetes have or will develop CKD (**1**). CKD, or diabetic nephropathy, is characterized by a progressive and persistent decline in kidney function, classified into 5 categorical stages according to the degree of renal filtration impairment, or renal filtration rate (eGFR), with stage 5 constituting end-stage renal disease (ESRD) (**2**). Predictably, subsequent to the high prevalence of CKD in this population, T2DM is attributed as the cause of over 44% of all annual new cases of ESRD (**3**). This high burden of CKD in T2DM is associated with a litany of adverse outcomes, comorbidities, reduced quality of life, and significant health-care costs (**3**).

Those with T2DM exhibit more rapid declines in kidney function above their age-matched counterparts. Indeed, in a 10-year prospective longitudinal study of 1682 participants with T2DM, and baseline eGFR <60 mL/min, the authors found between a 1 ("non-decliner") and 6 ("rapid decliner") mL/min annual decline in kidney function (filtration rate) in those with T2DM (**4**). The authors also found that HbA1c (a measure of glycemic control), and diabetes duration and severity (ie. presence of peripheral neuropathy), were significant modifiers of the annual rate of decline (**4**). Other studies have supported a faster rate of renal decline in those with T2DM, ranging from 1 mL/min per year for those without proteinuria, to nearly 3 mL/min per year in those with proteinuria (**5,2**). These data all support a faster rate of kidney decline in those with T2DM, as non-diabetic individuals of similar age experience <1 mL/min annual decline (**6,7,8**). However, a key modifiable factor in the rate of renal decline in CKD is physical activity and function.

It is now well established that those with CKD possess lower physical function, impaired physical performance and mobility, and exercise intolerance that contributes to early frailty, mobility

disability, and increased risk of mortality and poor patient outcomes (**9,10)**. Roshanravan and colleagues specifically demonstrate that in 385 participants with average eGFR of 41 mL/min (stage 3 CKD), performance on lower extremity functional tasks – such as gait speed, timed-up-and-go (TUG), and 6-minute walk distance, was at least 30% impaired compared to those without CKD (**11**). Moreover, these functional deficits drastically elevate the risk of death in those with CKD, as for instance, a small .1 m/second decline in gait speed increases mortality risk by 26%, while a 1-second increase in timed-up-and go (TUG) time elevated this risk by 8% (**11**). Yet, aside from increased risk of mortality, these functional deficits independently contribute to kidney functional decline and CKD progression. The Cardiovascular Health Study of 4011 older adults (age ≥65 years) shows that both energy expenditure and physical activity-mobility were inversely associated with rapid kidney functional decline (rapid defined as a loss of >3 mL/min per year in GFR) in patients with CKD (**12).** Similarly, the Seattle Kidney Study, examining those in stages 3-4 CKD, found that higher physical activity attenuated annual loss in kidney function by roughly 4% compared to sedentary behavior, and that just 60 minutes of weekly activity slows annual decline in eGFR by .5% (**13).** Though seemingly small effects, results from the Seattle study suggest that physical activity/mobility may independently delay ESRD initiation by almost 4 years compared to non-activity (**13**). These findings are echoed in the large dataset (5888 participants) of the Cardiovascular Health Study that showed that physical activity nearly cuts the risk of rapid kidney decline (>3 mL/min per year) in half compared to very low activity (16% risk vs. 30% risk) (**14).** Meanwhile, others have shown nearly 8 mL/min improvement in kidney function after 12 weeks of low-intensity aerobic activity and home-based walking (**15).** Additionally, other authors find that exercise intensity is also associated with lower incidence of rapid kidney decline (**14**).

In light of such findings, physical activity may be a potent intervention prescription for such patients. However, CKD progression, and especially ESRD, imparts a state of intolerance to such activity and exercise. Indeed, the Heart and Soul Study found that those with eGFR <60 mL/min (stage 3+ CKD) had 6x higher odds of possessing an exercise capacity below 5 METS, or moderate-level daily activity, and this was exacerbated with progression of disease (**16**). This exercise intolerance has also been demonstrated in those in ESRD receieving hemodialysis treatment (**17).** Given that skeletal muscle tissue is critical for performance of many daily functions in the body and is responsible for movement, impairments in skeletal muscle may be the focal point of CKD-induced functional and exercise capacity deficits. Indeed, reduced kidney function leads to the retention of uremic solutes, culminating in inflammation, hypercatabolism, oxidative stress, and insulin resistance which combine to promote skeletal muscle dysfunction **(9).** A direct assessment of this hypothesis was performed by Diesel and colleagues (1990), who aimed to determined if CKD-induced exercise intolerance was derived more from central cardiorespiratory origins or skeletal muscle origin (**17**)**.** Using measures of peak oxygen consumption during maximal exercise testing, serum chemistries (blood lactate, total hemoglobin, hematocrit), along with isokinetic dynamometry and ergometry, and peak heart rates, rates of ventilation and respiratory exchange ratio measures (RER), the investigators found significant correlations between isokinetic muscle strength and exercise duration, peak ventilation and peak blood lactate concentrations (**17**). However, no such relationships were found for the other cardiorespiratory measures and exercise duration. This study elegantly demonstrated that skeletal muscle strength predicts exercise capacity as opposed to blood-oxygen carrying capacity, and that altered skeletal muscle function explains the observed exercise and mobility intolerance in those with CKD (**17**). Others have attempted to investigate further, the cause of CKD-induced muscle impairments to better explain these functional and exercise deficits.

Low renal filtration rate is associated with marked muscle impairment and heightened risk for functional limitations. In fact, a recent study demonstrates significant reductions in knee extensor strength with progression of CKD (**18).** Moreover, a more mechanistic recent study demonstrated reduced calf muscle density in older adults with lower kidney function, theoretically due to increased adipose tissue accrual that subsequently interferes with metabolism and contractile mechanics (**19,20)**. By the same token, the authors also found more rapid declines in quadriceps muscle strength over time in those with lower eGFR (**19**). These results are intriguing, as lower extremity strength, specifically quadriceps strength, has been demonstrated to more strongly dictate functional mobility capacity, and risk of mortality in those with CKD (**10,9).** Indeed, many have theorized that functional mobility and exercise capacity deficits in this population are secondary to poor muscle performance and strength that increases the physiological and metabolic cost of such activities (**16**,**21**). Given that muscle size, among other factors, is critical for muscle strength and performance, loss of muscle mass may explain some of these mobility deficits and intolerance to exercise (**10).** Indeed, even minor losses of muscle contractile proteins (ie. Myosin, actin) can be association with large decrements in force due to resultant reduction in cross-bridge formation with contraction (**10)**. In concordance with this theory, the CKD hormonal and systemic milleiu promotes a state of protein-energy wasting and cachexia that targets contractile proteins (**22,23,24,25**). As evidence, individuals on hemodialysis with ESRD experience rampant muscle and whole-body degradation through the contractile-protein targeting ubiquitin proteasome pathway (**26)**.

Interestingly, however, it has been shown that in those undergoing hemodialysis in ESRD, muscle dysfunction and poor strength was only marginally correlated with muscle atrophy, and that these patients displayed poorer muscle function than matched controls for a given muscle mass, even after further controlling for age, comorbidities, physical activity and inflammation (**27)**. This finding, to

this point, remains unresolved, and the underlying mechanism driving inherent muscle performance impairment remains unknown in CKD. However, a key skeletal muscle component that influences exercise tolerance, muscle performance, and muscle breakdown and therefore a potential key player in muscle and mobility dysfunction in CKD is mitochondria and its capacity for oxidative phosphorylation.

Mitochondria are the powerhouses of biological tissues. In muscles, they link oxidation of substrates to phosphorylation that generates ATP. The contractile fibers then use ATP to generate force and motion (**27).** Of the two populations of mitochondria in skeletal muscle (subsarcolemmal, intermyofibrillar), intermyofibrillar mitochondria not only constitutes the vast majority (~80%), but also produce more ATP, via oxidative phosphorylation, to fuel cross-bridge cycling and muscle contraction (**28).** Thus, mitochondria provide the bridge between oxygen delivery and synthesis of ATP that fuels muscle contraction and exercise performance (**27).** This is supported by the findings of the Baltimore Longitudinal Study of Aging, in which the examiners investigated the relationship between in-vivo mitochondrial ATP-producing capacity (via 31-PMRS) and knee extensor muscle performance, and found that even after accounting for age, sex, height, and weight, mitochondrial function is significantly positively associated with muscle strength (and muscle strength per volume of muscle) (**29).** When combined with the findings by Diesel et al. (1990), that muscle strength deficits rather than oxygen delivery in CKD causes the observed limitations in exercise performance - skeletal muscle mitochondrial deficits emerge as a potential underlying mechanism, as these organelles translate oxygen into fuel for muscle performance. Indeed, others have demonstrated that mitochondrial ATP-producing capacity is closely linked to the capacity of muscles to generate contractile power as well (**27).** This has been clearly demonstrated in aging studies that show 50% reductions in ATP-generating capacity per mitochondria with older age are paralleled by reduced

power output per muscle volume (**27**), and these age-related reduction in mitochondrial function are strong predictors of walking speed, and more challenging gait tasks such as climbing stairs (**30).** This is intriguing, especially considering that CKD imparts a similar state of functional impairment and muscle weakness for a given muscle mass as well (**27).** Subsequent to these findings, improvements in mitochondrial oxidative metabolism and ATP-supplying capacity have been shown to directly relate to improved generation and maintenance of leg muscle power and endurance (**27**,**31).** Such reductions in ATP-production capacity of skeletal muscle mitochondria have been theorized to stem from either 1. More H^+ leak in the mitochondria that does not lead to phosphorylation, 2. Reduced oxidative capacity due to electron transport chain deficiencies, or 3. altered mitochondrial density and organization (**27).** Increase H^+ proton leak, otherwise known as uncoupling, in skeletal muscle has been linked to higher metabolic coast of locomotion, reduced exercise capacity, greater fatigability, and reduced mobility (**27**). This uncoupling promotes reduced muscle contractile capacity that limits speed and sustainability of functional tasks (**27**). This uncoupling of oxidative phosphorylation also promotes redox stress (**32**,**33)** that can result in DNA damage, protein oxidation, and apoptosis in skeletal muscle. Interestingly, those undergoing hemodialysis in ESRD demonstrate increased plasma isofuran levels indicative of mitochondrial oxidative stress, yet underlying mitochondrial function has not been thoroughly examined (**34).** Thus, mitochondrial function, and coupling efficiency constitutes a ripe area of investigation in the pathogenesis of CKD-induced muscle impairments and functional decrements, though this remains unstudied.

Thus, the purpose of this study is to determine how lower extremity skeletal muscle mitochondrial function (coupling efficiency, H^+ leak, electron transport chain function) and abundance is influenced by CKD progression in T2DM (across CKD stages), and, in-turn, how

mitochondrial health relates to lower extremity muscle performance, and overall physical function. In understanding the underlying energetic contributions to muscle and mobility impairments in CKD progression, we may gain a better understanding of not only which biological mechanisms hinder mobility to secondarily promote renal decline, but also the temporal nature of this process in the course of disease. This may inform key targets and windows of opportunity for conservative treatments to remedy functional deficits and improve activity engagement/tolerance and attenuate CKD progression in those most vulnerable – those with T2DM.

Methods

Participants

Twenty seven subjects participated in this study – all with diagnosed T2DM, 12 with diagnosed and clinically confirmed peripheral neuropathy (PN), and all with clinically diagnosed diabetic nephropathy (diabetes-induced CKD) by a nephrologist. Participants were stratified into early CKD stages (eGFR >60 mL/min, stages 1 and 2), middle-stage CKD (eGFR 30-59 mL/min, stage 3), and late CKD (eGFR<29 mL/min, stages 4 and5). Participants of each categorical stage/group of CKD progression were – n = 9 in early CKD (stage 1 and 2 - 7 male, 2 female), n=9 in middle-stage CKD (stage 3 - 6 male, 3 female), and n=9 in late-CKD (stages 4 and 5 - 5 male, 4 female). The groups were matched for age, diabetes severity (i.e. presence of PN), BMI, duration of T2DM, glycemic control, and gender composition (TABLE 1). Participants were recruited from the Washington University Volunteers for Health, the Center for Community Based Research, the Washington University Medical School Renal Clinic, and from the surrounding St. Louis community.

Study inclusion criteria included a diagnosis of T2DM based on clinical report of a diagnosis of DM from a physician, confirmation of medication usage for DM (insulin, oral hypoglycemic

agents or both) and verification of HbA1c levels either currently or at the time of diagnosis >6.5%, and/or OGTT ≥200 mg/dL. A diagnosis, particularly for those with eGFR ≤60 mL/min, of diabetic nephropathy based on nephrologist clinical assessment of patient medical history, degree of proteinuria (must be present at least at the microalbuminuria level – urinary ACR ≥30 mg/g), glycemic control, diabetic medication use, hypertension status, and rate of kidney decline (eGFR utilizing creatinine), all according to KDIGO guidelines.

Participants were excluded from the study if they weighed more than 350 pounds (due to equipment weight limit), had any infection or ulceration of either foot, severe foot deformity or amputation, or any serious medical co-morbidity. Serious medical comorbidities included - dialysis treatment, heart failure requiring medications, or New York Heart Association class 3 or class 4 heart failure, coagulation disorders (platelets <100,000, PT > 2 seconds above control, or INR >1.5), anemia (Hbg < 10g/dL), uncontrolled proliferative diabetic retinopathy, joint replacement or musculoskeletal injury that precludes intense muscular contraction, within 1 year of enrollment, symptoms that meet the requirement for class C or class D of the AHA risk stratification criteria, individuals who are participating in regular structured exercise programs, or may be pregnant or breast feeding, current cancer treatment, and organ transplant requiring immunosuppressant therapy. Each participant read and signed an IRB-approved protocol and informed consent that was approved by the Human Research Protection Office at Washington University in St. Louis, MO.

CKD Staging (eGFR)

CKD staging was performed using serum creatinine concentrations. Serum creatinine was measured with a standardized assay, and used to estimate GFR (eGFR) - computed based on the Chronic Kidney Disease Epidemiology Collaboration equation and was classified into 5 categories: eGFR ≥

90 mL/min per 1.73 m^2 (stage 1 CKD), 60-90 mL/min (stage 2 CKD), 30-60 mL/min (stage 3 CKD), 15-30 mL/min (stage 4 CKD), <15 mL/min (stage 5 CKD) with no kidney transplant or dialysis.

Laboratory Measures

Laboratory measures including serum creatinine (mg/dl) as above, BUN (mg/dl), HbA1c (%), and urine albumin:creatinine ratio (ACR – mg/g) to quantify degree of proteinuria.

Participant Demographics-

Participants age, duration of T2DM, weight, height, and BMI (calculated as weight in kg divided by the square of height in meteres, used to define obesity) were collected through participant interview, weight balance, and stadiometer, respectively at the initial visit, prior to any dynamometry or physical performance testing.

Neuropathy Assessment-

Determined by diminished or absent plantar sensation to light touch or pressure or vibration perception. Lower extremity sensation was assessed via biothesiometry and semmes Weinstein monofilament testing. Neuropathy was defined clinically as the inability to feel the 5.07 (10 gram) monofilament on at least one non-callused site on the plantar aspect of either foot or the inability to perceive vibration <25 volts on the biothesiometer (Biomedical Instrument, Newbury, OH, USA) applied to the hallux (**20**).

Physical Function –

Functional physical performance was assessed using the 9-item modified physical performance test (PPT). The PPT is a timed observational assessment of performance on nine daily physical activities including: 5 consecutive sit-to-stand chair rises without arm assistance, climbing a flight of stairs

with 10 steps, a 50-ft. walk test, turning 360 degrees, picking up a penny from the floor, donning/doffing a jacket, lifting a book onto an overhead shelf, a Romberg standing balance assessment with eyes open, and ability to ascend 4 flights of stairs (**20**). Each item is scored from 0-4 based on the time taken to complete each task, with a maximum score of 36 (higher scores indicate better physical function/performance). Each task is performed twice with the average time used to score the task. Interrater reliability, validity with other functional assessments, and predictive validity of lack of independence and mortality have all been well established for the mPPT (**35,36,37**). The mPPT possesses a test-retest reliability of .964, while individual sub-items have reliability ranging from .51-.99, and Cronbach alpha of .785 (**36,37**).

Muscle Performance Assessment-

Muscle performance of lower extremity major muscle groups was assessed via Biodex System 3 isokinetic dynamometer as described previously (**38**,**39,40**,**41**). Major muscle groups assessed were hip extensors, knee extensors, and ankle plantarflexors as these muscle groups are critical to ambulation and functional mobility (**42**). For each movement, the anatomical axis of rotation (ie. hip joint center/greater trochanter, knee joint femoral condyles, and ankle joint malleolus) was aligned to the dynamometer axis using visual inspection and manual palpation.

Participants upper extremities, trunk, and contralateral limb were secured with padded straps to ensure minimal accessory movement contributed to force production. Prior to each test, participants became familiar with procedures by performing 3-5 submaximal contractions, and the tested leg was weighted to correct for the effects of gravity on the torque measured, according to the specifications of the Biodex Manual. Range of motion was set for each movement to obtain ~110 degrees of hip flexion (from ~5° of hip extension), ~90 degrees of knee flexion (from terminal

extension), and maximal ankle plantarflexion and dorsiflexion. The isokinetic tests for each muscle group included 5 maximal concentric contractions each separated by 5 seconds. Isometric tests consisted of 4 maximal contractions held for 5 seconds each, separated by 10 seconds rest between repetitions. Isometric force production was assessed at 60 degrees of hip flexion, 60 degrees of knee flexion, and slight ankle dorsiflexion to achieve optimal muscle-specific sarcomere length (**43**,**44**). 3 minutes rest separated each test. Isokinetic strength was assessed for each joint extensor movement at 30°/sec and 120°/sec. To assess peak torque production (ft-lbs) as a measure of maximal muscle strength, the highest 3 repetitions were selected and averaged for each joint at each repetition speed. At each selected repetition, rate of torque production, seconds to peak torque, total work, and power was also assessed and averaged. Power was determined by the time-averaged integrated area under the curve at the constant velocity of movement in the available range of motion **(38**,**39**) To avoid sub-maximal performance or outliers, tests were re-done or data discarded if the coefficient of variation exceeded 10% for the knee and ankle, and 15% for the hip (**45**).

Finally, we also assessed muscle fatigueability/fatigue resistance of the aforementioned muscle groups using a fatigue protocol detailed as follows – participants performed 50 maximal repetitions at 90 degrees per second, with 2 second rest period between repetitions. Torque production was assessed for each repetition, and work was calculated across the first, second, and third portion of the fatigue set, and totaled for an index of fatigue resistance as detailed previously (**46,47**). Recovery from this fatigue task was tracked over 2 recovery phases. In phase 1, participants performed 5 maximal repetitions separated by 10 seconds of rest immediately following the fatigue set. In phase 2, participants performed 5 maximal repetitions separated by 25 seconds of rest. Torque production for each recovery repetition was recorded.

Fasting/medication/OGTT:

As renal decline can contribute to skeletal muscle insulin resistance, an oral glucose tolerance test and fasting glucose and insulin values were obtained to assess and control for any differences in insulin sensitivity, as this may confound the relationship between mitochondrial function and muscle performance. All diabetes medications (except insulin) were stopped 2 days before admission to the CRU to decrease residual drug effects on the metabolic measurements (long-acting GLP-1 agonist and thiazolidinediones were stopped 7 days before admission). Subcutaneous insulin was stopped after the final dose on the day prior to admission to the clinical research unit. Blood glucose concentration was checked by fingerstick twice daily at home (once before breakfast, and once posprandially after dinner before bedtime) for 2 days before admission (7 days before admission in subjects taking long-acting GLP-1 agonist or thiazolidinediones) to ensure adequate glycemic control was maintained prior to metabolic testing. Participants refrained from eating for 10 hours prior to administration of the 3-hour oral glucose tolerance test as previously described (**48**).

Participants fasting plasma glucose was assessed 10 minutes prior to administration of a 75g glucose drink. Plasma samples were subsequently obtained at the time of drink ingestion, and at 10, 20, 30 minutes, and then every half hour until 3 hours post-ingestion. Plasma glucose was assayed by automated glucose analyzer (Yellow Spring Instruments), and plasma insulin by enzyme-linked immunosorbent assay (**49**). Insulin sensitivity as a measure of basal insulin sensitivity during an OGTT was estimated using homeostasis model assessment of insulin resistance (HOMA-IR), calculated as [(fasting glucose (mg/dL)] x [fasting insulin (μU/mL)]/405 (**50**).

Body Composition:

Each participant was assessed for body composition with a whole-body, dual energy x-ray absorptiometry (DXA) (Hologic QDR 1000/W, software version 6.2 OD; Waltham MA) scan to

assess composite and regional lean and fat mass as described previously (**57**). Bilateral upper and lower extremity fat-free masses, region-specific lean mass (ie. thigh region), whole-body lean mass and fat masses were assessed.

***Muscle Biopsy*:**

Participants were positioned supine in a hospital bed with the thigh of their dominant leg exposed. Participants were then asked to contract the thigh so as to visualize the vastus lateralis (anterior to fascia lata, approximately 1/3rd of the distance from patella to great trochanter). The area was prepped and cleaned with iodine, and draped. The skin was anesthetized with 2% lidocaine solution injected into the dermis and allowed to take effect over a 3 minute period. A 1-2 cm incision was made through the skin and subcutaneous tissue, and a 5 mm Bergstrom needle was introduced with vacuum suction into the vastus lateralis. 2 passes of the biopsy needle were performed for each participant obtaining ~250-350 mg of skeletal muscle tissue as previously described (**58**). ~50-75 mg of the sample were immediately snap-frozen in liquid nitrogen and stored at -80°C until further analysis (mtDNA copy number, qPCR, enzyme testing, RNA-sequencing).

Mitochondrial Functional Analysis:

10 mg of the biopsy sample was immediately placed into ice-cold relaxing buffer, 50 mM K+-MES, 20 mM taurine, 0.5 mM dithiothreitol, 6.56 mM MgCl2, 5.77 mM ATP, 15 mM phosphocreatine, 20 mM imidazole, pH 7.1, adjusted with 5 N KOH at 0 °C, 10 mM Ca–EGTA buffer (2.77 mM CaK2EGTA + 7.23 mM K2EGTA; 0.1 μM free calcium) (**60**,**61**) and trimmed of surrounding epithelial and fat tissue. The sample was then transferred to an ice-cold glass plate, where fiber bundles were separated mechanically with sharp angular forceps over a standardized period of 5-10 minutes. Briefly, fibers were partially teased apart under dissection scope and stretched out but

remained connected in a meshlike framework, and immediately transferred into 2 mL freshly prepared saponin permeabilization solution (.003% saponin – weight/volume in relaxing buffer) and put on a rocker at 4°C for 20 minutes. The tissue was then equilibrated in respirometry media (110 mM sucrose, 60 mM K+-lactobionate, 0.5 mM EGTA, 3 mM MgCl2, 20 mM taurine, 10 mM KH2PO4, 20 mM HEPES adjusted to pH 7.1 with KOH at 37 °C; and 1 g/l BSA essentially fatty acid free) for 15 minutes. Samples were then blot dried, weighed, and split into two 3-mg samples, and placed into the respirometry chamber (1 sample per chamber). Chamber parameters were set to 37°C internal temperature, with a stirrer speed of 750 rpm (12.5 Hz), with oxygen flux data collection interval of 2 seconds, and filled with respirometry media (per chamber - 2.1 mL of respirometry media supplemented with 2.1 uL of 10μM blebbistatin and 6.3 mg creatine). O_2 flux was calculated as a time derivative of oxygen concentration using the DatLab4.3 Analysis software (OROBOROS), and was initially measured by adding malate (.5 mM), followed by glutamate (10 mM), and pyruvate (5 mM), in the absence of ADP (State 2-C1, ie. LEAK state respiration). State 3 respiration using complex 1 (C1) substrates (state 3-C1) was then achieved by the addition of ADP (5 mM). This was followed by the addition of succinate (10 mM) to reach state 3 respiration through both C1 and complex 2 (C2) (State 3-C1+C2). As a quality control measure, cytochrome c (10 μM) was then added to the chamber. As cytochrome c does not pass the intact outer mitochondrial membrane, any increase is oxygen flux with cytochrome c administration would indicate damage to the mitochondrial membrane during preparation. Oxygen flux changes that did not exceed 15% upon cytochrome c administration, were deemed evidence of non-damaging permeabilization as described previously (**62**). Next, carbonylcyanide-4-(trifluoromethoxy)-phenyl-hydrazone (FCCP) was titrated (3x, .5uM each injection) to evaluate maximum flux through the electron transfer system (ETS capacity – state E). FCCP is a protonophore that collapses the electrochemical proton potential

across the inner mitochondrial membrane, thereby removing the electrochemical backpressure on the proton pumps and represents maximal respiration in the uncoupled state **(60)**. Finally, Rotenone (.5 uM) was added to inhibit C1-mediated flux.

Additional flux-control ratios were calculated from the aforementioned analyses to further probe mitochondrial coupling efficiency. The oxidative phosphorylation system control ratio (P/E) was assessed to analyze for phosphorylation system deficits as lower ratios indicate phosphorylation deficit within mitochondria. The respiratory-control ratio (RCR – P/L) provides insight into the coupling efficiency of mitochondria, with higher values indicating improved coupling.

O_2 flux values are expressed relative to tissue wet weight per second. When possible, all respiration values were further normalized to citrate synthase activity (CS) as a measure of mitochondrial number. Inversely, the calculated phosphorylation control ratio (L/P) is indicative of increased dyscoupling. Similarly, the oxidative phosphorylation coupling efficiency ratio was also calculated (L-P)/P. Lastly, the ETS coupling efficiency was measured (E-L)/E, to assess coupling efficiency, as ratios closer to 1 indicate more efficient mitochondrial coupling.

mtDNA Copy Number-

To determine if mitochondrial density/abundance contributed to any differences found with respiratory function of these muscle samples, mtDNA copy number was performed. From the flash frozen sample, a ~15-20 mg portion was used for DNA extraction using a QIAgen DNeasy Blood and Tissue Kit (QIAGEN, Valencia, CA) according to the manufacturers instructions. Briefly, samples were lysed with 100 uL of the supplied buffer (Buffer ATL) for 50-90 minutes in the presence of proteinase K (2.5 mg/mL) in a 70°C water bath. The lysis was completed by adding 200 uL of buffer AL and incubating at 70°C for 10 minutes. The entire mixture is applied to a provided

spin column, centrifuged at 8000 rpm for 1 min., and washed twice with 500 uL supplied wash buffer (Buffer AW), and DNA is eluted three times with elution buffer (buffer AE). Following DNA isolation, precise quantitation of DNA was obtained via nanodrop. DNA concentrations ranged from 20-45 ng/uL per sample. To measure mtDNA copy number, oligonucleotide primers for mtDNA-encoded 12s ribosomal RNA and nucleus-encoded β2 microglobulin were used[Nuclear genome B2-microglobulin gene (forward 5'- TGCTGTCTCCATGTTTGATGTATCT-3', reverse 5'-TCTCTGCTCCCCACCTCTAAGT-3'), Mitochondrial genome 12s Ribosomal RNA (mt806F 5'-CCACGGGAAACAGCAGTGATT-3', mt929R 5'-CTATTGACTTGGGTTAATCGTGTGA-3')]. DNA was diluted to 2 ng/uL in DEPC water with both forward and reverse primers, and added to 10 uL of 2x PCR SYBR Green mastermix and 9.2 uL of DEPC water (total volume per reaction – 20 uL) per well in a 96-well plate and covered with optical adhesive. Sample PCRs were run in triplicate per gene probe. mtDNA and nDNA Ct values were averaged from the triplicate. To determine mtDNA content relative to nuclear DNA, the ΔCt method was used -- ΔCt = (*n*DNA Ct – *mt*DNA Ct), where relative mitochondrial DNA content = $2x2^{\Delta Ct}$ (**63**).

Mitochondrial Enzymatic Testing:

To more precisely determine mitochondrial quantity in these samples, enzymatic Citrate Synthase (CS) activity was determined spectrophotometrically as described previously (**64**). Briefly, CS was determined spectrophotometrically at 30 deg C by measuring decreased absorbance of the Acetyl CoA at 232 nM, due to the hydrolysis of the thioester in the formation of CoA-SH with CS activity. Due to the testing requirements of 50 mg of frozen muscle tissue, this and all enzymatic analysis was performed on a subset of 13 participants (n=5 in CKD stages 1&2, n=5 in stage 3, and n=3 in stages 4&5 CKD) whose biopsy samples were large enough to complete these analysis. Muscle samples

were homogenated in .5mL of medium consisting of 50 mM Tis HCL (pH 7.4) and .15M KCL and aliquotted and stored at -80 deg C for subsequent enzymatic analysis.

Citrate Synthase Activity (CS) - for the citrate synthase testing, each sample was run in duplicated with 5 uL aliquots per reaction as described previously (**64**). In a water bath, maintained at 30 deg celsius to increase reaction kinetics, samples were prepared by adding 1 mL of 100 mM Tris (pH 8.1), used as a buffer, 3.4 uL of .17 mM Oxaloacetic Acid, and 10 uL of .2M Acetyl CoA. The samples were poured into a quartz cuvette and inserted into a UNICO spectrophotometer maintained at 30 deg c. Readings were taken at 232 nM, the ideal wavelength for Acetyl CoA thioester absorption at 1 minute intervals for 10 minutes. The absorbance values were then plotted against time and the rate of absorbance decay determined and expressed per minute per milligram tissue as described previously (**65**). CS activity (expressed as umol/min/g) was used as a control factor in respiration measures as a secondary analysis of those 13 participants.

SDH enzymatic activity (Complex 2)- 10 uL of the 1:10 muscle homogenate is added to 100 uL of freshly made assay reagent as described previously (**64**). Briefly, fresh assay reagent consists of .5mL of 1M Imidazole HCL (pH 7.4) for a reaction concentration of 50mM, 1 mL of 1M succinate for a final concentration of 100 mM, .2 mLs of 500mM K_3FeCN_6 for an assay concentration of 10 mM, and finally, .2 mLs of 1% BSA (**64**). Once added, homogenate/assay mixture is incubated at room temperature for 60 minutes. Subsequently, 10 uL of 1N NaOH is added and heated at 60^0C for 20-minutes, followed by addition of 1mL fumarate indicator reagent (50mM 2-amino2 methyl propaneidol+200uM NAD+10mMglutamate+50ug/mL pig heart fumarase+2ug/mL GOT), and read at 340 nM in a UNICO spectrophotometer, using disposable semi-micro cuvettes after the final reaction was complete (15-30 minutes) and expressed as umoles/min/gram (**64**,**66**).

Cytochrome Oxidase, COX (Complex 4) - Enzymatic analysis of complex 4 of the ETC is based on the principle that absorption of cytochrome C at 550 nm changes with its oxidation state. Its oxidation by cytochrome oxidase (complex 4) is a measure of COX activity. The COX enzyme testing was thus conducted as described previously (**64**). Briefly, 5 uL of muscle homogenate is added to a cuvette containing .95 mL of .01M phosphate buffer (pH 7), and 50 uL of 1% reduced cytochrome C, and measured with a UNICO spectrophotometer at wavelength of 550 nm at 15, 30, 45, and 60 minutes. COX activity is expressed as described in citrate synthase above (**64**).

Transcriptome Analysis (RNA-Sequencing):

~20 mg of snap frozen tissue per participant, was ground into a fine powder in a liquid-nitrogen cooled mortar and pestal system. Ground samples were subsequently emptied into a vial containing 1mL of Trizol reagent (Invitrogen # 15596026) supplemented with 20 mg/mL glycogen and incubated for 10 minutes, and precipitated with chloroform, centrifuged at 13200 rpm (16000g) for 15 minutes, and the aqueous layer was transferred, precipitated with isopropanol and centrifuged at 13200 rpm (1600g) for 10 minutes. Finally the pellet was re-suspended in 75% ethanol and centrifuged at 11000 rpm for 5 minutes and allowed to air dry for 15 minutes and re-suspended in DEPC water. Concentration and quality of mRNA were measured using a nanodrop spectrophotometer. 1 ug of total RNA was subsequently utilized for RNA-sequencing and library preparation. Library preparation was performed using a Clontech SMARTER kit according to the manufacturer's protocol. The resulting cDNA ends were rendered blunt, an A base was added to the 3' ends, and Illumina sequencing adapters were ligated to the ends. The ligated fragments were then amplified for 12 cycles using primers that incorporated unique index tags, and the resulting fragments were sequenced on an Illumina HiSeq 2500 sequencing system using single reads that extended 50 bases and targeted 30M reads per sample as previously described (**63**). Briefly, RNA-

seq reads were aligned to the Ensembl top-level assembly with STAR version 2.0.4b. Gene counts were derived from the number of uniquely aligned unambiguous reads by Subread:featureCount version 1.4.5. Transcript counts were produced by Sailfish version 0.6.3. Sequencing performance was assessed for total number of aligned reads, total number of uniquely aligned reads, genes and transcripts detected, ribosomal fraction known junction saturation and read distribution over known gene models with RSeQC version 2.3.

All gene-level and transcript counts were then imported into the R/Bioconductor package EdgeR and TMM normalization size factors were calculated to adjust for samples for differences in library size. Ribosomal features as well as any feature not expressed in at least the smallest condition size minus one sample were excluded from further analysis and TMM size factors were recalculated to created effective TMM size factors. The TMM size factors and the matrix of counts were then imported into R/Bioconductor package Limma and weighted likelihoods based on the observed mean-variance relationship of every gene/transcript and sample were then calculated for all samples with the voomWithQualityWeights function. Performance of the samples was assessed with a spearman correlation matrix and multi-dimensional scaling plots. Gene/transcript performance was assessed with plots of residual standard deviation of every gene to their average log-count with a robustly fitted trend line of the residuals. Generalized linear models were then created to test for gene/transcript level differential expression. Differentially expressed genes and transcripts were then filtered for FDR adjusted p-values less than or equal to 0.05.

The biological interpretation of the large set of features found in the Limma results were then elucidated for global transcriptomic changes in known Gene Ontology (GO) and KEGG terms with *the R/Bioconductor packages GAGE and Pathview*. Briefly, GAGE measures for perturbations in GO or KEGG terms based on changes in observed log 2 fold-changes for the genes within that term

versus the background log 2 fold-changes observed across features not contained in the respective term as reported by Limma. For GO terms with an adjusted statistical significance of FDR <= 0.05, heatmaps were automatically generated for each respective term to show how genes co-vary or co-express across the term in relation to a given biological process or molecular function. In the case of KEGG curated signaling and metabolism pathways, Pathview was used to generate annotated pathway maps of any perturbed pathway with an unadjusted statistical significance of p-value <= 0.05.

Statistics-

Pearson Chi-square test for equality of proportions was used to determine the homogeneity of sex distribution, and neuropathy status between CKD-staged groups (stages 1 and 2, stage 3, and stages 4 and 5). CKD group baseline demographic variables (age, BMI, duration of diabetes, glycemic control – HbA1c, total body lean mass, and eGFR) were analyzed and compared via 1-way analysis of variance (ANOVA). CKD-group differences were also assessed via 1-way ANOVA for OGTT area under the curve and HOMA-IR (measures of insulin resistance), PPT score, lower extremity torque production and power, fatigue-related work production, all mitochondrial functional measures, and mitochondrial DNA copy number and enzymatic testing. Post-hoc testing for CKD-staged group differences was determined using Tukey's HSD or Games-Howell in the event of a violation of homogeneity of variance. Bivariate pearson correlation coefficients were used to assess relationships between eGFR and the aforementioned measures, including lab measures, and between mitochondrial function/abundance/enzyme measures (mtDNA copy number, complex 2, complex 1, and complex 4 enzymes) and muscle performance and PPT scores. All analyses were evaluated at an alpha level set at .05. RNA-seq.

Results-

Group Demographics-

As shown in Table 1, there were no group differences in gender composition, age, BMI, duration of diabetes, BMI, age, duration of diabetes, glycemic control (HbA1c), PN status, whole-body lean mass, insulin sensitivity (OGTT AUC) or albuminuria. The groups inherently differed in eGFR, as this was the defining criteria of the groups (early, middle, and late-stage CKD) ($p<.001$), and also differed in BUN, a measure of uremia ($p<.001$).

Physical Function-

As shown in Figure 1A and Table 2, eGFR was significantly positively correlated with PPT score ($r=.8$, $p<.001$), and other functional measures like the ability to rise from a chair ($r=.761$, $p<.005$), but was negatively correlated with 50-ft walk time ($r=-.68$, $p<.001$, Fig.1B), or in other words, worse kidney function was associated with slowed gait (from 4 ft./sec in stages 1&2, to 3 ft./sec in stage 3, and 2 ft./sec in stages 4&5). Similarly, PPT score and 50-ft walk time significantly declined with progression of CKD (Figure.1 C,B).

Muscle Performance-

eGFR was positively correlated with hip extensor torque production ($r=.82$, $p<.001$), knee extensor torque production ($r=.79$, $p<.001$), and knee extensor total work during fatigue task (a measure of fatigue resistance – $r=.83$, $p<.001$) (Table 2, Figure 2,C). With progression from early to middle to late CKD, there is a significant stepwise decline in knee extensor torque, power production, and hip extensor torque (Figure 2, A,D,C). Not surprisingly, knee extensor torque production and hip extensor torque both significantly positively correlated with PPT scores ($r=.78$, $p<.001$, $r=.88$, $p<.001$ respectively), and functional sub-tasks, uncluding the efficiency/speed in rising from a chair ($r=.78$, $p<.001$, $r=.72$, $p<.001$ respectively) (Table 2, Figure 3). Neuromuscular performance was

also assessed for hip and knee extensors, with no differences found between stages in regards to seconds-to-peak torque (a measure of muscle activation capacity) (knee extensors p=.4, hip extensors p=.18). As shown in Figure 3 (middle row, far right), knee extensor torque production significantly correlated with PPT score (r=.721, p<.001).

Mitochondrial Function/Coupling efficiency-

As shown in Figure 4A, there were no differences between groups in mitochondrial density as assessed via mtDNA copy number (Stage 1&2 – 2498.7 $\pm$ 798.7, Stage 3 – 2317.4 $\pm$ 570.6, and Stage 4&5 – 1637.4 $\pm$ 998.1, p>.05). Similarly, there were no significant differences between CKD stages on the 13-participant citrate synthase activity analysis (Figure 4B), supporting the copy number findings that mitochondrial number and density did not differ in our sample of CKD participants. However, there were progressive increases in mitochondrial LEAK-state respiration with progression of CKD (State L) (Figure 5A). This remained significant when normalizing LEAK respiration to mitochondrial number (citrate synthase) (Table 3) . Conversely, significant declines in mitochondrial complex-1-mediated respiration (state3-C1) were observed with progressive stage of CKD (Stage 1&2 CKD: 52.85 $\pm$11.4 pmol/sec, Stage 3 CKD: 39.9 $\pm$5.2 pmol/sec, Stage 4&5 CKD: 26.5 $\pm$7.5 pmol/sec, p<.001) (Figure 5B). After controlling for CS-activity, this relationship remained significant between early and late-sage CKD (p=.018, Table 3), with subsequent power analysis revealing 10 participants would be needed per stage for this measure to reflect our unadjusted respirometry measure differences. Similarly, CKD stage progression related to significant declines in mitochondrial maximal oxidative capacity (State3-C1+C2, P), with no difference observed between stage 3 and 4&5 (Figure 5C), and this relationship remained after normalizing to CS (Table 3). This same relationship was true of maximal mitochondrial electron transport capacity (State E-ETS) (FIgure 5D, Table 3). An example of respiration traces depicting the significant

differences between early and late-stage CKD is shown in Figure 5E. Moreover, LEAK-state respiration, maximal oxidative phosphorylation capacity, and complex-1-mediated respiration, all normalized to CS, significantly correlated with renal filtration (r=-.75, r=.81, r=.82, p<.001 respectively, Table 3), while CS-normalized complex 4 enzyme activity significantly positively correlated with renal filtration (r=.53, p=.02, Table 3), and exhibited significant functional declines in stage 3 CKD that persisted into later stages (stage 1&2: 4.29(1.96), vs. stage 3: 1.95(.61), vs. stage 4&5: 1.84(.35), p<.001, Figure.4D). No samples exhibited an increase in respiration exceeding 15% with cytochrome-c administration, indicating no damage was inflicted to the outer mitochondrial membrane in preparation.

To further probe mitochondrial function and coupling, mitochondrial respiratory flux control ratios were calculated from the aforementioned states and listed in Table 3. There were significant reductions in oxidative phosphorylation control ratio with CKD progression, where lower values indicate intrinsic mitochondrial deficits within the phosphorylation system (p=.017), though these differences were not observed between early stages of disease (stages 1&2 vs. stage 3). However, the respiratory control ratio, an index of mitochondrial coupling, whereby larger values reflect better coupling between phosphorylation system and ATP-production, was significantly different between stages, with progressive disease reflecting poorer coupling (p<.001). This was also true of the ETS coupling efficiency, where values closer to 1 are indicative of better coupling (p<.001). Conversely, while the PCR and OPC ratios both demonstrate impairment with CKD stage-wise progression (p=.001), PCR did not differ between middle and late stage CKD, while OPC did not differ between early and middle stage disease.

After demonstrating apparent intrinsic mitochondrial functional deficits across CKD stages, the mitochondrial measures were probed for their relationship to muscle performance, and functional

mobility. As shown in Figure 3. predictably, mitochondrial maximal oxidative phosphorylation capacity (P) significantly positively correlated with total knee extensor work performed over the fatigue task, with better phosphorylation capacity related to increased work production and fatigue resistance (r=.72) (Figure.3A). Interestingly, complex-1-mediated respiration (state3-C1), and max oxphos (P) both were strongly related to knee extensor torque (r=.75, r=.77 respectively, Figure 3 B,C) and power production (r=.67, r=.68 respectively) (Figure 3 G,H). Moreover, mitochondrial electron transport capacity (E), significantly correlated with knee extensor power production, although this was among the moderate correlations observed (r=.58, Figure. 3I). Given the strong relationship between mitochondrial functional measures and muscle performance, it was not surprising to see the strong positive relationship between these same measures and PPT scores (state3-C1 vs. PPT: r=.73, P vs. PPT: r=.74) (Figure 3, D,E).

Transcriptome Analysis (RNA-seq)-

The RNA-seq analysis resulted in approximately 19–28 million raw sequence reads for each of the 25 cDNA libraries generated from the human skeletal muscle samples. On average, 99% of the trimmed reads mapped to the human reference genome (Figure 6C). The muscle samples contained 44,000–66,000 transcripts, with ~5,000-8,000 genes detected. The ribosomal fraction was <5% across all samples. To determine the similarity between expression profiles, we used Pearson correlation plots. The correlation values indicate closely similar expression values for transcripts between biological samples. Differentially expressed genes in the stage 1&2 CKD group, stage 3 CKD group, and stage 4&5 CKD were filtered based on the highest fold change and significant *p*-values and the genes were annotated using Ensembl, leading to the identification of genes that were significantly altered between stages of disease (Figure 6A). As shown in Figure 6B, there were 448 differentially expressed genes between early and late-stage CKD, 440 differentially expressed genes

between early and middle-stage CKD, and 1775 differentially expressed genes between middle and late-stage CKD, all with p-value <.05.

GO and KEGG gene pathways that differed between CKD stage groups are shown in Figure 7. As demonstrated in Figure 7, oxidative phosphorylation, electron transport chain, couple ATP synthesis, and ETC complex-1 activity were the most significantly down-regulated gene pathways (GO and KEGG terms) (all FDR $\leq$.05) in late-stage CKD (stages 4&5) compared to early disease. Conversely, gene networks involved in regulatory region DNA binding, histone modification, chromatin modification, and complement cascade were all among the most significantly upregulated pathways in late-stage disease. Figure 7A (bottom), lists selected genes from the aforementioned GO and KEGG terms that were significantly altered in expression. In Figure 7B, the significant down-regulated gene networks/pathways in stage 3 CKD compared to early disease, include PI3K-Akt signaling, lipid localization, mitochondrial organization, oxidative phosphorylation, complex 1 assembly, and electron transport chain. Conversely, upregulated gene families were observed for the PPAR signaling pathway, mRNA spicing, and non-coding RNA metabolic processes. Tables 5 and 6 describe general functions of selected significantly differentially expressed genes from the selected GO and KEGG pathways. Figure 8 depicts a subunit visualization of the electron transport chain effected in late-stage CKD.

Discussion-

While mitochondria play a key role in energy metabolism of all organs, especially skeletal muscle, the available data on the effect of CKD on mitochondrial function, structure and abundance in skeletal muscle remains limited. This study demonstrates for the first time, to the authors knowledge, evidence of intrinsic mitochondrial respiration deficits as a potential key mechanism driving muscle

performance impairments and functional mobility loss in the progression of CKD across its stages in those with T2DM. Our cohort of participants did not differ in any potential confounding variables (ie. age, gender, peripheral neuropathy, BMI, duration of diabetes, glycemic control, insulin sensitivity, or lean mass), lending strong support to the analyzed connections between renal dysfunction and skeletal muscle health, energetics, and performance.

Our findings that CKD progression from early, to middle, to late stages was accompanied by impairments in a battery of physical function measures (ability to rise from a chair, gait speed, and PPT scores), even in early CKD (stage 3), relates strongly to studies of larger cohorts of those with CKD. For instance, Roshnaravan and colleagues, in a study of 385 participants with mean eGFR of 41 mL/min (eGFR <60 mL/min) found reduced performance in 6-minute walk distances, decreased grip strength, impaired ability to rise from a chair and walk, and gait speed reductions that increased the risk of death (**11**). Moreover, as weak quadriceps are accepted measures of muscle impairment most strongly associated with functional limitation and mobility disability among those with CKD, our findings that quadriceps and hip extensor torque production, power, and endurance/fatigue resistance, were all related to physical function was to be expected. However, this study demonstrates significant declines in quadriceps and hip extensor strength, knee extensor power, and reduced knee extensor endurance with CKD progression, with many of these decrements reaching significance at even early stages of disease (stage 3). Given that muscle size and neurological aspects are important in muscle strength, our results are intriguing, in that no difference in muscle size was noted with DXA analysis, while neurological activation of these muscle groups was similar between groups (time-to-peak-torque). However, previous research has shown reduced muscle density in the lower extremity of older adults with reduced kidney function theoretically due to adipose tissue and fibrotic accrual that reduces muscle quality (**19).** Such changes in quality cannot be readily detected

with DXA scanning, and warrant further investigation in T2DM-indued CKD (**10**). Additionally, even minor losses of muscle contractile proteins can be associated with even larger decrements in force – conditions that may promote functional changes that precede noticeable loss in muscle mass, as may be the case in our study (**10).** Indeed, in other works, muscle dysfunction is only marginally correlated with muscle atrophy in those in ESRD (stage 5 CKD), with these patients demonstrating poorer muscle function for a given muscle mass (**27**).

Recent studies have shown that impaired exercise capacity is induced prior to development of muscle atrophy, and theorize that this is mainly caused by mitochondrial dysfunction in muscle (**67**). Indeed, this is substantiated in a recent rodent model of CKD showing that in intermediate-stage CKD nephrectomy mouse, there were elevated uremic toxin intermediates (specifically indoxyl sulfate – IS) that stimulate myostatin, atrogin-1, and decreased Akt phosphorylation and exercise capacity, that all contribute to atrophy (**67**). However, upon administration of AST-120, a drug that impairs IS action by inhibiting its pro-reactive oxygen species stimulation on skeletal muscle mitochondria, exercise capacity was restored, along with mitochondrial function and muscle mass (**67**). These results suggest that mitochondrial redox stress is a key mechanistic link between poor kidney function and impaired muscle performance, findings that are reflected in our results.

We show significant increases in mitochondrial LEAK state respiration with progression of CKD, that remains even after normalizing to mitochondrial number (CS). The electron transport chain (ETC) is tasked with continual re-synthesis of ATP through generation of a proton gradient and proton-motive force between the mitochondrial matrix and intermembrane space (**68).** Loss of membrane potential, however, results when protons move back toward the matrix via non-specific leaks, often at specific ETC complexes or through channels such as the mitochondrial permeability transition pore (MPTP) or voltage-dependent anion channel (VDAC) (**69).** Leaking and uncoupling

is determined in part by efficiency of electron transfer. Reduced mitochondrial ETC activity causes cellular ROS production, as electrons accumulate in the early stages of the transport chain (primarily at complex 1), where they can be donated directly to molecular oxygen to give rise to superoxide anion (**70,71)**. Given our findings that complex-1 specific respiratory function (even after normalizing to CS) is impaired as early as stage 3 CKD, and to a greater extent in later stages, the presumable complex 1 deficit may cause electron leak at this protein, and increase ROS production and accumulation observed in this study. Indeed, other research has clearly demonstrated that superoxide radicals are largely produced from ETC complex 1 deficiencies as complex 1 marks the entry point for electron transport and proton gradient generation (**72,73).** Thus, in our study, while complex-1 mediated respiration is significantly diminished in stage 3 CKD, LEAK/ROS production appears elevated, though not to a significant extent until stages 4 and 5 CKD. In this respect, perhaps complex-1 deficiencies develop early in disease and contribute to steadily increasing ROS, which may further exacerbate ETC-complex dysfunction.

Indeed, it is now well established that mitochondrial ROS promotes mtDNA and nuclear DNA mutations in genes encoding ETC subunit proteins, and ROS itself directly damages specific ETC subunits to alter their respiratory function **(73,74).** Recent elegant studies have shown, using mass spectrometry and BN-Page, the effects of age-related mitochondrial ROS production on specific protein subunits of quadriceps mitochondrial ETC enzymes. They found that ROS specifically carbonylates FE-S subunit 1 and 2 of Complex 1, SDHA subunit of complex-2, and COX1 subunit of complex 4, that all related to decreased mitochondrial oxidative function (**73)**. Indeed, others have demonstrated that impairment in complex-1 function by as little as 20%, corresponds to ~10% decline in whole-mitochondrial respiration and oxidative function (**74).** Similar results have been demonstrated in $5/6^{th}$ nephrectomy rodent models of CKD, in which increased

skeletal muscle ROS relates strongly to impaired mitochondrial respiration, and poor ATP production (**75).** Moreover, prolongued ROS exposure, as may be the case in our study, has been shown to contribute to widening of the MPTP (**69).** This creates a positive feedback loop whereby ROS production promotes increased mitochondrial inner membrane permeability, exacerbating proton leak and subsequent ROS production. However, the clinical implications of our findings of increased LEAK and potential redox stress with progression of CKD, are striking. We found very strong relationships between mitochondrial respiratory function, and muscle performance measures (torque production/strength, power, and endurance).

Increased ROS in studies of CKD animals, results in declines in muscle specific-force, alters myofilament function, and promotes muscle fatigue (**76,77,78).** Others have observed similar findings, in which skeletal muscle exposure to ROS (ie. H2O2) reduces myofibrillar calcium sensitivity, calcium uptake, action potential amplitude, impairs sarcoplasmic reticulum calcium release, and carbonylates myosin heavy chain protein, thereby drastically reducing cross-bridge force production at the single fiber and whole-muscle levels (**79, 27, 80, 81).** Similarly, muscle fiber exposure to ROS prolongues time-to-peak tension and half-relaxation time - mechanisms that severely hamper muscle fiber power production (**81**). Thus, while we did not probe single-fiber contractile capacity or calcium-related contraction mechanics, these studies may provide potential mechanistic explanations for our findings between mitochondrial dysfunction and muscle force-generation impairments with CKD progression. Muscle endurance, similarly, is negatively affected by chronic-disease-associated ROS signaling. However, LEAK-state respiration, as studied in our participant samples may also be indicative of impaired coupling of electron transport to ATP-production, and as mentioned previously, premature proton leaking through mitochondrial membranes.

We demonstrate significant step-wise declines in the respiratory control ratio(RCR) with CKD progression, an index in which larger values indicate better coupling between the phosphorylation system and ATP-production. Interestingly, Roshanravan and colleagues (2016) determined, using 31-p MRS of the first dorsal interosseous muscle of non-diabetic CKD patients with mean eGFR of 39 mL/min (stage 3) compared to controls, that the mean mitochondrial coupling ratio was 34% lower in those with CKD (**82).** We report here, a strikingly similar 39% reduction from early to middle stage CKD (stage 3) in the RCR coupling index, albeit using different methodology, and this remained after normalizing for mitochondrial number (CS). Moreover, we find that this coupling deficit grows to a 63% reduction in late-stage CKD (39% lower than those in stage 3). Thus, skeletal muscle mitochondrial coupling efficiency appears significantly impaired early in CKD in those with T2DM. Once again however, this poor coupling may explain, in part, the poor resistance to fatigue exhibited with progression of CKD in our study – as mitochondrial uncoupling is associated with greater fatigability, reduced muscle endurance, and requires higher energy expenditure to accomplish the same physical tasks (**83,27)**. This, in conjunction with the aforementioned connections between increased LEAK and muscle deficits, may also lend mechanistic explanation for the reductions in gait speed seen with disease progression in our sample, along with impairments in repeatedly rising from a chair -- as those in middle and later stages of disease may bear a higher metabolic cost to complete these functional tasks.

As mentioned previously, the mitochondrial ROS production/exposure cycle may promote deficiencies in specific ETC complexes that further deteriorate ATP production capacity and energetic supply for skeletal muscle. However, we find significant reduction in complex-4 enzyme activity in middle and late-stage CKD (compared to stages 1 and 2), and a strong negative trend in complex-2 activity beginning in middle stage disease as well, before significant increases in LEAK

respiration. Moreover, we show strong positive correlations between the function of these complexes and renal function across the spectrum of filtration rates. While the underlying mechanism for our findings of complex-specific deficits with CKD progression, remains unclear, these results are supported by mitochondrial modeling data and rodent studies. In rats with 5/6th nephrectomy, after 12 weeks, the investigators discovered complex-4 enzyme activity to be reduced 13% in the gastrocnemius, with subunit 4 of the complex being significantly reduced in abundance (**84).** Other studies, albeit in younger populations with ESRD, have also found depressed complex-4 activity in skeletal muscle mitochondria (**85**). Though a seemingly small effect, computer modeling has shown that for every 5% decline in complex 4 function, maximal oxidative phosphorylation declines 1%, independent of other complexes (**74)**. While the negative trend in complex 2 enzymatic function remains to be confirmed with a larger sample size, our strong downward trend suggests that complex 2 deficits may also be present in the skeletal muscle mitochondria of those with the condition, even early on. Complex 2 is the only ETC component that is entirely encoded by mtDNA- hence, DNA mutations potentially caused by ROS exposure, may have a disproportionately larger impact on the function of this enzyme, and this warrants further study. However, CKD-associated uremic biproducts (indoxyl sulfate-IS, indole-3-acetic acid, etc.) have also been shown to inhibit mitochondrial complex-2 by as much as 20%, while indole-3-acetic acid specifically decreases electron transport capacity (ETS) by 18% **(86).** Similarly, we show deficits in ETS capacity beginning in stage 3 CKD, whicht remains deficient in later stages. It is theoretically plausible that these CKD-induced environmental exposures, over a prolonged period of time, may promote epigenetic re-programming of both mitochondrial and nuclear genes that govern mitochondrial function and organization to ultimately negatively impact mitochondrial ATP-production. The significant upregulated GO and KEGG gene pathways in middle and late-stage CKD (Figure 7)

suggest that epigenetic modification in skeletal muscle may be a ripe area for future investigation in this disease.

Thus, perhaps the uremic environment contributes directly to complex-specific deficits that together with increased LEAK and potential ROS production and uncoupling, results ultimately in impaired mitochondrial oxidative phosphorylation capacity. Our results demonstrate significant declines in mitochondrial oxidative phosphorylation capacity across stages of CKD, which may simply reflect a culmination of the aforementioned specific mitochondrial deficits. Once again however, our results reflect the animal literature that demonstrate state-3 mitochondrial respiration (maximal oxidative phosphorylation) to be impaired 39% in nephrectomy rats – as we found 27% reduction in stage 3, and 43% reduction in late-stage compared to stages 1 and 2 (**84).**

The skeletal muscle transcriptome analysis lends further support for mitochondrial respiratory and coupling deficits observed with CKD progression. Interestingly, the most significantly altered KEGG pathway or GO term in late-stage CKD was that of oxidative phosphorylation and electron transport chain function (Figure 7,A). As demonstrated, the oxidative phosphorylation gene network was downregulated with a striking mean log 2 fold change of -8. More specifically, this downregulation of genes governing oxidative phosphorylation spanned a wide range of critical mitochondrial regulatory functions. However, in middle stage CKD (stage 3), transcriptional differences are most evident in metabolism pathways, with contributions from altered gene expression in networks governing mitochondrial genome maintenance and protein synthesis (Figure 7,B).

Those in late-stage CKD (stages 4&5) demonstrate a global downregulation in genes encoding key mitochondrial electron transport chain subunits (Figure 6, 7A, 8). Differential

transcription or deficiencies in these mitochondrial subunits can have profound consequences for mitochondrial electron transport and respiration (**87**). As shown in Figures 7A,8, and table 5, those in late-stage CKD demonstrate significantly reduced expression of two complex 1 subunit genes (MTND3, MTND6), one subunit of complex 3 (MT-CYB), five subunits of complex 4 (COX5A, MT-CO3, COX6A2, COX7A2, MT-CO2), and four subunit proteins of complex 5 (MT-ATP6, MT-ATP8, ATP5MC3, ATP-MC1). Moreover, these muscles demonstrate significant reduction in expression of key complex assembly proteins (SURF1 – complex 4 assembly, and NDUFAF2 – complex 1 assembly) (Table 5). These results lend potential mechanistic insights into enzymatic results demonstrating significantly reduced complex 4 enzyme activity in later-stage CKD (FIG.4D), as RNA-seq data clearly indicates that complex 4 may be significantly impacted through inadequate subunit transcription and/or deficient complex assembly, a finding that echoes previous results in a rodent CKD-model (**84**). However, although not as diffuse across the ETC as later-stage transcriptional changes, we find reduced expression of NDUFAB1 in stage 3 CKD - a key complex 1 subunit charged with electron transfer from complex 1 to the ubiquinone carrier (**88**) (Figure 7B, Table 6). Others have demonstrated similar reductions in expression with aging, suggesting that this may be implicated in age-related increase in ROS production, and as shown here, potentially a player in CKD-associated respiration deficiencies and LEAK (**88**). Moreover, similar to late-stage CKD, we find reduced expression of complex assembly gene TMEM70 in stage 3 CKD - a key player in ATP-synthase biogenesis (**89**) (Figure 7B, Table 6). Indeed, it is well understood that mitochondrial functional deficiencies may disrupt nuclear and mitochondrial transcription, which may then negatively influence mitochondrial function to manifest a negative feedback cycle (**90**). Thus, while it is unclear whether these gene expression changes precede or follow mitochondrial respiratory deficits, deficient electron transport chain subunit protein transcription, and translation

may be a key mechanistic explanation for the mitochondrial deficits observed in late-stage CKD. However, beyond reductions in expression of these key subunits, their import to the mitochondria is also critical for mitochondrial function. As mitochondria are not formed de novo, nuclear-derived transcripts must translocate into the mitochondria via the TIM23 and TOM20 mitochondrial transporters (**91**).

Our results demonstrate, however, reductions in TIMM17A – an essential component of TIM23 – responsible for protein import into the mitochondria, in stages 4&5 CKD muscle (**91**) (Figure 7A, Table 5). It has been previously shown that TIMM17A expression is reduced under cellular stress conditions, resulting in impaired mitochondrial protein construction and stress signaling related to the mitochondrial unfolded protein response (**91**). Conversely, muscle in stage 3 demonstrates reduced expression of CSNK2A2 – a phosphorylator (activator) of the TOM20 mitochondrial ETC subunit protein importer (**92**) (Figure 7B, Table 6). When considered along with our finding of reduced expression of GRPEL2 and MRPL12 – a vital activator of mitochondrial RNA polymerase, this suggests potentially deficient protein transport and protein transcription in mitochondria in stage 3 CKD skeletal muscle (**93**,**94**).

As mentioned above, stress conditions that impair mitochondrial protein transport may be promoted by the increase in LEAK respiration observed in CKD progression, and potential accompanying ROS production. Interestingly, in stage 4&5 CKD muscle, the GPD2 gene was significantly upregulated - an electron transfer protein the shuttles electrons to the COQ carrier for complexes 1 and 2 (**95**). Given our findings of significantly reduced complex 1 function, and increased electron LEAK, and now transcriptomic evidence for upregulation of GPD2 – a protein known to contribute to electron backflow to complexes 1 and 2 and subsequent electron leak and ROS production, this may serve as a potential contributing mechanism to such cellular and

mitochondrial stress in late-stage CKD muscle (**95**). Moreover, we also find elevated expression of TP63 – a p53 family protein that stimulates ROS production through REDD1 gene pathways, and a reduction in the ROS-inhibiting TIGAR (**96**,**97**).

However, while not as prominent a finding in the transcriptome analysis, muscle in stage 3 CKD exhibits reduced expression of SOD2, the superoxide dismutase ROS scavenger (Figure 7B, Table 6). Also downregulated in stage 3, was TSPO – a gene expression pattern indicative of oxidative stress, as this is a cellular attempt at limiting mitochondrial permeability transition pore enlargement – a major site of electron leak, in the presence of oxidative stress (**98**) (Figure 7B, Table 6). Thus, in stage 3 CKD, while not significantly elevated above stages 1&2 CKD, LEAK and accompanying ROS may be poorly buffered secondary to SOD deficiency, thus causing compensatory limiting of mtPTP size via TSPO downregulation. This mechanism, though plausible given our transcript expression data, warrants further investigation. However, it is well understood that cellular stress signaling that may disrupt mitochondrial protein import and synthesis may derive from more than mitochondrial ROS production, and may also relate to skeletal muscle damage and metabolic signaling pathways.

Indeed, we report significant reductions in SH3BGRL3 expression in late-stage CKD muscle, a key gene governing sarcomere assembly at the z-disc (Figure 7A, Table 5.) (**99**). Additionally, we observe reduced expression of the myostatin and TGF-beta inhibitor DCN, which also promotes mitochondrial biogenesis (**100**). Lastly, we also observe significant upregulation of MDM2 – an E3 ubiquitin ligase that activates the FoXO3 atrophy pathway. Intriguingly however, elegant work by Arena and colleagues (2018), recently demonstrated that MDM2 is imported into skeletal muscle mitochondria, and impairs mitochondrial respiration and dynamics via repression of MT-ND6 complex 1 subunit transcription, with subsequent complex 1 deficits and increased ROS production,

and downstream impairment in skeletal muscle fatigue resistance (**101**). Specifically, the authors demonstrate that MDM2 impairs complex-1 mediated state 3 respiration (using glutamate, malate, pyruvate) by ~36%, a deficiency bearing striking similarity to our own ~48% reduction in complex-1 state 3 respiration in late-stage CKD with accompanying downregulation of MT-ND6. These results represent an intriguing potential mechanism observed in our study – later-stage (4&5) CKD upregulates the E3-ubiquitin ligase MDM2, an atrophy-pathway activator, which simultaneously impairs mitochondrial complex 1 function via attenuation of the production of its subunit-6 protein, to ultimately impair muscle performance. This potential mechanism is an exciting area of future study. Thus, given our genomic results, skeletal muscle integrity may be impaired in later-stages of CKD, potentially more so at the z-disc - a theory supported by other findings of z-disc streaming in uremic muscle (**102,103**), with disinhibition of atrophy signaling (via myostatin and TG-beta) that is detrimental to muscle health and mitochondrial function. However, the stage 3 skeletal muscle transcriptome suggests poor lipid handling and metabolism may play a more influential role in muscle integrity and quality than the implicated structural deficiencies of late-stage muscle.

Stage 3 CKD muscle exhibited striking reduction in adiponectin gene expression (Figure 7B, Table 6). Adiponectin plays a key role in mitochondrial fat metabolism via AMPK phosphorylation, while also negatively regulating TNF-alpha expression and inhibiting NF-KB signaling through cAMP-dependent pathway (**104**). It has been demonstrated previously, that reduced ADIPOQ expression results in increased oxidative stress, and inflammation (**104**). This finding is intruiging, especially when paired with the striking reductions in PPARG and leptin gene expression, as skeletal muscle secreted leptin, induced by PPARG, stimulates mitochondrial fatty acid oxidation via AMPK as well, and protects against adipose tissue accrual within skeletal muscle (IMAT) and suppresses skeletal muscle lipotoxicity (**105**). The substantial reduction in expression of these genes in stage 3

may predictably result in impairment in mitochondrial handling of fatty acid oxidation that may contribute to muscle adipose tissue accrual, and inflammatory pathway activation. Potential myocellular adipose accumulation may also be a consequence of the observed LDLR deficiency, STARD4, and ABCD2 downregulation, as all of these genes play key roles in fatty acid mitochondrial import and lipid metabolism (**106**, **107**, **108**) . Such alterations in mitochondrial metabolism may promote a different set of muscle health issues in middle-stage CKD.

Lastly however, muscle and mitochondrial health depends on a balance between mitochondrial synthesis and degradation (mitophagy). Our respiration results demonstrate increased LEAK-state respiration, and poor coupled respiration (Figure 5A, Table 4) that suggests these mitochondria may have a deregulation of membrane potential. With loss of membrane potential or increased ROS production, PINK1 protein is stabilized on the mitochondrial membrane, whereby it recruits Parkin to ubiquitinate and degrade defective mitochondrial proteins and also signal the autophagasome to sequester and degrade the defective mitochondria (**109**). This autophagasome is formulated, in-part through the interaction of BCL2 and BECN1 (Beclin-1) protein, with Beclin-1 dissociation from BCL2 activating autophagasome formation and autophagy of deficient mitochondria (**109**). However, we observe significant reductions in expression of PINK, and BECN1 and BCL2 genes in stages 4&5 CKD muscle, suggesting mitophagy and general autophagy may be attenuated in late-stage CKD (Figure 7A, Table 5). This may promote accumulation of defective mitochondria, and could partially explain the non-significant difference in mitochondrial abundance in this stage (Figure 4A,B), as mitochondria are not being degraded, and deficient mitochondria accumulate to result in poor muscle respiration (**109**). However, in such an environment with increased concentration of deficient mitochondria, cells may upregulate mitochondrial fusion genes to remodel mitochondria to maintain energy homeostasis, and indeed, in late-stage CKD muscle, we

observe significantly increased expression of mitochondrial-membrane protein MSTO1, a newly discovered player in mitochondrial fusion (Figure 7A, Table 5) (**110**,**111**). Similarly, we also observe reduced expression of PINK1 in stage 3 CKD. Interestingly, in stage 3 CKD, we also observe reduced BAG4 expression – an anti-apoptotic stress protein that negatively regulates PARKIN, a PINK-ligand that assists in autophagy of mitochondrial proteins and whole-mitochondria (**112**). The downregulation of BAG4 may be in response to mitochondrial damage, to activate mitophagy, however, with insufficient PINK transcription, mitophagy may be deficient in stage 3 CKD muscle. However, further investigation is required to followup on these findings to determine the effects of CKD on mitochondrial turnover and quality control pathways.

Divergent from late-stage transcriptome changes, middle-stage CKD exhibits consistently downregulated genes that play a role in mitochondrial and nuclear DNA maintenance. Specifically, we observe deficits in RRM2B, DNA2, and SLC25A33 gene expression – all genes that participate in mitochondrial genome maintenance, and repair, and govern mtDNA stability, with DNA2 specifically serving as the predominant means of repairing small mitochondrial DNA lesions induced via oxidative stress (**113**, **114**, **115**) (Figure 7B, Table 6). SLC25A33 is of particular interest in that it also plays a key role in regulation of mitochondrial membrane potential and regulates mitochondrial DNA replication/transcription, and governs the ratio of mitochondrial:nuclear encoded protein components of the ETC (**115**, **116**). Its downregulation may promote an environment of dysregulated mitochondrial membrane potential, dynamics, and altered protein incorporation. Mitochondrial regulation requires maintenance of the mitochondrial membrane potential for importing nuclear encoded proteins involved in mitochondrial respiration, DNA replication and transcription, and similar to late-stage CKD muscle, we find reductions in gene expression of other key import/export related mechanisms aside from the TIM/TOM proteins.

SLC35F6, dowregulated in stage 3 CKD muscle, stimulates mitochondrial membrane potential via interaction with inner-membrane bound ATP transporter ANT2, to transport ATP out of the cytosol and ADP into the matrix (**117**). Its reduced expression may result in poor membrane potential regulation, and altered ATP:ADP ratios that may promote shifts in metabolism and altered respiration. This de-regulation of mitochondrial membrane potential may be exacerbated by our findings of reduced BCL2L1, a BCL2 family member, located in the outer membrane to regulate mitochondrial VDAC opening. VDAC opening controls the production of ROS and release of cytochrome C, and inducers of apoptosis, with a loss of BCL2L1 regulation resulting in increased VDAC opening and subsequent permeation pathway creation for metabolites, electrons, and apoptotic proteins into and out of the mitochondria (**118**). This pathway constitutes a potential theoretical mechanism for the uremic milleui to infiltrate and negatively influence mitochondrial function, and for electron slippage and ROS generation.

Thus, the skeletal muscle transcriptome highlights mitochondrial structure, function, and signaling as significant downregulated processes in both middle and late-stage CKD muscle. These findings lend potential mechanistic insights to support the respiratory deficits and coupling inefficiency observed in mitochondria with CKD progression. While this study marks the first use of transcriptomics to track skeletal muscle biological changes in CKD stages, these gene pathways require further study to more completely elucidate the direct connections between gene expression and mitochondrial function in this disease.

Conclusion-

T2DM-induced CKD progression, and its associated uremic environment, independent of diabetic severity or duration, negatively impacts physical function, potentially via impairment of

muscle force generation, power, and reduced fatigue resistance. We demonstrate, for the first time, that these muscle performance decrements strongly relate to intrinsic mitochondrial functional deficits that begin early in stage 3 CKD, which may in-turn, derive from altered expression of gene networks involved in mitochondrial respiration, structure, and turnover pathways. Further investigation is needed to probe the quality of skeletal muscle in CKD and its progression, and investigations aimed at determining the precise genomic and epigenetic influences of the uremic environment on specific mitochondrial-governing genes is needed, and an exciting avenue of future research.

Tables for Chapter 2:

TABLE 1	Stage 1&2 (60+ mL/min)	Stage 3 (30-59 mL/min)	Stage 4&5 (<29 mL/min)	P-value
Gender (M,F)	**7,2**	**6,3**	**5,4**	**Fishers Exact (p=.47)**
Age (SD)	**55 (9.8)**	**61 (6.4)**	**62 (7.3)**	**1-way ANOVA (p=.13)**
BMI (SD)	**33.5 (5.6)**	**33.7 (5.6)**	**38.9 (6.3)**	**1-way ANOVA (p=.10)**
Years of DM (SD)	**14 (6.3)**	**13 (7.6)**	**17 (7)**	**1-way ANOVA (p=.37)**
HbA1c (SD)	**8.01 (2.1)**	**7.85 (1.8)**	**7.5 (2.1)**	**1-way ANOVA (p=.88)**
Neuropathy (Yes, No)	**5,4**	**5,4**	**5,4**	**1-way ANOVA (p=.8)**
Whole-body lean mass (kg)	**59.24 (10.1)**	**55.64 (14.7)**	**57.08 (9)**	**1-way ANOVA (p=.8)**
OGTT AUC (SD)	**40180 (10911)**	**47394 (11510)**	**39752 (12010)**	**1-way ANOVA (p=.37)**
HOMA (SD)	**5.9 (3.8)**	**3.8 (3.1)**	**3.8 (3.6)**	**1-way ANOVA (p=.5)**
BUN (SD)	**18 (2.95)**	**31.2 (6.55)**	**58.2 (21)**	**1-way ANOVA (p<.001) *Stage 1&2 vs. Stage 3 ^Stage 1&2 vs. Stage 4&5 #Stage 3 vs. Stage 4&5**
Albumin:Creatinine (ACR)	**279 (530)**	**729 (1100)**	**1086 (790)**	**1-way ANOVA p=.16**
Kidney Function (eGFR)	**87.8 (20.1)**	**46.3 (7.4)**	**18.9 (7.6)**	**1-way ANOVA (p<.01) *Stage 1&2 vs. Stage 3 ^Stage 1&2 vs. Stage 4&5 #Stage 3 vs. Stage 4&5**

TABLE1 – Demographics.

Participant demographics were compared using 1-way ANOVA, and chi-square was used for sex distribution, and peripheral neuropathy status between groups. Values listed are mean and standard deviation in (). The following symbols represent post-hoc pairwise comparisons in the event of significant F-test - *(between Stage 1&2 and Stage 3), ^(between stage 1&2 and Stage 4&5), #(Between stage 3 and Stage 4&5)

Table 2

	eGFR	PPT Score	Hip Extensor Torque (30^0/sec)	Knee Extensor Torque (30^0/sec)	Knee Extensor Work (fatigue)	BUN	Chair Rise Score	50-ft walk time
eGFR	r=1 p=----	r=.805 p<.001	r=.821 p<.001	r=.795 p<.001	r=.83 p<.001	r=-.768 p<.001	r=.761 p=.005	r=-.68 p<.001
PPT Score	r=.805 p<.001	r=1 p=----	r=.68 p<.001	r=.722 p<.001	r=.74 p<.001	r=-.877 p<.001	r=.87 p<.001	r=-.95 p<.001
Hip Extensor Torque (30^0/sec)	r=.821 p<.001	r=.68 p<.001	r=1 p=----	r=.898 p<.001	r=.823 p<.001	r=-.549 p<.001	r=.723 p<.001	r=-.608 p<.001
Knee Extensor Torque (30^0/sec)	r=.795 p<.001	r=.722 p<.001	r=.898 p<.001	r=1 p=----	r=.904 p<.001	r=-.551 p<.001	r=.784 p<.001	r=-.651 p<.001
Knee Extensor Work (fatigue)	r=.83 p<.001	r=.74 p=.003	r=.823 p=.002	r=.904 p<.001	r=1 p=----	r=-.635 p<.001	r=.769 p<.001	r=-.654 p<.001
BUN	r=-.761 p<.001	r=-.877 p<.001	r=-.55 p<.001	r=-.55 p<.001	r=-.635 p<.001	r=1 p=----	r=-.697 p<.001	r=.821 p<.001
Chair Rise Score	r=.761 p=.005	r=.87 p<.001	r=.723 p<.001	r=.784 p<.001	r=.769 p<.001	r=-.697 p<.001	r=1 p=----	r=-.789 p<.001
50-ft walk time	r=-.68 p<.001	r=-.95 p<.001	r=-.608 p<.001	r=-.651 p<.001	r=-.654 p=.001	r=.821 p<.001	r=-.789 p<.001	r=1 p=----

TABLE 2- Correlation Matrix. Bivariate pearson correlation coefficients were calculated between measures of physical function (PPT score, Chair Rise Score, 50-ft. walk time), muscle performance (Hip and knee extensor torque, knee extensor work fatigue), and serum chemistries (eGFR, BUN). Color coding is as follows --

r= (-.25)-(-.5), r=(-.5)-(-.75), r=(-.75)-(-1) , r=.25-.5, r=.5-.75, r=.75-1

Table 3

	Stage 1&2 (60+ mL/min) n=5	Stage 3 (30-59 mL/min) n=5	Stage 4&5 (<29 mL/min) n=3	P-value
LEAK (L) respiration (normalized to CS activity – pmol/sec/mg/CS)	**.325 (.06)**	**.44 (.06)**	**.82 (.12)**	**1-way ANOVA (p<.05) ^Stage 1&2 vs. Stage 4&5 #Stage 3 vs. Stage 4&5**
Complex 1 respiration (normalized to CS activity – pmol/sec/mg/CS)	**4.3(.54)**	**3.46(.46)**	**2.9(.6)**	**1-way ANOVA (p=.018) ^Stage 1&2 vs. Stage 4&5 -power analysis: 10 subjects needed per stage to reach stage-wise significance**
Max Oxphos Capacity (P) (normalized to CS activity – pmol/sec/mg/CS)	**7.52(.87)**	**5.7(.72)**	**5.4(.55)**	**1-way ANOVA (p=.004) *Stage 1&2 vs. Stage 3 ^Stage 1&2 vs. Stage 4&5**
Max ETS Capacity (E) (normalized to CS activity – pmol/sec/mg/CS)	**9.3(1.3)**	**6.9(.97)**	**7.2(.31)**	**1-way ANOVA (p=.001) ^Stage 1&2 vs. Stage 4&5 #Stage 3 vs. Stage 4&5**
Correlations				
			eGFR (mL/min)	
LEAK (normalized to CS)			**r=-.75 (p<.001)**	
Complex 4 Enzyme Activity			**r=.53 (p=.02)**	
Complex 1 respiration (normalized to CS)			**r=.82 (p<.001)**	
Max Oxphos (P) (normalized to CS)			**r=.81 (p<.001)**	

TABLE 3- Top: Mitochondrial respiration normalized to mitochondrial content (citrate synthase activity) performed on a 13-participant subset of the study population, was compared across stage groups using 1-way ANOVA. Values listed are mean and standard deviation in (). The following symbols represent post-hoc pairwise comparisons in the event of significant F-test - *(between Stage 1&2 and Stage 3), ^(between stage 1&2 and Stage 4&5), #(Between stage 3 and Stage 4&5). Bottom: Bivariate Pearson Correlations were calculated to compare respiration measures/states normalized to mitochondrial content (citrate synthase activity) with renal filtration rate (eGFR), and mitochondrial ETC complex 4 enzyme activity was also correlated.

Table 4

	Stage 1&2 (60+ mL/min)	Stage 3 (30-59 mL/min)	Stage 4&5 (<29 mL/min)	P-value
Oxidative phosphorylation control ratio (P/E), (SD)	**.79 (.07)**	**.81(.036)**	**.67(.15)**	**1-way ANOVA (p=.017) ^Stage 1&2 vs. Stage 4&5 #Stage 3 vs. Stage 4&5**
Respiratory Control Ratio (RCR) (P/L), (SD)	**22 (4.3)**	**13.1 (2.4)**	**7.9 (3.2)**	**1-way ANOVA (p<.001) *Stage 1&2 vs. Stage 3 ^Stage 1&2 vs. Stage 4&5 #Stage 3 vs. Stage 4&5**
Phosphorylation Control Ratio -PCR (L/P), (SD)	**.047 (.007)**	**.078 (.015)**	**.15 (.08)**	**1-way ANOVA (p=.001) *Stage 1&2 vs. Stage 3 ^Stage 1&2 vs. Stage 4&5**
Oxidative Phosphorylation Coupling Efficiency Ratio OPC ((L-P)/P), (SD)	**-.95 (.007)**	**-.92 (.015)**	**-.84(.08)**	**1-way ANOVA (p=.001) ^Stage 1&2 vs. Stage 4&5 #Stage 3 vs. Stage 4&5**
ETS Coupling Efficiency ((E-L)/E), (SD)	**.963 (.007)**	**.936 (.01)**	**.908 (.026)**	**1-way ANOVA (p<.001) *Stage 1&2 vs. Stage 3 ^Stage 1&2 vs. Stage 4&5 #Stage 3 vs. Stage 4&5**

TABLE 4- CKD-stage groups were compared in mitochondrial flux control ratios using 1-way ANOVA. Letters denote the following – P = max oxidative phosphorylation capacity (State 3-C1+C2), E = ETS capacity, L = state2-C1 (LEAK). Values listed are mean and standard deviation in (). The following symbols represent post-hoc pairwise comparisons in the event of significant F-test - *(between Stage 1&2 and Stage 3), ^(between stage 1&2 and Stage 4&5), #(Between stage 3 and Stage 4&5)

Table 5

Stage 4&5 vs. Stage 1&2 Significant GO and KEGG terms: selected genes	
Oxidative Phosphorylation	
SPATA18 (+1.5x)	encodes a p53-induced protein that induces lysosomal eliminiation of oxidized mitochondrial proteins, contributing to mitochondrial quality control. Responsible for repairing or degrading unhealthy mitochondria in response to mitochondrial damage. Involved also in degradation of damaged mitochondria by promoting MIV vacuole formation that engulf and degrade unhealthy mitochondria via lysosomes. Upregulation could be indicative of the prescense of diffuse intra-mitochondrial damage in late-stage ckd muscle.
PINK1 (-1.34x)	part of the pink/parkin2 mitophagy pathway, whereby pink1 must accumulate on outer membrane of defective mitochondria where it activates parkin2, which then recruits autophagy receptors like p62 causing them to be shuttled to the autophagasome for degradation. Lack of pink1 can lead to impaired mitophagy
BCL2 (-1.4x)	autophagy regulatory protein -- autophagasome formation requires the interaction of BCL2 and BECN1 (Beclin-1) protein, with Beclin-1 dissociation from BCL2 activating autophagasome formation and autophagy of deficient mitochondria
BECN1 (-1.3x)	part of mitochondrial autophagy pathway. Forms crucial component of phagaphore which targets and removes defective mitochondria. Downregulation leads to impaired mitophagy and poor mitochondrial turnover
MSTO1 (+1.6x)	cytoplasmic protein and interacts with the mitochondrial fusion machinery. Important component required for mitofusion of damaged mitochondria
TP63 (+1.61x)	encodes a member of the p53 family of transcription factors - p63. p63 regulates REDD1 gene transcription, which stimulates ROS production/increase. Thus, increased p63 increases ROS via REDD1
TIGAR (-1.72x)	p53 target, protects against oxidative stress in muscle cells by inhibiting glycolysis and decreasing ROS levels. It regulates intracellular ROS levels and if reduced, results in increased ROS production, and enhanced sensitivity to stress-related apoptosis
TIMM17A (-1.23x)	essential component of TIM23 that is responsible for protein import into the mitochondria. TIMM17A is reduced under stress conditions -- results in the impaired biogenesis of mitochondrial proteins that depend on TIM23 and triggers stress-induced signaling pathway related to the mitochondrial unfolded protein response (mtUPR).
Electron Transport Chain	
GPD2 (+1.8x)	a respiratory chain dehydrogenase that transfers electrons to COQ. ROS producer that normally shuttles cytoplasmic reducing equivalents to complex 1. Can often promote reverse electron flow back to complex 1 or complex 2, and has been shown to a major site of electron leak. FROM The function and the role of the mitochondrial glycerol-3-phosphate dehydrogenase in mammalian tissues
MTND3 (-1.42X)	encodes core subunit 3 of complex 1 -- NADH dehydrogenase
MT-ND6 (-1.4x)	encodes subunit 6 (nqo6) of complex 1 -- NADH dehydrogenase
NDUFAF2 (-1.3x)	encodes complex 1 assembly factor
MT-ATP6 (-1.46x)	encodes subunit 6 of complex 5-- ATP synthase
MT-ATP8 (-1.4x)	encodes subunit 8 of complex 5 -- ATP synthase
ATP5MC1 (-1.3x)	encodes subunit c of complex 5 proton channel
ATP5MC3 (-1.3x)	encodes subunit c of complex 5
MT-CYB (-1.4x)	encodes subunit 3 of complex 3 – Coenzyme Q (CoQ)
COX5A (-1.3x)	encodes subunit 4 of complex 4 -- Cytochrome C Oxidase (COX)
MT-CO2 (-1.35x)	encodes subunit 2, of complex 4 – Cytochrome C Oxidase (COX): subunit 2 transfers electrons to the core of the complex
COX6A2 (-1.3x)	encodes subunit 6a2 of complex 4 – Cytochrome C Oxidase (COX): subunit 6a2 regulates assembly of cytochrome c oxidase
MT-CO3 (-1.31x)	encodes subunit 3 of complex 4 – Cytochrome C Oxidase (COX): subunit 3 serves as the core of the complex
COX7A2 (-1.3x)	encodes subunit 7a-L of complex 4 – Cytochrome C Oxidase (COX)
SURF1 (-1.3x)	a 30 kDa transmembrane protein localized in the inner mitochondrial membrane. SURF1 promotes the association of COX2 with the COX assembly intermediate composed of COX1, COX4 and COX5A. Reduced expression may hinder construction of COX complex (complex 4) of the ETC
Muscle structural Integrity	
SH3BGRL3 (-1.4X)	in sarcomere asembly, Enah protein loclizes to the z-line to provide construction assistance for sarcomere assembly. Lack of SH3BGRL3 gene expression results in insufficent Enah protein recruitment to z-disc for sarcomere construction
DCN (-2.1x)	decorin protein. counters the action of myostatin, and TGF-beta mediated fibrosis. Also promotes mitochondrial biogenesis via PGC-1a
MDM2 (+1.7)	member of E3 ubiquitin ligase, activates FOXO3 atrophy pathways. MDM2 gets imported into mitochondria to control respiration and mitochondrial dynamics, and represses transcription of NADH-dehydrogenase6 (MT-ND6) which inhibits complex 1 activity and enhances mitochondrial ROS production

Table 5 (above)

Table of significantly differentially expressed genes from Figure 7A (genes down or upregulated in late-stage CKD vs. early stage 1&2), their relative fold change, and their basic function listed to the right.

Table 6

Stage 3 vs. Stage 1&2 Significant GO and KEGG terms: selected genes	
Lipid Localization	
TSPO (-1.4x)	Promotes transport of cholesterol across mitochondrial membranes and may play a role in lipid metabolism. TSPO plays a central role in regulation of mitochondrial function modulating the crosstalk between inner membrane anion channel (IMAC) and permeability transition pore. In response to oxidative stress, and impaired antioxidant systems, TSPO is downregulated to prevent excessive superoxie anion efflux from the mitochondrial matrix and as an attempt to ensure the permeability transition pore is not enlarged
ADIPOQ (-7.4x)	involved in the control of fat metabolism and insulin sensitivity,with anti-inflammatory activities. Stimulates AMPK phosphorylation and activation in skeletal muscle, enhancing glucose utilization and fatty-acid combustion. Antagonizes TNF-alpha by negatively regulating its expression in and also by counteracting its effects. Inhibits NF-kappa-B signaling through a cAMP-dependent pathway. Muscle with reduced ADIPOQ shows increased oxidative stress, inflammation. Restoration of adiponectin alleviates oxidative stress and inflammation in skeletal muscle
LEP (-4.8X)	leptin stimulates fatty acid oxidation in muscle via aAMPK, resulting in decreased IMAT accrual and suppresses lipotoxicity
STARD4 (-2.55x)	play a role in lipid metabolism
LDLR (-2.5x)	deficiency leads to elevated LDL levels and myocellular adipose accumulation
ABCD2 (-2.3x)	peroxisomal import of fatty acids into mitochondria
PPARG (-1.4x)	stimulates adiponectin production from muscle (pairs with the reduced adipoq). Also plays role in mitochondrial biogenesis
Mitochondrial Organization	
MRPL12 (-2.4x)	encodes mitochondrial ribosome, for mitochondrially encoded protein transcription. Loss of mitochondrial ribosomes would impair transcription of key mitochondrial-encoed proteins.
SLC25A33 (-1.3x)	mitochondrial transporter that participates in mt genome maintenance, and regulation of mitochondrial membrane potential and mitochondrial respiration. With IGF-1 stimulation, it can regulate cell growth and proliferation by controlling mitochondrial DNA repcliation and transcription, AND controls the ratio of mitocondria-to-nuclear encoded components of the ETC, resulting in control of mitochondrial ROS
TMEM70 (-2.4x)	encodes a protein that plays a role in biogenesis of mitochondrial ATP synthase. Impaired expression can result in reduced oxidative phosphorylation via inadequate ATP-synthase
RRM2B (-1.8x)	nuclear-encoded mitochondrial maintenance gene, and repair of damaged mitochondrial DNA.
DNA2 (-1.8x)	encoded protein is a conserved helicase/nuclease involved in the maintenance of mitochondrial and nuclear DNA stability
CTTN (-1.6x)	encodes cortactin protein, which has been postulated, though still debated, to play a role in mitochondrial fission. Downregulation may impede mitochondrial quality control mechanisms, specifically attenuating mitochondrial division
SLC35F6 (-1.6x)	mitochondrial biogenesis requires maintenance of mitochondrial membrane potential for importing nuclear-encoded proteins involved in oxphos, mtDNA replication and transcription. SLC35F6 stimulates mitochondrial membrane potential by interacting with ATP transporter ANT2 embedded in the mitochondrial inner membrane to transport ATP out to the cytosol while importing ADP into the mitochondrial matrix
CSNK2A2 (-1.44x)	CSNK2 phosphorylates TOMM receptor complex (TOMM is responsible for recognition and translocation of synthesized mitochondrial precursor proteins, and its phosphorylation is mandatory for TOMM biogenesis and proper mitochondrial protein import. Loss of TOMM phosphorylation can result in impaired protein subunit import into mitochondria
GRPEL2 (-1.52x)	essential component of the "presequence translocase-associated motor" complex (PAM), that regulates protein import into the mitochondrial matrix. It also binds to several essential regulators of mitochondrial function. It also interacts with longevity-regulating mitochondrial Hsp70, and is also linked to mitochondrial function. It stimulates Hsp70, and plays a role in mitochondrial unfolding response
Oxidative phosphorylation	
NDUFAB1 (-1.94x)	nuclear-encoded subunit of complex 1, functions in the transfer of electrons from NADH to chain. Reduces in expression with age, potentially connected to complex-1 respiratory deficiencies
PINK1 (-1.4X)	part of the pink/parkin2 mitophagy pathway, whereby pink1 must accumulate on outer membrane of defective mitochondria where it activates parkin2, which then recruits autophagy receptors like p62 causing them to be recruited to the autophagasome for degradation. Lack of pink1 can lead to impaired mitophagy. FROM Increased mitophagy in the skeletal muscle of spinal and bulbar muscular atrophy patients. PINK1 also controls mitochondrial fission, and if fission is interfered with, this leads to increased oxidized proteins and decreased mitochondrial respiration. With lack of PINK1, PARKIN cant efficiently localize to damaged mitochondria
SOD2 (-1.63x)	encodes superoxide dismutase 2, anti-oxidant that scavenges superoxide radicals ROS products. If downregulated, could result in inefficient ROS handling. Reducing SOD2 leads to fragmentation of mitochondria
BCL2L1 (-1.5x)	BCL2L1 proteins belong to BCL2 family, located in the outer mitochondrial membrane and regulate mitochondrial membrane VDAC opening, which regulates mitochondrial membrane potential, and thus controls the production of ROS and release of cytochrome C, inducers of cell apoptosis. Loss of BCL2L1 would promote increased VDAC opening. permeation pathway for metabolites and mobile ions between the cytosol and mitochondria. VDACs are also involved in cell death by interacting with apoptotic proteins and releasing apoptotic metabolites to the cytosol
BAG4 (-1.4x)	encodes mitochondrial-expressed stress protein Bag-4 that is anti-apoptotic. It is a negative regulator of PARKIN translocation following mitochondrial damage.PARKIN gets recruited to PINK1 sites on mitochondria to degrade them
STAT2 (-1.3x)	required for DRP-1 mediated mitochondrial fission, resulting in altered mitochondrial morphology. Reduced STAT2 results ins altered JAK-STAT pathway signaling, and reduced mitochondrial fission
TMEM70 (-2.4x)	essential role in biogenesis of mitochondrial ATP synthase (complex 5)
NCF2 (-1.8x)	protects against cell apoptosis vai beneficial p53-stimulated ROS production. If downregulated, results in increased cell apoptosis
NDUFV3 (+1.6x)	May be the terminally assembled subunit of Complex I. Could be compensatory increase

Table 6 (above)

Table of significantly differentially expressed genes from Figure 7B (genes down or upregulated in middle-stage CKD vs. early stage 1&2), their relative fold change, and their basic function listed to the right.

Figures for Chapter 2:

Figure 1

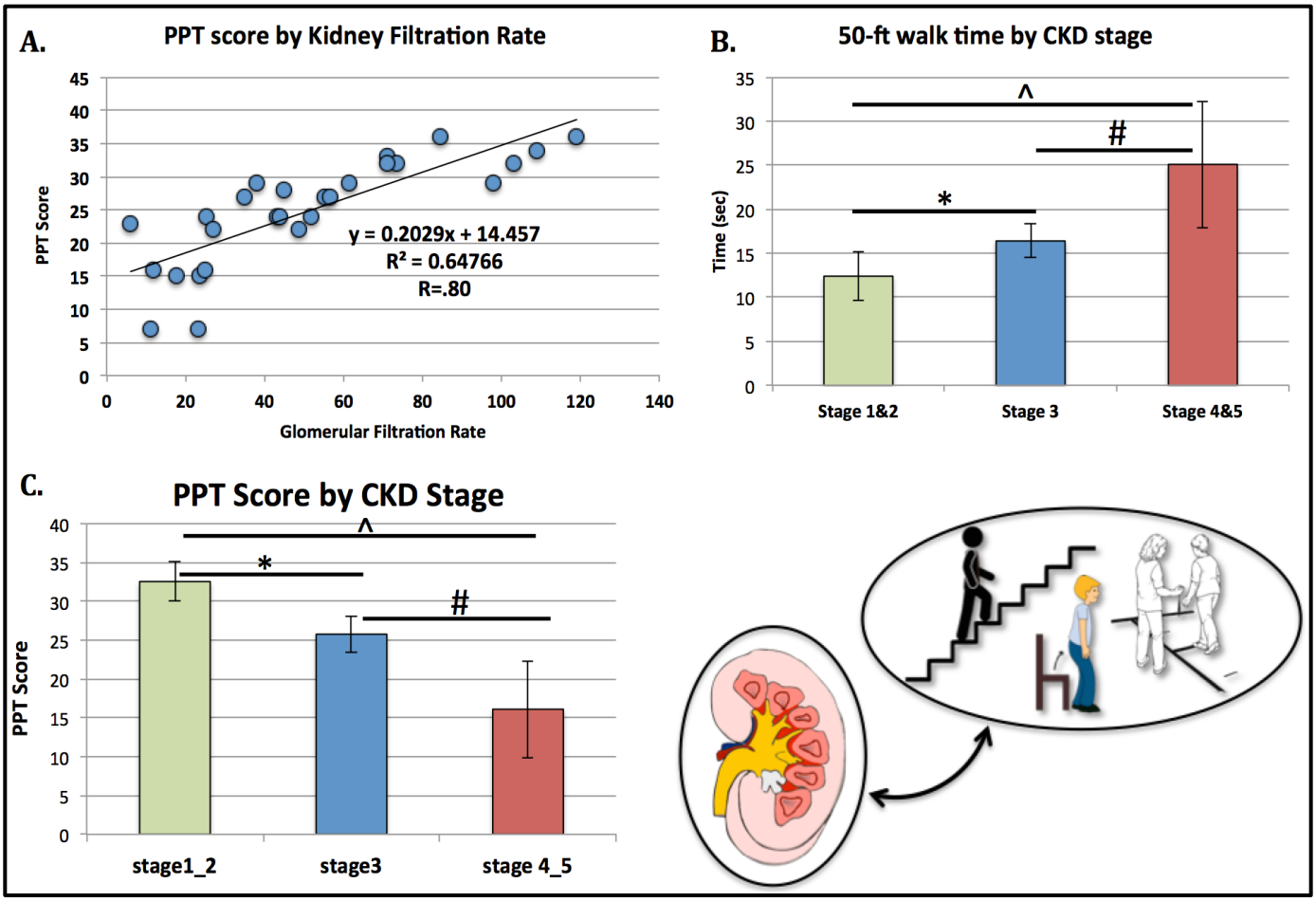

FIGURE 1 – Physical function capacity was assessed across CKD-stage groups with 1-way ANOVAs. Bar heights represent group mean and error bars represent ± SD. The following symbols represent significant post-hoc tests of pairwise comparisons: *(between Stage 1&2 and Stage 3), ^(between stage 1&2 and Stage 4&5), #(Between stage 3 and Stage 4&5). A. Pearson Bivariate Correlation with eGFR (glomerular filtration rate) plotted on the x-axis, and PPT score (0-36) plotted on the y-axis (higher scores indicate better functional performance) (not pictured – $p<.001$). B. 50-ft walk time, higher values indicate slower gait speed. C. PPT (physical performance test) score ($F=36$, $p<.001$).

Figure 2

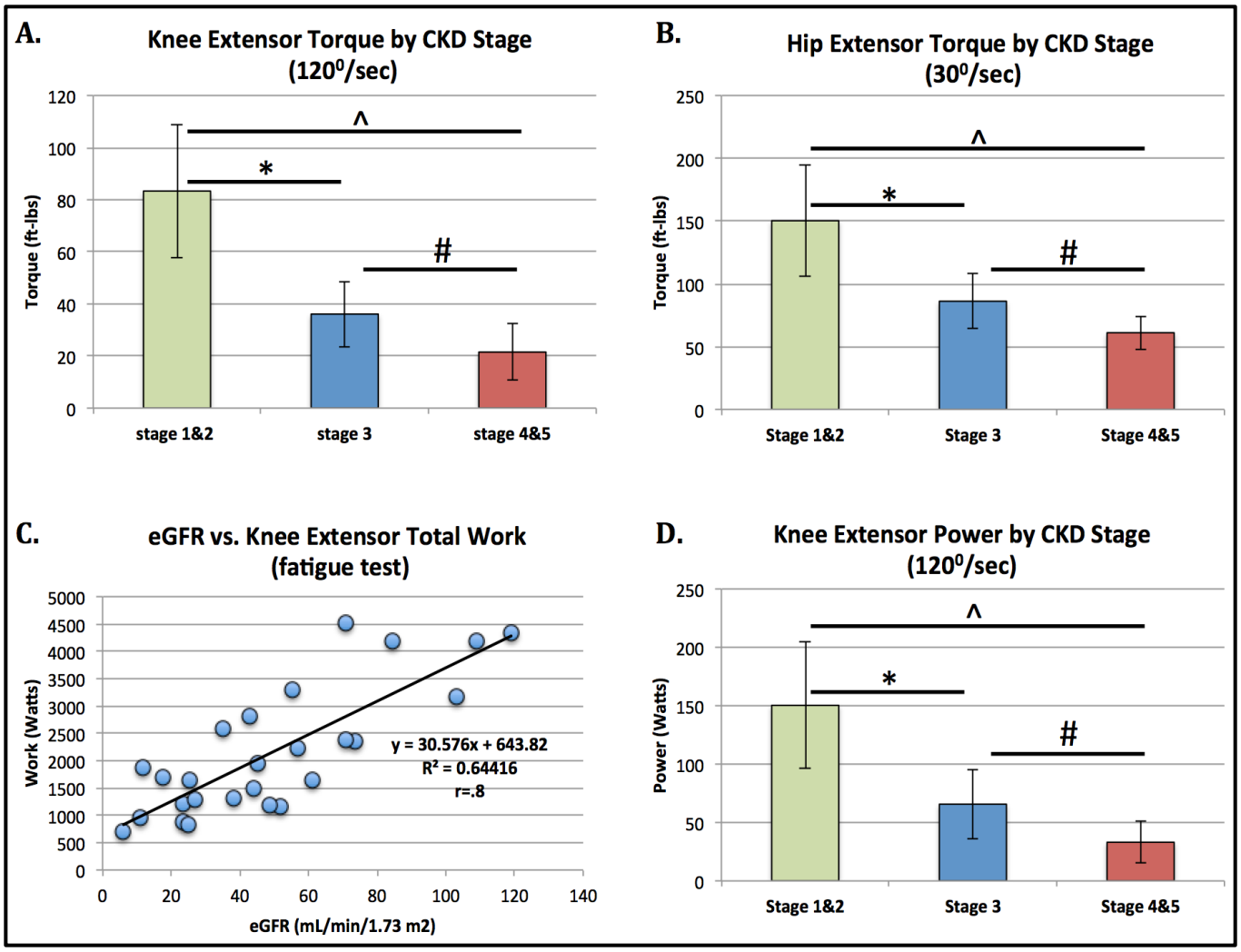

FIGURE 2-

Lower extremity muscle strength (hip extensor, knee extensor torque), and knee extensor power were assessed across CKD-stage groups with 1-way ANOVAs. Bar heights indicate group means, with errors bars indicating ± SD. The following symbols represent significant post-hoc tests of pairwise comparisons: *(between Stage 1&2 and Stage 3), ^(between stage 1&2 and Stage 4&5), #(Between stage 3 and Stage 4&5). A. Group differences in knee extensor torque (assessed at isokinetic speed of 120^0/sec, knee extensor torque measured in ft-lbs) ($F=20$, $p<.001$). B. Hip extensor torque (30^0/sec, ft-lbs) ($F=22$, $p<.001$). D. Knee extensor power (30^0/sec, measured in watts) ($F=11$, $p<.001$). C. Pearson correlation plotting total knee extensor work over fatigue task (50 repeated contractions) (measured in watts- Y axis), against renal filtration rate (eGFR – X axis) ($p<.001$).

Figure 3

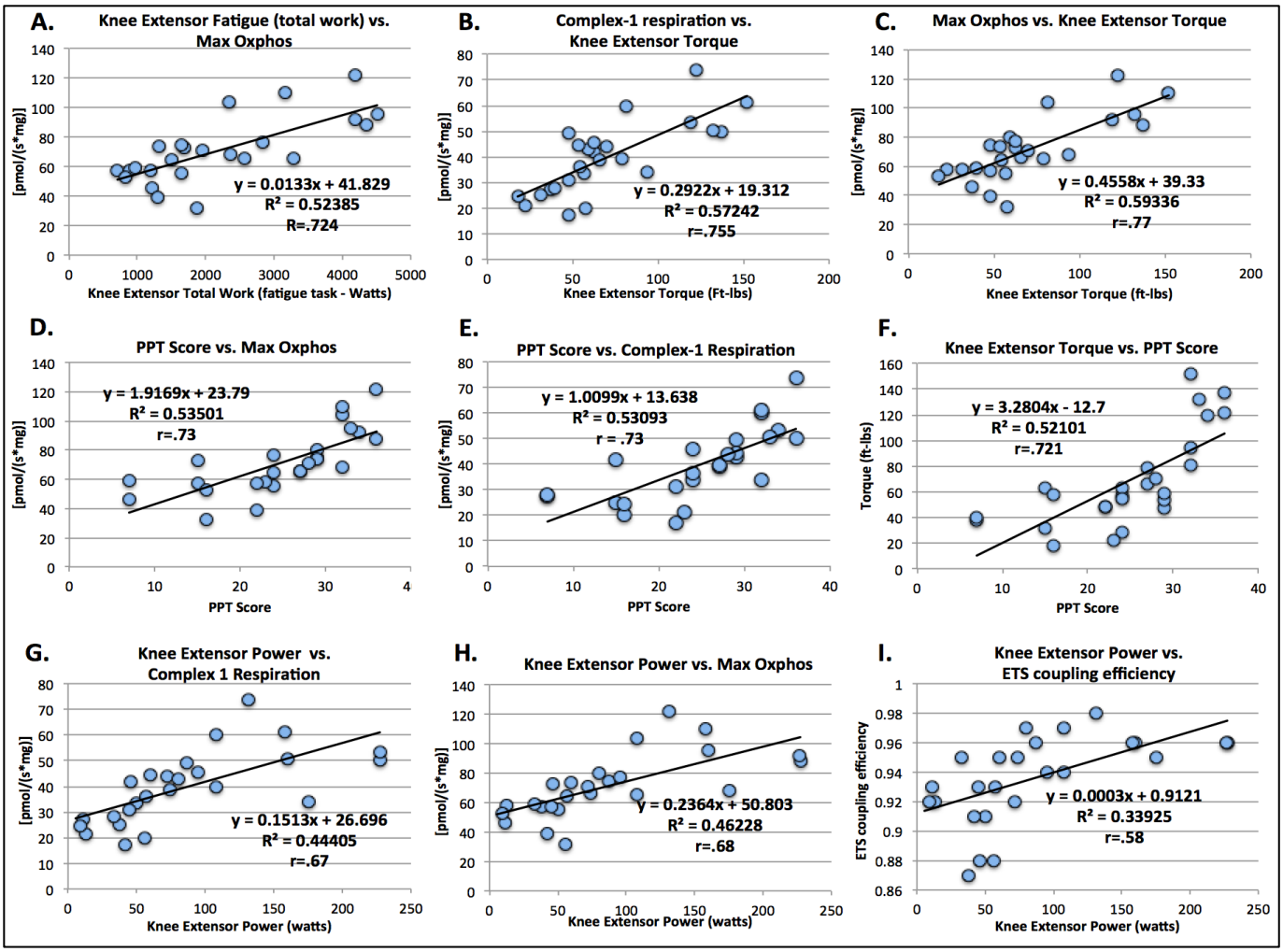

FIGURE 3- Bivariate pearson correlation plots depicting interrelationships between mitochondrial respiration states, muscle performance, and physical function. All depicted correlations are significant ($p<.05$). Abbreviations: Max Oxphos (State3-C1+C2), Complex-1 respiration (State3-C1), ETS coupling efficiency (ETS capacity/ aka E). Knee extensor power was assessed as in Figure 2 (120^0/sec isokinetic speed), with knee extensor torque assessed in ft-lbs.

Figure 4

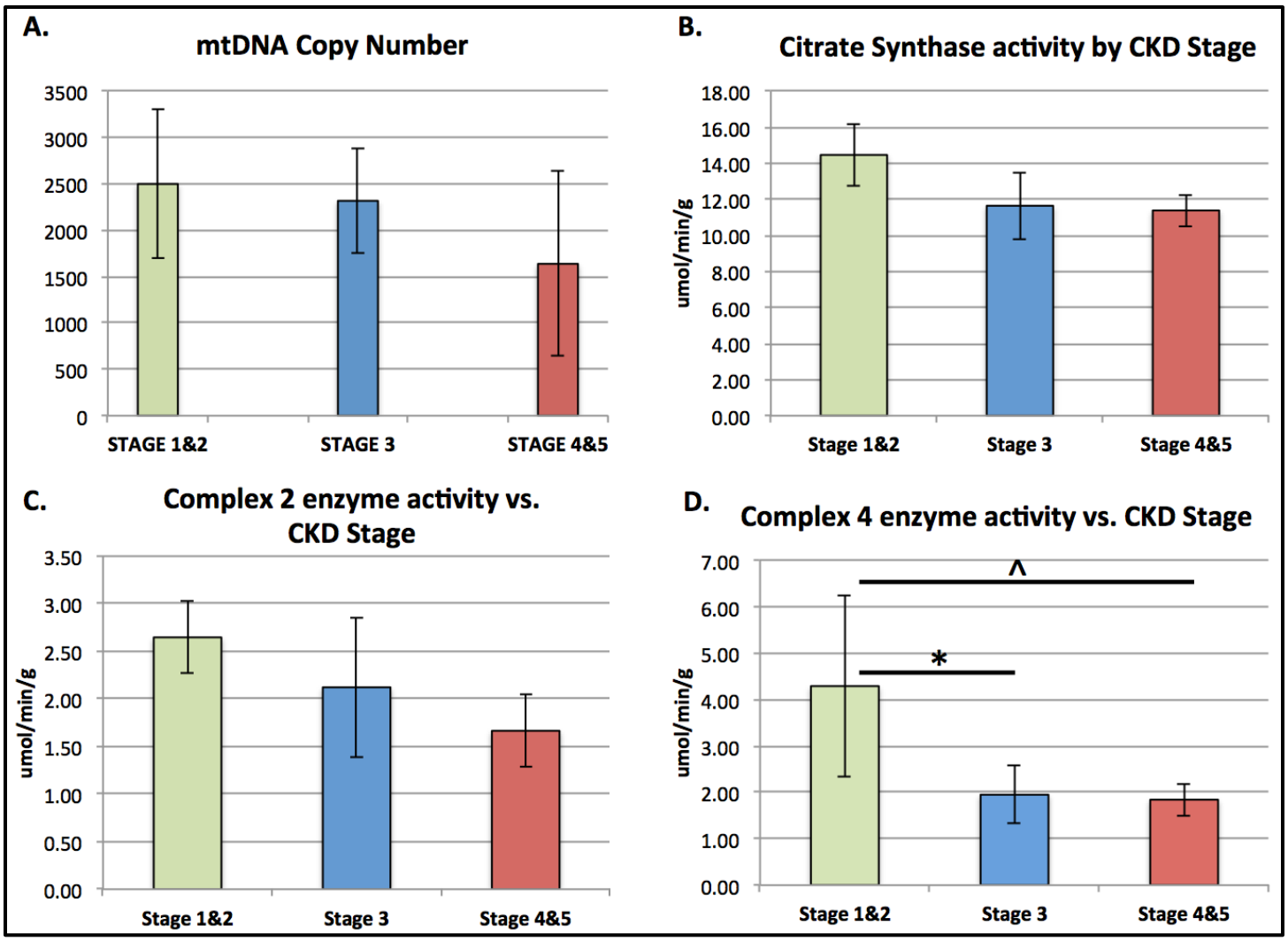

FIGURE 4 – Analysis of mitochondrial density, number, and ETC complex enzyme activity. **A.** Mitochondrial DNA copy number, y-axis is unitless (F=3, p=.07), all samples were included in mtDNA copy number analysis (n=26) depicting no significant difference between CKD stage groups. For remaining analysis (B-D), analysis was performed on a 13-participant subset of samples (Stage 1&2 n=5, Stage 3 n=5, Stage 4&5 n=3). **B.** Citrate synthase enzyme activity assessment. Y-axis = umol/min/gram muscle. as in A, no significant differences were observed between groups (F=1.2, p=.33). **C.** Mitochondrial ETC complex 2 (Succinate Dehydrogenase – SDH) enzyme activity measured in umol/min/g (y-axis), an assessment of complex-2 specific function in isolation. Although there appears to be a trend, there is no significant difference between CKD stage groups in complex 2 function (F=3, p=.08). **D.** Mitochondrial ETC complex 4 (Cytochrome Oxidase - COX) enzyme activity measured as in C (umol/min/g). The 1-way ANOVA F-test was significant (F=5.1, p=.02), with post-hoc tests revealing significant differences between stages 1&2 and 3 (*, p<.05), and stages 1&2 and 4&5 (^, p<.05).

Figure 5

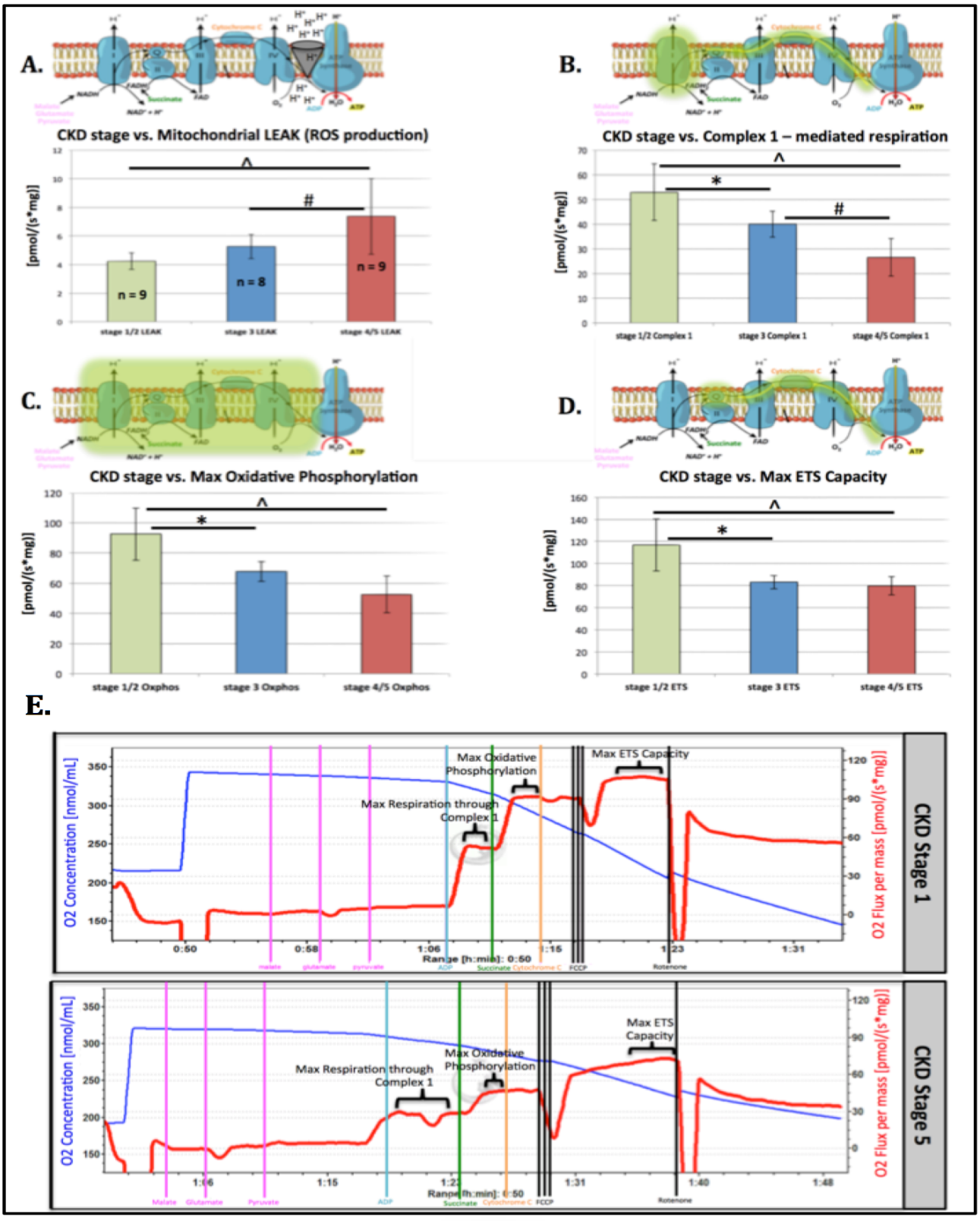
A.
CKD stage vs. Mitochondrial LEAK (ROS production)
[pmol/(s*mg)]
n = 9
n = 8
n = 9
stage 1/2 LEAK
stage 3 LEAK
stage 4/5 LEAK
B.
CKD stage vs. Complex 1 – mediated respiration
[pmol/(s*mg)]
stage 1/2 Complex 1
stage 3 Complex 1
stage 4/5 Complex 1
C.
CKD stage vs. Max Oxidative Phosphorylation
[pmol/(s*mg)]
stage 1/2 Oxphos
stage 3 Oxphos
stage 4/5 Oxphos
D.
CKD stage vs. Max ETS Capacity
[pmol/(s*mg)]
stage 1/2 ETS
stage 3 ETS
stage 4/5 ETS
E.
O2 Concentration [nmol/mL]
O2 Flux per mass [pmol/(s*mg)]
Max Oxidative Phosphorylation
Max Respiration through Complex 1
Max ETS Capacity
Malate
Glutamate
Pyruvate
ADP
Succinate
Cytochrome C
FCCP
Rotenone
CKD Stage 1
CKD Stage 5

FIGURE 5 (above) - Mitochondrial respiration assessment. across CKD-stage groups with 1-way ANOVAs. Bar heights indicate group means, with errors bars indicating ± SD. The following symbols represent significant post-hoc tests of pairwise comparisons: *(between Stage 1&2 and Stage 3), ^(between stage 1&2 and Stage 4&5), #(Between stage 3 and Stage 4&5). All respiration measures are depicted in rate of oxygen consumption per second per mg of tissue wet weight (Y-axis: pmol/s/mg). **A**. LEAK-state respiration between CKD stages ($F=8$, $p=.002$), with stage 1&2 (*) and stage 3 (#) exhibiting significantly less LEAK than late-stage 4&5 ($p<.05$). **B.** Complex 1 respiration (State3-C1) between CKD stages ($F=21$, $p<.001$), with stage 1&2 (^), stage 3(#) significantly higher than late-stage (4&5), and stage 1&2 (*) higher than stage 3. **C.** Maximal ox-phos (State3-C1+C2) between CKD stages ($F=21$, $p<.001$), with stage 1&2(*) being higher than stage 3, and stage 1&2 (^) being higher than stage 4&5 ($p<.05$). **D.** Maximal ETS respiration between stages ($F=15.5$, $p<.001$) with stage 1&2(*) being higher than stage 3, and stage 1&2 (^) being higher than stage 4&5 ($p<.05$). **E.** Representative oxygraph tracings depicting mitochondrial respiration (pmol/s/mg – red trace) over the experimental protocol between mitochondria in early (stage 1) CKD and late (stage 5) CKD, with plateaus labeled according to their respective respiration state (Complex 1 respiration, Maximal oxidative phosphorylation, and maximal ETS). Also depicted are color-coded lines indicating time-specific addition of substrates to the respiration chamber.

Figure 6

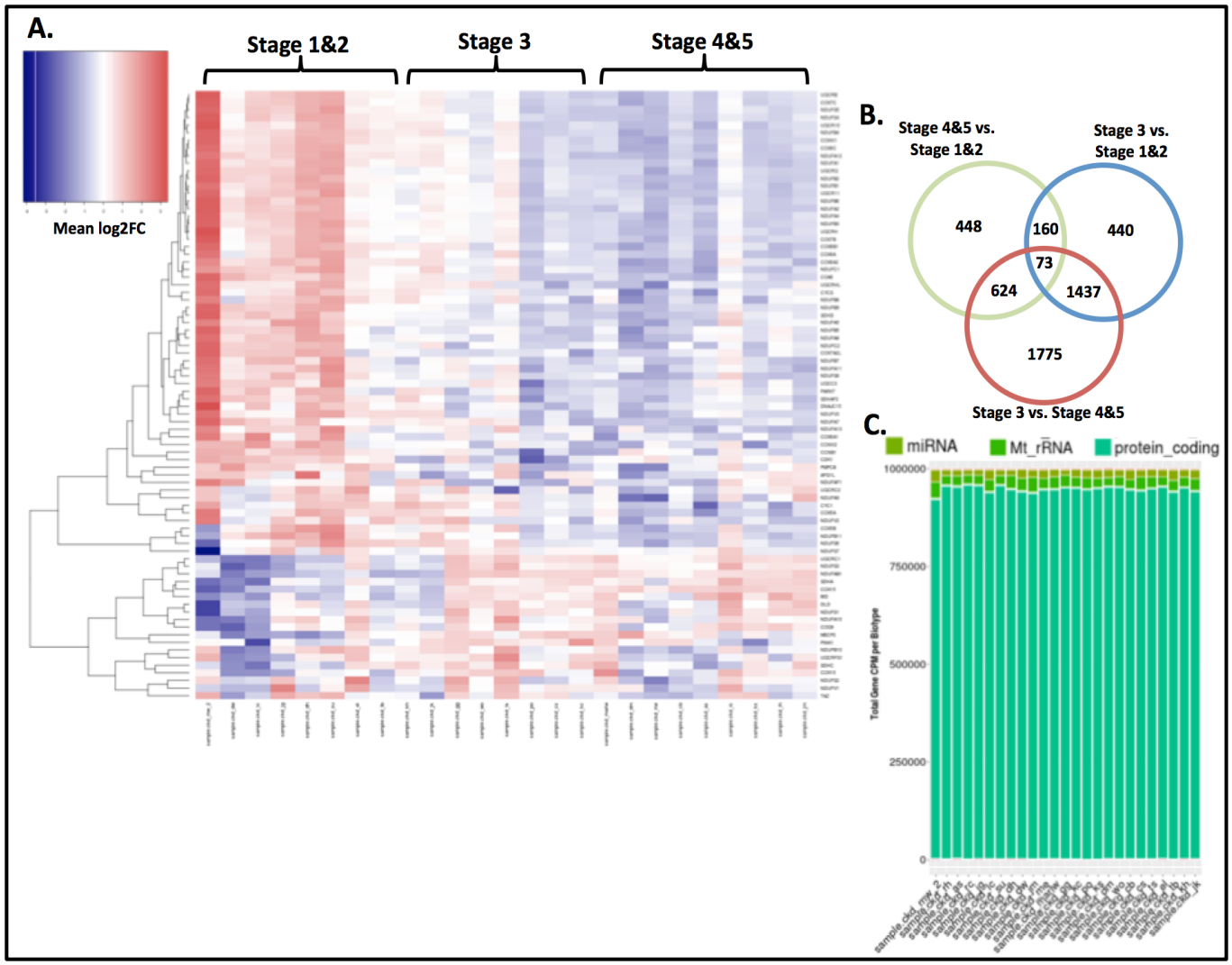

FIGURE 6

RNA-sequencing output detaling overall transcript differences between samples and CKD-stages. **A.** Heat-map depicting significantly differentially expressed genes (p<.05) across all samples. Columns represent participant muscle samples, rows depict genes. Color scheme is shown in the upper left, with increasing shade of red depicting relative upregulated genes, and increasing shade of blue depicting downregulated genes (scale = mean log 2-fold change). The heat map clusters on CKD stage, as shown at top. **C**. Venn diagram depicting the number of significantly differentially expressed genes per condition comparison (green circle = stage 4&5 vs. stage 1 – 448 differentially expressed transcripts) (blue circle = stage 3 vs. stage 1&2 – 440 differentially expressed transcripts) (red circle = stage 3 vs. 4&5 – 1775 differentially expressed transcripts). **C.** Bar graph depicting total gene counts per biotype. Each bar represents the biotype breakdown per participant. The transcripts analyzed contained mostly protein-coding mRNA (teal) across all samples, followed by mitochondrial rRNA (green), and small proportions of miRNA (mustard).

Figure 7

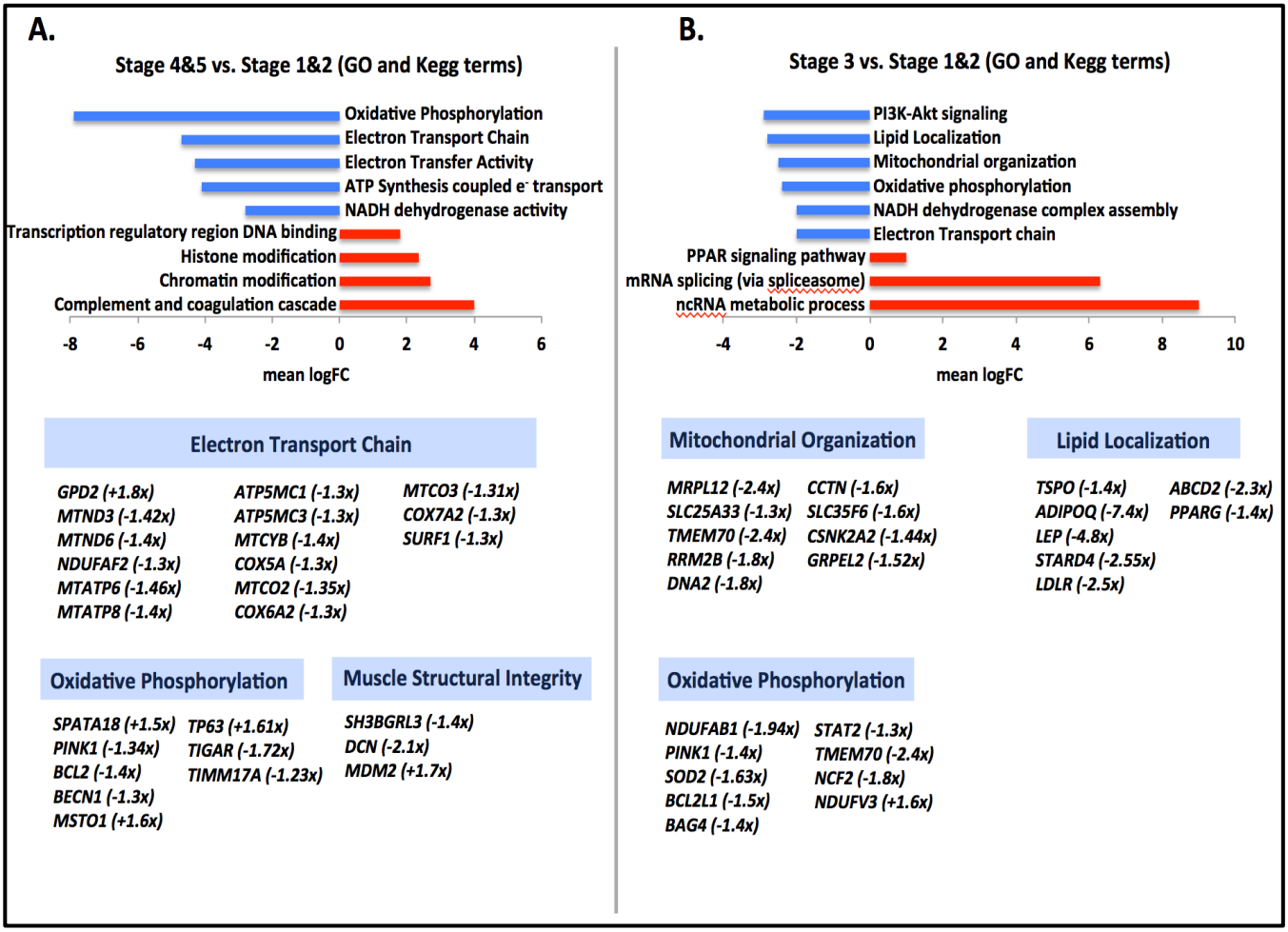

FIGURE 7

Selected GO terms and KEGG pathways from a larger list of top 25 down and upregulated gene networks across stage-wise transcript analysis. Bar charts depict top downregulated (blue bars) or upregulated (red bars) gene networks, with their accompanying network label listed next to its corresponding bar (all GO terms list have FDR ≤.05, and all KEGG terms have p-value <.05). Pathway up or downregulation is expressed in mean log-fold-change units, and was determined to be significant when compared to background log 2 fold change for genes not contained within the network/pathway. Below/bottom are selected genes from the significant GO or KEGG pathways that are differentially expressed, and the fold change listed in parentheses next to the gene term. **A.** Comparing late-stage CKD muscle transcriptome to early stage 1&2 (early CKD is the reference). Oxidative phosphorylation and mitochondrial ATP-synthesis components were significantly downregulated in late-stage CKD compared to early, with specific genes listed at the bottom. **B.** Comparing middle-stage CKD to early stage 1&2 (early is the reference). Metabolic pathways including PI3K-Akt signaling, lipid handling and localization, and oxidative phosphorylation were significantly downregulated in middle-stage CKD compared to early.

Figure 8

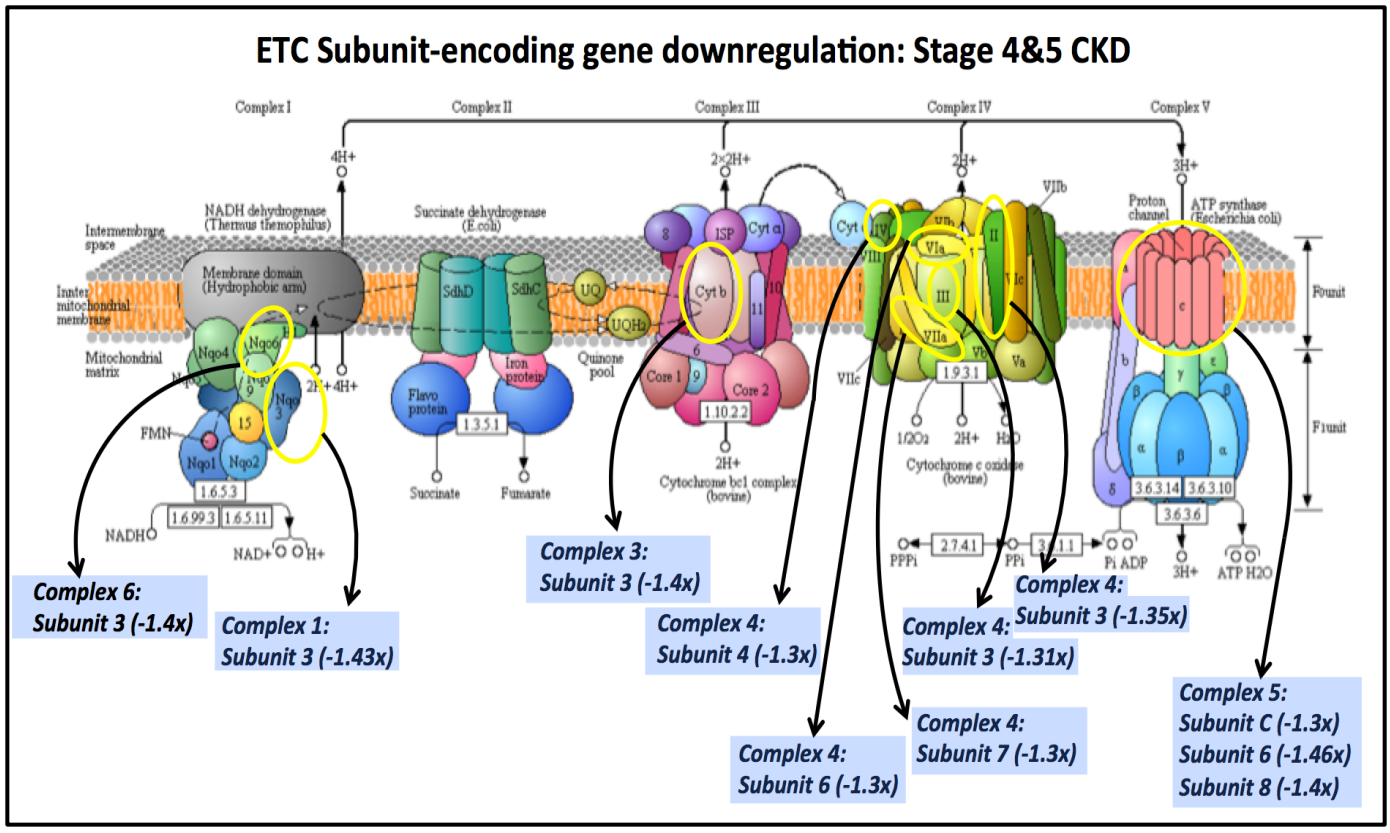

Figure 8

KEGG oxidative phosphorylation pathway annotation for stage 4&5 CKD muscle. Significant selected downregulated genes in the electron transport chain GO term were used to annotate the mitochondrial electron transport chain subunits they encode (subunits circled in yellow, and connected to their corresponding gene with black arrow, and highlighted in blue). Not pictured – NDUFAF2 (complex 1 assembly factor) and SURF1 (complex 4 assembly factor). All listed genes are significantly downregulated in late-stage (4&5) CKD compared to early (stage 1&2).

References

1. Center for Disease Control and Prevention (CDC). National Chronic Kidney Disease Fact Sheet: General Information and National Estimates on Chronic Kidney Disease in the United States, 2014. Atlanta, GA: US Dept. of Health and Human Services, CDC; 2014.

2. Tuomilehto, J., & Wolf, E. (1987) Primary prevention of diabetes mellitus. *Diabetes Care*. 10(2); 238-248.

3. Bailey, R.A., Wang, Y., Zhu, V., & Rupnow, M.F. (2014) Chronic kidney disease in US adults with type 2 diabetes: an updated national estimate of prevalence based on kidney disease: improving global outcomes (KDIGO) staging. *BMC Res Notes*, 7, 415

4. Zapponi, G., Targher, G., Chonchol, M., Ortalda, V., et al. (2012) Predictors of estimated GFR decline in patients with type 2 diabetes and preserved kidney function. *Clin J Am Soc Nephrol*, 7(3); 401-8.

5. Hemmelgarn, B.R., Zhang, J., Manns, B.J., Tonelli, M., et al. (2006) Progression of kidney dysfunction in the community-dwelling elderly. *Kidney Int*, 69(12); 2155-61.

6. Lindeman RD, Tobin J, Shock NW. Longitudinal studies on the rate of decline in renal function with age. J Am Geriatr Soc. 1985 Apr;33(4):278–285

7. Rule AD, Amer H, Cornell LD, et al. The association between age and nephrosclerosis on renal biopsy among healthy adults. Ann Intern Med. 2010 May 4;152(9):561–567

8. Denic, A., Glassock, R.J., & Rule, A.D. (2016) Structural and functional changes with the aging kidney. *Adv Chronic Kidney Dis*, 23(1); 19-28.

9. Roshanravan, B., Gamboa, J., & Wilund, K. (2017) Exercise and CKD: skeletal muscle dysfunction and practical application of exercise to prevent and treat physical impairments in CKD. *Am J Kidney Dis*, 69(6); 837-52.

10. Carrero, J.J., Johansen, K.L., Lindholm, B., et al. (2016) Screening for muscle wasting and dysfunction in patients with chronic kidney disease. *Kidney Int*, 90(1): 53-66.

11. Roshanravan, B., Robinson-Cohen, C., Patel, K.V., Ayers, E., et al. (2013) Association between physical performance and all-cause mortality in CKD. *J Am Soc Nephrol*, 24(5); 822-30.

12**.** Robinson-Cohen C, Katz R, Mozaffarian D, Dalrymple LS, de Boer I, Sarnak M, Shlipak M, Siscovick D, Kestenbaum B. (2009) Physical activity and rapid decline in kidney function among older adults. *Arch Intern Med*. 169:2116–2123

13. Robinson-Cohen, C., Littman, A.J., Duncan, G.E., et al. (2014) Physical activity and change in estimated GFR among persons with CKD. *J Am Soc Nephrol*, 25(2); 399-406.

14. Robinson-Cohen, C., Katz, R., Mozaffarian, D., et al. (2009) Physical activity and rapid decline in kidney function among older adults. *Arch Intern Med*, 169(22): 2116-2123.

15**.** Toyama K, Sugiyama S, Oka H, Sumida H, Ogawa H (2010) Exercise therapy correlates with improving renal function through modifying lipid metabolism in patients with cardiovascular disease and chronic kidney disease. *J Cardiol* 56: 142–146

16. McManus, D., Slipak, M., Ix, J.H., Ali, S. et al. (2007) Association of cystatin c with poor exercise capacity and heart rate recovery: data from the heart and soul study. *Am J Kidney Dis*, 49(3); 365-72.

17. Diesel, W., Noakes, T.D., Swanepoel, C., & Lambert, M. (1990) Isokinetic muscle strength predicts maximum exercise tolerance in renal patients on chronic hemodialysis. *Am J Kidney Dis*, 16(2): 109-14.

18. Otobe, Y., Hiraki, K., Hott, C. et al. (2017) The comparison of the muscle strength in pre-dialysis chronic kidney disease patients and the average levels in healthy individuals. *Physical Therapy Japan*, 6(44): 401-407.

19. Roshanravan B, Patel KV, Robinson-Cohen C, et al. (2015) Creatinine clearance, walking speed, and muscle atrophy: a cohort study. *Am J Kidney Dis*. 65(5):737-747.

20. Bittel, D.C., Bittel, A.J., Tuttle, L.J., Hastings, M.K., et al. (2015) Adipose tissue content, muscle performance and physical function in obese adults with type 2 diabetes mellitus and peripheral neuropathy. *J Diabetes Complications*, 29(2); 250-257.

21. Anand, S., Johansen, K.L., & Tamura, M.K. (2014) Aging and chronic kidney disease: the impact on physical function and cognition. *J Gerontol A Biol Sci Med Sci*, 69A(3); 315-322.

22. Wang, X.H., & Mitch, W.E. (2014) Mechanisms of muscle wasting in chronic kidney disease. *Nat Rev Nephrol*, 10(9): 504-16

23. Serratric, G., Toga, M., Roux, H. et al. (1967) Neuropathies, myopathies and neuromyopathies in chronic uremic patients. *Presse Med*, 75; 1835-1838

24. Kaltsatou, A., Sakkas, G.K., Poulianiti, K.P., Koutedakis, Y., et al. (2015) Uremic myopathy: is oxidative stress implicated in muscle dysfunction in uremia. *Front Physiol*, 2015(6); 102.

25. Campistol, J.M. (2002) Uremic myopathy. *Kidney International*, 62(5); 1901-1913.

26. Kosmadakis, G.C., Bevington, A., Smith, A.C. et al (2010) Physical exercise in patients with severe kidney disease. *Nephron Clin Pract*, 115(1): c7-c16.

27. R.L. Marcus, P.C. LaStayo, T.A. Ikizler, *et al.* (2015) Low Physical Function in Maintenance Hemodialysis Patients Is Independent of Muscle Mass and Comorbidity, *J Ren Nutr*, 25 (2015), pp. 371-375

27. Conley, K.E. (2016) Mitochondria to motion: optimizing oxidative phosphorylation to improve exercise performance. *J Exp Biol*, 219(pt2): 243-9.

28. Powers, S.K., Wiggs, M.P., Duarte, J.A. et al. (2012) Mitochondrial signaling contributes to disuse muscle atrophy. *Am J Physiol Endocrinol Metab*, 303(1): E31-9.

29. Zane, A.C., Reiter, D.A., Shardell, M., et al. (2017) Muscle strength mediates the relationship between mitochondrial energetics and walking performance. *Aging Cell*, 16(3): 461-68.

30. Choi S, Reiter DA, Shardell M, Simonsick EM, Studenski S, Spencer RG, Fishbein KW, Ferrucci L (2016) 31P magnetic resonance spectroscopy assessment of muscle bioenergetics as a predictor of gait speed in the baltimore longitudinal study of aging. *J. Gerontol. A Biol. Sci. Med. Sci*. 71, 1638–1645

31. Hoppeler H, Howald H, Conley K, et al. (1985) Endurance training in humans: aerobic capacity and structure of skeletal muscle. *J Appl Physiol*. 59(2):320-327.

32. Siegel MP, Kruse SE, Knowels G, et al. (2011) Reduced coupling of oxidative phosphorylation in vivo precedes electron transport chain defects due to mild oxidative stress in mice. *PLoS One*. 6(11):e26963.

33. Siegel MP, Wilbur T, Mathis M, et al. (2012) Impaired adaptability of in vivo mitochondrial energetics to acute oxidative insult in aged skeletal muscle. *Mech Ageing Dev*. 133(9-10):620-628.

34. Gamboa JL, Billings FT, Bojanowski MT, et al. (2016) Mitochondrial dysfunction and oxidative stress in patients with chronic kidney disease. *Physiol Rep*. 4(9)

35. Brown M, Sinacore DR, Binder EF, Kohrt WM. Physical and performance measures for the identification of mild to moderate frailty. *J Gerontol A Biol Sci Med Sci* 2000; 55:M350–M355

36. Reuben DB, Siu AL. An objective measure of physical function of elderly outpatients: the Physical Performance Test. *J Am Geriatr Soc*.1990;38:1105–12.

37. Reuben DB, Siu AL, Kimpau S. (1992) The predictive validity of self-report and performance-based measures of function and health. *J Gerontol*. 47:M106–10.

38. Tuttle, L.J., Sinacore, D.R., & Mueller, M.J. (2012) Intermuscular adipose tissue is muscle specific and associated with poor functional performance. *J Aging Res*, 2012; 172957

39. Hilton, T.N., Tuttle, L.J., Bohnert, K.L., Mueller, M.J., & Snacore, D.R. (2008) Excessive adipose tissue infiltration in skeletal muscle in individuals with obesity, diabetes mellitus, and peripheral neuropathy: association with performance and function. *Phys Ther*, 88(11); 1336-44.

40. Tuttle, L.J., Hastings, M.K., & Mueller, M.J. (2012) A moderate-intensity weight-bearing exercise program for a person with type 2 diabetes and peripheral neuropathy. *Phys Ther*, 92(1); 133-41.

41. Meyer, C., Corten, K., Wesseling, M. et al. (2013) Test-retest reliability of innovated strength tests for hip muscles. *Plos One.*

42. Kirn, D.R., Reid, K.F., Hau, C. et al. (2016) What is a clinically meaningful improvement in leg-extensor power for mobility-limited older adults. *J Gerontol A Biol Sci Med Sci*, 71(5), 632-6.

43. Worrell, T.W., Karst, G., Adamczyk, D. et al. (2001) Influence of joint position on electromyographic and torque generation during maximal voluntary isometric contractions of the hamstrings and gluteus maximus muscles. *J Orthop Sports Phys Ther*, 31(12); 730-40.

44. Frey-Law, L.A., Laake, A., Avin, K.G. et al. (2012) Knee and elbow 3D strength surfaces: peak torque-angle-velocity relationships. *J Appl Biomech*, 28(6): 726-37.

45. Harbo, T., Brincks, J., & Andersen, H. (2012) Maximal isokinetic and isometric muscle strength of major muscle groups related to age, body mass, height, and sex in 178 healthy subjects. *Eur J Appl Physiol*, 112(1): 267-75

46. Pincivero, D.M., Lephart, S.M., & Karunakara, R.A. (1997) Reliability and prevision of isokinetic strength and muscular endurance for the quadriceps and hamstrings. *Int J Sports Med*, 18(2): 113-7.

47. Roshanravan B, Patel KV, Fried LF, et al. (2017) Association of muscle endurance, fatigability, and strength with functional limi- tation and mortality in the Health Aging and Body Composition Study. *J Gerontol A Biol Sci Med Sci*. 72(2):284-291.

48. Entrekin, K., Work, B., & Owen, J. (1998) Does a high carbohydrate preparatory diet affect the 3-hour oral glucose test in pregnancy. *J Matern Fetal Med*, 7(2): 68-71.

49. Smith, G.I., Yoshino, J., Kelly, S.C., et al. (2016) High-protein intake during weight loss therapy eliminates the weight-loss induced improvement in insulin action in obese postmenopausal women. *Cell Rep*, 17(3): 849-861.

50. Matthews DR, Hosker JP, Rudenski AS, Naylor BA, Treacher DF, Turner RC. (1985) Homeostasis model assessment: insulin resistance and beta-cell function from fasting plasma glucose and insulin concentrations in man. *Diabetologia*. 28:412–419

51. Matsuda, M., & DeFronzo, R.A. (1999) Insulin sensitivity indices obtained from oral glucose tolerance testing: comparison with the euglycemic insulin clamp. *Diabetes Care*, 22(9): 1462-1470.

52. DeFronzo, R.A., & Matsuda, M. (2010) Reduced time points to calculate the composite index. *Diabetes Care*, 33(7): e93.

53. Abdul-Ghani, M.A., Tripathy, D., & DeFronzo, R.A. (2006) Contributions of beta-cell dysfunction and insulin resistance to the pathogenesis of impaired glucose tolerance and impaired fasting glucose. *Diabetes Care*, 29(5): 1130-9.

54. Utzschneider, K.M., Prigeon, R.L., Faulenbach, M.V. et al. (2009) Oral disposition index predicts the development of future diabetes above and beyond fasting and 2-h glucose levels. *Diabetes Care*, 32(2): 335-41.

55. Steensberg, A., van Hall, G., Osada, T., et al. (2000) Production of interleukin-6 in contracting human skeletal muscles account for the exercise-induced increase in plasma interleukin-6. *J Physiol*, 529 (Pt1): 237-242.

56. Rauchhaus, M., Doehner, W., Francis, D.P., et al. (2000) Plasma cytokine parameters and mortality in patients with chronic heart failure. *Circulation*, 102(25): 3060-7.

57. Merriwether, E.N., Host, H.H., & Sinacore, D.R. (2012) Sarcopenic indices in community-dwelling older adults. *J Geriatr Phys Ther*, 35(3): 118-25.

58. Shanely, R.A., Zwetsloot, K.A., Triplett, N.T., et al. (2014) Human skeletal muscle biopsy procedures using the modified bergstrom technique. *J Vis Exp*, (91): 51812

59. Meng, H., Janssen, P.M., Grange, R.W. et al. (2014) Tissue triage and freezing for models of skeletal muscle disease. *J Vis Exp*, (89)

60. Pesta, D., & Gnaiger, E. (2012) High-resolution respirometry: Oxphos protocols for human cells and permeabilized fibers from small biopsies of human muscle. *Methods Mol Biol*, 810: 25-58.

61. Greggio, C., Jha, P., Kulkarni, SS. et al. (2017) Enhanced respiratory chain supercomplex formation in response to exercise in human skeletal muscle. *Cell Metab*, 25(2): 301-311.

62. Gonzalez-Freire, M., Scalzo, P., D'Agostino, J. et al. (2018) Skeletal muscle ex vivo mitochondrial respiration parallels decline in vivo oxidative capacity, cardiorespiratory fitness, and muscle strength: the Baltimore longitudinal study. *Aging Cell*, 17(2).

63. Rooney, J.P., Ryde, I.T., Sanders, L.H. et al. (2015) PCR based determination of mitochondrial DNA copy number in multiple species. *Methods Mol Biol*, 1241:23-38.

64. Pestronk, A., Keeling, R., & Choksi, R. (2018) Sacropenia, age, atrophy and myopathy: mitochondrial oxidative enzyme activities. *Muscle & Nerve*, Accepted. doi: 10.1002/mus.25442

65. Leek, B.T., Mudaliar, S.R., Henry, R. et al. (2001) Effect of acute exercise on citrate synthase activity in untrained and trained human skeletal muscle. *Am J Physiol Regul Integr Comp Physiol*, 280(2): R441-7.

66. Chi, M.M, Hintz, C.S., Coyle, E.F., et al. (1983) Effects of detraining on enzymes of energy metabolism in individual human muscle fibers. *Am J Physiol*, 244(3): C276-87.

67. Enoki, Y., Watanabe, H., Arake, R. et al. (2017) Potential therapeutic interventions for chronic kidney disease-associated sarcopenia via indoxyl-sulfate induced mitochondrial dysfunction. *J Cachexia, Sarcopenia Muscle*, 8(5): 735-747.

68. Park, S.Y., Gifford, J.R., Andtbacka, R.H., et al. (2014) Cardiac, skeletal, and smooth muscle mitochondrial respiration: are all mitochondria create equal. *Am J Physiol Heart Circ Physiol*, 307(3):H346-52.

69. Sivitz, W.I., & Yorek, M.A. (2010) Mitochondrial dysfunction in diabetes: from molecular mechanisms to functional significance and therapeutic opportunities. *Antioxid Redox Signal*, 12(4): 537-77.

70. Wallace, D. C. (1999). Mitochondrial diseases in man and mouse. *Science*. 283: 1482–1488.

71. Brambilla, L., G. Cairo, P. Sestili, V. O'Donnel, A. Azzi, and O. Cantoni. (1997). Mitochondrial respiratory chain deficiency leads to overexpression of antioxidant enzymes. *FEBS Lett*. 418: 247–250

72. Raha S. Robinson BH. (2000) Mitochondria, oxygen free radicals, disease and ageing. *Trends Biochem Sci.* 25:222–230

73. Choksi, K.B., Nuss, J.E., DeFord, J.H., & Papaconstantinou, J. (2008) Age-related alterations in oxidatively damaged proteins of mouse skeletal muscle mitochondrial electron transport chain complexes. *Free Radic Biol Med*, 45(6): 826-838.

74. Korzeniewski, B. (2015) Effects of oxphos complex deficiencies and ESA dysfunction in working intact skeletal muscle: implications for mitochondrial myopathies. *Biochimica et Biophysica Acta- Bioenergetics*, 1847(10): 1310-1319

75. Martinez Cantarin, M.P., Whitaker-Menezes, D., Lin, Z., & Falkner, B. (2017) Uremia induces adipose tissue inflammation and muscle mitochondrial dysfunction. *Nephrol Dial Transplant*, 32(6): 943-951.

76. Clanton TL, Zuo L, Klawitter P. (1999) Oxidants and skeletal muscle function: physiologic and pathophysiologic implications. *Proc Soc Exp Biol Med*. 222:253–262.

77. Andrade FH, Reid MB, Allen DG, Westerblad H. (1998) Effect of hydrogen peroxide and dithiothreitol on contractile function of single skeletal muscle fibres from the mouse. *J Physiol*. 509:565–575.

78. Reid MB. (2008) Free radicals and muscle fatigue: of ROS, canaries, and the IOC. *Free Radic Biol Med*. 44:169–179.

79. Andrade, F.H., Reid, M.B., Allen, D.G., & Westerblad, H. (1998) Effect of hydrogen peroxide and dithiothreitol on contractile function of single skeletal muscle fibres from the mouse. *J Physiol*, 509(Pt2): 565-75

80. Couillard,A,, Koechlin, C,, Cristol, J.P, Varray, A., & Prefaut, C. (2002). Evidence of local exercise-induced systemic oxidative stress in chronic obstructive pulmonary disease patients. *Eur Respir J* 20, 1123–1129.

81. Westerblad H & Allen DG (2011). Emerging roles of ROS/RNS in muscle function and fatigue. *Antioxid Redox Signal* 15,2487–2499.

82. Roshanravan, B., Kestenbaum, B., Gamboa, J., et al. (2016) CKD and muscle mitochondrial energetics. *Am J Kidney Dis*, 68(4):658-659.

83. Rabinovich, R.A., & Vilaro, J. (2010). Structural and functional changes of peripheral muscles in chronic obstructive pulmonary disease patients. *Curr Opin Pulm Med,* 16, 123–133.

84. Yazdi, P.G., Moradi, H., Yang, J.Y., Wang, P.H., & Vaziri, N.D. (2013) Skeletal muscle mitochondrial depletion and dysfunction in chronic kidney disease. *Int J Clin Exp Med*, 6(7): 532-9.

85. Miró O, Marrades RM, Roca J, et al. (2002) Skeletal muscle mitochondrial function is preserved in young patients with chronic renal failure. *Am J Kidney Dis*. 39:1025–1031

86. Mutsaers, H.A., Wilmer, M.J., Reijnders, D., et al. (2013) Uremic toxins inhibit renal metabolic capacity through interference with glucuronidation and mitochondrial respiration. *Biochim Biophys Acta*, 1832(1): 142-50.

87. Vartak, R., Deng, J., Fang, H., & Bai, Y. (2015) Redifining the roles of mitochondrial DNA-encoded subunits in respiratory complex 1 assembly. *Biochim Biophys Acta*, 1852(7): 1531-9.

88. Mercken, E. M., Capri, M., Carboneau, B. A., Conte, M., Heidler, J., Santoro, A., … de Cabo, R. (2017). Conserved and species-specific molecular denominators in mammalian skeletal muscle aging. *NPJ Aging and Mechanisms of Disease*, *3*, 8

89. Braczynski, A. K., Vlaho, S., Müller, K., Wittig, I., Blank, A.-E., Tews, D. S., … Mittelbronn,

M. (2015). ATP Synthase Deficiency due to TMEM70 Mutation Leads to Ultrastructural Mitochondrial Degeneration and Is Amenable to Treatment. *BioMed Research International*, *2015*, 462592.

90. Kim, H., Kim, M.J., Jeong, E., Chung, J. et al (2010) Mitochondrial transcription factor B1 is required for mitochondrial function and oxidative stress resistance in drosophila. *Genes and Genomics*, 32(5): 455-461

91. Sokol, A.M., Sztolsztener, M.E., Wasilewski, M., Heinz, E., & Chacinska, A. (2014) Mitochondrial protein translocases for survival and wellbeing. *FEBS Lett*, 588(15): 2484-95.

92. Kravic, B., Harbauer, A.B., Romanello, V., Simeone, L., et al. (2018) In mammalian skeletal muscle, phosphorylation of TOMM22 by protein kinase CSNK2/CK2 controls mitophagy. *Autophagy*, 14(2): 311-335.

93. Templeman, N.M., Flibotte, S., Chik, J.H.L., Sinha, S. et al. (2017) Reduced circulating insulin enhances insulin sensitivity in old mice and extends lifespan. *Cell Rep*, 20(2): 451-463.

94. Wang, Z., Cotney, J., & Shadel, G. S. (2007). Human Mitochondrial Ribosomal Protein MRPL12 Interacts Directly with Mitochondrial RNA Polymerase to Modulate Mitochondrial Gene Expression. *The Journal of Biological Chemistry*, *282*(17), 12610–12618

95. Mracek, T., Drahota, Z., & Houstek, J. (2013) The function and the role of the mitochondrial glycerol-3-phosphate dehydrogenase in mammalian tissues. *Biochimica et Biophysica Actaci, 1827(3): 401-410.*

96. Ellisen, L.W., Ramsayer, K.D., Johannessen, C.M., Yang, A., et al. (2002) REDD1, a developmentally regulated transcriptional target of p63 and p53, links p63 to regulation of reactive oxygen species. *Mol Cell*, 10(5): 995-1005.

97. Qi, Z., He, J., Zhang, Y., Shao, Y., & Ding, S. (2011) Exercise training attenuates oxidative stress and decreases p53 protein content in skeletal muscle of type 2 diabetic goto-kakizaki rats. *Free Radic Biol Med*, 50(7): 794-800.

98. Morin, D., Musman, J., Pons, S., Berdeaux, A., & Ghaleh, B. (2016) Mitochondrial translocator protein (TSPO): From physiology to cardioprotection. *Biochem Pharmacol*, 105: 1-13.

99. Jang, D. G., Sim, H. J., Song, E. K., Medina-Ruiz, S., Seo, J. K., & Park, T. J. (2015). A thioredoxin fold protein Sh3bgr regulates Enah and is necessary for proper sarcomere formation. *Developmental Biology*, *405*(1), 1–9.

100. Li, Y., Li, J., Zhu, J., Sun, B. et al. (2007) Decorin gene transfer promotes muscle cell differentiation and muscle regeneration. *Mol Ther*, 15(9): 1616-22.

101. Arena, G., Cisse, M.Y., Pyrziak, S., Chatre, L., et al (2018) Mitochondrial MDM2 regulates

respiratory complex 1 activity independently of p53. *Mol Cell*, 69(4): 594-609.

102. Bautista, J.E., Gil-Necija, J., Castill, I. et al. (1983) Dialysis myopathy: report of 13 cases. *Acta Neuropathol*, 61: 71-75

103. Peter, A.K., Cheng, H., Ross, R.S., Knowlton, K.U., & Chen, J. (2011) The costamere bridges sarcomeres to the sarcolemma in striated muscle. *Prog Pediatr Cardiol*, 31(2): 83-88

104. Liu, Y., & Sweeney, G. (2014) Adiponectin action in skeletal muscle. *Best Pract Res Clin Endocrinol Metab*, 28(1): 33-41.

105. Minokoshi, Y., Toda, C., & Okamoto, S. (2012). Regulatory role of leptin in glucose and lipid metabolism in skeletal muscle. *Indian Journal of Endocrinology and Metabolism*, *16*(Suppl 3), S562–S568.

106. Miljkovic, I., Kuipers, A., Kuller, L., Sheu, Y., Bunker, C., Patrick, A., … Zmuda, J. (2013). Skeletal Muscle Adiposity is associated with Serum Lipid and Lipoprotein Levels in Afro-Caribbean Men. *Obesity (Silver Spring, Md.)*, *21*(9), 1900–1907

107. Calderon-Dominguez, M., Gil, G., Medina, M. A., Pandak, W. M., & Rodríguez-Agudo, D. (2014). The StarD4 subfamily of steroidogenic acute regulatory-related lipid transfer (START) domain proteins: new players in cholesterol metabolism. *The International Journal of Biochemistry & Cell Biology*, *49*, 64–68

108. Morita, M., & Imanaka, T. (2012) Peroxisomal ABC transporters: structure, function and role in disease. *Biochimica et Biophysica Acta*, 1822(9): 1287-1396.

109. Tryon, L. D., Vainshtein, A., Memme, J. M., Crilly, M. J., & Hood, D. A. (2014). Recent advances in mitochondrial turnover during chronic muscle disuse. *Integrative Medicine Research*, *3*(4), 161–171.

110. Eisner, V., Lenaers, G., & Hajnóczky, G. (2014). Mitochondrial fusion is frequent in skeletal muscle and supports excitation–contraction coupling. *The Journal of Cell Biology*, *205*(2), 179–195

111. Westermann, B. (2012) Bioenergetic role of mitochondrial fusion and fission. *Biochim Biophys Acta*, 1817(10): 1833-8.

112. Hasson, S. A., Kane, L. A., Yamano, K., Huang, C.-H., Sliter, D. A., Buehler, E., … Youle, R. J. (2013). High-content genome-wide RNAi screens identify regulators of parkin upstream of mitophagy. *Nature*, *504*(7479), 291–295.

113. Cho, E.-C., Kuo, M.-L., Cheng, J., Cheng, Y.-C., Hsieh, Y.-C., Liu, Y.-R., … Yen, Y. (2015). RRM2B-Mediated Regulation of Mitochondrial Activity and Inflammation under Oxidative Stress. *Mediators of Inflammation*, *2015*, 287345

114. Ronchi, D., Di Fonzo, A., Lin, W., Bordoni, A., Liu, C., Fassone, E., … Comi, G. P. (2013). Mutations in *DNA2* Link Progressive Myopathy to Mitochondrial DNA Instability. *American Journal of Human Genetics*, *92*(2), 293–300.

115. Di Noia, M. A., Todisco, S., Cirigliano, A., Rinaldi, T., Agrimi, G., Iacobazzi, V., & Palmieri, F. (2014). The Human *SLC25A33* and *SLC25A36* Genes of Solute Carrier Family 25 Encode Two Mitochondrial Pyrimidine Nucleotide Transporters. *The Journal of Biological Chemistry*, *289*(48), 33137–33148.

116. Lytovchenko, O., & Kunji, ERS (2017) Expression and putative role of mitochondrial transport proteins in cancer. *Biochim Biophys Acta*, 1858(8): 641-654.

117. Uittenbogaard, M., Brantner, C. A., & Chiaramello, A. (2018). Epigenetic modifiers promote mitochondrial biogenesis and oxidative metabolism leading to enhanced differentiation of neuroprogenitor cells. *Cell Death & Disease*, *9*(3), 360

118. Maurya, S.R., & Mahalakshmi, R. (2016) VDAC-2: Mitochondrial outer membrane regulator masquerading as a channel? *FEBS J*, 283(10): 1831-6.

Chapter 3

Deterioration of skeletal muscle health and function in progressive CKD: impairments in myogenesis and the skeletal muscle transcriptome

Background

Chronic Kidney Disease (CKD) affects nearly two thirds of those with diabetes, and is an early complication of type 2 diabetes, a population exceeding 29 million persons in the United States (**1**). CKD, or diabetic nephropathy, is characterized by a progressive and persistent decline in kidney function, categorized into 5 stages defined by the degree of renal filtration rate impairment (**2**). CKD configures well to a geriatric syndrome model, specifically in its propensity to promote a physical frailty state. Reduced renal filtration rate is associated with marked muscle impairment and heightened risk for functional limitations (**3**). Many have theorized that such functional mobility limitations and exercise capacity deficits in this population are secondary to poor muscle performance and strength (**4,5**). Indeed, work by Diesel and colleagues (1990) find that skeletal muscle strength predicts exercise capacity, as opposed to blood-oxygen carrying capacity, and that altered skeletal muscle function explains the observed exercise and mobility intolerance in those with CKD (**6**). Given that skeletal muscle tissue is critical for many functions in the body and is responsible for movement, impairments in skeletal muscle may be the focal point of CKD-induced functional and exercise capacity deficits. Indeed, reduced kidney function leads to the retention of uremic solutes, promoting inflammation, hypercatabolism, oxidative stress, and insulin resistance contributing to skeletal muscle dysfunction (**7).** Given that muscle size, among other factors, is critical for muscle strength and performance, loss of muscle mass may explain some of these mobility deficits and intolerance to exercise (**7).** Indeed, even minor losses of muscle contractile proteins (ie. Myosin, actin) can be associated with large decrements in force generation due to consequential reduction in cross-bridge formation with contraction (**7).** In support of this observation, decreased muscle fiber size and number observed in CKD is due in large part to the synergistic proteolytic effects of uremia-induced inflammatory cytokines (IL-6, TNFa, CRP) and activation of ubiquitin-proteasome-mediated contractile protein degradation (**9**) that increases the

risk of morbidity and mortality in CKD and hampers muscle performance and mobility (**10,9**). However, skeletal muscle is a highly plastic tissue that responds to a variety of physiological and pathological stimuli due, in part, to the constant turnover or remodeling of muscle proteins, organelles and cell populations. Given the muscle degradation and multifactorial metabolic impairments in CKD, it is not surprising that investigators have observed a myriad abberant morphological features of skeletal muscle in CKD beyond atrophy alone, including – loss of myofiber myofilaments, reduced mitochondrial content with mitochondrial damage and reduced muscle density, and internalized nuclei with z-band damage and cellular degeneration (**11,12**). This constellation of muscle cellular alterations implicates not only dysfunction of systems governing muscle protein degradation and mitochondrial dysfunction, but also systems governing new muscle fiber formation and injury repair.

Skeletal muscle is composed of multinucleated contractile muscle cells called myofibers. As the nuclei of myofibers are terminally differentiated in mature muscle (unable to divide, proliferate, or regenerate), a distinct cell population - the satellite cell (SC), residing on the periphery of the fiber, between its sarcolemma and basal lamina, is charged with repair, regeneration, and maintenance of muscle tissue (**13).** The fundamental process by which SCs perform these duties, is via a transition of specific yet overlapping steps that proceed from quiescence, to activation, proliferation, differentiation, and finally muscle cell fusion (**13**).

One primary means by which SCs "maintain" myofibers, including protein synthesis and breakdown, is through myonuclear domain maintenance. Each of the several hundred myonuclei of a myofiber regulates the gene products and cellular signaling networks in a finite volume of cytoplasm – termed its myonuclear domain (MND) (**14)**. This has been demonstrated through findings that mRNA products of single myonuclei are confined to the immediate cytoplasmic space, and nuclear-

encoded and synthesized proteins are restricted to specific targets immediate to its parent nucleus (**14**). SCs provide a continual source for new myonuclei at a rate sufficient to maintain constant MND size during skeletal muscle growth, and degradation (**15**). Moreover, MND size relates to the amount or capacity for protein synthesis, and if SCs are deficient in nuclear addition (via fusion), myonuclei may be overwhelmed, resulting in deficient protein synthesis for their cytoplasmic domain, resulting in dysfunctional proteostasis (**15**). It has also been postulated that mitochondrial content and demand may also require dynamic myonuclear addition via SC activation and fusion. Indeed, it is now well established that anterograde and retrograde signaling between nucleus and surrounding mitochondria is crucial for many fundamental cellular processes, especially proper mitochondrial function. Roughly 1500 proteins necessary for mitochondrial function are nucleus-encoded, and are then imported into the mitochondria to perform their functions (eg. NRF-1 stimulates mitochondrial DNA replication, PGC-1a, electron transport chain proteins and subunits, and mitochondrial turnover genes). Thus, SC function may be crucial in dictating the metabolic capacity, both for protein synthesis and maintenance, and energetic efficiency of myofibers. This is supported by recent elegant work by Fry and colleagues (**16)** who demonstrate that by inhibiting SC fusion (via genetic deletion of a key fusion protein-- myomaker), overload-induced muscle hypertrophy was attenuated, along with protein synthesis. The authors argue that this is likely due to the inability to add myonuclei to the muscle fiber, and thus, transcription of contractile proteins is blunted, while additional protein synthetic factors – ribosomes for protein translation or secondary signaling molecules secreted by SCs – are also diminished (**16**). Interestingly, other work also demonstrates that SC deficiency leads to diminished muscle performance (**17**). This may be due to impairments in nuclear metabolic and protein synthesis capacity, but this may also result from poor muscle quality and repair that is seen with SC deficiency as well.

SCs reside underneath the basal lamina in a quiescent state, and upon injury, become activated to generate a pool of myogenic progenitors (MPs) that differentiate and fuse to each other or existing myofibers to restore structure and function to muscle (**16**). Every functional satellite cell is critical for the repair of subtle and focal damages that occur in normal day-to-day muscle utilization. This injury triggered repair process occurs in 3 sequential and overlapping stages – 1. an inflammatory response, 2. activation, differentiation, and fusion of SCs, and 3. maturation and remodeling of newly formed myofibers. This injury-SC-repair process begins with sarcolemmal disruption, resulting in increased myofiber permeability that upregulates calcium-dependent proteolysis of myofibrillar and cytoskeletal proteins along with activation of the complement cascade and inflammatory response (**18)**. This inflammatory response recruits leukocytes to the cite of myofiber damage, followed by pro-inflammatory (M1) macrophages that phagocytose debris, and anti-inflammatory (M2) macrophages that promote SC proliferation and differentiation (**18**). The SC activation, proliferation, and differentiation is driven by myogenic regulatory factors, where SCs are progressed down the myogenic pathway, starting with their expression of Myogenic factor 5 (Myf5 -- drives SC proliferation and amplifies SC number), and MyoD which commits these SC to a myogenic end-point as they form myoblasts (**13**). These myoblasts then differentiate and fuse under the direction of Myogenin, to create myotubes and synthesize the major muscle contractile protein -- myosin heavy chain, after which, myotubes fuse with existing myofibers in both growth and repair (**13**). How SC proliferation and differentiation is balanced is poorly understood, but is known to involve extrinsic signals from muscle and non-muscle cell types (**19).** SC, not surprisingly, are regulated by their surrounding niche that consists of endothelial cells, inflammatory cells, macrophages, fibroblasts, extracellular matrix components, cytokines, and second messenger growth

factors, in addition to mechanical cues (**19**). Thus, impairments and/or disruptions in any of these factors may predictably alter SC function, and proper myofiber repair and maintenance.

The initiating inflammatory response of myofiber repair, requires an orchestrated response consisting of leukocyte infiltration signaling circulatory monocytes and chemoattractant molecules that produce downstream inflammatory cytokines and extracellular matrix proteins (ie. fibronectin, collagen 6) (**20**). It has been clearly shown that even slight imbalances in immune cell populations due to sustained and excessive inflammatory signals in muscles, can disrupt the cellular dynamics of the niche, and provide inappropriate environmental cues to SCs (**20**). In fact, sustained inflammation and accompanying persistent expression of ECM proteins impairs the differentiation capacity of SCs (**21**). Moreover, the ECM remodeling in such an environment alters elastic properties of muscle tissue, making it more fibrotic, stiff, and negatively impacting SC capacity to proliferate, fuse, and self-renew (**22**). However, persistent inflammation may not be the only factor that impairs SC reparative processes.

As demonstrated in several studies, fibrosis, and poor muscle quality may best be attributed to inability to maintain myofiber integrity due to a loss or imbalance of SC-fibroblast paracrine communication (**16**). Fibroblasts regulate expansion of SCs by preventing their premature differentiation (**23**), while SCs secrete micro-RNAs (ie. MiR-206) that regulate fibroblast collagen production and ECM deposition, while also possessing the capacity to remodel the basal lamina constituents directly (**23,24,25**). However, increased ECM is characteristic of regenerating muscle, and is synthesized by muscle-resident fibroblasts, largely to serve as scaffolds to maintain structural and functional integrity, myofiber orientation, and to sequester and present growth factors necessary for SC repair (**26)**. Yet, excessive ECM with regeneration can impede muscle function and hinder muscle regeneration, and prevent SC self-renewal (**26**,**22**). Conversely, with loss of SCs, there is

noticeable increase in fibroblast density and ECM deposition in muscle, and these fibroblasts retain a multipotent capacity, as certain subpopulations can differentiate into adipocytes, thus promoting intramuscular adipose tissue infiltration in addition to unchecked fibrosis (**19)**. Thus, pathological deterioration of the SC niche or systemic changes can influence SC fate decision and disrupt normal cellular responses to injury, and attenuate the formation of healthy or even new myofibers that leads to loss of muscle function and mass (**27**,**28**). However, aside from inflammatory and neighboring cell paracrine interaction potentially impairing SC reparative function, second-messenger signaling factors also play a large role in the SC niche.

Notch signaling regulates SC proliferation, differentiation, and cell fate determination (**29**). Delta and Jagged family ligands bind to SC transmembrane Notch receptors resulting in cleavage and nuclear translocation of the Notch intracellular domain to activate MRF and gene expression (**29**). However, for SCs to progress from proliferation to differentiation, signaling must switch from notch to Wnt, with Wnt and notch signaling interacting to promote efficient transition between these two cellular states and proper progression down the myogenic lineage (**30)**. However, in aging studies, increased Wnt signaling during SC proliferation can convert SCs myogenic lineage to a fibrogenic one, resulting in further fibrosis (**27**). Conversely, the age-related deficiency in Notch signaling in SCs impairs their activation, proliferation, and muscle repair following injury (**31)**. Similar to Notch signaling, insulin-like growth factor 1 (IGF-1) binds to, and activates IGF-1R in SCs to induce expression of MRFs and SC activation (**32**). These co-regulating signaling molecules add another level of complexity to the control mechanisms that dictate SC-mediate muscle maintenance.

Thus, SCs play a vital role in maintaining myofiber protein synthesis rates, energetic capacity, muscle quality (fibrosis, adipose infiltration), and function. Progressive CKD represents a

deteriorating health state characterized by elevated inflammation, contractile protein catabolism, skeletal muscle mitochondrial/energetic deficiencies, and systemic signaling factor alterations (ie. increased Angiotensin-2 production that may suppress SC MRF gene transcription via SC angiotensin receptors). Given this physiological imbalance and the aforementioned muscle morphological alterations in CKD - fiber atrophy, loss of myofilaments, reduced mitochondrial content, mitochondrial damage, reduced muscle density, and z-band damage and myocellular degeneration - SC function represents a critical area of research that may provide key mechanistic insights into skeletal muscle impairments that are so prevalent in this population. As satellite cells are controlled by both intrinsic and extrinsic regulatory cues and relate to both muscle degenerative disease and sarcopenia, novel discoveries in this area may bring new opportunities to enhance muscle function and mass in the uremic environment of CKD (**33).** Based on studies demonstrating the negative impact of the uremic milleui on mesenchymal stem cells (**34**), endothelial progenitor cells (**35**), bone marrow-derived stromal cells (**34**), investigation into the effect of CKD on SCs is needed. However, to-date, no studies have evaluated the impact of CKD or its progression on satellite cell function and muscle health in humans, nor have the muscle and whole-body functional relationships to SC function been explored in this population.

Thus, the purpose of this study is to determine how skeletal muscle SC abundance and function is affected by CKD progression and its associated systemic milleui in those with T2DM, and subsequently, how SC alterations relate to muscle health, quality, performance, and overall physical mobility across the spectrum of CKD severity. In understanding the functional status of this key skeletal muscle regulatory cell population, we may gain new insights not only into the biological underpinnings of skeletal muscle impairment in those with CKD, but also when these mechanisms become apparent. This may inform key targets and windows of opportunity for conservative

treatments to improve muscle health and remedy functional deficits to improve activity engagement/tolerance and attenuate CKD progression in those most vulnerable – those with T2DM.

Methods

Participants

Twenty seven subjects participated in this study – all were diagnosed with T2DM, 12 with diagnosed and clinically confirmed peripheral neuropathy (PN), and all with clinically diagnosed diabetic nephropathy (diabetes-induced CKD) by a nephrologist. Participants were categorized into early CKD stage (eGFR >60 mL/min, stages 1 and 2), middle-stage CKD (eGFR 30-59 mL/min, stage 3), and late CKD (eGFR<29 mL/min, stages 4 and5). Participants of each categorical stage/group of CKD progression were – n = 9 in early CKD (stage 1 and 2 - 7 male, 2 female), n=9 in middle-stage CKD (stage 3 - 6 male, 3 female), and n=9 in late-CKD (stages 4 and 5 - 5 male, 4 female). The groups were matched for gender composition, age, BMI, duration of T2DM, glycemic control (HbA1c, OGTT AUC), diabetes severity (presence of PN) (Table 1). Participants were recruited from the Washington University Volunteers for Health, the Center for Community Based Research, the Washington University Medical School Renal Clinic, and from the surrounding St. Louis community.

Study inclusion criteria included a diagnosis of T2DM based on clinical report of a diagnosis of DM from a physician, confirmation of medication usage for DM (insulin, oral hypoglycemic agents or both) and verification of HbA1c levels either currently or at the time of diagnosis >6.5%, and/or OGTT $\geq$200 mg/dL. A diagnosis, particularly for those with eGFR $\leq$60 mL/min, of diabetic nephropathy based on nephrologist clinical assessment of patient medical history, degree of proteinuria (must be present at least at the microalbuminuria level – urinary ACR $\geq$30 mg/g),

glycemic control, diabetic medication use, hypertension status, and rate of kidney decline (eGFR utilizing creatinine), all according to KDIGO guidelines (**35**)

Participants were excluded from the study if they weighed more than 350 pounds (equipment weight limit), had any infection or ulceration of either foot, severe foot deformity or amputation, or any serious medical co-morbidity. Serious medical comorbidities included - dialysis treatment, heart failure requiring medications, or New York Heart Association class 3 or class 4 heart failure, coagulation disorders (platelets <100,000, PT > 2 seconds above control, or INR >1.5), anemia (Hbg < 10g/dL), uncontrolled proliferative diabetic retinopathy, joint replacement or musculoskeletal injury that precludes intense muscular contraction, within 1 year of enrollment, symptoms that meet the requirement for class C or class D of the AHA risk stratification criteria, individuals who are participating in regular structured exercise programs, or may be pregnant or breast feeding, current cancer treatment, and organ transplant requiring immunosuppressant therapy. Each participant read and signed an IRB-approved protocol and informed consent that was approved by the Human Research Protection Office at Washington University in St. Louis, MO.

CKD Staging (eGFR):

CKD staging was performed using serum creatinine concentrations. Serum creatinine was measured with a standardized assay, and used to estimate GFR (eGFR) - computed based on the Chronic Kidney Disease Epidemiology Collaboration equation and was classified into 5 stages: eGFR $\geq$ 90 mL/min per 1.73 m^2 (stage 1 CKD), 60-90 mL/min (stage 2 CKD), 30-60 mL/min (stage 3 CKD), 15-30 mL/min (stage 4 CKD), <15 mL/min (stage 5 CKD) with no kidney transplant or dialysis.

Laboratory Measures:

Laboratory measures including serum creatinine (mg/dl) as above, blood-urea nitrogen -- BUN (mg/dl), HbA1c (%), oral glucose tolerance test – OGTT area under the glucose curve (AUC), and urine albumin:creatinine ratio (ACR – mg/g) to quantify degree of proteinuria.

Participant Demographics:

Participants age, duration of T2DM, weight, height, and BMI (calculated as weight in kg divided by the square of height in meters, used to define obesity) were collected through participant interview, weight balance, and stadiometer, respectively at the initial visit, prior to any dynamometry or physical performance testing.

Neuropathy Assessment:

Peripheral neuropathy was determined by diminished or absent plantar sensation to light touch or pressure or vibration perception. Lower extremity sensation was assessed via biothesiometry and semmes Weinstein monofilament testing. Peripheral neuropathy was defined clinically as the inability to feel the 5.07 (10 gram) monofilament on at least one non-callused site on the plantar aspect of either foot or the inability to perceive vibration threshold <25 volts on the biothesiometer (Biomedical Instrument, Newbury, OH, USA) applied to the hallux (**36**).

Physical Function:

Functional physical performance was assessed using the 9-item modified physical performance test (PPT). The PPT is a timed observational assessment of performance on nine daily physical activities including: 5 consecutive sit-to-stand transfers without arm assistance, climbing a flight of stairs with 10 steps, a 50-ft. walk test, turning 360 degrees, picking up a coin from the floor, donning/doffing a jacket, lifting a book onto an overhead shelf, a Romberg standing balance assessment with eyes

open, and ability to ascend 4 flights of stairs (**36**). Each item is scored from 0-4 based on the time taken to complete each task, with a maximum score of 36 (higher scores indicate better physical function/performance). Each task is performed twice with the average time used to score the task. Interrater reliability, validity with other functional assessments, and predictive validity of lack of independence and mortality have all been well established for the mPPT (**36,37,38,39**). The mPPT possesses a test-retest reliability of .964, while individual sub-items have reliability ranging from .51-.99, and Cronbach alpha of .785 (**38,39**).

Stair Vertical Power-

Stair vertical power was calculated from the stair-climbing component of the PPT, using the equation as previously described (**36**)

Stair Power = [(weight in Kg)(9.8)(1.95)] / (avg. stair climb time in seconds)

1.95 → cumulative height of the 10 steps (each step is 19.5 cm), in meters

Muscle Performance Assessment:

Muscle performance of lower extremity major muscle groups was assessed via Biodex System 3 isokinetic dynamometer as described previously (**40,41,42,43**). Major muscle groups assessed were hip extensors and knee extensors as these muscle groups are critical to ambulation and functional mobility (**44**). For each movement, the anatomical axis of rotation (ie. hip joint center/greater trochanter, knee joint femoral condyles) was aligned to the dynamometer axis using visual inspection and manual palpation.

Participants upper extremities, trunk, and contralateral limb were secured with padded straps to ensure minimal accessory movement contributed to force production. Prior to each test,

participants became familiar with procedures by performing 3-5 submaximal contractions, and the tested leg was weighted to correct for the effects of gravity on the torque measured, according to the specifications of the Biodex Manual. Range of motion was set for each movement to obtain ~110 degrees of hip flexion (from ~5° of hip extension), ~90 degrees of knee flexion (from terminal extension). The isokinetic tests for each muscle group included 5 maximal concentric contractions each separated by 5 seconds. Isometric tests consisted of 4 maximal contractions held for 5 seconds each, separated by 10 seconds rest between repetitions. Isometric force production was assessed at 60 degrees of hip flexion, 60 degrees of knee flexion, to achieve optimal muscle-specific sarcomere length (**45,46**). 3 minutes rest separated each test. Isokinetic strength was assessed for each joint extensor movement at 30°/sec and 120°/sec. To assess peak torque production (ft-lbs) as a measure of maximal muscle strength, the highest 3 repetitions were selected and averaged for each joint at each repetition speed. At each selected repetition, rate of torque production, seconds to peak torque, total work, and power was also assessed and averaged. Power was determined by the time-averaged integrated area under the curve at the constant velocity of movement in the available range of motion **(40,41**) To avoid sub-maximal performance or outliers, tests were re-done or data discarded if the coefficient of variation exceeded 10% for the knee and ankle, and 15% for the hip (**47**).

Finally, we also assessed muscle fatigueability/fatigue resistance of the aforementioned muscle groups using a fatigue protocol detailed as follows – participants performed 50 maximal repetitions at 90 degrees per second, with 2 second rest period between repetitions. Torque production was assessed for each repetition, and work was calculated across the first, second, and third portion of the fatigue set, and totaled for an index of fatigue resistance as detailed previously (**48,49**). Recovery from this fatigue task was tracked over 2 recovery phases. In phase 1, participants performed 5 maximal repetitions separated by 10 seconds of rest immediately following the fatigue

set. In phase 2, participants performed 5 maximal repetitions separated by 25 seconds of rest. Torque production for each recovery repetition was recorded.

Fasting/medication/OGTT:

As renal decline can contribute to skeletal muscle insulin resistance, an oral glucose tolerance test and fasting glucose and insulin values were obtained to assess and control for any differences in insulin sensitivity, as this may confound the relationship between mitochondrial function and muscle performance. All diabetes medications (except insulin) were stopped 2 days before admission to the Clinical Research Unit (CRU) to decrease residual drug effects on the metabolic measurements (long-acting GLP-1 agonist and thiazolidinediones were stopped 7 days before admission). Subcutaneous insulin was stopped after the final dose on the day prior to admission to the CRU. Blood glucose concentration was checked by fingerstick twice daily at home (once before breakfast, and once posprandially after dinner before bedtime) for 2 days before admission (7 days before admission in subjects taking long-acting GLP-1 agonist or thiazolidinediones) to ensure adequate glycemic control was maintained prior to metabolic testing. Participants refrained from eating for 10 hours prior to administration of the 3-hour oral glucose tolerance test as previously described (**50**).

Participants fasting plasma glucose was assessed 10 minutes prior to administration of a 75g glucose drink. Plasma samples were subsequently obtained at the time of drink ingestion, and at 10, 20, 30 minutes, and then every half hour until 3 hours post-ingestion. Plasma glucose was assayed by automated glucose analyzer (Yellow Spring Instruments), and plasma insulin by ELISA (**51**). Insulin sensitivity as a measure of basal insulin sensitivity during an OGTT was estimated using homeostasis model assessment of insulin resistance (HOMA-IR), calculated as [(fasting glucose (mg/dL)] x [fasting insulin (μU/mL)]/405 (**52**).

***Plasma Cytokines**:*

Fasting blood samples for cytokine measurement were drawn prior to the glucose challenge, into pre-cooled glass tubes containing EDTA and gently inverted 10x to mix. Samples were subsequently spun at 1300g, at 4°C for 10 minutes, and the supernatant aliquoted as plasma and stored at -80°C for future analysis. IL-6 and TNF-alpha concentrations (pg/mL) were assessed via high-sensitivity ELISA from R&D Systems (Minneapolis, MN, USA) (**53**,**54**).

Body Composition:

Each participant was assessed for body composition with a whole-body, dual energy x-ray absorptiometry (DXA) (Hologic GDR 1000/W, software version 6.2 OD; Waltham MA) scan to assess composite and regional lean and fat mass as described previously (**55**). Bilateral upper and lower extremity fat-free masses, region-specific lean mass (ie. thigh region), whole-body lean mass and fat masses were assessed.

***Muscle Biopsy*:**

Participants were positioned supine in a hospital bed with the thigh of their dominant leg exposed. Participants were then asked to contract the thigh so as to visualize the vastus lateralis (anterior to fascia lata, approximately 1/3rd of the distance from patella to great trochanter). The area was prepped and cleaned with iodine, and draped. The skin was anesthetized with 2% lidocaine solution injected into the dermis and allowed to take effect over a 3 minute period. A 1-2 cm incision was made through the skin and subcutaneous tissue, and a 5 mm Bergstrom needle was introduced with vacuum suction into the vastus lateralis. Two passes of the biopsy needle were performed for each participant obtaining ~250-350 mg of skeletal muscle tissue as previously described (**56**).

A 50-75 mg portion of the sample were immediately snap-frozen in liquid nitrogen and stored at -80°C until further analysis (RNA-sequencing), while 50-120 mg of muscle tissue were prepared for immediate flow cytometry analysis and muscle SC isolation. When enough sample remained, 50 additional mg of tissue were blotted with gauze to remove excess moisture, and oriented with fibers directed vertically and embedded in cork-mounted tragacanth gum and frozen in liquid-nitrogen-cooled isopentane for 10-20 seconds for cryosectioning and histology.

Muscle Morphology (H&E staining):

Samples frozen for histology were sectioned at 8um with a Leica Cryostat on Superfrost Plus slides, and fixed for 5 minutes with ice-cold acetone and stained with Harris haematoxylin and eosin (H&E) according to standard procedures as previously described (**57**). Briefly, mounted cryosectioned samples were immersed in filtered Harris Hematoxylin for 1 minute, followed by tap water rinse, and subsequent immersion in EOSIN stain for 1-2 minutes. After thorough rinsing, the sample was dehydrated in ascending alcohol solutions (50,70,80,95%x2,100%x2) in Columbia staining dish. Samples were then cleaned with xylene (3-4x), and mounted with coverslips with Permount for non-contractile tissue quantification.

Sections were examined at 10x magnification at 5 representative locations in the muscle cross section by a blinded rater. Images were captured with a Leica DC500 camera and Leica IM50 software. Subsequently, ImageJ software was used with the haeomatoxylin/eosin (H&E) color deconvolution plugin (Rasband, W.S., ImageJ, US National Institutes of Health, Bethesda, Maryland, USA http://rsb.info.nih.gov/ij/, 1997–2008) to determine the fibrotic/non-contractile percentage of the entire cross section of each image per sample. This plugin was used as it is outfitted with stain vectors to accurately separate green, blue and red stain components, which is

based on the primary and secondary 3D colour space (RGB and CYM) (http://www.dentistry.bham.ac.uk/landinig/software/cdeconv/cdeconv.html). Healthy contractile tissue was separated from non-contractile using ImageJs automatic threshold on the eosin component (obtained after H&E color deconvolution). This allowed for calculation of the percentage of fibrotic/non-contractile tissue ((whole area – muscle occupied area)/whole area) as described previously (**58**).

Satellite Cell Isolation/Cell quantification –

Muscle SC isolation was adapted from standard methods and criteria (**59**,**60**). Briefly, muscle samples were immediately placed in a 15 mL conical tube containing pre-warmed (37^0C) digestion buffer (Dulbecco's Modified Eagle Medium [DMEM; Gibco/Invitrogen, Carlsbad, CA, USA]; 20 mg/mL collagenase type 1 [Sigma, St. Louis, MO, USA]; 6mg/mL dispase II [Roche, Mannheim, Germany]; 6ku/mL penicillin [Gibco/Invitrogen]; 5mg/mL streptomycin [Gibco/Invitrogen]), and placed in a 37^0C water bath for 30 minutes, with agitation every 10 minutes. Samples were transferred to a 21cm^2 tissue culture plate and fibers were visualized and pulled apart using surgical fine-tip forceps in a sterile tissue culture hood. After the tissue was sufficiently broken apart, the dish was placed in an incubator for 50 minutes (5% CO_2, 37^0C), with gentle agitation every 10 minutes. The plate and mixture were then manually triturated through a 5mL plastic serological pipette to further disrupt the tissue, and incubated for an additional 10 minutes. Following incubation, the mixture was filtered through a 70 um mesh cell strainer (VWR #352350) into a 50-mL conical tube. The plate was subsequently washed with 4 mL of low-glucose DMEM (1g/L) and passed through the filter. The mixture was then passed through a 40 um mesh cell strainer (VWR #352340) into a new 50-mL conical tube and transferred to a 15-mL conical tube. The mixture was centrifuged at 800 rpm for 10 minutes at 4^0C to obtain a pellet containing mononuclear cells. The pellet was re-

suspended in 1 mL of fluorescence-activated cell sorting (FACS) buffer (2.5% goat serum; 1mmol/l ethylenediaminetetraacetic acid in phosphate buffer saline [PBS] at pH 7.4). 20 uL of the cell suspension was then added to 980 uL of FACS buffer for 4 conditions (1 for each cell surface marker probe, and 1 for unstained cell control) for fluorescence minus-one controls (FMO). 200 uL of FACS buffer was used to restore the original cell suspension to 1 mL volume. Cell-surface markers were then labeled by adding the following fluorophore conjugated antibodies to the cell suspensions: NCAM (unconjugated, BD Biosciences, #561903, San Jose, CA, USA, 1:200), CD31 (FITC, eBioscience/ThermoFisher Scientific, #11031941, Grand Island, NY, USA, 1:200), and CD45 (Pac-Blue, Biolegend, #304022, San Diego, CA, USA, 1:200), and secondary antibody goat anti-mouse IgG (Alexa-Fluor 647, ThermoFisher, #A21236, Grand Island, NY, USA, 1:200). Cell suspensions with primary antibodies were incubated for 20 minutes on a rocker, in a 4^0C cold room, and pelleted, and washed with 3 mL of FACS buffer. Cells were then pelleted and re-suspended in 1 mL of FACS buffer (5 suspensions total – 3 FMOs, 1 unstained control, and sample suspension). Secondary antibody was then added to conjugate to the NCAM (CD56) antibody, and incubated for 20 minutes on a rocker in a 4^0C cold room, after which, cells were pelleted, washed, and re-suspended as previously, and ready for FACS sorting.

Flow cytometry was conducted using a FACS Aria II-1 (BD Biosciences, San Jose, CA, USA) instrument at the Washington University School of Medicine Pathology Department Flow Cytometry Core (St. Louis, MO, USA; https://pathology.wustl.edu/research/core-facilities/flow-cytometry-fluorescence-activated-cell-sorting/). Optical alignment and fluidics of the cytometer were verified daily by a trained technician using BD Cytometer Setup and Tracking Software (BD Biodsciences). The excitation and emission wavelengths used were NCAM (Alexa-Fluor 647)

excitation=650 nm, emission=668 nm, CD31 (FITC) excitation=494, emission=519, and CD45 (Pac-Blue) excitation=401, emission=452.

Gating strategies were optimized using multiple preliminary experiments that included unstained and FMO controls. Initial gaiting was set based on two-dimensional plot of forward scatter (FWSC – indicative of cell size) and side scatter (SSC – indicative of internal cell complexity/granularity) to focus on intact cells while excluding cell debris. Next, gating was established on two-dimensional plotting of the intact cells on forward scatter area (FSC-A) and forward scatter width (FSC-W) to remove any dublets, debris clumps and non-single-cells. This single-cell population was further refined by establishing a gate set on two-dimensional plotting of side-scatter area (SSC-A) and side-scatter width (SSC-W), to ensure that mononuclear single cell population was being applied to the established antibody gating scheme for cell quantification. From this established population, satellite cell (NCAM+) gating was performed with a 1-dimensional gate placed so that <1% of cells within the FMO suspensions were positive, and a confirmatory gate was placed on a two-dimensional plot of CD45 and CD31, to ensure that Satellite Cells were CD31-/CD45-/NCAM+. Gating for endothelial cells and inflammatory cells was performed on a 2-dimensional plot of CD31 and CD45, with CD34+/CD45- cells demarcated as endothelial cells, and CD45+/CD31- cells designated as inflammatory cells (leukocytes). All samples - FMOs, unstained suspension, and labeled biopsy sample were run in the same session, and the established gating parameters were applied to every sample sorted. All cell population were expressed as a percentage of the total mononuclear cell population, and compared via 1-way ANOVA between CKD groups. Sorted satellite cells (NCAM+) were collected in FBS and immediately plated in 21cm^2 collagen-coated dishes (10 ug/cm^2 Rat Tail Collagen Type 1 dissolved in 20 mM acetic acid, Sigma-Aldrich,

#C3867, St. Louis, MO, USA) with growth media (20% FBS, 1% Pen/Strep, 1:1 low glucose DMEM to Hams F10, 4 ng/mL bFGF) in a cell culture incubator (37^0C in 5% CO_2-95% air).

Satellite Cell Culturing-

Once plated, isolated satellite cells were left to proliferate and expand, with growth media changed every 4 days, until the contents of the 21 cm^2 dish were ~75% confluent (~5 days - 1 week). Once 75% confluent, cells were split into two collagen-coated 21 cm^2 dishes for expansion. After ~3 days (~75% confluency), cells were split further (passage 2) into two 60 cm^2 collagen-coated dishes for final expansion to ~75% confluence (~3-5 days), at which time, cells were trypsinized (.25% trypsin-EDTA, Simga-Aldrich, #T4049, St. Louis, MO, USA), pelleted and frozen for later analysis (freeze media – 90% FBS+10% dimethylsulfoxide/DMSO).

For cell culture studies, frozen primary satellite cells were thawed and expanded in collagen-coated 60 cm^2 dishes (each passage split 1:4 in dishes). All subsequent experiments were performed with cells at passage 3-4. Cells were fed growth media every 3 days, until ~75% confluent, at which time, cells were trypsinized, pelleted, counted and plated into 16 matrigel-coated 9.6 cm^2 dishes (matrigel concentration – 200 ug/mL, or 26.7 ug/cm^2) (GFR-phenol-red-free, Corning, #356231, Bedford, MA, USA). 14 dishes were plated with 100,000 cells (~10,400 cells per cm^2) for myogenic analysis, while 2 dishes were plated with 30,000 cells each (~3,125 cells per cm^2) for cell proliferation assay.

Cellular proliferation was measured with the Click-iT ethynyl-2'-deoxyuridine (EdU) imaging kit (Invitrogen) following the manufacturers protocol. EdU is a nucleoside analog of thymidine, and is incorporated into DNA during DNA synthesis, thus preferentially staining the nucleus of proliferating cells. Briefly, satellite cell cultures were incubated for 12 hours at 37^0C with

growth media containing 1 mM EdU solution, after which, cells were fixed in 3.7% formaldehyde solution for 15 minutes, and rinsed with PBS. Fixed cells were then permeabilized with 1% Triton-X solution for 15 minutes and rinsed with PBS, and subsequently incubated for 40 minutes at room temperature in EdU reaction cocktail. Detection of EdU occurs through a click reaction (copper-catalyzed covalent reaction between azide and an alkyne). Labelled cells were then incubated at room temperature for 10 minutes, with Hoechst 33342 to stain cell nuclei blue. Cells were finally rinsed with PBS and imaged using a dual purpose phase contrast and fluorescence microscope (EVOS FL Cell Imaging System, Life Technologies, Paisley, UK) at 10x magnification at 5 random locations per dish (2 dishes total). EdU-stained cells were counted with ImageJ software and quantified as a fraction of the total number of cells in the field of view per image, and averaged over all images and expressed as a percentage (**61**).

Myogenic analysis was performed over a 5-day period. Plated cells were allowed to grow to confluence (~2-3 days), at which time, to promote differentiation of confluent satellite cells into myotubes, growth media was changed to differentiation media consisting of low-glucose DMEM (1g/L) (GIBCO/Invitrogen) supplemented with 5% horse serum (ThermoFisher #16050-122) and 1% pen/streptomycin antibiotic, denoted as *day 0*. To assess the timeline and myogenic capacity of primary satellite cells, 2 plates were fixed in ice-cold 100% methanol at *days 1* (24 hours post differentiation media administration), *day 2*, *day 3*, and *day 5*. Fixed cells were subsequently stained for constituent protein myosin heavy-chain (MyHC) (MF-20, mouse anti-human, Developmental Studies Hybridoma Bank, Iowa, USA), and nuclei (Hoechst 33342, Invitrogen). Briefly, fixed cells were washed twice with 1x PBS, and blocked in 2% BSA with primary antibody against myosin heavy chain protein (MF-20, diluted 1:30) for 1 hour at room temperature. Cells were then washed thrice with PBS, and incubated in secondary antibody (Alexa-Fluor 647, goat anti-mouse,

ThermoFisher, #A21236, Grand Island, NY, USA, diluted 1:400 in 2% BSA) for 20 minutes at room temperature, protected from light. Cells were then washed thrice with PBS, and finally incubated in Hoechst nuclear stain (diluted 1:1000 in 1x PBS) for 2 minutes at room temperature. Cells were thoroughly rinsed with PBS and viewed on a dual purpose phase contrast and fluorescence microscope (EVOS FL Cell Imaging System, Life Technologies, Paisley, UK). At each day, 5 representative images were taken at random locations in each of the two plates (10 total images per day) at 20x magnification, and the proportion of cells that had fused into multinucleated MyHC+ myotubes were expressed as a percentage of total nuclei in the field of view, averaged over all 10 images per day, per participant, and reported as the *fusion index* as previously described (**61**).

Simultaneously, to examine the coordination of myogenic regulatory factor (MRF) gene program, 2 plates of cells were extracted for gene expression profiling using Trizol reagent (Invitrogen # 15596026) at *day 1*, *day 3*, and *day 5*. Quantitative RT-PCR was used to assess mRNA expression of chief MRF genes that drive differentiation (*myod, myogenin, MyHC)*. Briefly, trizoled cells were thawed and incubated with 20 mg/mL glycogen for 10 minutes, and precipitated with chloroform, centrifuged at 13200 rpm (16000g) for 15 minutes, and the aqueous layer was transferred, precipitated with isopropanol and centrifuged at 13200 rpm (1600g) for 10 minutes, and finally the pellet was re-suspended in 75% ethanol and centrifuged at 11000 rpm for 5 minutes and allowed to air dry for 15 minutes and re-suspended in DEPC water. Concentration and quality of mRNA were measured using a nanodrop spectrophotometer. qPCR was subsequently performed on isolated RNA as described previously (**62**). Briefly, 1 ug of RNA was diluted in DEPC water and combined with reverse-transcription master mix (consisting of dNTP, 100 mM DTT, 5x buffer, random hexamers and RTase) per sample and subsequently cycled at 37^0C for 60 minutes, 99^0C for 5 minutes, and 4^0C, to obtain cDNA. Subsequentely, 1 uL of cDNA was added to qPCR mastermix

(consisting of 12.5 uL SYBR Grenn, 6.5 uL DEPC water, and 2.5 uL of forward and reverse primer) per well in a 96-well plate and covered with optical adhesive. Sample PCRs were run in duplicate per gene probe. PCR was carried out at 50^0C for 2 min, 95^0C for 10 min., 95^0C for 15 sec., and 60^0C for 1 minute for 40 cycles. (PRIMERS LISTED BELOW). The cycle threshold (Ct) value for detection of gene of interest was normalized against the Ct value of GAPDH, and relative changes compared to stage 1&2 SCs were calculated according the ΔΔCt method.

Primers-

MyoD: Forward 5' - ACTTTGCTATCTACAGCCGGG- 3'
Reverse 5'- TAGAAGTCGTCCGTTGTGGC- 3'
Myogenin: Forward 5' - CAGTGCACTGGAGTTCAGCG- 3'
Reverse 5'- TTCATCTGGGAAGGCCACAGA- 3'
Myosin HC: Forward 5' - TTGCTGTCTTCTGCTCTCATC- 3'
Reverse 5'- GGAGCAGCTATGCCGAACAC - 3'
GAPDH: Forward 5' - CTCTGACTTCAACAGCGACA- 3'
Reverse 5'- TCTCTCTCTTCCTCTTGTGC- 3'

Transcriptome Analysis (RNA-sequencing)-

Approximately 20 mg of snap frozen tissue per participant, was ground into a fine powder in a liquid-nitrogen cooled mortar and pestal system. Ground samples were subsequently emptied into a vial containing 1mL of Trizol reagent (Invitrogen # 15596026) supplemented with 20 mg/mL glycogen and incubated for 10 minutes, and precipitated with chloroform, centrifuged at 13200 rpm (16000g) for 15 minutes, and the aqueous layer was transferred, precipitated with isopropanol and centrifuged at 13200 rpm (1600g) for 10 minutes, and finally the pellet was re-suspended in 75% ethanol and centrifuged at 11000 rpm for 5 minutes and allowed to air dry for 15 minutes and re-

suspended in DEPC water. Concentration and quality of mRNA were measured using a nanodrop spectrophotometer. 1 ug of total RNA was subsequently utilized for RNA-sequencing and library preparation. Library preparation was performed using a Clontech SMARTER kit according to the manufacturer's protocol. The resulting cDNA ends were rendered blunt, an A base was added to the 3' ends, and Illumina sequencing adapters were ligated to the ends. The ligated fragments were then amplified for 12 cycles using primers that incorporated unique index tags, and the resulting fragments were sequenced on an Illumina HiSeq 2500 sequencing system using single reads that extended 50 bases and targeted 30M reads per sample as previously described (**63**). Briefly, RNA-seq reads were aligned to the Ensembl top-level assembly with STAR version 2.0.4b. Gene counts were derived from the number of uniquely aligned unambiguous reads by Subread:featureCount version 1.4.5. Transcript counts were produced by Sailfish version 0.6.3. Sequencing performance was assessed for total number of aligned reads, total number of uniquely aligned reads, genes and transcripts detected, ribosomal fraction known junction saturation and read distribution over known gene models with RSeQC version 2.3.

All gene-level and transcript counts were then imported into the R/Bioconductor package EdgeR and TMM normalization size factors were calculated to adjust for samples for differences in library size. Ribosomal features as well as any feature not expressed in at least the smallest condition size minus one sample were excluded from further analysis and TMM size factors were recalculated to created effective TMM size factors. The TMM size factors and the matrix of counts were then imported into R/Bioconductor package Limma and weighted likelihoods based on the observed mean-variance relationship of every gene/transcript and sample were then calculated for all samples with the voomWithQualityWeights function. Performance of the samples was assessed with a spearman correlation matrix and multi-dimensional scaling plots. Gene/transcript

performance was assessed with plots of residual standard deviation of every gene to their average log-count with a robustly fitted trend line of the residuals. Generalized linear models were then created to test for gene/transcript level differential expression. Differentially expressed genes and transcripts were then filtered for FDR adjusted p-values less than or equal to 0.05.

The biological interpretation of the large set of features found in the Limma results were then elucidated for global transcriptomic changes in known Gene Ontology (GO) and Kyoto Encyclopedia of Genes and Genomes (KEGG) terms with *the R/Bioconductor packages GAGE and Pathview*. Briefly, GAGE measures for perturbations in GO or KEGG terms based on changes in observed log 2 fold-changes for the genes within that term versus the background log 2 fold-changes observed across features not contained in the respective term as reported by Limma. For GO terms with an adjusted statistical significance of FDR <= 0.05, heatmaps were automatically generated for each respective term to show how genes co-vary or co-express across the term in relation to a given biological process or molecular function. In the case of KEGG curated signaling and metabolism pathways, Pathview was used to generate annotated pathway maps of any perturbed pathway with an unadjusted statistical significance of p-value <= 0.05.

Statistics-

Pearson Chi-square test for equality of proportions was used to determine the homogeneity of sex distribution, and neuropathy status between CKD-staged groups (stages 1 and 2, stage 3, and stages 4 and 5). CKD group baseline demographic variables (age, BMI, duration of diabetes, glycemic control – HbA1c, total body lean mass, and eGFR) were analyzed and compared via 1-way analysis of variance (ANOVA). CKD-group differences were also assessed via 1-way ANOVA for OGTT area under the curve and HOMA-IR (measures of insulin resistance), PPT score, PPT sub-items stair power production and chair rise capacity, lower extremity torque production and power (knee

extensors, hip extensors), SC quantification, SC proliferation capacity (EDU+ %), SC myogenic capacity (fusion index %) at differentiation days 1,2,3, and 5, and all gene expression measures. Post-hoc testing for CKD-staged group differences was determined using Tukey's HSD or Games-Howell in the event of a violation of homogeneity of variance. Bivariate pearson correlation coefficients were used to assess relationships between eGFR and the aforementioned measures, including lab measures, and between SC function/abundance measures and muscle quality, muscle performance and PPT scores. All analyses were evaluated at an alpha level set at .05.

Results

Group Demographics-

As shown in Table 1, there were no group differences in gender composition, PN status, BMI, age, duration of diabetes, whole-body lean mass, glycemic control (HbA1c), insulin sensitivity (OGTT AUC) or albuminuria, though stages 3 and 4&5 CKD groups on average presented with macro-albuminuria (>300 mg/dL), while early stage CKD presented with microalbuminuria (30-300 mg/dL). The groups inherently differed in eGFR, as this was the defining criteria of the groups (early, middle, and late-stage CKD) ($p<.001$), and also differed in BUN, a measure of uremia ($p<.001$).

Physical Function-

As shown in Figure 1, eGFR was significantly positively correlated with PPT score ($r=.8$, $p<.001$), along with other functional measures -- lower extremity power output while climbing stairs (Figure 2), or in other words, worse kidney function was associated with impaired functional mobility, and muscle power output to propel stair climbing. Similarly, PPT score ($F=36.1$, stage 1&2 vs. stage 3-$p=.005$, stage 1&2 vs. stage 4&5-$p<.001$, stage 3 vs. 4&5-$p<.001$), stair power ($F=14.7$, stage 1&2

vs. stage 3-p=.02, stage 1&2 vs. stage 4&5-p<.001, stage 3 vs. 4&5-p=.047), and chair rise score (F=13.9, stage 1&2 vs. stage 3-p=.048, stage 1&2 vs. stage 4&5-p<.001, stage 3 vs. 4&5-p=.027) significantly declined with stage-wise progression of CKD (Figure.1 B,C).

Muscle Performance-

As shown in Figure 3, knee extensor torque (Figure.3A, F= 16.9, stage 1&2 vs. stage 3- p=.014, stage 1&2 vs. stage 4&5- p=.001, stage 3 vs. 4&5- p=.037) and power (Figure.3C, F=11.4, stage 1&2 vs. stage 3- p=.04, stage 1&2 vs. stage 4&5- p=.002, stage 3 vs. 4&5- p=.023) significantly decline across CKD stages. Similar relationships were observed for hip extensor torque (Figure.3B, F=10.1, stage 1&2 vs. stage 3- p=.01, stage 1&2 vs. stage 4&5- p=.01, stage 3 vs. 4&5- p=.07), and hip extensor power (Figure.3D, F=19.36, stage 1&2 vs. stage 3- p=.009, stage 1&2 vs. stage 4&5- p=.003, stage 3 vs. 4&5- p=.014). Moreover, as shown in Figure 2, eGFR was strongly and significantly positively correlated with knee extensor torque (r=.79, p<.001) and power (r=.84, p<.001) production. Not surprisingly, knee extensor torque and power production significantly positively correlated with stair power production in the functional PPT assessment (r=.78, r=.87, p<.001 respectively) (Figure.2). Importantly, these muscle performance changes were not attributable to altered neuromuscular properties, as no differences were found between staged groups in regards to seconds-to-peak torque (a measure of muscle activation capacity) (knee extensors p=.4, hip extensors p=.18, not shown).

Laboratory Measures* (*blood chemistries)-

As demonstrated in Figure.2, eGFR was significantly strongly negatively correlated with BUN levels (r=-.77, p<.001). Similarly, eGFR was moderately negatively correlated with plasma inflammatory cytokine concentration (IL-6 - r=-.51, p=.006, TNF-a – r=-.47, p=.014). As shown in Figure 4,

systemic IL-6 concentration is slightly elevated in stage 3, but exhibits a robust and significant increase in later stages of disease (stages 4&5, F=6.8, stage 1&2 vs. stage 3- p=.5, stage 1&2 vs. stage 4&5- p=.034, stage 3 vs. stage 4&5- p=.08). The same relationship is demonstrated in TNF-a concentration, though a more noticeable increased in stage 3 is seen with this pro-inflammatory cytokine (F=3.9, stage 1&2 vs. stage 3- p=.6, stage 1&2 vs. stage 4&5- p=.03, stage 3 vs. stage 4&5- p=.1). In examining the interrelationships between these cytokines with BUN levels and functional and muscle performance, Figure 2 shows that both IL-6 and TNF-a cytokine concentrations are significantly strongly positively correlated with BUN (r=.71, r-.56 for IL-6 and TNF-a respectively), however, while both cytokines were negatively correlated with knee extensor torque and power production, only IL-6 cytokine concentrations was significant (r=-.4, r=-.46 with knee extensor torque and power respectively). However, both IL-6 (r=-.54) and TNFa (r=-.37) were negatively correlated with functional stair power production (Figure.2).

Satellite Cell and Inflammatory cell abundance-

SC count (% of mononuclear cell population) significantly declines from early to middle and late CKD stages, as demonstrated in Figure 5A. (F=9.6, stage 1&2 vs. stage 3- p=.015, stage 1&2 vs. stage 4&5- p=.001, stage 3 vs. stage 4&5- p=.47). Additionally, renal filtration rate (eGFR) was significantly positively correlated with SC pool size (r=.707, p<.001, Fig.5B). Conversely, filtration rate was significantly negatively correlated with CD45+ muscle-resident inflammatory cell population (leukocytes) (r=-.695, p<.001, Figure.5D). Interestingly, SC pool size/count was significantly positively correlated with functional stair power production (r=.57, p=.004), knee extensor torque and power production (r=.68, r=.62, p<.001, p=.001 respectively, Figure. 2).

Figure 2 further shows that SC count within skeletal muscle was also negatively correlated with the uremic environment (BUN – r=-.45, p<.001), and moderately negatively correlated with inflammatory cytokine concentration IL-6 (r=-.39) and TNF-a (r=-.33, not-significant). However, CD45 population size did not reach significance in its relationships to any of the other measures, aside from eGFR.

Satellite Cell Proliferative Capacity –

Subsequent to the above findings that SC content is reduced with stage-wise progression of CKD, EdU click-it reaction analysis was performed on selected primary SCs from individuals of each stage as shown in Figure 6A, to determine if cell proliferation may be a potential mechanism driving SC loss in this population. As demonstrated in Figure.6B, SC proliferation, demarcated as % of EdU+ cells after 12 hour incubation period, significantly declines as early as stage 3 CKD, and remains attenuated in later stages. Representative EdU images are shown in Figure.6C (F=27.1, stage 1&2 vs. stage 3 – p=.01, stage 1&2 vs. stage 4&5- p=.001, stage 3 vs. 4&5- p=.058). In light of these findings, it was not surprising that SC proliferative capacity was significantly positively correlated with eGFR (r=.83, p<.001), SC count (r=.71, p=.01), negatively correlated with uremia (BUN – r=-.85, p<.001), IL-6 concentration (r=-.57, p=.03), TNF-a (-.51, p=.048), and was also strongly associated with knee extensor torque and power production (r=.93, r=.87, p<.001) (Fig.2).

Muscle Quality –

With the above findings of reduced SC pool size, and impaired proliferative capacity in-vitro, we sought to characterize the morphological quality of skeletal muscle in this population as shown in Figure 7. H&E staining revealed relatively healthy muscle tissue in early CKD stages (Figure.7B),

however, stage 3 CKD muscle was characterized by increased presence of fibrotic and adipose tissue infiltration (black arrows), which was exacerbated in later stages of disease (Figure.7B). As shown in Figure.7A, when plotted relative to renal function, non-contractile tissue infiltration of skeletal muscle of the quadriceps increases with worsening kidney function (lower eGFR), and this relationship was strongly negative and significant ($r=-.75$, $p<.001$). Not surprisingly, the degree of non-contractile tissue infiltration in the quadriceps was strongly and significantly negatively correlated with knee extensor torque production and power ($r=-.72$, $r=-.75$, $p=.005$, $p=.003$ respectively) (Figure.2). Similarly, non-contractile tissue infiltration significantly negatively correlated with functional stair power ($r=-.51$, $p=.044$). While the degree of non-contractile tissue infiltration was significantly positively correlated with CKD-associated systemic factors (BUN: $r=.79$, IL-6: $r=.57$, TNF-a: $r=.67$, $p=.001$, $p=.042$, $p=.012$ respectively), one of its strongest relationships was to SC proliferative capacity ($r=-.81$, $p<.001$), but not SC number ($r=-.2$, $p>.05$).

Satellite Cell Myogenic Capacity-

Due to the striking degree of non-contractile infiltration in the vastus lateralis with progressive CKD, and its strong relationship to SC proliferative function, we sought to examine the myogenic capacity of these SCs in-vitro by inducing differentiation into myotubes and tracking both the myogenic gene program (MRF expression patterns), and fusion capacity with immunostaining and microscopy (Figure.8A). As demonstrated in Figure.8B, SCs from those in early-stage CKD demonstrated strong myogenic capacity, with myosin-expressing myotube formation and ~38% cell fusion after only 1 day of differentiation, while those in stage 3 and 4&5 CKD exhibit little to no myotube formation in this time period (stage 1 vs. stage 3, $p=.006$, stage 1 vs. 4&5 – $p<.001$). This is also visualized in Figure.8C, as myotube formation is clearly present after only 1 day in early-stage disease, but almost

completely absent in middle and fully absent in late-stage disease (not shown). This relationship continues over the course of differentiation, where robust myotube formation, with a surprising ~95% fusion, was achieved in early-stage SCs by day 2 of differentiation (Figure.8B,C), while myotube formation was significantly less robust with reduced fusion in middle and late stage CKD (stage 1 vs. stage 3, p=.041, stage 1 vs. 4&5 – p=.005) (Figure.8B,C). At day 3, where the myogenic program slows down considerably, and all stages begin to plateau, early-stage CKD SCs maintain their thick, fusion-laden myotube morphology, while middle-stage CKD is not significantly different in their degree of fusion at this time, and late-stage SCs demonstrate slightly improved myotube formation from day 2 albeit with significantly less fusion and myotubes that are not as robust as early-stage cells (stage 1 vs. stage 3, p=.18, stage 1 vs. 4&5 – p=.02). Although not depicted in part C, at day 5, early-stage SCs maintain their morphology achieved at day 2, and this is significantly larger than middle-stage SCs (p=.043), and later-stage (p=.015). Interestingly, at no point during the 5-day differentiation experiment did the degree of fusion between middle stage CKD (stage 3) and later-stage (stage 4&5) differ significantly in their fusion capacity (all days – p>.05). The degree of SC fusion at day 5, was subsequently correlated with the aforementioned measures, and shown in Fig.2. Not surprisingly, the degree of SC fusion was the strongest relationship of all measures to the degree of non-contractile tissue infiltration in muscle (r=-.9, p<.001). The fusion index also strongly correlated with SC proliferative capacity (r=.83, p<.001), and is negatively related to the systemic milleui of CKD (BUN: r=-.73, IL-6: r=-.40, TNF-a: r=-.35, p=.003, p=.15, p=.22 respectively). Interestingly, SC fusion index significantly related to knee extensor torque and power production (r=.81, r=.86, p<.001 respectively), though this may be an indirect relationship mediated through non-contractile tissue accrual secondary to poor SC-mediated myogenesis.

Satellite Cell MRF expression-

Given the SC myogenic deficits, we sought to determine the expression pattern of key MRFs over the 5-day SC differentiation period. As shown in Figure 9A, MyoD expression was attenuated in stage 3 CKD across all studied days (day 1: -31%, day 3: -46%, day5: -57%), and was even more attenuated in late-stage SCs (day 1: -53%, day 3: -64%, day5: -63%), though only MyoD expression on day 1 of differentiation significantly differed between middle and late-stage cells. Myogenin expression was similarly attenuated across all days studied, in both middle (day 1: -52%, day 3: -38%, day5: -62%) and late-stage SCs (day 1: -62%, day 3: -36%, day5: -47%), with no differences observed between middle and late-stage cells (Figure 9B). Myosin heavy chain gene expression was attenuated in middle-stage CKD only after day 1 of differentiation (day 1: -90%), with no difference observed in days 3 or 5 compared to early-stage SCs (Figure 8C). However, myosin heavy chain expression was attenuated at all days in stage 4&5 cells compared to stage 1&2 cells (day 1: -80%, day3: -70%, day5: -68%) (Figure 9C).

Skeletal Muscle Transcriptome-

The RNA-seq analysis resulted in approximately 19–28 million raw sequence reads for each of the 25 cDNA libraries generated from the human skeletal muscle samples. On average, 99% of the trimmed reads mapped to the human reference genome. The muscle samples contained 44,000–66,000 transcripts, with ~5,000-8,000 genes detected. The ribosomal fraction was <5% across all samples. To determine the similarity between expression profiles, we used Pearson correlation plots. The correlation values indicate closely similar expression values for transcripts between biological samples. Differentially expressed genes in the stage 1&2 CKD group, stage 3 CKD group, and stage 4&5 CKD were filtered based on the highest fold change and significant *p*-values and the genes were annotated using Ensembl, leading to the identification of genes that were significantly altered

between stages of disease. As shown in Figure 10 (center graphic), there were 448 differentially expressed genes between early and late-stage CKD, 440 differentially expressed genes between early and middle-stage CKD, and 1775 differentially expressed genes between middle and late-stage CKD, all with p-value <.05.

GO and KEGG gene pathways that differed between CKD stage groups are shown in Figure 10. As demonstrated in Figure.10, A, extracellular matrix organization and structure, MAPK signaling, molecular transducer activity, growth factor activity, g-protine coupled receptor activity and ribosome constituted the most significant down-regulated gene pathways (GO and KEGG terms) (all FDR $\leq$.05) in late-stage CKD (stages 4&5) compared to early disease. Conversely, gene networks involved in miRNA bidning, phagasome, chromatin binding, mRNA transport, histone modification, mRNA processing, cytokine/cytokine-receptor interaction, DNA repair, and complement cascade were all the most significantly upregulated in late-stage disease. Shown in Figure.10, A, are selected genes from the above GO and KEGG terms that were significantly altered in expression. In (Figure.10, B), the significant down-regulated gene networks/pathways in stage 3 CKD compared to early disease, include signaling receptor activity, molecular transducer activity, cell morphogenesis/differentiation, MAPK signaling, protein kinase activity, focal adhesion pathway, and hippo pathway signaling. Conversely, upregulated gene families were observed for the spliceosome, proteasome, transcription factor binding, and chromatin DNA binding networks. As in Figure 10, Tables 2 and 3 describe general functions of selected significantly differentially expressed genes from the selected GO and KEGG pathways. Figure 11 depicts a subunit visualization of the 26S Proteasome that is upregulated in stage 3 CKD.

Discussion

CKD represents a health state characterized by systemic hormonal, protein, metabolic bi-product and genetic alterations and imbalances, with resulting demonstrable muscle morphological characteristics. However, this study, for the first time, demonstrates the negative effect of CKD progression on skeletal muscle reparative and maintenance capacity – through loss of SCs, attenuated SC myogenic gene expression and myogenic capacity. Moreover, theses findings were strongly related to the progressive deterioration in muscle quality with CKD progression, that may serve as the connection between cellular dysfunction and altered muscle contractile performance and physical mobility deficits that are apparent even early in CKD. Our cohort of participants did not differ in any potential confounding variables (ie. age, gender, peripheral neuropathy, BMI, duration of diabetes, glycemic control, insulin sensitivity, or lean mass), lending strong support to the analyzed connections between renal dysfunction and skeletal muscle health, cellular regulation, and performance.

Our findings that CKD progression – from early, to middle, to late-stages demonstrated impairments in physical function (PPT scores, ability to rise from a chair, power production to traverse stairs) that becomes significant upon stage 3 disease, is reflected in numerous other studies (**7, 67, 68, 69**). Moreover, as proximal lower extremity muscle performance (notably the quadriceps) is most strongly associated with functional limitation and mobility disability among those with CKD, our findings that quadriceps and hip extensor torque production and power were significantly reduced with disease progression, in parallel with reductions in function, is not surprising. A potential link between CKD progression and muscle performance impairments, may be the systemic milleui imparted by renal dysfunction. Urea, a major nitrogenous end product of protein and amino acid catabolism and filtered by the renal glomeruli, predictably increases in circulation and intra/extracellular fluid with worsening kidney function. Our findings of moderate-strong

relationships between BUN levels and knee extensor power and strength, and functional stair power production suggest a possible negative influence of urea on muscle function. Indeed, elevated urea concentrations are known to disrupt proteins, and specifically alter the tertiary structure of skeletal muscle myosin. Moreover, urea targets the globular catalytic domain of myosin through ATPase interference at the myosin head, thereby interfering with ATP binding and cross-bridge cycling for contraction (**70)**. The kidneys also play a major role in the clearance of pro-inflammatory cytokines, and thus, our findings of elevated circulating levels of IL-6 and TNF-a in later-stage non-dialyzed CKD patients is reflected in numerous other studies as well (**71,72).** These cytokines have a wide range of negative effects on skeletal muscle, as chronic low-level IL-6 exposure and TNF-a can upregulate skeletal muscle atrophy pathways. Specifically, these cytokines can phosphorylate ribosomal p70 S6 kinase to promote atrophy, activate caspase-3 to target myofibrillar proteins for breakdown, transcriptionally activate the ubiquitin proteasome system, upregulate atrogenes atrogin-1 and MuRF1, and inhibit protein synthesis via phospho-inactivation of IRS-1 and 2 receptors (**73)**. However, the negative effects of such cytokine exposure extend beyond atrophy-induction. Myofibers treated with TNF-a demonstrate failure to maintain contractile force, and both TNF-a and IL-6 have been associated with hand grip strength loss, and lower knee extensor strength (**73,74,75,76).** Thus, the systemic milleui of CKD – elevated urea, and pro-inflammatory cytokines, may combine to partially explain the skeletal muscle performance decrements with CKD progression that in-turn, impairs functional mobility. However, IL-6 cytokine concentration significantly correlated with muscle performance only to a moderate extent, while TNF-a did not, and BUN levels were only slightly stronger in their relationship. Moreover, lean mass assessment with DXA did not differ between stages. While not ruling out an active atrophy process, this suggests that the elevated cytokine concentration in later stages had not promoted enough muscle mass loss to become

significant. This suggests that the systemic factors of CKD do not fully explain the poor muscle performance and health with CKD progression. Thus, to further probe into the mechanistic causes of muscle dysfunction and poor health in CKD, we examined reparative SC function.

SCs are the engine of muscle regeneration and in healthy conditions, satellite cells possess a tremendous capacity to regenerate muscles with their ability to proliferate extensively, differentiate and self-renew (**77).** In muscle injury, induced experimentally or with exercise, sarcolemmal damage triggers SC activation by disturbing the niche of SC (**78).** Moreover, muscle injury not only activates SC locally, but also alerts SCs in distant, uninjured muscles via yet unknown circulating factors, transitioning them into a G_{alert} phase (**79).** However, prolongued or chronic G_{alert} leads to SC pool depletion and regenerative failure (**79**). CKD represents a state of repeated muscle damage, as evidenced by the pervasive findings of z-disc streaming, increased serum CK levels, and centrally nucleated myofibers in muscle biopsy analyses (**11**). Thus, our findings of reduced SC abundance in skeletal muscle with progressive CKD, may be due to SC exhaustion secondary to chronic activation. Such a phenomenon would be similar in mechanism to neuromuscular diseases such as DMD, metabolic myopathies like Pompe disease, and even natural aging, In these health conditions, SC depletion is due to continuous regeneration attempts, and subsequent exhaustion of the SCs (**80).** In such cases of exhaustion, as demonstrated in DMD (mdx mouse model), a subpopulation of SCs no longer proliferate to replenish the SC pool (**80**). In aging studies, reduced SC pool size has been attributed to reduced SC proliferative capacity and a switch to senescence, a finding suggested in our results as well (**81,82)**. Indeed, aging studies have demonstrated a reduction in the SC pool size from 4-5% in adulthood to ~1% in those 60-80 years old (**83**). We demonstrate a strikingly reduced SC pool (.866%) in those with advanced CKD, to levels that reflect an extremely aged condition, and even those in stage 3 disease exhibit reductions below those of typical adults (~2%). While the

precise mechanisms driving proliferative senescence remain poorly understood, a study by Collins and colleagues (2007) shows that when aged muscle stem cells were engrafted into young mice, their capacity to proliferate and re-populate the SC pool were partly restored – a finding that the authors suggested, points to circulating agents of the systemic environment as significant players that partially regulate SC abundance (**84).** In the only study to-date to examine SCs functionality in CKD, the authors, using a murine nephrectomy model that recapitulates ESRD, demonstrate a 44% decline in SC proliferative capacity as measured by SC BrDU incorporation, while we report a reasonably similar 27% decline in stage 4&5 SCs (**33)**. Thus, the systemic milleui of CKD (elevated BUN and inflammatory cytokines) may in fact exert their negative effects on muscle performance indirectly through negative influence on the SC pool size and proliferative capacity, a hypothesis that is suggested in Figure 2. Indeed, while unconfirmed in our study, findings of disrupted cell division kinetics in endothelial cells in CKD lends theoretical support for this explanation (**85**). As other studies have demonstrated- there seems to be a negative impact of the uremic milleui on mesenchymal stem cell (MSC) proliferation, abundance, and overall competence. Work by Noh and colleagues (2011) clearly demonstrate reduction in mesenchymal stem cell proliferation by 50% in the presence of uremia-associated systemic bi-products p-crestol, and indoxyl sulfate (**34**). While we find a smaller, ~27% reduction in proliferative capacity in late-stage CKD SCs, our experiments were conducted on primary cells in ideal culture conditions. However, under experimental conditions similar to our own, the authors also found reduced MSC proliferation and differentiation under ideal in-vitro conditions in those cells obtained from CKD patients as well (**34**). Interestingly, the authors posit that this phenomenon is similar to cellular metabolic or hyperglycemic memory observed in diabetes, in that the uremic environment imparts a metabolic and epigenetic imprint on these stem cells that ultimately impair their kinetics, performance, and lead to deficient cellular

function (**34**). This point leads to one more potential explanation for the loss of SCs observed in this study, with CKD progression. A popular theory applied to the loss of SC with aging, is that SC intrinsic properties, determined via epigenetic mechanisms – ie. DNA methylation, play a large role.

DNA methylation can influence the accessibility of methylated enhancer regions to transcription factors, can alter histone deacetylases and methyltransfersases to promote tight DNA packing and prevent RNA polymerase or transcription factor binding and subsequently, repress gene expression. A recent study has shown that aged SCs present with different methylation patterns that are modified by the systemic environment and its constituent hormones, metabolites, and proteins, and that these methylation marks related to poor SC proliferation and abundance with age (**86**). Others have similarly found that SC hypermethylation in older age interferes with their capacity for self-renewal, leading to SC pool exhaustion (**86**,**87**). While we did not assess epigenetic alteration to SCs in CKD, this represents a promising area of future study. However, we have previously demonstrated evidence of increased mitochondrial ROS production and inefficient respiratory coupling in ATP production with progression of CKD. A consensus theory behind SC epigenetic alterations in other conditions involves continual ROS exposure through mitochondrial deficiencies in skeletal muscle that leads to SC DNA damage and recruitment of epigenetic machinery to repress gene transcription – a plausible and exciting area of future study (**88**, **89**, **90**, **91**). Indeed, our transcriptomic analysis revealed epigenetic gene networks (histone modification, miRNA binding, chromatin binding) to be among the most significantly upregulated in middle and late-stage CKD compared to early CKD (Figure.10). However, aside from SC proliferation deficiency and loss of SCs, even in early CKD (stage 3), SC myogenic deficits were striking. The end-results of poor SC myogenic capacity, is poor myofiber repair and subsequent poor muscle quality (**18**).

As demonstrated in Figure 7, renal function and muscle quality deteriorate in-parallel . Of particular note, selected muscle of those with advanced CKD (eGFR <25 mL/min) demonstrated >25% non-contractile composition. The evident fibrotic and adipose tissue accrual, seen even in stage 3 CKD, strongly implicates deficient SC reparative function.

Indeed, with loss of SCs, as shown in this study, there is noticeable increase in fibroblast density and ECM deposition in muscle, as muscle injury is repaired poorly and injured contractile tissue is replaced with non-contractile accumulation. Moreover, these fibroblasts retain a multipotent capacity and can differentiate into adipocytes, thus promoting intramuscular adipose tissue infiltration in addition to unchecked fibrosis, a possibility given our observations of adipose tissue infiltration as early as stage 3 CKD (Figure 8B, dark arrows) (**19)**. However, it is difficult to discern the directionality of this relationship in our findings, as excessive ECM with regeneration can impede muscle function and hinder muscle regeneration, and prevent SC self-renewal to exhaust the SC pool as well (**22**). In any case, poor myofiber repair and subsequent poor muscle quality decreases specific tension generating capacity in skeletal muscle. This is supported in our findings that reduced SC proliferative and myogenic capacity is strongly related to non-contractile tissue deposition, which is in-turn strongly negatively related to muscle performance and mobility.

Interestingly, SCs from middle and late-stage disease did not exhibit significant differences in their myogenic capacity or in their upregulation of the necessary MRFs, yet both were deficient when compared to early CKD (stages 1 &2).

With damage, SCs exit from quiescence and engage in a highly orchestrated and self-regulating myogenic program. We report delayed and deficient myotube formation and SC fusion in-vitro in both CKD stages 3 and 4&5. This myogenic program is driven by overlapping gene

expression patterns, beginning with MyoD and Myf5 to drive SC activation. In fact, deficient MyoD activation causes SC withdrawal from the cell cycle and attenuates progression to differentiation and repair, effectively delaying myogenic differentiation (**92).** We demonstrate, after 5 days of differentiation, a 58% reduction in MyoD expression in stage 3 disease, and 64% reduction in stages 4&5. These findings are strikingly similar to the findings of Zhang et al (2010), that exhibit a ~55% reduction in MyoD expression in SCs from CKD mice after 5 days of differentiation (**33).** Moreover, we find attenuated MyoD expression 1 day and 3 days after differentiation induction as well (Figure 9). This may be a potential genetic cause explaining the delayed and deficient myogenesis we observe in middle and late-disease SCs (Figure 8).

Differentiating SCs fuse to each other or existing myofibers to restore structure and function to muscle (**93**,**16,18)**. Thus fusion of myoblasts are crucial in muscle repair and maintenance, and altered fusion causes delayed, deficient, and inadequate regeneration (**94).** This fusion process is dependent upon genetic expression of Myogenin and Mrf4 – two immediate downstream targets of MyoD (**18).** Subsequently, a large portion of Myogenin and Mef2 target genes encode muscle-specific structural, transmembrane, and contractile genes such as those encoding actins, myosins, and troponins, in addition to adhesion molecules, and binding factors that facilitate cell-cell communication and fusion (**18 ,95**). Similar to our MyoD expression results, SCs from middle and late-stage CKD exhibit attenuated myogenin expression across all studied days (1, 3, and 5 days post-differentiation). This strongly suggests that CKD progression may negatively influence the myogenic program to alter key MRF expression patterns, and hamper proper SC regenerative function. Of note however, were our findings that although deficient compared to early disease (stages 1&2 CKD), middle and late-stage SCs are still capable of producing myotubes in-vitro, with late-stage SCs even achieving ~60% fusion by day 5. However, if these new myonuclei retain poor

myogenic expression, contractile protein may not be properly transcribed, deficient, and muscle morphology may be altered as well.

Interestingly, the fact that these cells demonstrate altered MRF expression and proliferation/fusion kinetics in-vitro, strongly suggests that the CKD environment may impose epigenetic alterations that are in-turn remembered by these cells and demonstrated in culture conditions (**96**). Indeed, the work by Zhang and colleagues (2010) also demonstrates in-vitro impairment in SC myotube formation and fusion with 30% reduction in Myogenin expression at 5-days post-differentiation in a murine CKD model (**33).** While we found myogenin to be attenuated to a greater extent (~50% in middle and late stage CKD), both findings suggest that the systemic environment of CKD negatively influences genetic expression of SCs, and this is committed to cellular memory even outside this environment. While it is unclear what particular mechanisms or CKD-associated factors result in impaired MRF activation in these SCs, our findings of poor muscle quality with evidence of excess fibrosis and adipose tissue accumulation in progressively declining kidney function (Figure 8), suggests that SC dysfunction may stem from other muscle-resident sources.

We demonstrate a progressive increase in muscle-resident leukocytes with worsening kidney function in CKD (Figure 5C). The injury-SC-repair process activates the complement cascade and inflammatory response that immediately recruits leukocytes to the muscle tissue (**18).** This is subsequently followed by signaling cascades that produce down-stream pro-inflammatory macrophages and cytokines and signal the production of extracellular matrix constituents like collagen and fibronectin from other cell types like fibroblasts (**18**). However, even slight imbalances in immune cell populations in muscle can disrupt cellular dynamics of the SC niche, as sustained inflammation promotes persistent expression of ECM proteins and impairs SC differentiation and

proliferative function (**97**). While we demonstrate a kidney function-associated rise in the leukocyte population, and increased circulating inflammatory cytokines (IL-6 and TNF-a in late-stage CKD) others have demonstrated prolongued macrophage infiltration in CKD muscle after injury that persists beyond 2 weeks, with accompanying increase in IL-6 (2.5x) and TNF-a (5x) gene expression and increase muscle fibrosis (**33).** The authors conclude that CKD facilitates a "more intense" macrophage infiltration in muscle. Our data suggests that this may indeed be the case, and may be due to increased muscle resident leukocyte population (CD45+), even in non-injured CKD muscle.

Thus, a potential explanation for the progressively poor muscle quality, even in middle-stage CKD, may be a cyclical process whereby the CKD environment and accompanying inflammation may impair SC proliferative function and myogenic capacity at a genetic level, to hinder adequate muscle repair. At this time other muscle-resident cell populations (ie. fibroblasts) contribute excessively and are disinhibited by the associated SC dysfunction. This creates a progressive thickening of the muscle ECM, and potentially promotes transdifferentiation of other cells (ie. fibro-adipogenic progenitors -- FAPs) leading adipose tissue accrual, and muscle replacement with non-contractile tissue. The resultant biophysical properties of the SC niche further negatively influence the remaining SCs to inhibit their function. While this is speculative, transcriptomic analysis via RNA-sequencing suggests this may indeed be the case.

RNA-seq results demonstrate significant gene pathway alterations in CKD progression, beginning in stage 3 disease that lends further support to the morphological and functional differences demonstrated in this study. In both Stage 3 CKD, and later stages (4&5) of disease, gene pathways governing cell morphogenesis, focal adhesion and molecular transducer and cell signaling networks are negatively affected compared to early-stage CKD, and many genes within these pathways carry particular significance in regulating SC function and myogenesis (Figure 10).

In stage-3 CKD, genes of particular interest included CDC42, CRKL, DOCK1, PTEN, Myf5, SKIL, EFNA5, WNT5A, FZD4, and TCF7 as all of these genes were significantly downregulated (Table 3), and all carry direct action on SC function. These genes govern a host of pro-SC-function duties ranging from -- actin-fiber recruitment to facilitate SC fusion and myogenesis; encoding SC adaptor proteins that facilitate growth-factor signaling networks (ie. MAPK) to fuel SC proliferation; encoding signaling proteins that activate key transcriptional networks (ie. Akt-mTOR pathway) to ensure adequate SC proliferation and self-renewal; direct MRFs (ie. Myf5) that guide SCs to myoblast lineage; transcription factors that alter epigenetic marks to promote myogenesis; interstitial second-messenger proteins that stimulate SC motility and regulate interstitial cell concentration; and SC Wnt signaling (Figure.10, Table 3) (**98**, **99**, **100**, **101**, **79**, **102**, **103**, **104**, **105**, **106**, **107**). Interestingly, cell signaling networks in later-stage disease were more strongly connected to inflammatory reactions, although within the molecular transducer gene network, we also found significant attenuation in expression of genes that govern SC function as well – with reductions in IGF-1 expression, but upregulation in RPTOR gene expression, a canonical mTOR signaling protein known to stimulate SC cycle shifts to G_{alert}; upregulation in CDKN1A a pro-atrophy cyclin-dependent kinase inhibitor that mediates p53 inhibition of SC proliferation while simultaneously stimulating protein degradation and inhibiting protein synthesis; and downregulation of BCL2, an anti-apoptotic gene that promotes autophagy and clearance of deficient or defective contractile proteins and organelles (Figure.10, Table 2) (**108**, **33**, **109**, **110)**. In this regard, early and late-stage CKD seem to have differential gene-driven negative effects on SC-mediate myogenesis and general muscle maintenance. This is perhaps best supported by the different gene pathways outside cell signaling and molecular transduction, that play important roles in muscle health.

Stage 3 CKD skeletal muscle demonstrated notable attenuation in gene expression of numerous muscle-integrity-related genes. For instance, the downregulation of the gene encoding cortactin (Table 3) may promote muscle fragility through inadequate transcription/translation of its actin binding filament that is important for muscle cytoskeletal structure (**111**). Similarly, the stage 3 reduction in CAV3 expression (Table 3) suggests that there may be a significant loss of caveolin3 protein, a key muscle membrane constituent that maintains sarcolemmal integrity in response to mechanical strain and aids in membrane repair, while also playing an important role in myoblast fusion (**112**, **113**). Lastly, the finding of attenuated expression of fibronectin 1, a protein that contributes to myogenesis and SC differentiation, has also been shown, that when down-regulated, promotes myofiber disorganization (**114**, **115**). Thus, in middle-stage CKD, there may be a shift in the transcriptome that promotes a loss of skeletal muscle architectural integrity, with simultaneous impairment in SC-response and SC signaling networks. However, we observe ECM-integrity genes to be upregulated in late-stage CKD, perhaps as an adaptive compensatory mechanism to bolster a more fragile architecture with disease progression. Specifically, we find upregulation of COL19A1, a collagen fibril-associated cross-bridge protein that serves as a scaffold for ECM deposition, along with increased expression of COL27A1 and TNC **(116)**. Interestingly, TNC encodes an ECM protein expressed only in actively remodeling muscle tissue as a result of microdamage (**117**). TNC exerts a strong proliferative effect on interstitial cells, and has even been shown to make SCs de-adhesive to their niche, so as to engage in the myogenic program (**117**). However, we did observe reduced MYOC gene expression, a gene encoding the myocillin protein link between the dystrophin-associated protein complex (DAPC) and intracellular signaling machinery. Myocillin not only acts as the bridge to translate extracellular mechanical signals into metabolic change (ie. Akt activation), but also serves to stabilize the DAPC link to the ECM (**118**). This represents an intriguing possibility

that may partially explain the increase in fibrosis observed with CKD progression that warrants further study. Thus, there appears to be a significant alteration in key muscle integrity and ECM-related genes in both middle and late-stage CKD that may help explain both the observed poor muscle quality (Figure.10, Tables 2 and 3) with worsening kidney function, but also the poor SC functional capacity. However, while middle and late-stage CKD skeletal muscle seem to both share alterations in these gene pathways, muscle in later stage CKD (stages 4&5), exhibits a unique upregulation in the cytokine/cytokine-receptor signaling gene networks indicative of active inflammatory processes that may present its own set of negative consequences on muscle health.

Consistent with our findings of significantly elevated circulating inflammatory cytokines (IL-6 and TNF-a) in late-stage CKD, we found significant upregulation of genes involved in inflammatory cytokine signaling in skeletal muscle in late-stage CKD. Specifically, activators of NF-KB, the primary inflammatory-responsive muscle regulatory network were increased in their expression – IL1R, EDA2R, TNF-a receptor TNFRSF10D, CX3CL1 all act as pro-inflammatory receptors that activate canonical NF-KB signaling in skeletal muscle (Figure.10, Table 2) (**119**, **120**, **121**, **122**, **123**). Moreover, we also observe increased expression of LBP, a lipopolysaccharide binding protein that acts a key mediator of IL-6 and IL-1 signaling (**124**). However, as mentioned previously, inflammatory signaling in skeletal muscle is carried out through a coordinated network of different cell types and paracrine and autocrine signaling. Keeping this in mind, our results suggest that many aspects of this signaling cascade are upregulated in late-stage CKD as genes governing the inflammatory response and leukocyte recruitment were also significantly increased in expression.

Of interest was the upregulation of CX3CR1, a chemokine gene involved in leukocyte adhesion, signaling, and migration that positively regulates macrophage inflammatory cytokine

expression, and also serves as cell-surface protein found on inflammatory macrophages that invade injured muscle after phagocytosis of injured debris (Table 2) (**125**). Similarly, we observe increased expression of ADAMTS12, a matrix metalloproteinase induced by inflammatory cytokines (ie. TNF-a and IL-1B) in the ECM to mediate inflammatory response and guide collagen-producing-cell fate (**126**). We also report elevated expression of other inflammatory genes known to be responsive to cell stress (PRKAB1), induction of the sarcoplasmic and cytoplasmic inflammasome (NLRC4), and chemokine signaling (Figure.10, Table 2) (**127**, **128**, **129**). Of particular interest however, was the novel finding of drastic upregulation of the major histocompatibility complex 2 (MHC II complex) in those with stage 4&5 CKD. MHC class 2 expression in muscle is induced when the muscle becomes immunologically activated, often in response to inflammatory cell types. We specifically find very large increases in expression of MHC class 2 component genes – HLA-DRB1 (+2.83x), HLA-DRB5 (+5x), HLA-DRA (+2.4x), HLA-DPB1 (+3.8x), and HLA-B (+8x) (Figure 10, Table 2). While a rare finding, this has been uniquely demonstrated previously as a feature of inflammatory myositis, and has been postulated to potentially precede leukocyte muscle infiltration (**130**). Yet, despite the striking transcriptomic evidence of active inflammatory signaling in late-stage CKD muscle, CCR1 gene expression was attenuated by more than 2-fold. CCR1 is a myoblast receptor, that upon interaction with inflammation-stimulated MIp1a secretion by macrophages, engages in proliferation and asymmetric division (**131**) (Figure.10). Thus, this receptor is a critical component to SC activation in response to injury-induced inflammatory signaling, and its reduction in CKD skeletal muscle may impede proper SC kinetics in the face of inflammatory stimulation. While inflammatory transcriptome changes were much more evident in late-stage CKD, we find altered expression of genes involved in inflammatory cytokine signaling in middle-stage as well. Specifically, we observed a downregulation of PTPRS, a muscle cell surface receptor that normally

inhibits TNF-a production and NF-KB signaling, suggesting a potential avenue of disinhibition of inflammatory signaling (**132**) (Figure.10, Table 3). Similar to late-stage CKD, we also observe upregulation of CXCL12, a chemoattractant that attracts monocytes and lymphocytes with muscle damage (**133**). Thus, the transcriptome in stage 3 CKD supports the theory of muscle damage, altered structural integrity, and inflammatory signaling is also present, though to a lesser extent, in middle stage CKD. Intruigingly however, one of the most significantly upregulated gene networks in stage 3 CKD involved key structural protein subunits of the 26S proteasome – the degradative complex of the ubiquitin proteasome pathway (Figure.11). This suggests that even in middle-stage CKD, the degradative process may be stimulated above that in early-stage disease.

Conclusion

T2DM-induced CKD progression, and its associated uremic environment, independent of diabetic severity or duration, negatively impacts physical function, potentially via impairment of muscle force generation, and power. We demonstrate, for the first time, that these muscle performance decrements strongly relate to intrinsic changes in skeletal muscle maintenance and health that is dictated by changes in the muscle transcriptome, SC and inflammatory abundance, SC functional capacity (proliferative and myogenic capacity), and myogenic gene program with CKD progression. Of particular importance – our findings suggests CKD-associated changes across all levels of skeletal muscle health and performance, begin as early as stage 3 disease. Future studies are needed to investigate the direct mechanisms driving such changes (ie. uremic environment-associated epigenetic alterations), and how therapeutic intervention may address these detrimental adaptations.

Tables for Chapter 3:

Table 1

TABLE 1	Stage 1&2 (60+ mL/min)	Stage 3 (30-59 mL/min)	Stage 4&5 (<29 mL/min)	P-value
Gender (M,F)	7,2	6,3	5,4	Fishers Exact (p=.47)
Age (SD)	55 (9.8)	61 (6.4)	62 (7.3)	1-way ANOVA (p=.13)
BMI (SD)	33.5 (5.6)	33.7 (5.6)	38.9 (6.3)	1-way ANOVA (p=.10)
Years of DM (SD)	14 (6.3)	13 (7.6)	17 (7)	1-way ANOVA (p=.37)
HbA1c (SD)	8.01 (2.1)	7.85 (1.8)	7.5 (2.1)	1-way ANOVA (p=.88)
Neuropathy (Yes, No)	5,4	5,4	5,4	1-way ANOVA (p=.8)
Whole-body lean mass (kg)	59.24 (10.1)	55.64 (14.7)	57.08 (9)	1-way ANOVA (p=.8)
OGTT AUC (SD)	40180 (10911)	47394 (11510)	39752 (12010)	1-way ANOVA (p=.37)
BUN (SD)	18 (2.95)	31.2 (6.55)	58.2 (21)	1-way ANOVA (p<.001) *Stage 1&2 vs. Stage 3 ^Stage 1&2 vs. Stage 4&5 #Stage 3 vs. Stage 4&5
Albumin:Creatinine (ACR – mg/g)	279 (530)	729 (1100)	1086 (790)	1-way ANOVA p=.16
Kidney Function (eGFR)	87.8 (20.1)	46.3 (7.4)	18.9 (7.6)	1-way ANOVA (p<.01) *Stage 1&2 vs. Stage 3 ^Stage 1&2 vs. Stage 4&5 #Stage 3 vs. Stage 4&5

Table 1

Demographics. Participant demographics were compared using 1-way ANOVA, and chi-square was used for sex distribution, and peripheral neuropathy status between groups. Values listed are mean and standard deviation in (). The following symbols represent post-hoc pairwise comparisons in the event of significant F-test - *(between Stage 1&2 and Stage 3), ^(between stage 1&2 and Stage 4&5), #(Between stage 3 and Stage 4&5)

Table 2

Stage 4&5 vs. Stage 1&2 Significant GO and KEGG terms: selected genes	
Cytokine/Cytokine-receptor interaction	
IL1R (+1.47x)	upstream activator of NFKB through IL1 pro-inflammatory signaling
EDA2R (+1.61x)	positive activator of NF-KB signaling
TNFRSF10D (+1.7x)	TNF-family receptor, induces NFK-B pathway, part of TNF-alpha signaling pathway
CX3CL1 (+1.63x)	Positive regulatory of canonical NF-KB signaling (upregulates NFKB signaling, and induces authophagy)
LBP (+2.1x)	lipopolysaccharide-binding protein, binds lipopolysaccharides to modulate inflammatory pathways. Levels of LBP are greater in presence of cytokines like IL-6 and IL-1
PRKAB1 (+1.6x)	upregulated in response to cellular stress, connected to AMPK stress signaling
CXC3R1 (+1.63x)	Monocyte receptor subtype. chemokine involved in adhesion, signaling, and migration of leukocytes. After monocytes phagocytose the injured muscle, macrophages that are CXC3R1-positive take over to promote muscle regeneration, and positively attracts macrophages (acts as a chemokine receptor for tissue-resident macrophages), and positively regulates macrophages inflammatory cytokine expression.
HLA-DRB1 (+2.83x) ***HLA-DPB1 (+3.8)*** ***HLA-DRB5 (+5x)*** ***HLA-B (+8)*** ***HLA-DRA (+2.4x)***	MHC complex 2 constituent proteins. Its expression is induced in skeletal muscle when the muscle becomes immunologically activated – often in response to inflammatory cell signaling. This is a feature of inflammatory myositis, and may precede leukocyte infiltrations into muscle.
ACKR1 (+1.5x)	chemokine receptor
ECM Organization	
COL19A1 (+2.1x)	encodes collagen type 19 alpha 1, a fibril-associated collagen that serves as cross-bridge between fibrils and other ECM molecules.

	Serves as scaffold for ECM construction
COL27A1 (+1.53x)	ECM collagen member
TNC (+1.5x)	ECM protein expressed only in actively remodeling muscle tissue from micro-damage. Exerts strong proliferative effect on interstitial cells, and shown to make SCs de-adhesive to their niche so they can engage in myogenic program
Molecular Transducer Activity	
IGF1 (-1.5x)	Growth hormone/signaling protein involved in SC proliferation, differentiation, and myogenesis-mediated regeneration. Its attenuated signaling shown to a potential key factor in murine models of skeletal muscle SC dysfunction in CKD
RPTOR (+1.4x)	Links mTORC1 signaling in SCs. Responsible for G_{alert} phase transition in SCs
CDKN1A (+2x)	Pro-atrophy, cyclin-dependent kinase inhibitor that mediates p53 inhibition of SC proliferation while simultaneous stimulating protein degradation and inhibiting protein synthesis
MYOC (-1.9x)	Encodes the protein link between the dystrophin-associated protein complex (DAPC) and intracellular signaling machinery. Myocillin not only acts as the bridge to translate extracellular mechanical signals into metabolic change (ie. Akt activation), but also serves to stabilize the DAPC link to the ECM
PIK3R (-1.6x)	Receptor link between IGF-1 signaling and muscle protein synthesis. PIK3R is recruited to activated IRS sites to signaling activation of Akt, which then inhibits protein breakdown through repression of FoXO family degradative transcription factors, while also stimulating protein-synthesis mTOR pathway

Table 2

Table of significantly differentially expressed genes from Figure 10A (genes down or upregulated in late-stage CKD vs. early stage 1&2), their relative fold change, and their basic function listed to the right.

Table 3

Stage 3 vs. Stage 1&2 Significant GO and KEGG terms: selected genes	
Cell Morphogenesis	
CDC42 (-1.42x)	When deficient, results in impaired actin fiber recruitment to myoblast contact sites, essential for SC fusion and myogenesis -- (FROM "The small G-proteins Rac1 and Cdc42 are essential for myoblast fusion in the mouse")
CORTACTIN (-1.6x)	Actin binding filament, important in the cytoskeletal structure of muscle
PTPRS (-1.45x)	cell surface receptor, normally down regulates NFK-B and TNFa production
CX3CL12 (+1.5x)	Acts to induce rapid chemotaxis, and positive attractor of monocytes and T-lymphocytes. Has been shown to be upregulated following exercise-induced damage
Myf5 (-1.4x)	Myogenic SC lineage director. Downregulation could be indicative of fewer of SCs.
FZD4 (-1.8x)	receptor for wnt5a
CMKLR1 (-2.3x)	g-protein-coupled receptor activated by leukocyte attractants and adipokines. When reduced in expression, it impairs SC differentiation
Signaling Receptor Activity	
ACTB (-1.5x)	Beta actin, links dystrophin complex to the cytoskeleton
WNT5a (-1.42x)	With early muscle damage, WNT5A should be upregulated, promotes slow myofiber type, modulates chromatin structure of MyoD and Myf5 promoters to induce their expression, and promotes SC proliferation and self-renewal (through upregulation of B-catenin)
TCF7 (-1.74x)	encodes crucial B-catenin co-factor, and downstream effector of Wnt signaling (decreased expression along with WNT5a)

FGF1 (-1.81x)	growth factor, expressed in SCs, promotes SC differentiation
CRKL (-1.6x)	SC adaptor protein that facilitates Fibroblast Growth Factor signaling to SCs, which then activates MAPK signaling that fuels SC proliferation. If its down, this may inhibit SC proliferation
FN1 (-1.92x)	Fibronectin, contributes to myogenesis and differentiation, when downregulated leads to disorganization of myofibers
CCND2 (-2.25x)	cyclin D2, it directly interacts with cyclin-dependent kinase Cdk4 to block myogenic switch during fusion
Focal Adhesion Pathway	
DOCK1 (-1.5x)	plays a major role in governing SC fusion
PTEN (-1.9x)	present in quiescent SCs, when downregulated, leads to premature SC differentiation, lack of proliferation and SC pool reduction and regenerative failure, and once activated, these SCs cannot return to quiescence
CAV3 (-1.8x)	Major muscle membrane protein of caveolae. If downregulated, leads to reduced sarcolemmal integrity in response to mechanical strain. Also interacts with dysferlin in sarcolemmal membrane repair, and plays an important role in myoblast fusion
SKIL (-2.3x)	Ski-like protooncogene -- encodes a repressor of TGF-b signaling, and enhances muscle differentiation through modulation of the myogenin promoter via activation of the MEF2 complex and inhibition of the histone deacetylase activity, AND activates the enhancer and promoter of myosin proteins and muscle creatine kinase
EFNA5 (-2.65x)	Ephrin A5, target of NFK-B signaling. Ephrin A5 stimulates myoblast motility and proliferation (via NG2+ interstitial cells). When downregulated, causes significant reduction in myoblast mottility and increases number of interstitial cells

Table 3

Table of significantly differentially expressed genes from Figure 10B (genes down or upregulated in middle-stage CKD vs. early stage 1&2), their relative fold change, and their basic function listed to the right.

Figures for Chapter 3:

Figure 1

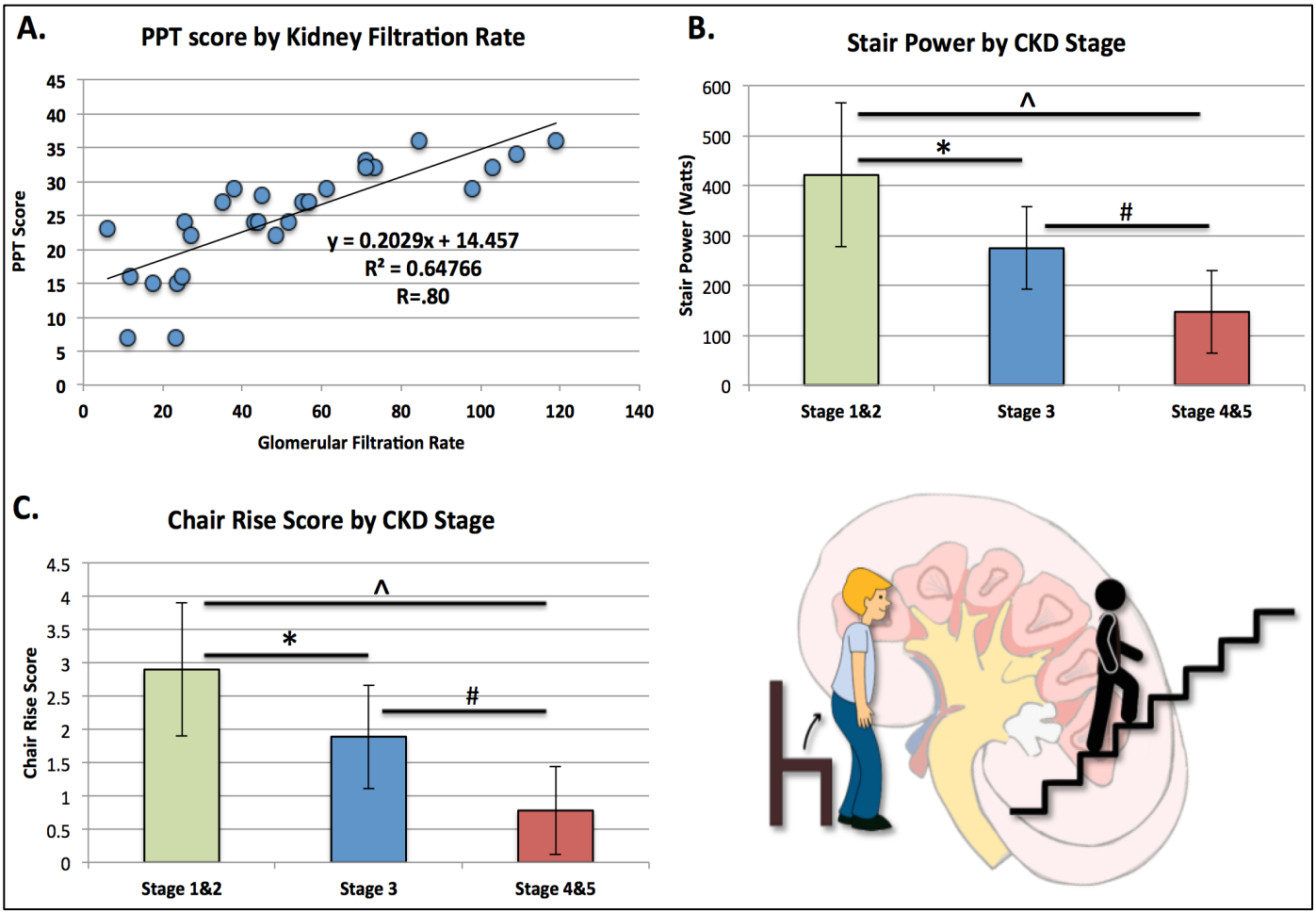

FIGURE 1 – Physical function capacity was assessed across CKD-stage groups with 1-way ANOVAs, and Bivariate pearson correlations. Bar heights represent group mean and error bars represent ± SD. The following symbols represent significant post-hoc tests of pairwise comparisons: *(between Stage 1&2 and Stage 3), ^(between stage 1&2 and Stage 4&5), #(Between stage 3 and Stage 4&5). **A**. Pearson Bivariate Correlation with eGFR (glomerular filtration rate) plotted on the x-axis, and PPT score (0-36) plotted on the y-axis (higher scores indicate better functional performance) (not pictured – p<.001). **B**. Calculated stair power (watts), higher values indicate more lower extremity power produced to ascend stairs (F=14.7, p<.001). **C**. Chair rise score (from the physical performance test) (F=13.9, p<.001). As shown in **B,** and **C**, there are significant step-wise declines in stair power and chair rise capacity as CKD stage progresses.

Figure 2

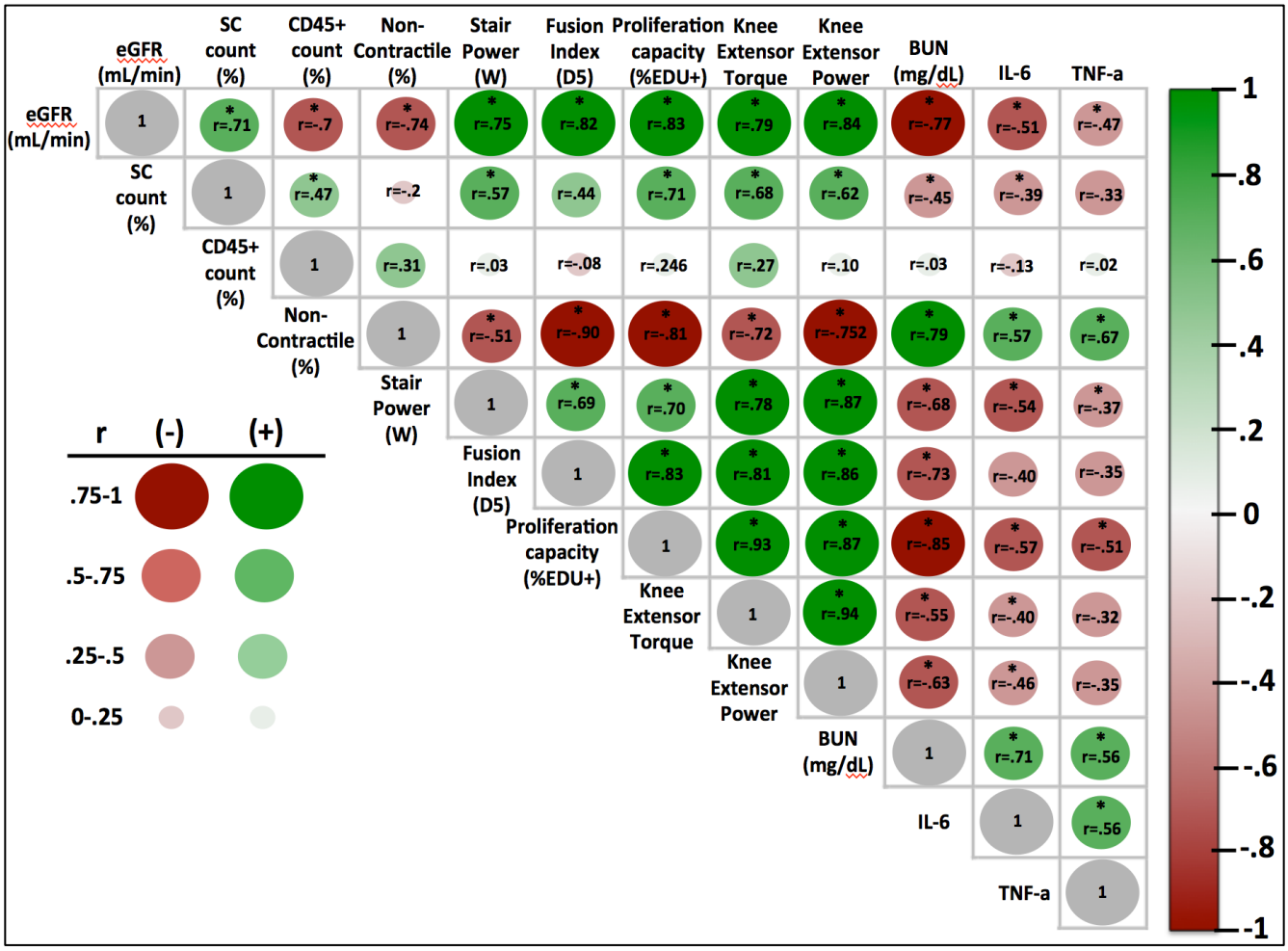

FIGURE 2- Bivariate pearson correlation matrix depicting interrelationships between renal filtration rate (eGFR), serum markers (BUN, inflammatory cytokines – IL-6, TNF-a), functional performance (stair power), muscle performance (knee extensor torque and power), muscle quality (non-contractile % = % of muscle sample that is non-contractile tissue), SC count and function, and muscle-resident leukocyte population (CD45+). Color key is shown bottom left. Stronger correlations are reflected by higher r-value range, and darker shade (red = negative correlation, green = positive correlation). This range is also displayed at right in bar format. Correlation r-values are inset within each correlation pair circle, with an * denoting significant correlation ($p<.05$). Gray circles mark variables correlating with itself. (Note – knee extensor torque was assessed at 30^0/sec isokinetic speed, Knee extensor power assessed at 30^0/sec and expressed in watts. Hip extensor muscle performance not included here due to the quadriceps-specific cellular measures included in correlation matrix).

Figure 3

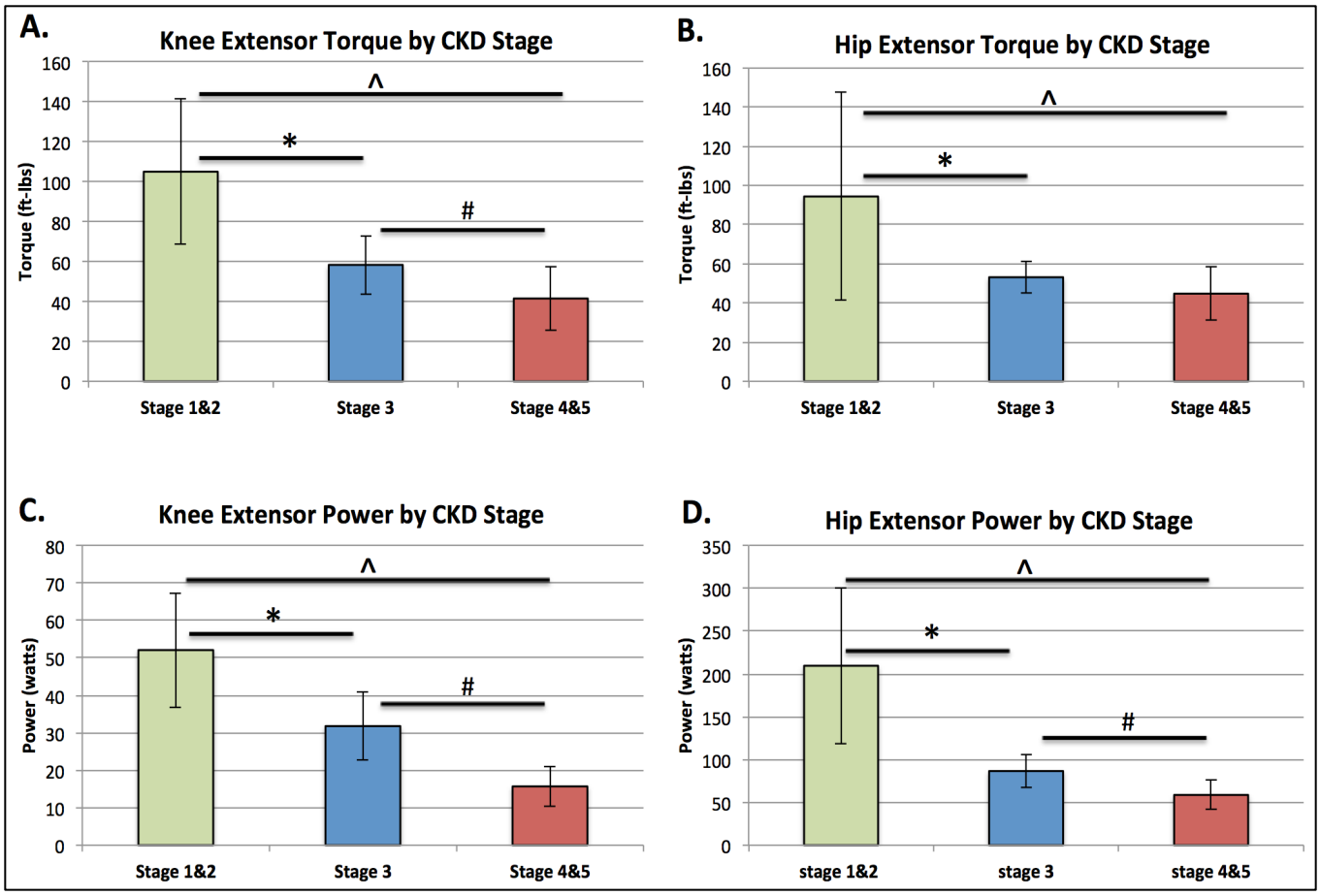

FIGURE 3-
Lower extremity muscle strength (hip extensor, knee extensor torque), and power (hip extensor power and knee extensor power) were assessed across CKD-stage groups with 1-way ANOVAs. Bar heights indicate group means, with errors bars indicating $\pm$ SD. The following symbols represent significant post-hoc tests of pairwise comparisons: *(between Stage 1&2 and Stage 3), ^(between stage 1&2 and Stage 4&5), #(Between stage 3 and Stage 4&5). **A**. Group differences in knee extensor torque (assessed at isokinetic speed of 30^0/sec, knee extensor torque measured in ft-lbs) ($F=16.9$, $p<.001$). **B**. Hip extensor torque (120^0/sec, ft-lbs) ($F=8.8$, $p=.01$). **C**. Knee extensor power (30^0/sec, measured in watts) ($F=11.4$, $p<.001$). **D**. Hip extensor power (30^0/sec, watts), ($F=19$, $p<.001$).

Figure 4

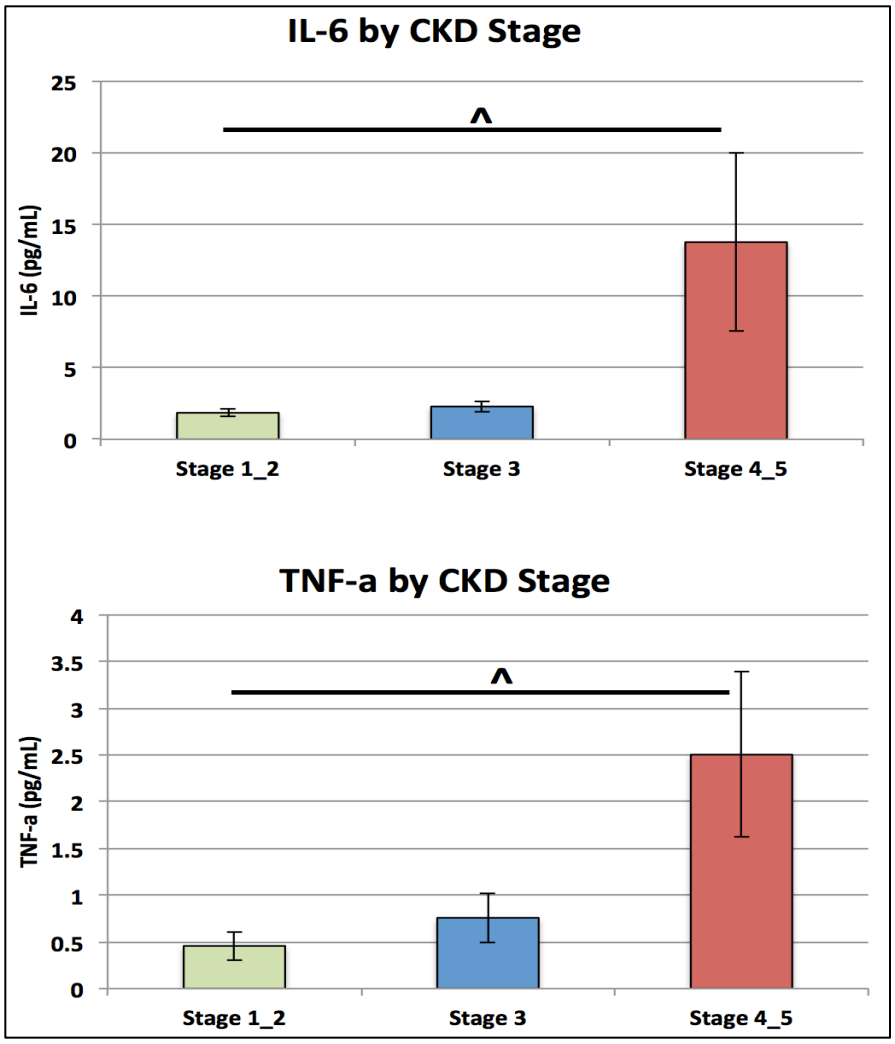

FIGURE 4-

Plasma inflammatory cytokine concentration (pg/mL) was assessed across CKD-stage groups with 1-way ANOVAs, specifically comparing TNF-α, and IL-6. Bar heights indicate group means, with errors bars indicating ± SEM. *TOP***.** IL-6 concentration by CKD Stage (F=6.8, p=.005), ^ denotes post-hoc significant difference between stage 1&2 and stage 4&5 (p<.005). *BOTTOM*. TNF-α concentration by CKD Stage (F=3.9, p=.035), as above, ^ denotes post-hoc significant difference between stage 1&2 and stage 4&5 (p<.005).

Figure 5

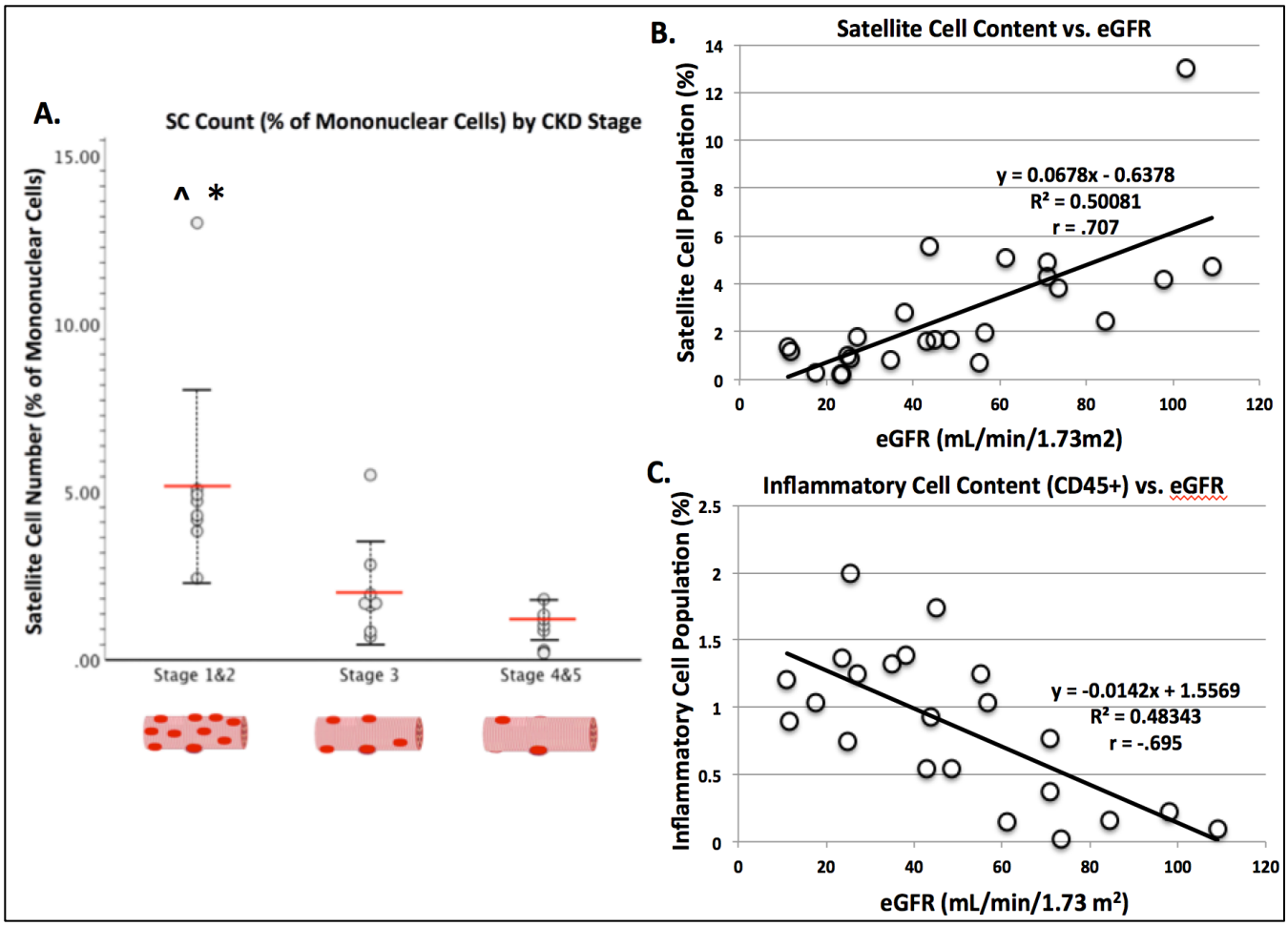

FIGURE 5-
Fluorescence Activated Cell Sorting (FACS) Results for SC and CD45+ (leukocytes) cells in all samples. SC count was assessed across CKD-stage groups with 1-way ANOVA. The following symbols denote significant post-hoc tests: *(between Stage 1&2 and Stage 3), ^(between stage 1&2 and Stage 4&5), #(Between stage 3 and Stage 4&5). **A**. FACS results counting SC population, expressed as the % of mononuclear cells (y-axis) in the sample. Red horizontal lines indicate the average count for that stage, with SD bars. Small circles represent each individual's SC count ($F=9.6$, $p=.001$). Inset above Stage 1&2 are the ^ and * symbols denoting significant differences between stage 1&2 and 4&5, and stage 1&2 and stage 3 respectively. **B.** Pearson bivariate correlation chart plotting SC count (% of mononuclear cells – y-axis) against renal filtration rate (eGFR – x-axis) (not shown, $p<.001$). **C**. Pearson bivariate correlation chart plotting CD45+ (leukocyte) population expressed once again as % of mononuclear cell population (y-axis) against eGFR (x-axis) (not shown, $p<.05$).

Figure 6

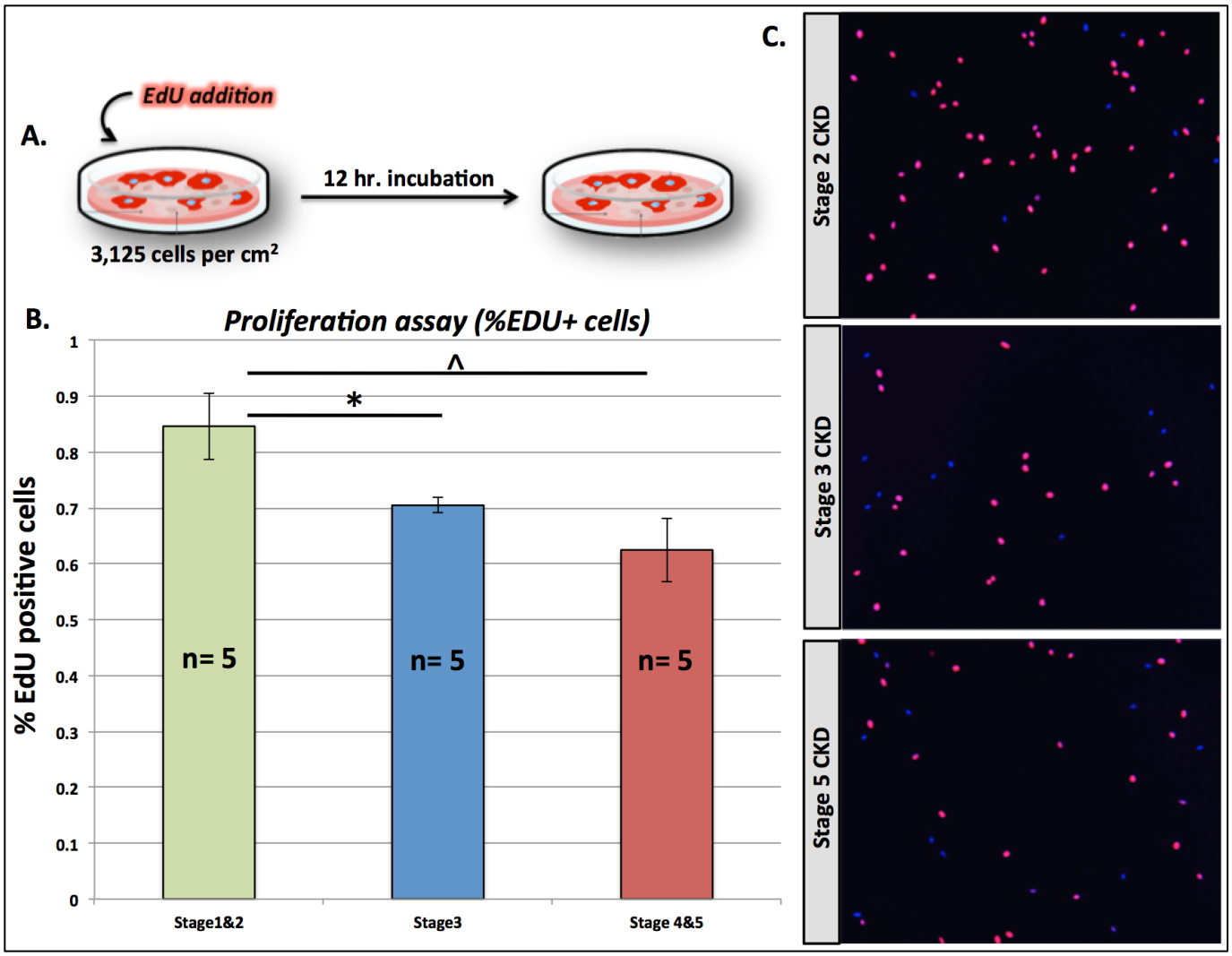

FIGURE 6-
SC in-vitro proliferative capacity, assessed with EdU click-it-reaction. **A**. Experiment setup – SCs were plated at 3,125 cells per cm^2 on matrigel-coated dishes, and incubated for 12 hours at 37^0C with growth media containing 1 mM EdU solution. Cells were then fixed, stained and imaged to track the % of EdU+ cells out of all cells in 5 random locations over 2 dishes per sample. % of EdU+ cells assessed across CKD-stage groups with 1-way ANOVA. The following symbols denote significant post-hoc tests: *(between Stage 1&2 and Stage 3), ^(between stage 1&2 and Stage 4&5), #(Between stage 3 and Stage 4&5). **B.** Bar graph depicting stage-specific group differences in % of EdU+ cells (EdU+/Total cells – Y-axis) (marker of proliferative capacity) ($F=27$, $p<.001$). **C**. Representative EdU images (10x). *TOP* – SCs in early (stage 2) CKD demonstrate high proportion of EdU+ cells (red). *MIDDLE*- SCs in middle (stage 3) CKD. *BOTTOM* – SCs in late-stage CKD. (Blue = DAPI staining of all cells).

Figure 7

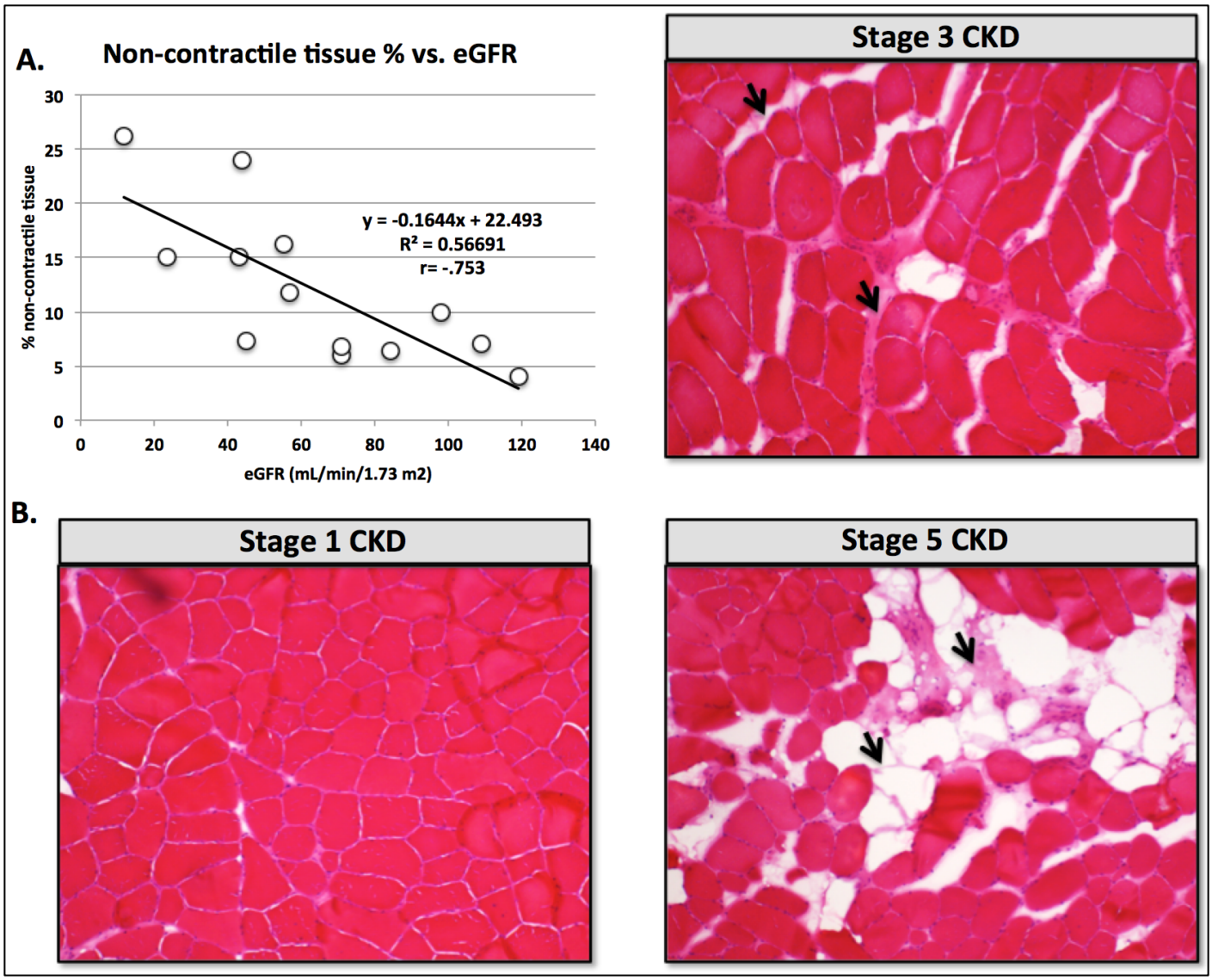

FIGURE 7-
Muscle histology (H&E) to assess gross muscle quality on a subset of 13 participants where enough muscle sample was extracted. **A**. Bivariate pearson correlation depicting the negative relationship between renal filtration rate (eGFR-axis), and % of non-contractile tissue infiltration in muscle [((whole area – healthy area)/whole area) = %non-contractile, y-axis] (not pictured p=.004). **B.** Representative cross-sectional images of the H&E-stained muscle samples. *BOTTOM LEFT* – cross-section from early (stage 1) CKD. *UPPER RIGHT* – cross-section of middle (stage 3) CKD muscle. Arrows highlighting presence of intermuscular adipose tissue and likely connective/fibrotic tissue. *BOTTOM RIGHT*- cross-section from late (stage 5) CKD, with arrows highlighting presence of intermuscular adipose tissue and connective/fibrotic tissue.

Figure 8

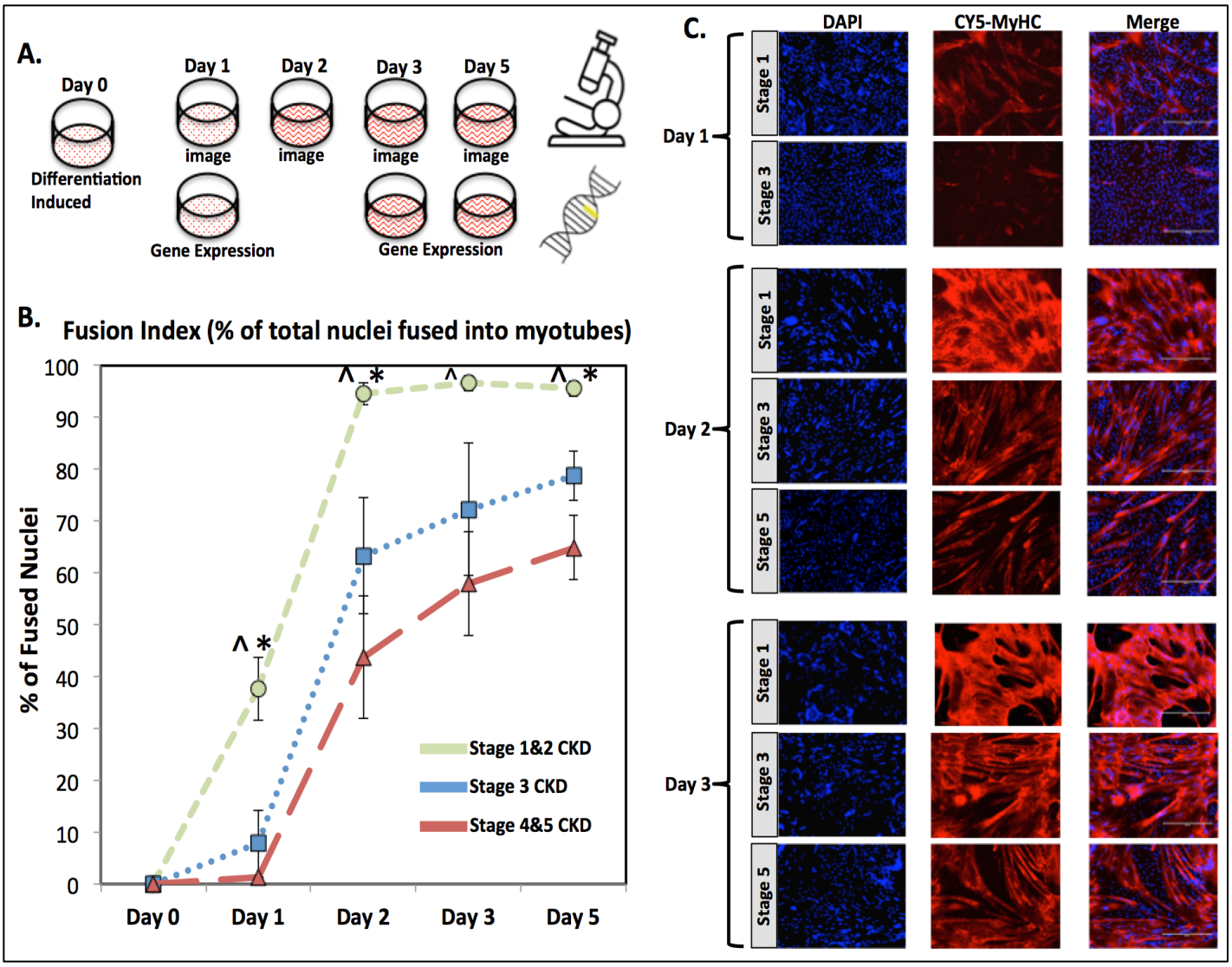

FIGURE 8-
SC in-vitro myogenic capacity. **A**. Experiment setup – SCs were plated at 10,400 cells per cm^2 on matrigel-coated dishes, and grown to confluence. At day 0, growth media was changed to differentiation media, with day 1 denoting 24 hours post-differentiation induction and so on through day 5. Cells were fixed and imaged at 20x magnification at days 1,2, 3 and 5 post-differentiation after staining for MyHC, and DAPI ([fusion index = # of cells that had fused into multinucleated MyHC+ myotubes / total nuclei in the field of view], averaged over all 10 images per day, per participant. Cells were also collected in trizol at days 1, 3, and 5, for RNA extraction and MRF gene expression patterns. **B.** Plot of SC fusion kinetics over the 5-day experimental protocol for early (stage 1&2 -- green), middle (stage 3 -- blue), and late (stage 4&5 -- red) CKD SCs. Each dot represents the average fusion % for that day for that group (with SD bars). For each time point, 1-way ANOVAs were used to assess for differences in degree of fusion between the 3 groups. The following symbols denote significant post-hoc tests: *(between Stage 1&2 and Stage 3), ^(between

stage 1&2 and Stage 4&5), #(Between stage 3 and Stage 4&5), these symbols are placed over the respective day, above stage 1&2 cells. **C**. Representative immunostained images of SCs from early (stage 1 CKD), middle (stage 3 CKD), and late (stage 5 CKD), at day 1 (*top panel segment*), day 2 (*middle panel segment*), and day 3 (*bottom panel segment*). Images from left to right depict DAPI (blue – cell nuclear stain), MyHC (stained with Cy5/Alexa-Fluor 647), and the merged image (MyHC + DAPI). Inset within the merged image is scale bar, with these images taken at 10x magnification.

Figure 9

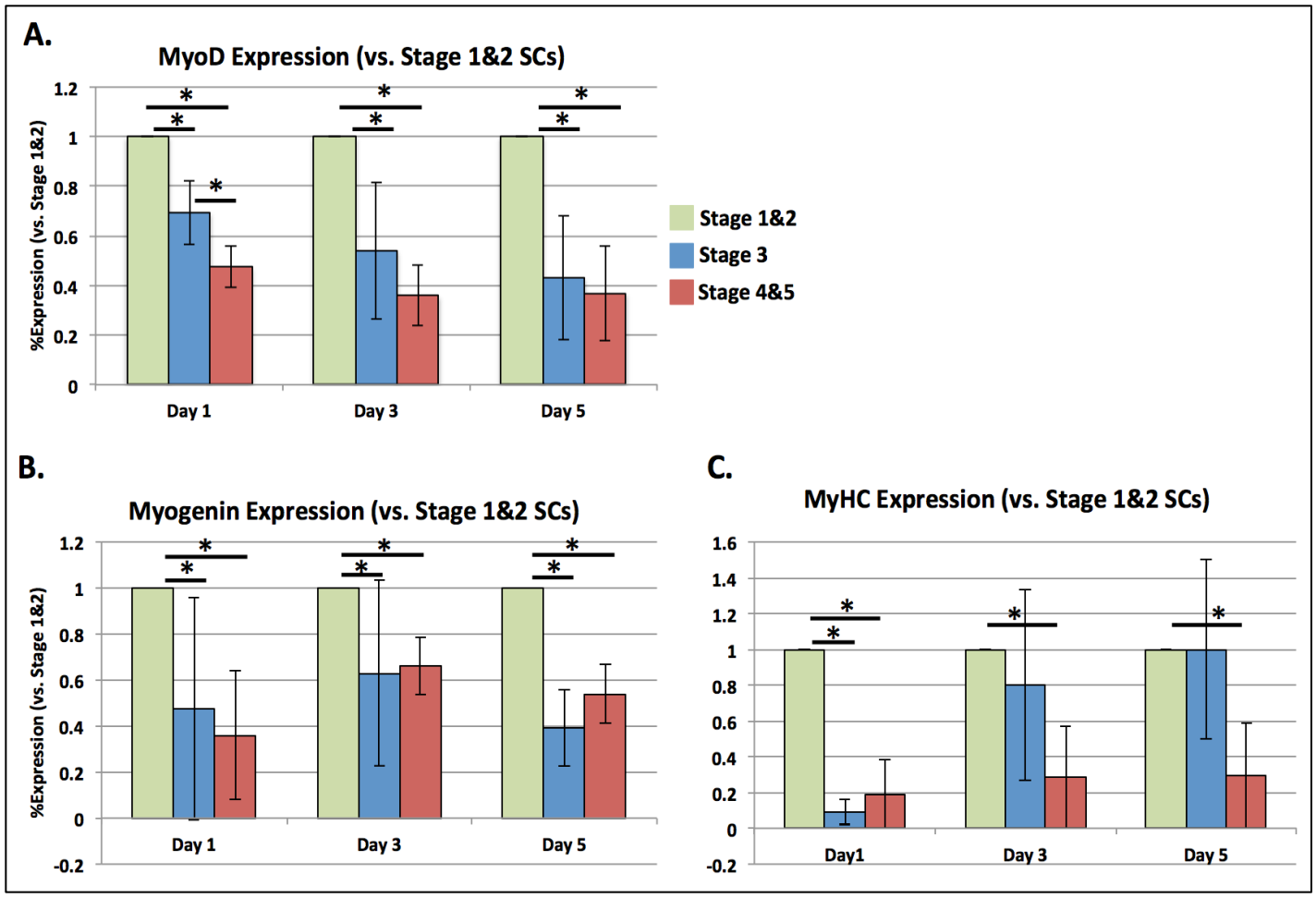

FIGURE 9-
SC myogenic gene expression (RT-PCr) across the differentiation experiment (days 1, 3, and 5) for stage 1&2 CKD (reference – green bars), stage 3 (blue bars), and stage 5 (red bars). Groups were assessed for gene expression differences with 1-way ANOVAs. Bar heights indicate gene expression relative to reference (stage 1&2), with errors bars indicating ± SD. The * symbol with accompanying line, denotes significant post-hoc differences between the denoted groups. **A**. Group differences in MyoD gene expression at day 1 (24-hours post-differentiation induction), day 3, and day 5. Significant differences were observed on day 1 (between all groups), day 3 (between stage 1&2 and middle and late-stage groups), and day 5 (between stage 1&2 and middle and late-stage groups) (all $p<.05$). **B**. Group differences in Myogenin gene expression. Significant differences were observed on day 1 (between stage 1&2 and middle and late-stage groups), day 3 (between stage 1&2 and middle and late-stage groups), and day 5 (between stage 1&2 and middle and late-stage groups). **C.** Group differences in MyHC gene expression. Significant differences were observed on day 1 (between stage 1&2 and middle and late-stage groups), on day 3 (between stage 1&2 and late-stage CKD), and on day 5 (between stage 1&2 and late-stage CKD) (all $p<.05$).

Figure 10

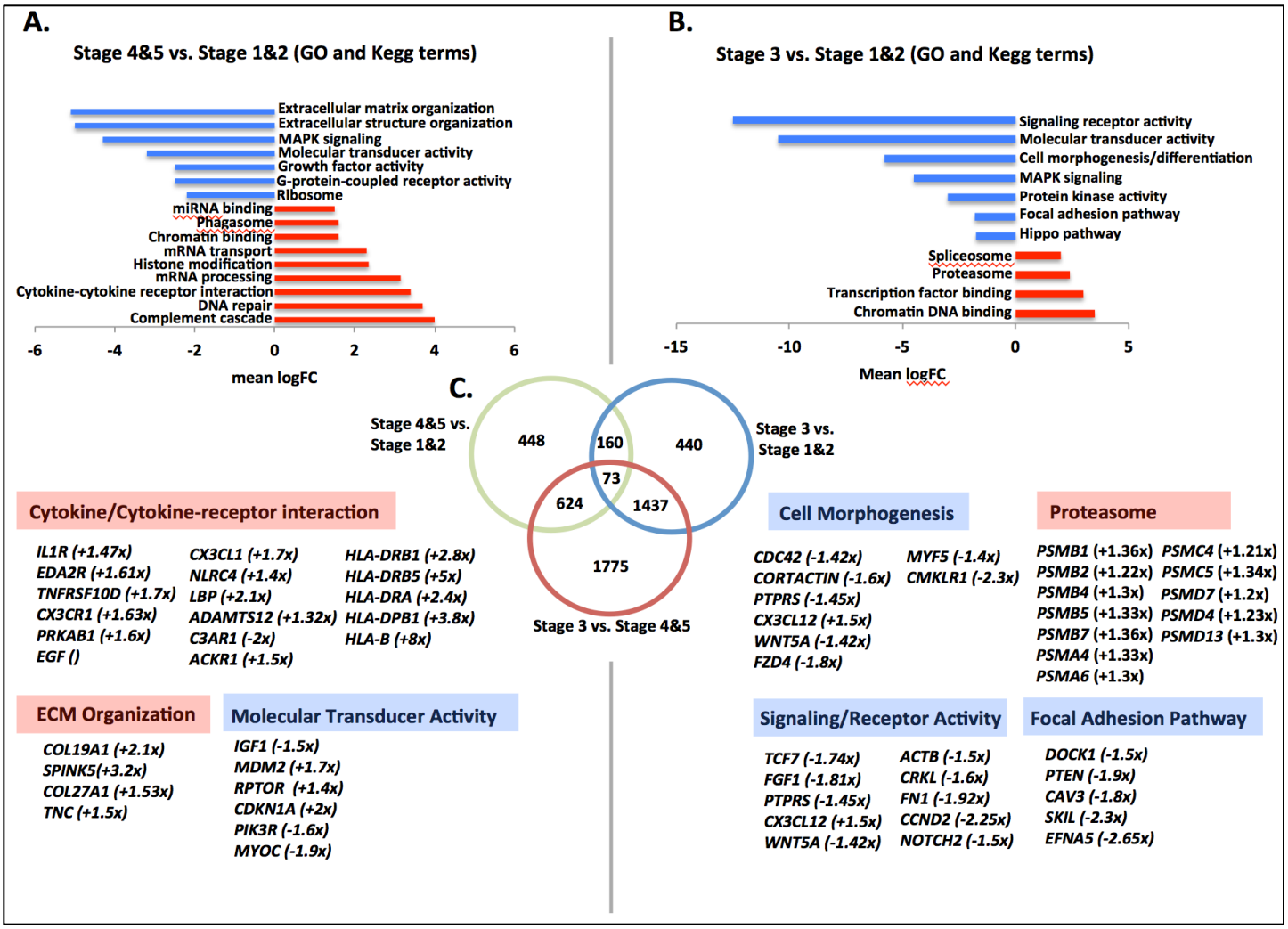

FIGURE 10

Selected GO terms and KEGG pathways from a larger list of top 25 down and upregulated gene networks across stage-wise transcript analysis. Bar charts depict top downregulated (blue bars) or upregulated (red bars) gene networks, with their accompanying network label listed next to its corresponding bar (all GO terms list have FDR ≤.05, and all KEGG terms have p-value <.05). Pathway up or downregulation is expressed in mean log-fold-change units, and was determined to be significant when compared to background log 2 fold change for genes not contained within the network/pathway. Below/bottom are selected genes from the significant GO or KEGG pathways that are differentially expressed, and the fold change listed in parentheses next to the gene term. **A.** Comparing late-stage CKD muscle transcriptome to early stage 1&2 (early CKD is the reference). Extracellular matrix organization, molecular transducer activity, MAPK signaling, growth factor activity, and g-protein coupled receptor activity components were significantly downregulated in late-stage CKD compared to early. Conversely, late-stage CKD demonstrates significant upregulation in cytokine/cytokine-receptor interaction, DNA repair, complement cascade, and epigenetic mechanisms (ie. histone modification, chromatin binding, miRNA binding). Specific

significantly differentially expressed genes from some of these pathways are listed at the bottom. **B.** Comparing middle-stage CKD to early stage 1&2 (early is the reference). Genes governing signaling receptor activity, molecular transducer activity, cell morphogenesis, MAPK signaling, focal adhesion and hippo pathway were significantly downregulated in middle-stage CKD compared to early. However, pathways governing the degradative proteasome, transcription factor binding, and epigenetic chromatin binding are significantly upregulated. Below, are listed specific genes that significantly differentially expressed in some of these selected pathways.

Figure 11

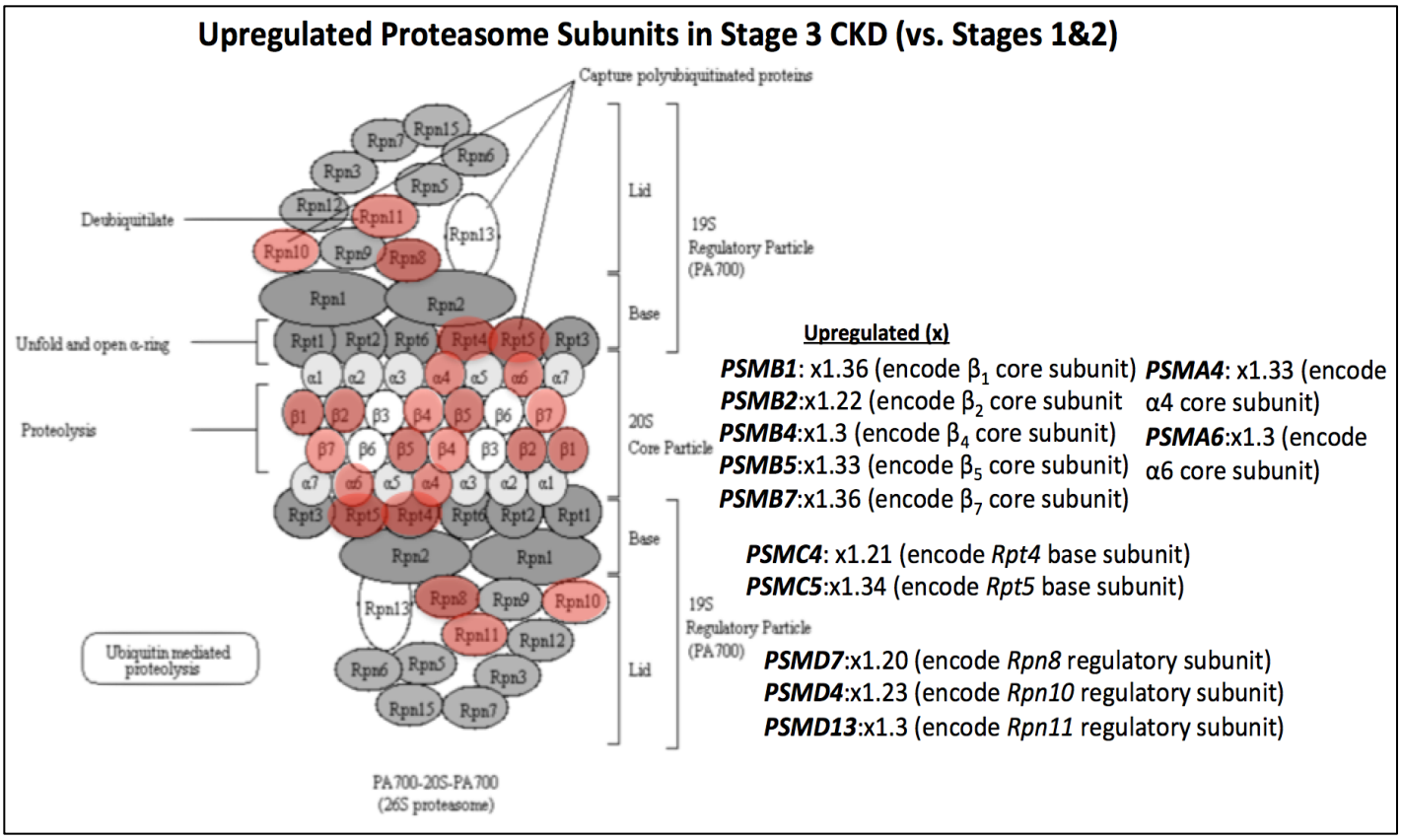

FIGURE 11

KEGG pathway image of the 26S ubiquitin proteasome responsible for contractile muscle protein degradation. Each labeled circle represents a protein subunit of the proteasome. The chart depicts the upregulation of many key proteasome structural subunit protein genes (as shown in figure 10, listed at right, with the fold differences between stage 3 CKD and stage 1&2, with stage 1&2 being the reference), the proteasome subunit they encode (listed next to the gene), and highlited in red in the proteasome construction (left). Note – significant upregulation in core subunit proteins responsible for protein degradation.

References

1. Center for Disease Control and Prevention (CDC). National Chronic Kidney Disease Fact Sheet: General Information and National Estimates on Chronic Kidney Disease in the United States, 2014. Atlanta, GA: US Dept. of Health and Human Services, CDC; 2014.

2. Zapponi, G., Targher, G., Chonchol, M., Ortalda, V., et al. (2012) Predictors of estimated GFR decline in patients with type 2 diabetes and preserved kidney function. *Clin J Am Soc Nephrol*, 7(3); 401-8.

3. Otobe, Y., Hiraki, K., Hott, C. et al. (2017) The comparison of the muscle strength in pre-dialysis chronic kidney disease patients and the average levels in healthy individuals. *Physical Therapy Japan*, 6(44): 401-407.

4. McManus, D., Slipak, M., Ix, J.H., Ali, S. et al. (2007) Association of cystatin c with poor exercise capacity and heart rate recovery: data from the heart and soul study. *Am J Kidney Dis*, 49(3); 365-72.

5. Anand, S., Johansen, K.L., & Tamura, M.K. (2014) Aging and chronic kidney disease: the impact on physical function and cognition. *J Gerontol A Biol Sci Med Sci*, 69A(3); 315-322.

6. Diesel, W., Noakes, T.D., Swanepoel, C., & Lambert, M. (1990) Isokinetic muscle strength predicts maximum exercise tolerance in renal patients on chronic hemodialysis. *Am J Kidney Dis*, 16(2): 109-14.

7. Roshanravan, B., Gamboa, J., & Wilund, K. (2017) Exercise and CKD: skeletal muscle dysfunction and practical application of exercise to prevent and treat physical impairments in CKD. *Am J Kidney Dis*, 69(6); 837-52.

8. Neirynck, N. Glorieux, G., Schepers, E., Dhondt, A., Verbeke, F., & Vanholder, R. (2015) Pro-inflammatory cytokines and leukocyte oxidative burst in chronic kidney disease: culprits or innocent bystanders. *Nephrol Dial Transplant*, 30(6); 943-51.

9. Wang, X.H., & Mitch, W.E. (2014) Mechanisms of muscle wasting in chronic kidney disease. *Nat Rev Nephrol*, 10(9): 504-16

10. Neirynck, N. Glorieux, G., Schepers, E., Dhondt, A., Verbeke, F., & Vanholder, R. (2015) Pro-inflammatory cytokines and leukocyte oxidative burst in chronic kidney disease: culprits or innocent bystanders. *Nephrol Dial Transplant*, 30(6); 943-51.

11. Campistol, J.M. (2002) Uremic myopathy. *Kidney International*, 62(5); 1901-1913.

12. Marcus, R.L., LaStayo, P.C., Ikizler, T.A., Wei, G. et al. (2015) Low physical function in maintenance hemodialysis patients is independent of muscle mass and comorbidity. *Journal of Renal Nutrition*, 25(4); 371-375.

13. Dayanidhi, S., & Lieber, R.L. (2014) Sketal muscle satellite cells: mediators of muscle growth during development and implications for developmental disorders. *Muscle Nerve*, 50(5): 723-32.

14. Liu, J.X., Hoglund, A.S., Karlsson, P., Lindblad, J. et al (2009) Myonuclear domain size and myosin isoform expression in muscle fibers from mammals representing a 100,000-fold difference in body size. *Exp Physiol*, 94(1)

15. Schultz, E. (1989) Satellite cel behavior during skeletal muscle growth and regeneration. *Med Sci Sports Ecerc*, 21, S181-S186

16. Goh, Q., & Millay, D.P. (2017) Requirement of myomaker-mediated stem cell fusion for skeletal muscle hypertrophy. *Elife, 10(6)*

17. Jackson JR, Kirby TJ, Fry CS, Cooper RL, et al. (2015). Reduced voluntary running performance is associated with impaired coordination as a result of muscle satellite cell depletion in adult mice. *Skeletal Muscle*. 41 doi: 10.1186/s13395-015-0065-3

18. Yin, H., Price, F., & Rudnicki, M.A. (2013) Satellite cells and the muscle stem cell niche. *Physiol Rev*, 93(1): 23-67.

19. Murphy, M.M., Lawson, J.A., Mathew, S.J., Hutcheson, D.A., & Kardon, G. (2011) Satellite cells, connective tissue fibroblasts and their interactions are crucial for muscle regeneration. *Development*, 138(17): 3625-37

20. Bentzinger, C.F., Wang, Y.X., Dumont, N.A., & Rudnicki, M.A. (2013) Cellular dynamics in the muscle satellite cell niche. *EMBO Rep*, 14(12): 1062-72.

21. Serrano AL, Muñoz-Cánoves P (2010) Regulation and dysregulation of fibrosis in skeletal muscle. *Exp Cell Res* 316: 3050–3058

22. Gilbert, P.M. et al. (2010) Substrate elasticity regulates skeletal muscle stem cell self-renewal in culture. *Science* 329: 1078–1081

23. Fry, C.S., Kirby, T.J., Kosmac, K., McCarthy, J.J., & Peterson, C.A. (2017) Myogenic progenitor cells control extracellular matrix production by fibroblasts during skeletal muscle hypertrophy. *Cell Stem Cell*, 20(1): 56-69.

24. Kovanen V. (2002) Intramuscular extracellular matrix: complex environment of muscle cells. *Exerc Sport Sci Rev* 30: 20–25

25. Boonen KJ, Rosaria-Chak KY, Baaijens FP, van der Schaft DW, Post MJ (2009) Essential environmental cues from the satellite cell niche: optimizing proliferation and differentiation. *Am J Physiol Cell Physiol* 296: C1338–C1345

26. Cornelison D. D. (2008). Context matters: in vivo and in vitro influences on muscle satellite cell activity. *J. Cell. Biochem.* 105, 663-669

27. Brack AS, Conboy MJ, Roy S, Lee M, Kuo CJ, Keller C, Rando TA (2007) Increased Wnt signaling during aging alters muscle stem cell fate and increases fibrosis. *Science* 317: 807–810

28. Bentzinger CF, Wang YX, Rudnicki MA (2013) Treating muscular dystrophy by stimulating intrinsic repair. *Regen Med* 8: 237–240

29. Artavanis-Tsakonas S, Rand MD, Lake RJ (1999) Notch signaling: cell fate control and signal integration in development. *Science* 284: 770–776

30. Brack AS, Conboy IM, Conboy MJ, Shen J, Rando TA. (2008) A Temporal Switch from Notch to Wnt Signaling in Muscle Stem Cells Is Necessary for Normal Adult Myogenesis. *Cell stem cell.* 2(1):50–59.

31. Snijders, T., Nederveen, J.P., McKay, B.R., Joanisse, S. et al. (2015) Satellite cells in human skeletal muscle plasticity. *Front Physiol*, 2105; 6:283

32. Relaix F., Montarras D., Zaffran S., Gayraud-Morel B., Rocancourt D., Tajbakhsh S., et al. . (2006). Pax3 and Pax7 have distinct and overlapping functions in adult muscle progenitor cells. *J. Cell Biol*. 172, 91–102.

33. Zhang, L., Wang, X. H., Wang, H., Du, J., & Mitch, W. E. (2010). Satellite Cell Dysfunction and Impaired IGF-1 Signaling Cause CKD-Induced Muscle Atrophy. *Journal of the American Society of Nephrology : JASN*, *21*(3), 419–427

34. Lanza D, Perna AF, Oliva A et al (2015) . Impact of the uremic milieu on the osteogenic potential of mesenchymal stem cells. *PLoS One* 10: e0116468

35. Jourde-Chiche N, Dou L, Sabatier F et al (2009) Levels of circulating endothelial progenitor cells are related to uremic toxins and vascular injury in hemodialysis patients. *J Thromb Haemost* 7: 1576–1584

34. Noh H, Yu MR, Kim HJ et al (2012) Uremia induces functional incompetence of bone marrow-derived stromal cells. *Nephrol Dial Transplant*; 27: 218–225

35. Levin, A., & Stevens, P.E. (2013) KDIGO 2012 Clinical Practice Guidelines for the evaluation and management of chronic kidney disease. *Kidney International*, 3(1): 1-136.

36. Bittel, D.C., Bittel, A.J., Tuttle, L.J., Hastings, M.K., et al. (2015) Adipose tissue content, muscle performance and physical function in obese adults with type 2 diabetes mellitus and peripheral neuropathy. *J Diabetes Complications*, 29(2); 250-257.

37. Brown M, Sinacore DR, Binder EF, Kohrt WM. Physical and performance measures for the identification of mild to moderate frailty. *J Gerontol A Biol Sci Med Sci* 2000; 55:M350–M355

38. Reuben DB, Siu AL. An objective measure of physical function of elderly outpatients: the Physical Performance Test. *J Am Geriatr Soc*.1990;38:1105–12.

39. Reuben DB, Siu AL, Kimpau S. (1992) The predictive validity of self-report and performance-based measures of function and health. *J Gerontol*. 47:M106–10.

40. Tuttle, L.J., Sinacore, D.R., & Mueller, M.J. (2012) Intermuscular adipose tissue is muscle specific and associated with poor functional performance. *J Aging Res*, 2012; 172957

41. Hilton, T.N., Tuttle, L.J., Bohnert, K.L., Mueller, M.J., & Snacore, D.R. (2008) Excessive adipose tissue infiltration in skeletal muscle in individuals with obesity, diabetes mellitus, and peripheral neuropathy: association with performance and function. *Phys Ther*, 88(11); 1336-44.

42. Tuttle, L.J., Hastings, M.K., & Mueller, M.J. (2012) A moderate-intensity weight-bearing exercise program for a person with type 2 diabetes and peripheral neuropathy. *Phys Ther*, 92(1); 133-41.

43. Meyer, C., Corten, K., Wesseling, M. et al. (2013) Test-retest reliability of innovated strength tests for hip muscles. *Plos One*.

44. Kirn, D.R., Reid, K.F., Hau, C. et al. (2016) What is a clinically meaningful improvement in leg-extensor power for mobility-limited older adults. *J Gerontol A Biol Sci Med Sci*, 71(5), 632-6.

45. Worrell, T.W., Karst, G., Adamczyk, D. et al. (2001) Influence of joint position on electromyographic and torque generation during maximal voluntary isometric contractions of the hamstrings and gluteus maximus muscles. *J Orthop Sports Phys Ther*, 31(12); 730-40.

46. Frey-Law, L.A., Laake, A., Avin, K.G. et al. (2012) Knee and elbow 3D strength surfaces: peak torque-angle-velocity relationships. *J Appl Biomech*, 28(6): 726-37.

47. Harbo, T., Brincks, J., & Andersen, H. (2012) Maximal isokinetic and isometric muscle strength of major muscle groups related to age, body mass, height, and sex in 178 healthy subjects. *Eur J Appl Physiol*, 112(1): 267-75

48. Pincivero, D.M., Lephart, S.M., & Karunakara, R.A. (1997) Reliability and prevision of isokinetic strength and muscular endurance for the quadriceps and hamstrings. *Int J Sports Med*, 18(2): 113-7.

49. Roshanravan B, Patel KV, Fried LF, et al. (2017) Association of muscle endurance, fatigability, and strength with functional limi- tation and mortality in the Health Aging and Body Composition Study. *J Gerontol A Biol Sci Med Sci*. 72(2):284-291.

50. Entrekin, K., Work, B., & Owen, J. (1998) Does a high carbohydrate preparatory diet affect the 3-hour oral glucose test in pregnancy. *J Matern Fetal Med*, 7(2): 68-71.

51. Smith, G.I., Yoshino, J., Kelly, S.C., et al. (2016) High-protein intake during weight loss therapy eliminates the weight-loss induced improvement in insulin action in obese postmenopausal women. *Cell Rep*, 17(3): 849-861.

52. Matthews DR, Hosker JP, Rudenski AS, Naylor BA, Treacher DF, Turner RC. (1985) Homeostasis model assessment: insulin resistance and beta-cell function from fasting plasma glucose and insulin concentrations in man. *Diabetologia*. 28:412–419

53. Steensberg, A., van Hall, G., Osada, T., et al. (2000) Production of interleukin-6 in contracting human skeletal muscles account for the exercise-induced increase in plasma interleukin-6. *J Physiol*, 529 (Pt1): 237-242.

54. Rauchhaus, M., Doehner, W., Francis, D.P., et al. (2000) Plasma cytokine parameters and mortality in patients with chronic heart failure. *Circulation*, 102(25): 3060-7.

55. Merriwether, E.N., Host, H.H., & Sinacore, D.R. (2012) Sarcopenic indices in community-dwelling older adults. *J Geriatr Phys Ther*, 35(3): 118-25.

56. Shanely, R.A., Zwetsloot, K.A., Triplett, N.T., et al. (2014) Human skeletal muscle biopsy procedures using the modified bergstrom technique. *J Vis Exp*, (91): 51812

57. Selected Histochemical and Histopathological Methods. Thompson, S.W. (1966). CC Thomas Publishers, Chicago, IL.

58. Van Putten, M., de Winter, C., van Roon-Mom, W., van Ommen, G.J., et al. (2010) A 3 month mild functional test regime does not affect disease parameters in young mdx mice. *Neuromuscul Disord*, 20(4): 273-80.

59. Conboy, M.J., Cerletti, M., Wager, A.J., & Conboy, I.M. (2010) Immuno-analysis and FACS sorting of adult muscle fiber-associated stem/precursor cells. *Methods Mol Biol*, 621: 165-73.

60. Smith, L. R., Chamber, H. G., & Lieber, R. L. (2013). Reduced satellite cell population may lead to contractures in children with cerebral palsy. *Developmental Medicine and Child Neurology*, *55*(3), 264–270.

61. Cheng, C. S., El-Abd, Y., Bui, K., Hyun, Y.-E., Hughes, R. H., Kraus, W. E., & Truskey, G. A. (2014). Conditions that promote primary human skeletal myoblast culture and muscle differentiation

in vitro. *American Journal of Physiology - Cell Physiology*, *306*(4), C385–C395.

62. Guardiola, O., Lafuste, P., Brunelli, S., Iaconis, S. et al. (2012) Cripto regulates skeletal muscle regeneration and modulates satellite cell determination by antagonizing myostatin. *PNAS*, 109(47): E3231-E3240.

63. Andley, U.P., Tycksen, E., McGlasson-Naumann, B.N., & Hamilton, P.D. (2018) Probing the changes in gene expression due to α-crystallin mutations in mouse models of hereditary human cataract. *Plos One*, Jan 16

67**.** Robinson-Cohen C, Katz R, Mozaffarian D, Dalrymple LS, de Boer I, Sarnak M, Shlipak M, Siscovick D, Kestenbaum B. (2009) Physical activity and rapid decline in kidney function among older adults. *Arch Intern Med*. 169:2116–2123

68. Robinson-Cohen, C., Littman, A.J., Duncan, G.E., et al. (2014) Physical activity and change in estimated GFR among persons with CKD. *J Am Soc Nephrol*, 25(2); 399-406.

69. Robinson-Cohen, C., Katz, R., Mozaffarian, D., et al. (2009) Physical activity and rapid decline in kidney function among older adults. *Arch Intern Med*, 169(22): 2116-2123.

70. Ortiz-Costa, S., Sorenson, M.M., & Sola-Penna, M. (2002) Counteracting effects of urea and methylamines in function and structure of skeletal muscle myosin. *Arch Biochem Biophys*, 408(2): 272-8

71. Kaizu, Y., Kimura, M., Yoneyama, T., & Miyaji, K. (1998) Interleukin-6 may mediate malnutrition in chronic hemodialysis patients. *Am J Kidney Dis*, 31(1): 93-100

72. Stenvinkel, P., Ketteler, M., Johnson, R.J., Lindholm, B. et al (2005) IL-10, IL-6, and TNF-alpha: central factors in the altered cytokine network of uremia—the good, the bad, and the ugly. *Kidney Int*, 67(4): 1216-33

73. Serrano, A.L., Baeza-Raja, B., Perdiguero, E., Jardi, M., & Munoz-Canoves, P. (2008) Interleukin-6 is an essential regulator of satellite cell-mediated skeletal muscle hypertrophy. *Cell Metab*, 7(1): 33-44.

73. Adams, G.R., Vaziri, N.D (2006) Skeletal muscle dysfunction in chronic renal failure: effects of exercise. *Am J Physiol Renal Physiol*, 290(4): F753-61

74. Cesari M, Penninx BWJH, Pahor M, et al. (2004) Inflammatory markers and physical performance in older persons: the InCHIANTI study. *J Gerontol Med Sci.* 59A:242-248.

75. Ferrucci L, Penninx BWJH, Volpato S, et al. (2002) Change in muscle strength explains accelerated decline of physical function in older women with high interleukin-6 serum levels. *J Am Geriatr Soc.* 50:1947-1954.

76. Visser M, Pahor M, Taaffe DR, et al. Relationship of interleukin-6 and tumor necrosis factor-alpha with muscle mass and muscle strength in elderly men and women: the Health ABC Study. *J Gerontol Med Sci.* 2002;57A:M326-M332.

77. Dumont, N. A., & Rudnicki, M. A. (2016). Targeting muscle stem cell intrinsic defects to treat Duchenne muscular dystrophy. *NPJ Regenerative Medicine*, *1*, 16006

78. Schaaf, G. J., van Gestel, T. J., Brusse, E., Verdijk, R. M., de Coo, I. F., van Doorn, P. A., … Pijnappel, W. P. (2015). Lack of robust satellite cell activation and muscle regeneration during the progression of Pompe disease. *Acta Neuropathologica Communications*, *3*, 65.

79. Yue, F., Bi, P., Wang, C., Li, J., Liu, X., & Kuang, S. (2016). Conditional Loss of *Pten* in Myogenic Progenitors Leads to Postnatal Skeletal Muscle Hypertrophy But Age-dependent Exhaustion of Satellite Cells. *Cell Reports*, *17*(9), 2340–2353

80. Heslop L, Morgan JE, Partridge TA. Evidence for a myogenic stem cell that is exhausted in dystrophic muscle. J Cell Sci. 2000;Pt 1:2299–2308

81. Sousa-Victor P., Gutarra S., Garcia-Prat L., Rodriguez-Ubreva J., Ortet L., Ruiz-Bonilla V., et al. (2014). Geriatric muscle stem cells switch reversible quiescence into senescence. Nature 506, 316

82. Barberi L., Scicchitano B. M., De Rossi M., Bigot A., Duguez S., Wielgosik A., et al. (2013). Age-dependent alteration in muscle regeneration: the critical role of tissue niche. Biogerontology 14, 273

83. Renault V, Thornell LE, Eriksson PO et al. . Regenerative potential of human skeletal muscle during aging. *Aging Cell* 2002; 1: 132–139

84. Collins CA, Zammit PS, Ruiz AP, Morgan JE, Partridge TA (2007) A population of myogenic stem cells that survives skeletal muscle aging. *Stem Cells*. 25(4):885–994.

85. Goligorsky, M.S., Yasuda, K., & Ratliff, B. (2010) Dysfunctional endothelial progenitor cells in chronic kidney disease. *JASN*, 21(6): 911-919

86. Liu L, Cheung TH, Charville GW, Hurgo BMC, Leavitt T, Shih J, et al. (2013) Chromatin modifications as determinants of muscle stem cellquiescence and chronological aging. *Cell Re*. 4(1):189–204

86. Chakkalakal JV, Jones KM, Basson MA, Brack AS (2012) The aged nichedisrupts muscle stem cell quiescence. *Nature*. 490(7420):355–360

87. Bernet JD, Doles JD, Hall JK, Kelly Tanaka K, Carter Ta, Olwin BB (2014) p38 MAPK signaling underlies a cell-autonomous loss of stemcell self-renewal in skeletal muscle of aged mice. *Nat Med*;20(3):265–271

88. Claflin DR, Jackson MJ, Brooks SV (2015) Age affects the contraction-induced mitochondrial redox response in skeletalmuscle. *Front Physiol*. p. 6.

89. Liu D, Sartor M, Nader G, Pistilli EE, Tanton L, Lilly C, et al. (2013) Microarray analysis reveals novel features of the muscle agingprocess in men and women. *J Gerontol A Biol Sci Med Sci*;68(9):1035–1044.

90. Signer RAJ, Morrison SJ (2013) Mechanisms that regulate stem cell agingand life span. *Cell Stem Cell*;12(2):152–165

91. Zampieri M, Ciccarone F, Calabrese R, Franceschi C, Bürkle A, Caiafa P (2015) Reconfiguration of DNA methylation in aging. *Mech Ageing Dev*. pii:S0047-6374(15)00007-X.

92. Zammit, P.S., Relaix, F., Nagata, Y., Ruiz, A.P. et al. (2006) Pax7 and myogenic progression in skeletal muscle satellite cells. *Journal of Cell Science*, 19: 1824-1832

93. Relaix F, Zammit PS. (2012) Satellite cells are essential for skeletal muscle regeneration: the cell on the edge returns centre stage. *Development*.139:2845–2856. doi: 10.1242/dev.069088.

94. Charrin, S., Latil, M., Soave, S., Polesskaya, et al. (2013) Normal muscle regeneration requires tight control of muscle cell fusion by tetraspanins CD9 and CD81. *Nature Communications*, 1674(2013)

95. Meadows, E., Cho, J.H., Flynn, J.M., & Klein, W.H. (2008) Myogenin regulate a distinct genetic program in adult muscle stem cells. *Dev Biol*, 322(2): 406-414

96. Sharples, A.P., Polydorou, I, Hughes, D.C., Owens, D.J., et al. (2016) Skeletal muscle cells possess a memory of acute early life TNF-a exposure: role of epigenetic adaptation. *Biogerontology*, 17(3): 603-17

97. Chevrel G, Hohlfeld R, Sendtner M (2006) The role of neurotrophins in muscle under physiological and pathological conditions. *Muscle Nerve* 33: 462–476

98. Vasyutina, E., Martarelli, B., Brakebusch, C., Wende, H., & Birchmeier, C. (2009). The small G-proteins Rac1 and Cdc42 are essential for myoblast fusion in the mouse. *Proceedings of the National Academy of Sciences of the United States of America*, *106*(22), 8935–8940.

99. Pawlikowski, B., Vogler, T.O., Gadek, K., & Olwin, B.B. (2017) Regulation of skeletal muscle stem cells by fibroblast growth factors. *Dev Dyn*, 246 (5): 359-367.

100. Laurin, M., Fradet, N., Blangy, A., Hall, A., Vuori, K., & Côté, J.-F. (2008). The atypical Rac activator Dock180 (Dock1) regulates myoblast fusion *in vivo*. *Proceedings of the National Academy of Sciences of the United States of America*, *105*(40), 15446–15451

101. Yue, F., Bi, P., Wang, C., Shan, T., Nie, Y., Ratliff, T. L., … Kuang, S. (2017). *Pten* is

necessary for the quiescence and maintenance of adult muscle stem cells. *Nature Communications*, *8*, 14328

102. Francetic, T., & Li, Qiao. (2011) Skeletal myogenesis and Myf5 activation. *Transcription*, 2(3): 109-114

103. Zhang, H., & Stavnezer, E. (2009). Ski Regulates Muscle Terminal Differentiation by Transcriptional Activation of *Myog* in a Complex with Six1 and Eya3. *The Journal of Biological Chemistry*, *284*(5), 2867–2879.

104. Gu, J.-M., Wang, D. J., Peterson, J. M., Shintaku, J., Liyanarachchi, S., Coppola, V., … Guttridge, D. C. (2016). An NF-κB – EphrinA5 – Dependent Communication between NG2+ Interstitial Cells and Myoblasts Promotes Muscle Growth in Neonates. *Developmental Cell*, *36*(2), 215–224.

105. von Maltzahn, J., Chang, N.C, Bentzinger, C.F., & Rudnicki, M.A. (2012) Wnt signaling in myogenesis. *Trends Cell Biol*, 22(11): 602-609

106. Karczewska-Kupczewska, M, Stefanowicz, M, Matulewicz, N, Nikołajuk, A, Strączkowski, M (2016) Wnt signaling genes in adipose tissue and skeletal muscle of humans with different degrees of insulin sensitivity. *J Clin Endocrinol Metab*, 101(8): 3079-87

107. Majmundar, A. J., Lee, D. S. M., Skuli, N., Mesquita, R. C., Kim, M. N., Yodh, A. G., … Simon, M. C. (2015). HIF modulation of Wnt signaling regulates skeletal myogenesis *in vivo*. *Development (Cambridge, England)*, *142*(14), 2405–2412.

108. Malam, Z. & Cohn, R.D. (2014) Stem cells on alert: priming quiescent stem cells after remote injury. *Cell Stem Cell*, 15(1): 7-8

109. Calura, E., Cagnin, S., Raffaello, A., Laveder, P., Lanfranchi, G., & Romualdi, C. (2008). Meta-analysis of expression signatures of muscle atrophy: gene interaction networks in early and late stages. *BMC Genomics*, *9*, 630.

110. Dominov, J.A., Houlihan-Kawamoto, C.A., Swap, C.J., & Miller, J.B. (2001) Pro- and anti-apoptotic members of the Bcl-2 family in skeletal muscle: a distinct role for Bcl-2 in later stages of myogenesis. *Dev Dyn*, 220(1): 18-26.

111. Nazari, H., Khaleghian, A., Takahashi, A., Harada, N., Webster, N. J. G., Nakano, M., … Nakaya, Y. (2011). Cortactin, an Actin Binding Protein, Regulates GLUT4 Translocation via Actin Filament Remodeling. *Biochemistry. Biokhimiia*, *76*(11), 1262–1269.

112. The Three Musketeers of Skeletal Membrane Repair♦: Membrane Repair Defects in Muscular Dystrophy Are Linked to Altered Interaction between MG53, Caveolin-3, and Dysferlin. (2009). *The Journal of Biological Chemistry*, *284*(23), e99922.

113. Volonte, D., Peoples, A. J., & Galbiati, F. (2003). Modulation of Myoblast Fusion by Caveolin-3 in Dystrophic Skeletal Muscle Cells: Implications for Duchenne Muscular Dystrophy and Limb-Girdle Muscular Dystrophy-1C. *Molecular Biology of the Cell*, *14*(10), 4075–4088

114. Bentzinger, C. F., Wang, Y. X., von Maltzahn, J., Soleimani, V. D., Yin, H., & Rudnicki, M. A. (2013). Fibronectin regulates Wnt7a signaling and satellite cell expansion. *Cell Stem Cell*, *12*(1), 75–87.

115. Lukjanenko, L., Jung, M. J., Hegde, N., Perruisseau-Carrier, C., Migliavacca, E., Rozo, M., … Bentzinger, C. F. (2016). Loss of fibronectin from the aged stem cell niche affects the regenerative capacity of skeletal muscle in mice. *Nature Medicine*, *22*(8), 897–905

116. Mouw, J. K., Ou, G., & Weaver, V. M. (2014). Extracellular matrix assembly: a multiscale deconstruction. *Nature Reviews. Molecular Cell Biology*, *15*(12), 771–785

117. Flück, M., Mund, S. I., Schittny, J. C., Klossner, S., Durieux, A.-C., & Giraud, M.-N. (2008). Mechano-regulated Tenascin-C orchestrates muscle repair. *Proceedings of the National Academy of Sciences of the United States of America*, *105*(36), 13662–13667

118. Joe, M. K., Kee, C., & Tomarev, S. I. (2012). Myocilin Interacts with Syntrophins and Is Member of Dystrophin-associated Protein Complex. *The Journal of Biological Chemistry*, *287*(16), 13216–13227

119. Li, H., Malhotra, S., & Kumar, A. (2008). Nuclear Factor-kappa B Signaling in Skeletal Muscle Atrophy. *Journal of Molecular Medicine (Berlin, Germany)*, *86*(10), 1113–1126.

120. Hindi, S. M., Sato, S., Xiong, G., Bohnert, K. R., Gibb, A. A., Gallot, Y. S., … Kumar, A. (2018). TAK1 regulates skeletal muscle mass and mitochondrial function. *JCI Insight*, *3*(3), e98441

121. Llano-Diez, M., Gustafson, A., Olsson, C., Goransson, H., & Larsson, L. (2011) Muscle wasting and the temporal gene expression pattern in a novel rat intensive care unit model. *BMC Genomics*, 12:602

122. Hussain, K. M., Lee, R. C. H., Ng, M. M.-L., & Chu, J. J. H. (2016). Establishment of a Novel Primary Human Skeletal Myoblast Cellular Model for Chikungunya Virus Infection and Pathogenesis. *Scientific Reports*, *6*, 21406.

123. Stromberg, A., Olsson, K., Dijksterhuis, J.P., Rullman, E., et al. (2016) CX3CL1 – a macrophage chemoattractant induced by a single bout of exercise in human skeletal muscle. *Am J Physiol Regul Integr Comp Physiol*, 310(3): R297-304

124. Amino acid sequence and distribution of mRNA encoding a major skeletal muscle laminin binding protein: an extracellular matrix-associated protein with an unusual COOH-terminal polyaspartate domain. (1988). *The Journal of Cell Biology*, *107*(2), 699–705.

125. Arnold, L., Perrin, H., de Chanville, C. B., Saclier, M., Hermand, P., Poupel, L., … Combadiere, C. (2015). CX3CR1 deficiency promotes muscle repair and regeneration by enhancing macrophage ApoE production. *Nature Communications*, *6*, 8972.

126. Lin, E. A., & Liu, C. (2009). The emerging roles of ADAMTS-7 and ADAMTS-12 matrix metalloproteinases. *Open Access Rheumatology : Research and Reviews*, *1*, 121–131.

127. Nitert, M. D., Dayeh, T., Volkov, P., Elgzyri, T., Hall, E., Nilsson, E., … Ling, C. (2012). Impact of an Exercise Intervention on DNA Methylation in Skeletal Muscle From First-Degree Relatives of Patients With Type 2 Diabetes. *Diabetes*, *61*(12), 3322–3332

128. Pillon, N.J., & Krook, A. (2017) Innate immune receptors in skeletal muscle metabolism. *Exp Cell Res*, 360(1): 47-54

129. Rayavarapu, S., Coley, W., Kinder, T. B., & Nagaraju, K. (2013). Idiopathic inflammatory myopathies: pathogenic mechanisms of muscle weakness. *Skeletal Muscle*, *3*, 13.

130. Englund, P., Lindroos, E., Nennesmo, I., Klareskog, L., & Lundberg, I. E. (2001). Skeletal Muscle Fibers Express Major Histocompatibility Complex Class II Antigens Independently of Inflammatory Infiltrates in Inflammatory Myopathies. *The American Journal of Pathology*, *159*(4), 1263–1273

131. Yahiaoui, L., Gvozdic, D., Danialou, G., Mack, M., & Petrof, B. J. (2008). CC family chemokines directly regulate myoblast responses to skeletal muscle injury. *The Journal of Physiology*, *586*(Pt 16), 3991–4004.

132. Sajnani-Perez, G., Chilton, J.K., Aricescu, A.R., Haj, F., & Stoker, A.W. (2003) Isoform-specific binding of the tyrosine phosphatase PTP-sigma to a ligand in developing muscle. *Mol Cell Neurosci*, 22(1): 37-48.

133. Brzoska, E., Kowalewska, M., Markowska-Zagrajek, A., Archacka, K. et al. (2012) sdf-1 (CXCL12) improves skeletal muscle regeneration via the mobilization of Cxcr4 and CD34 expressing cells. *Biol Cell*, 104(12): 722-37

Chapter 4

Summary of overall findings

Summary of Overall Findings

The objectives of this research were to 1. Determine the relationship between diabetes-induced renal dysfunction or CKD progression and its systemic environment, on skeletal muscle performance and overall physical function and when this becomes apparent, and 2. Determine the physiological mechanisms that promote muscle and functional impairment in CKD progression, and when this occurs in the course of disease.

Chapter 1 aimed to accomplish objective 1. Our results suggest that muscle performance of the lower extremity, particularly the quadriceps, and physical function decline in-parallel with progression of CKD in T2DM, with these declines becoming significant and clinically evident in stage 3. Moreover, we find that CKD-stage, and renal filtration/function (eGFR) are both significant predictors of overall physical function, with increasing CKD stage/worsening kidney filtration predicting worse functional mobility, and this is true even after for controlling for potentially confounding age and diabetes-related variables (HbA1c, BMI). Additionally, CKD-associated metabolic bi-products, like BUN are significant negative predictors of functional mobility, and those in stage 3+ CKD demonstrate functional deficits that reflect a pre-mature geriatric state.

These data shed new light on the deleterious effects of poor kidney function on overall health. We demonstrate, for the first time, that CKD imparts significant reductions in performance of key lower extremity muscle groups like the quadriceps, as early as stage 3, which carries strong relationships to functional mobility deficits that may independently contribute to CKD exacerbation.

Chapter 2 aimed to provide mechanistic insights into the physiological ways in which poor kidney function with CKD progression negatively affects muscle health, performance, and overall physical function. Specifically, chapter 2 examined the CKD-stage specific functional status of

skeletal muscle mitochondrial ATP production, and electron transport chain kinetics, as these are critical cellular processes to fuel muscle cross-bridge cycling, contraction and movement. We find that skeletal muscle mitochondrial electron transport chain function is reduced with progression of CKD, once again, with significant reductions in ATP-production capacity emerging as early as stage 3 CKD. Moreover, we report mitochondrial abundance is maintained with CKD progression, suggesting these ATP-production deficits are secondary to intrinsic mitochondrial deficits. These suggestions are further bolstered with our ETC complex-specific enzyme tests demonstrating significaint complex 4 functional deficits in stage 3 and 4&5 CKD. Lastly, using RNA-sequencing, we find gene pathway alterations may drive these intrinsic mitochondrial deficits in middle and late-stage CKD, primarily through attenuated transcription of key ETC complex subunit proteins and assembly factors, reduced expression of mitochondrial turnover and transport channels, and altered expression of genes that govern reactive oxygen species handling and generation. Most importantly, we demonstrate that intrinsic mitochondrial function is strongly related to lower extremity muscle performance and physical function.

These data mark the first time anyone has investigated intrinsic mitochondrial function with CKD progression, and highlights new time-frames and potential targets of conservative treatment, to improve muscle health, function, and attenuate the functional declines seen in this disease.

Chapter 3 aimed to answer, in-tandem with chapter 2, the second objective of this research – to determine the physiological ways in which poor kidney function with CKD progression negatively affects muscle health, performance, and overall physical function. However, while chapter 2 focused on skeletal muscle energetics as a contributing mechanism, chapter 3 studies muscle regenerative and maintenance capacity. Specifically, chapter 3 examines the CKD-stage specific status of muscle-resident stem cells (Satellite Cells -- SC), a cell population charged with

maintaining muscle integrity and repairing muscle fibers after injury. We find the muscle-resident SC pool to decline significantly at stage 3 CKD, and remain reduced in late-stage disease. Moreover, we demonstrate that such SC loss may be secondary to their poor capacity to renew themselves through duplication and division. Additionally, we report impaired myogenic capacity of these SCs secondary to altered gene activation patterns, that relate strongly to findings of poor muscle quality with progressive CKD stage (increased fibrotic and adipose tissue accrual). Similar to chapter 2, using transcriptomics, we report significant dowregulation in gene networks that influence muscle SC behavior and myogenesis, with concomitant upregulation in epigenetic mechanisms, and inflammatory cytokine signaling pathways with progression of CKD stage. This inflammatory signaling is supported by our findings of increased circulating pro-inflammatory cytokines (IL-6 and TNF-a), and increased muscle-resident leukocytes with worsening kidney function.

As in chapter 2, the investigation in chapter 3 marks the first time anyone has studied myogenesis in human skeletal muscle with CKD progression in those most at risk – type 2 diabetics. This data lends new insights into the mechanisms that may relate the CKD-associated environment with muscle gene pathway changes, reparative capacity, and cell-cell interactions that are all crucial in ensuring proper muscle health and function.

In summary, our data suggests that the progression of diabetes-induced chronic kidney disease, is paralleled by impairments in skeletal muscle ATP-producing capacity, and these energetic deficits are accompanied by CKD-associated reductions in muscle SC abundance, and reparative function. Both changes perhaps stem from alterations in gene pathway expression that is imparted by the altered uremic environment. These impairments may promote the development of poor muscle quality and performance that ultimately impairs functional capacity, even in middle-stage CKD.

Clinical Implications

Based on these results, it is clear that skeletal muscle impairments, even on a cellular level, become significant in middle-stage CKD (stage 3). Stage 3 also marks the point of entry for many of these patients, into nephrology care. In light of this, these results suggest that conservative exercise prescription, specifically targeted to the underlying energetic and cellular factors earlier in CKD progression (ie. stage 2 or 3) may prove highly beneficial in attenuating the progression of muscle impairment with CKD. Healthcare workers should aim to educate patients regarding the importance of maintained mobility and exercise, specifically activities that target large lower extremity muscle groups such as the quadriceps studied in this work. Of particular emphasis should be stimuli that promote improved mitochondrial respiration and SC abundance and myogenic function – cellular adaptations often reported in exercise physiology literature for both aerobic and resistance training regimens.

Future Studies

As mentioned in chapter 2 and 3, this work provides many avenues of potential future investigation. The use of transcriptome analysis via RNA-sequencing revealed epigenetic mechanisms to be significantly upregulated in both middle and late-stage CKD. Chromatin binding pathways, histone modifications, and miRNA signaling were all among the most significantly upregulated gene networks seen in CKD skeletal muscle. Such factors have been shown in other conditions, to be induced by environmental changes (i.e hyperglycemia of diabetes), to promote changes in DNA packing and to prevent or allow RNA polymerase or transcription factor binding and subsequently, repress or upregulate gene expression. An exciting avenue of future research would be to further probe the specific epigenetic alterations imparted by CKD and its uremic

environment, and how this translates into skeletal muscle health and function. Such work may even highlight epigenetic marks in those in various stages of CKD that may predispose them to deficient muscle energetics or SC-mediated repair processes. This could potentially serve as a biomarker from which to proactively introduce treatment before the onset of symptoms or functional loss. Similarly, we highlight several potential mechanisms by which CKD and its associated signaling factors may negatively affect mitochondrial function. Further investigations aimed at determining the precise influences of the uremic environment on specific mitochondrial-governing genes and how this relates to function, is needed.

From a clinical perspective however, based on our results, construction and implementation of a targeted exercise program would be immensely useful and informative. Specifically, an exercise regimen (ie. resistance training) may be implemented in early/middle stage CKD to track the outlined cellular adaptations (intrinsic mitochondrial function, SC abundance, SC function, transcriptome changes) and subsequently follow these patients longitudinally to monitor their muscle performance and functional mobility in-tandem with their CKD status. Such an investigation that addresses the point of intersection between disease and functional outcome before the end-stage of the disease, is needed in this population.